FUNCTIONAL AND COMPLEX TOPOLOGICAL APPLICATIONS OF PLASMA POLYMERIZED ULTRATHIN FILMS

A Dissertation
Presented to
The Academic Faculty

by

Kyle D. Anderson

In Partial Fulfillment
Of the Requirements for the Degree
Doctor of Philosophy in the
School of Materials Science and Engineering

Georgia Institute of Technology
August 2012

FUNCTIONAL AND COMPLEX TOPOLOGICAL APPLICATIONS OF PLASMA POLYMERIZED ULTRATHINFILMS

Approved by:

Dr. Vladimir V. Tsukruk, Advisor
School of Materials Science and Engineering
Georgia Institute of Technology

Dr. Timothy J. Bunning, Co-Advisor
Materials and Manufacturing Directorate
Air Force Research Laboratory

Dr. David Bucknall
School of Materials Science and Engineering
Georgia Institute of Technology

Dr. Anselm Griffin
School of Materials Science and Engineering
Georgia Institute of Technology

Dr. Zhiqun Lin
School of Materials Science and Engineering
Georgia Institute of Technology

Date Approved: April 20th, 2012

Dedicated to

My Family

ACKNOWLEDGEMENTS

First of all I would like to express my sincere thanks to my parents, sister and extended family for their support in my continued educational efforts. It is with this solid foundation that I have built my life and without them I would not be where I am today.

I would also express my sincere thanks to Prof. V. Tsukruk whom I began working with at the very beginning of my college career at Iowa State University. As an inexperienced pre-freshman, he extended me an offer to spend the summer with his group based only on a resume with a three-week summer science camp polymer project and to this day, that opportunity has greatly shaped the course of my life and career. Prof. Tsukruk has continued to provide me with many excellent opportunities over the years to enhance my education through collaborations with Wright-Patterson AFB and the University of Bayreuth in Germany during my time at Georgia Tech. His guidance and motivation in the endeavor of graduate school has been paramount to its completion. A special thanks to Dr. Timothy Bunning of the AFRL with whom I had an opportunity to work closely with during my time in graduate school. Dr. Bunning's mentorship during my time at Wright-Patterson has contributed greatly to the successful completion of this work and my development as a scientist. I would also like to thank my thesis committee, Prof. A. Griffin, Prof. D. Bucknall and Prof. Z. Lin for their valuable inputs and for reviewing this work.

I would also like to thank the many mentors and peers I have had the opportunity to learn from at Iowa State and Georgia Tech especially Dr. M. McConney, Prof. S. Singamaneni, Dr. R. Gunawidjaja, Prof. E. Kharlampieva, Dr. D. Zimnitsky, Dr. M. LeMieux, Dr. S. Peleshanko, Prof. S. Mallapragada, Dr. C. Harrison, Prof. M. Misovich, Prof. J. Cochran, Prof. S. Chumbley, Dr. M. Ornatska, Dr. K. Genson, Prof. C. Jiang, Prof. H. Ko, Dr. T. Clark, Dr. K. Campbell, Dr. J. Vernon, Dr. R. Kodyath, Mr. K. Marczewski, Ms. M. Luo, Mr. Z. Combs, Mr. S. Young, Mr. R. B. Weber. I would also like to thank the many collaborators who have provided invaluable assistance in this work: Dr. R. Naik, Dr. J. Slocik, Dr. R. Jakubiak, Dr. H. Jiang, Dr. M. Dickerson, Mr. J. Enlow, Dr. K. Eyink Prof. A. Fery, Dr. A. Schweikart, Dr. N. Pazos-Peréz, Dr. O. Kaftan, Mr. C. Kuttner, Mr. D. Kluge and Prof. E. L. Thomas' group at MIT for providing IL structures. I am very grateful for the financial support from the National Defense Science & Engineering Graduate Fellowship (NDSEG) fellowship program, AFOSR (FA9550-08-1-0446 and FA9550-09-1-0162 projects), AFRL, AFRL BIONIC Center and the AFRL Bio-X STT program is duly acknowledge and appreciated. Finally, I would like to give a very special thanks to Lindsey Goodman for her continued love and support during this process.

TABLE OF CONTENTS

Page

LIST OF TABLES

Page

LIST OF FIGURES

Page

LIST OF SYMBOLS AND ABBREVIATIONS

ACN	Acrylonitrile
AFM	Atomic Force Microscopy
CVD	Chemical Vapor Deposition
FTIR	Fourier Transform Infrared Spectroscopy
HEMA	2-Hydroxyethyl methacrylate
His	Histidine
IL	Interface Lithography
NIPAAM	N-isopropylacrylamide
PDMS	Polydimethylsiloxane
PECVD	Plasma Enhanced Chemical Vapor Deposition
PP	Plasma Polymerized
PS	Polystyrene
PTFE	Polytetrafluoroethylene
SEM	Scanning Electron Microscopy
TTIP	Titanium Isopropoxide
Tyr	Tyrosine
XPS	X-ray Photoelectron Spectroscopy

SUMMARY

This study is focused on the fabrication of plasma polymerized ultrathin films and the elucidation of their unique properties with an emphasis on the solvent-less, dry polymerization process to introduce post-deposition functionality, robustness, and shape preservation. Two major classes of materials are the subject of this study: biological monomers, specifically the amino acids tyrosine and histidine and synthetic organic and inorganic monomers including acrylonitrile, 2-hydroxyethyl methacrylate, N-isopropylacrylamide, titanium isopropoxide and ferrocene. The unique chemical and physical properties of highly cross-linked ultrathin plasma polymerized amino acid and synthetic polymer films are demonstrated along with their functional response and robustness on both planar and complex surface structures. The work emphasizes the facile ability of plasma polymerization to create unique, tailored ultrathin coatings.

Chemical functionality retention (OH, NH_2) of the tyrosine and histidine amino acids is demonstrated by the subsequent mineralization of gold or titania nanoparticles on the plasma polymerized ultrathin films using a wet chemical approach. Inorganic nanoparticle mineralization is further investigated as a method to modify the optical properties of composite nanocoatings. Plasma co-polymerization of tyrosine and synthetic monomers is used to create nanocomposite coatings with unique surface functionalities, responsive behavior, optical characteristics and a high level of integration between monomers. The fabrication of novel plasma polymerized Janus microspheres, micropatterned substrates and free-standing films also demonstrate numerous plasma polymerized materials which exhibit unique structural properties. Overall, facile plasma polymerization of novel, functional ultrathin films and complex topological coatings having potential biocompatible and optical applications is established.

CHAPTER 1 : Introduction

1.1 Background

Polymeric and soft matter ultrathin films deposited through different vacuum coating techniques have been an area of increasing interest as these materials are adapted for use in surface modification, sensing, optical, electronic, photonic, responsive and biological applications.[1,2,3,4,5,6] Chemical vapor deposition (CVD) is a versatile method for fabricating thin films of many different materials using a vapor phase polymerization reaction, which virtually eliminates the need for and challenges associated with wet chemical synthesis of thin films on various surfaces.[7] These types of CVD coating methods are easily and uniformly applied to many different micro- and nano-scale surfaces, which require unique surface modifications and are difficult to achieve through other means due to synthetic mechanisms, wetting and agglomeration problems or substrate incompatibility. CVD techniques have traditionally been applied to inorganic materials in the semiconductor industry and more recently to carbon structures such as carbon nanotubes and graphene.[8,9,10,11] Many different methods of CVD exist, but all rely on the use of a vacuum system and vaporization of the monomer species for deposition onto the target surface.[12] CVD offers a facile method to overcome many surface coating issues (grafting, adhesion, film density, uniformity) while providing conformal, uniform coverage in a single, dry chemical fabrication step.

The origins of polymeric CVD work are traced back to work by Gorham where the polymerization of poly-p-xylylene was investigated under heating in vacuum.[13] This work established the basis for much of the future CVD polymerization work by demonstrating

how a monomer can become reactive through heating, as in this case, and form long chains with other reactive molecules. However, the heat required for such cleavage and reactive species formation was in excess of 600ºC, a temperature which would be destructive to many monomers, thus limiting the general applicability of this method. This early example of CVD did however establish a general model and the principles for how two active species can combine with others in a rapid step-growth type reaction to form a thin film on a target substrate. For more widely applicable depositions of a broader range of materials, other methods of creating vaporized reactive species have been explored at much lower, and even at room temperatures.

CVD methods have been widely used to polymerize materials directly on a variety of surfaces.[7,12,14,15,16] CVD processes have been designed to allow organic monomers to undergo *in situ* polymerization during the deposition process resulting in a stable film of polymerized material on the surface. Polymerization is initiated by a range of different stimuli including RF plasma initiation (PECVD), introduction of a vaporized chemical initiator (iCVD), photoinitiation (piCVD), oxidative (oCVD), hot-wire (HWCVD) and physical vapor deposition (Table 1.1).[17,18,19,20,21,22,23,24,25,26,27] Many methods have been studied which seek to provide a better means of facilitating formation of soft matter thin films and each deposition method has the effect of creating a polymerized film on a target substrate with different variations in the cross-linking density and morphology depending on the CVD method used and the reaction mechanisms.[28] This leads to films with a wide range of unique surface properties that can be tailored for many specialized applications. These types of different CVD methods have all been employed for use in the fabrication of soft matter thin films with different polymers covering a wide range of chemistries and applications. Each system presents a unique set of advantages and drawbacks making them uniquely suited for a specific process, but no broad,

overarching technique is currently available which adequately addresses every processing issue to the extent which would allow universal applicability to every scenario.

Table 1.1: Compilation of common thin film fabrication techniques[7]

Technique	Description	Attributes
Vapor Deposition (VDP)	Physical vapor deposition process where monomer and adsorbed on surface, may require surface modification for adhesion/growth	Material is physically deposited on a surface. Surface initiator may be needed to ensure grafting. Post deposition curing used.
Chemical Vapor Deposition	Any process whereby a monomer is vaporized, undergoes a chemical reaction/interaction and is adsorbed on a surface in a chemically altered state.	Widely used in microelectronic fabrication for inorganic material deposition. Readily adapted for use with organic monomers under varying levels of vacuum
Plasma Enhanced CVD	Use of RF plasma in continuous wave or pulsed modes to radicalize a monomer allowing it to undergo a rapid chemical reaction in a single step uniformly coating a surface at low temperatures	Highly cross-linked, uniform, robust films with good surface adhesion. Can suffer from high internal stresses which cause film delamination. Compatible with solid, liquid and gas monomers
Initiated CVD	Use of a chemical initiator vaporized simultaneously with the monomer to initiate chemical reaction/chain formation via radicals. Activated by UV light or heat	Films show high deposition rate and high functional group retention. Uses a chemical initiator to begin polymerization and an additional cross-linking agent.
Oxidative CVD	Use of an oxidizing agent vaporized simultaneously with the monomer to induce reaction	Used in the deposition of conductive monomers and show high conductivities
Hot-wire CVD	Heated filament wire used to activate a monomer, usually through decomposition	Lacks use of chemical initiator. Heating of input gases decomposes them to a state where they become reactive.

A key advantage of several of these processes is the retention of specific chemical functionalities, which allow the construction of chemically tailored surfaces and interfaces that can be designed for specific interactive, detection and responsive applications. Controlling the surface chemistry, chemical cross-linking, and functional group retention allows the design of films tailored for specific uses. The primary focus of the work in this dissertation is centered on the use of the plasma enhanced CVD

(PECVD) method for fabricating functional thin films on complex surfaces. Plasma polymerized films can be constructed from a wide range of monomers for many different applications ranging from sensors to implant coatings to optical modifying agents to biofunctional films.[1,14,23,29,30,31,32,33,34]

Other examples of physical vapor depositions based on monomer heating have also been studied with different materials, including some amino acids, but these demonstrations typically require a surface modification of the substrate with an initiator or a specific substrate to be used in order to allow the reaction to progress.[35,36] While some studies of physically vapor deposited amino acids have been carried out and analyzed, they have tended to show large structural formations such as nanotubes and other features formed by the monomers during the deposition.[37,38] These types of amino acid nanotubes are not an entirely unique phenomena of vapor deposition as examples of their formation have been documented through the use of wet chemical means.[39] The use of a more uniform coating technique such as PECVD has not been explored in detail to assess the functionality of amino acid films as biomineralization agents and surface modification agents on 2D and 3D surfaces. While there are many different methods which are viable for the surface deposition and polymerization of many monomers, this dissertation work will focus primarily on those systems created by PECVD.

1.1.1 Plasma Enhanced Chemical Vapor Deposition

PECVD is a specific form of CVD which has been adapted from its common use to deposit dielectrics to successfully deposit a wide range of monomers covering many common polymers, ranging from styrene, acrylonitrile and benzene to responsive materials such as poly(2-vinyl pyridine) and poly(N-isopropylacrylamide) to functional

amino acids.[40,41,42,43,44,45,46,47,48] PECVD represents a versatile “dry” chemistry fabrication method which is capable of utilizing precursors in solid, liquid or gas form for facile, rapid and solvent free fabrication of ultrathin coatings for use in many systems (Figure 1.1).[29,49,50,51,52] There is a growing interest in the deposition of biological molecules via PECVD which can potentially be used to enhance surface functionalities and structures for cell viability and can also help to bridge the interface between inorganic and biological components of integrated systems and biomedical applications.[14,31,36,53,54,55,56]

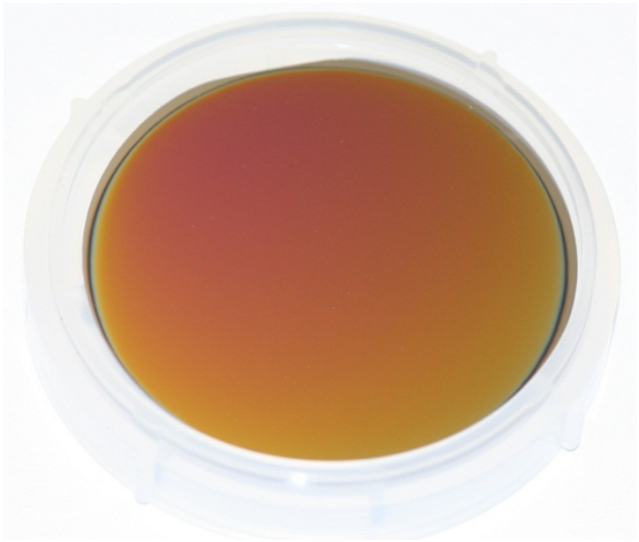

Figure 1.1: Representative image of PECVD deposited film of histidine coating a 50 mm silicon wafer.

PECVD relies on using a radio frequency (RF) plasma generated at 13.56 MHz at room temperature, to induce radicalization of monomer species in the reaction chamber. While several methods can be used to generate plasma in a low-pressure chamber including electron cyclotron resonance, inductive coupling and capacitive coupling, the configuration used in this work is a capacitively coupled parallel plate configuration with the substrate placed downstream, perpendicular to the plasma stream.[18] The substrates can either be immersed directly in the plasma (i.e. between the parallel plates) or placed

outside of the plasma (downstream). The plasma excitation and radicalization of the carrier gas and vapor phase monomer gives the excited species the opportunity to react with any surface in the plasma chamber, forming a film through two basic steps: formation of a radical or reactive species and propagation of the polymer chain or network. PECVD itself has several varieties including flowing afterglow, plasma zone and pulsed plasma deposition, which further offer different deposition regimes for coatings. A major concern in all plasma work is the integrity of the monomer as it is being exposed to the plasma. Direct influx of the monomer into the plasma zone has a high probability of causing large scale destruction to the monomer. By "softening" the radicalization, either through the use of a plasma pulsing regime or introducing the monomer downstream of the plasma zone (flowing afterglow), many monomers are able to be deposited with greater stability and with excellent retention of the monomeric chemistry and functionality.[57] With less applied power, the monomers are still radicalized on certain functional groups, but generally do not undergo full-scale alteration or destruction of the monomer. This type of radicalization makes PECVD a versatile and "gentle" deposition technique in the same class as iCVD or oCVD, two other widely used polymerization methods. As no solvents are used and the reactions are carried out at low applied powers and substrate temperatures, the process is considered to be amenable to a wide range of monomers. Since the plasma radicalization process is non-selective, all species will undergo the reaction and adhere to the target surfaces. This is in contrast to other, more specialized deposition techniques which may rely on a specific chemical initiator in the reaction which is not as universal in nature as the plasma.

While the plasma polymerization reactions on the surface seems to have elements of both a radical and step-growth polymerization scheme, the process is truly unique and is

used to form polymeric films under vacuum conditions with reactive species more often bonding with each other, rather than with an unradicalized monomer. This differs from other polymerization where a radical may be formed by an initiator and proceed to interact with a monomer, passing the radical along a growing chain. Plasma polymerization is a method intended to prepare unique polymers (highly cross-linked networks) that cannot otherwise be created by alternate polymerization methods as opposed to a specific way of polymerizing monomers.[26] These films are typically seen to have nonlinear, highly branched and highly cross-linked structures. Due to the presence of many free radicals and the fact that chain termination is favored over chain propagation, this leads to many small molecular weight chains being formed and terminated which ultimately results in a high degree of cross-linking and networked structures. Other CVD methods, such as iCVD tend to produce more linear polymer chains in contrast to the film structures formed via PECVD. One feature of plasma deposited films is their excellent substrate adhesion. This high adhesion allows the films to resist solvent treatments, mechanical wear and multiple exposures to heat, humidity and ambient atmosphere for long periods of time. The surface adhesion is a result of the plasma stream radicalizing sites on the substrate, which act as bonding sites for the incident radical monomers to adhere to. By using surface free radicals to initiate grafting of the monomer to the substrate, the ability of the film to remain firmly attached to the substrate is greatly increased.

1.1.2 Plasma Chemistry

The nature of the chemical reactions as they occur during plasma reactions is difficult to determine precisely owing to the fact that *in situ* measurements are challenging. However, by exerting careful control over the reaction variables such as power,

pressure, monomer and carrier gas flow rate, temperature and atmospheric content, many materials can be reliably deposited multiple times under identical conditions. Even with careful control in place, PEVCD is still subject to a degree of variation and all conditions should be monitored as closely as possible. While plasma polymerization may appear at first glance to be similar to a radicalization or step growth polymerization reaction, it is worth noting that it likely proceeds along a different path in part to its deposition under vacuum conditions.

Radiation polymerization, where a monomer is ionized by exposure to radiation which causes the emission of an electron, is similar to the type of reaction that occurs under

$$e^- + Ar \rightarrow Ar^* + e^-$$
$$M + e^- \rightarrow M^* + e^-$$
$$M + Ar^* \rightarrow M^* + Ar$$

Figure 1.2: General mechanistic reactions of plasma depositions resulting in the formation of monomer radicals. Adapted from Singamaneni et. al.[29]

plasma conditions, but does not typically yield polymer structures when under vacuum.[26] The same type of polymerization under vacuum is seen, however, with the example of Parylene heating and cracking, which results in reactions between two reactive species to form a polymer and is much more akin to a step growth type polymerization.[13,26] Using RF plasma to generate molecular radicals is the primary means by which plasma polymerization begins to occur (Figure 1.2).[58,59] As opposed to atomic ionization, molecular ionization requires less energy input to the monomer and can easily break low energy bonds and cause the formation of reactive, excited species. This tends to give rise to many side reactions, making a defined, linear polymerization model difficult in the plasma reaction.

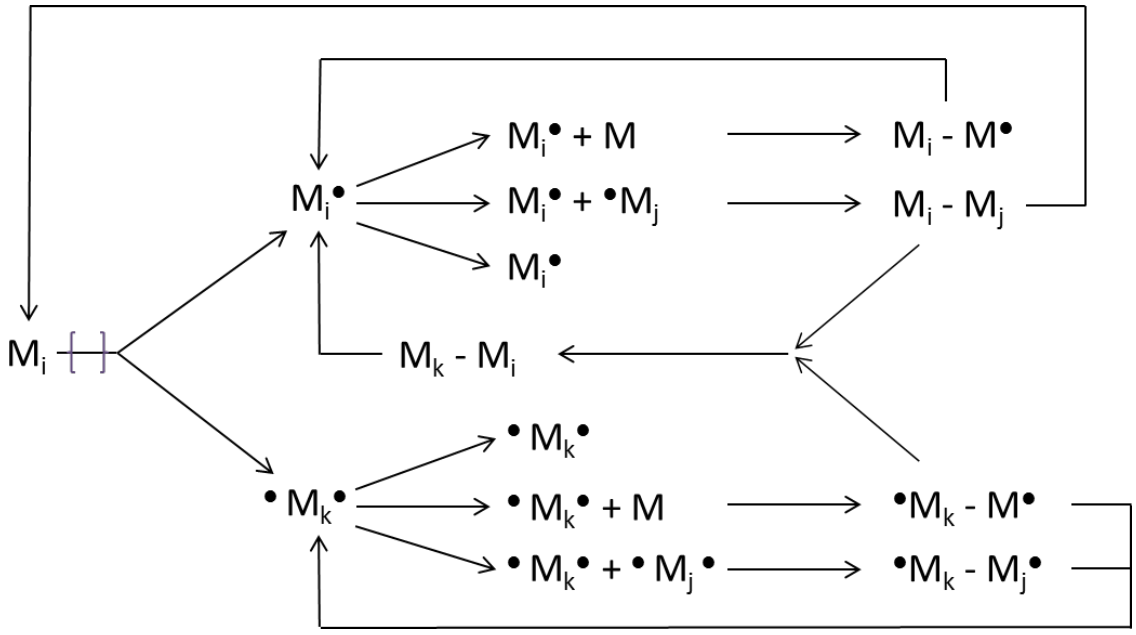

Figure 1.3: Possible polymerization routes of a monomer that can occur during plasma polymerization. Adapted from Yasuda.[26]

The radicals are formed both on the monomer while in the plasma stream and on the target substrate, especially after the film begins to deposit, enhancing the films adhesion. Radical formation typically follows the example shown (Figure 1.3) where the monomer can either be directly radicalized in the plasma or through interaction with another radicalized species. Once radicalized, the monomer can either combine with another radicalized monomer or transfer its radical to another monomer. Two radicalized monomers can combine to form a dimer causing termination, which can either end the reaction or the dimer can become re-radicalized in the plasma stream. Due to the number of radicals in the system, there can be a significant amount that become trapped in the final film if they do not react before becoming completely encapsulated by other deposited material. Recently, some discussion regarding the role various ions and gas phase reactions play in the surface polymerization has appeared in literature.[60,61,62] Much of this work has involved the study of the possible formation of

charged oligomers forming in the gas phase prior to deposition on the surfaces in contrast to chains only growing once monomers were attached to the substrate. Studies of hexamethyl disiloxane (HMDS) have shown that under varying plasma deposition conditions, the flux of ions on the surface will vary and that as pressure increases, there is an increase of radical and neutral species in the film as measured by mass spectrometry and time of flight secondary ion mass spectroscopy (ToF-SIMS).[63] However, the debate over the role of surface ions in plasma systems and contributions of these ions to the films and their underlying mechanistic reactions continues in the literature.[64,65,66,67,68,69]

The ratio of radicals to ordinary monomer has a great impact on how the film characteristics develop. Controlling the radical formation is achieved through several means. First, the power applied to the plasma induces radical formation and generally, lower power plasmas will create statistically fewer radicals. The power setting applied to soft matter depositions is much lower than most industrial or inorganic depositions and allow the monomers tested to deposit well without dissociations of the monomer itself. The goal is to induce radicalization so that the monomers will react while still retaining their original structure and functionality. The second factor of radical formation is concerned with the placement of the monomer inlet. Monomers which flow directly through the plasma generating zone will also tend to radicalize more readily as opposed to ones introduced downstream, in the flowing afterglow of the reactor. Flowing afterglow reactions also help preserve the integrity of the monomer which leads to greater retention of the original chemical functionalities by exposing the monomer to a lower intensity of power. In addition to these considerations, other variables that are observed to control the plasma deposition process are the pressure of the reaction chamber and the flow rates of the carrier gas and monomer into the chamber as well as

the temperature of the chamber, substrate and monomer. Varying these conditions can have a significant impact on the resulting films.

1.2 Soft Matter in PECVD

PECVD has proven to be a simple method to rapidly deposit monomers onto substrates in stable, robust thin films. The fact that the system is compatible with a wide range of monomers lends itself well to potential future industrial applications as it can easily be adapted to new materials. The use of organic molecules with PECVD is significant since PECVD was originally developed around inorganic chemistries for different oxides, nitrides, metal silicides and transition metals.[8,70] It is significant that such a process was adapted for use with soft matter and is compatible at low temperatures and low powers. The ability to take a monomer and deposit it as a stable thin film on a substrate is not necessarily a trivial exercise with some synthesis methods requiring complex chemistries, harsh solvents and extensive surface modifications for molecular attachment. Many of these issues are eliminated in PECVD since the plasma induces radicalization in the monomer and activates the substrate surface allowing the monomer to form a bond to the substrate and form a cross-linked film on top. Control of cross-linking is critical in the films to allow them to retain features such as responsiveness, surface activity, stability, stiffness and definition of optical characteristics, such as refractive index.[71] With this in mind, it is seen that PECVD of soft materials is being applied in diverse fields from optical to biomedical applications. In this study, monomers of both synthetic and biological origin are investigated.

1.2.1 Organic plasma polymerizable materials

PECVD is distinct from other forms of polymerization due to the nature of the reaction occurring and means of initiating and controlling film growth. While similarities between

plasma polymerization and other methods such as step or chain growth exist, there are fundamental differences in the plasma process that make these films truly unique as have been explained.[26] PECVD draws its immense material versatility from the mechanism it uses to create thin films; the radicalization induced by the plasma. The films also acquire a unique architecture of a highly cross-linked network since the reactions occur randomly in the plasma chamber and are not specifically directed as the films form on the substrate. Inorganic thin films such as silanes and nitrides that were the original focus of PECVD studies deposit very well forming hard, inorganic layers, but generally fall short in many applications where polymers excel, one being responsiveness. These inorganic films generally do not exhibit a response to external stimuli the way a polymer film does and are typically better suited for use in microelectronic applications.

PECVD had been widely adapted as a method and has been used with many different polymers including polystyrene, polyacrylonitrile and polyethylene oxide, responsive monomers including poly(N-isopropylacrylamide) (pNIPAAM) and poly(2-hydroxyethyl methacrylate) (pHEMA), halogenated molecules such as pentafluoroethane and hexaflurobenzene which show unique insulating properties and organometallics like ferrocene and titanium isopropoxide.[41,49,72,73,74,75,76,77,78] Two of the more extensively studied polymeric materials deposited with CVD have been NIPAAM and HEMA, which both show a responsive behavior. These types of responsive materials, and these two in particular, are of great interest because of the idea of being able to create a one-step facile surface coating with unique responsive properties that can then be tailored to exhibit specific responses. Each year more reports of different and novel monomers are seen for new applications as PECVD, along with other CVD methods, become more common and widely used for thin film fabrication.

Several reports look to detail the unique internal structure of plasma polymerized films through methods such as X-ray and neutron reflectivity.[79,80,81,82,83] While most chemical characterization of plasma polymerized films has been limited to techniques such as FTIR, UV-VIS or XPS, obtaining a better understanding of the structure of the films is necessary when studying their interactions and responses. Films of benzene and octafluorocyclobutane showed structural variations near the polymer/substrate interface and the polymer/air interface on the order of several nanometers in thickness. The bulk of the films were generally seen to be homogenous, but through variation of the chamber pressure during deposition, the cross-linking density could be varied significantly and

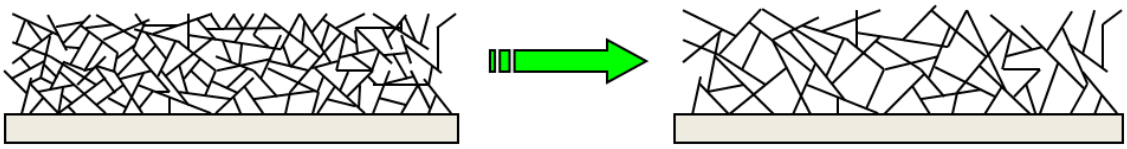

Figure 1.4: Schematic representation of high and low cross-link density in plasma polymerized films.

was typically lower near the substrate than in the bulk of the film (Figure 1.4).[84] These studies also probed the surface roughness of co-polymerized films and found them to be very smooth, on the order of 3-6 Å, and homogenous in composition.[85] Several other important characteristics were noted by Foster et al.: The structure was uniform throughout the films, thin transition layers were observed of about 7 nm thickness near the substrate and near the surface and a decrease in the cross-linking density of the film near the surface. These studies offer excellent insight into the nature of the plasma polymerized films and how they are controlled through the deposition parameters. Applied plasma power greatly affects the composition and morphology of the copolymer

film, especially in copolymers and it will affect the structure of all films by changing the ratio of radical to monomer molecules which affects the cross-linking.

The plasma deposition conditions also have a significant bearing on the long term stability of the plasma polymerized films. Since any use of PECVD on a commercial scale would require films to be stable for extended periods, this is an area of interest as the process is adapted for more applications. One study characterized the aging effect on allyl alcohol and acrylic acid PECVD films and found little change in the films or their composition over 400 days.[86] Some oxygen increase is seen in allylamine films, as it is absorbed from the atmosphere. Films were measured by XPS to evaluate the carbon/oxygen and carbon/nitrogen ratio at various time intervals to characterize any change in the films. The depositions were run under low power (5W) and showed remarkably stable films over an extended period of time when fabricated under appropriate conditions. Confirmation of the robustness and stability of the films demonstrates that PECVD can be used as a viable method to produce films for applications requiring long-term stability.

One common monomer used in many PECVD studies is NIPAAM due to the ability of poly(NIPAAM) to exhibit characteristics of a thermally responsive, swellable hydrogel, making it a material desirable for many applications. Deposition conditions have also been studied in regards to the responsive nature of pNIPAAM where the substrate temperature and chamber pressured were varied to assess the impact on water uptake by the film.[40,41] QCM-D studies at different temperatures confirmed that films with higher degrees on intermolecular hydrogen bonding indeed showed lower moisture uptake capacities and that processing conditions contributed greatly to overall film stability. For some of the listed conditions, the films measured were unstable while others were very

stable in water and illustrates clearly how that even using the same monomer, changes in the deposition (in this case, pressure and substrate temperature) has a major impact on the end result. These studies provide highly relevant information regarding the plasma deposition conditions and their effect on the resulting film which can be applied broadly to future studies. Ratner et al. have shown the ability of PNIPAAM to retain a temperature functionality after coating, which allows changes in the mechanical properties of the film as it undergoes an LCST transition around 30ºC.[31,49] The ability to plasma polymerize PNIPAAM is of interest since it exhibits a transition range near body temperature which can be controlled through various means while promoting cell growth and tissue engineering applications, especially in conjunction with grafted RGD peptide.[87]

Another monomer extensively studied with PECVD and other various CVD processes is pHEMA, which is noted for its swelling and responsive characteristics. Plasma deposition techniques have also been extensively characterized for this material, especially as they relate to the control of the cross-linking density of the film. The first studies of PECVD pHEMA were related to the chemical structure following plasma exposure and noted that the material was observed to undergo more dramatic changes in structure and cross-linking as higher applied powers in conjunction with lower deposition pressures would cause a greater loss of functional groups than films fabricated under lower power conditions.[43] While some cross-linking is essential and contributes to the stability of the film, excessive amounts will limit the response through multiple side reactions and may diminish the number of functional groups on the surface. Overall, though, there is typically a loss in the swelling capacity of such films as characterized by a decrease in the swelling ratio.[74,88] Pulsed plasma deposition methods, where the plasma is rapidly cycled on and off, have also been used

successfully as a method of preserving hydroxyl functional groups with pHEMA depositions.[89]

One example of pHEMA polymerization utilized a low power plasma along with the cross-linking agent ethylene glycol diacrylate (EGDA).[74] This is unique since most cases of plasma polymerization rely on the plasma itself to be the initiator of cross-linking rather than a chemical cross-linker. However, the films cross-linked with the EGDA were observed to be much more robust under long term water exposure, indicating their potential application in tissue scaffolding and slow drug delivery applications.[74] A second study was conducted showing pHEMA to be a useful as a biocompatible material capable of coating complex biological geometries and supporting significant cell attachment.[75] This example shows how the influx of two monomers can lead to co-polymerization, an important feature of CVD for building films of tailored architectures and chemistries.

Translating swellable and responsive types of behavior to CVD deposited pHEMA has been studied extensively and several key examples have been demonstrated with a retained structure of functional groups and response analyzed through extensive chemical analysis.[75] Gleason et al. have demonstrate pHEMA in an adjustable optical stack where, combined with titania layers, a shift in the optical properties of the film is observed when exposed to an excess of water.[27] The system was constructed using both iCVD for the PHEMA layers and hot-filament CVD for the titania layers, and while not plasma enhanced, provides an excellent example of the use of other CVD methods with the HEMA monomer, which compliment many of the aims and objectives of general PECVD use.

Most reports of novel materials are ones involving the use of monomers that begin in the gas or liquid phase since these are the easiest to vaporize and induce into the plasma stream and compatible with the majority of reactor constructions. A limited number of reports are available using direct sublimation of solid precursor monomers where the monomers are heated directly into the plasma stream for reaction and deposition. The use of solid precursors is utilized in fewer cases in CVD studies, but has the potential to open access to many materials systems and is worthy of further exploration. One such example is that of ferrocene which readily sublimes upon heating from a dry powder form to be easily deposited upon the target surface for optical modification.[73]

Since the governing reaction mechanism in PECVD can generally be universally applied, only two major constraints are of primary concern when depositing a new material: 1) The monomer must have the ability to be vaporized into the plasma stream via boiling, heating, sublimation or direct vaporization. 2) The applied power of the plasma stream must not cause significant damage/dissociation to the monomer before it reacts on the surface. Given these two premises, a variety of techniques exist which allow the monomer to be successfully deposited on the target substrate.

1.2.2 Biologically derived plasma polymerizable materials

At the simplest level, biological molecules such as proteins and peptides are constructed from amino acids. Amino acids serve as the basic building blocks of many complex systems and are at the core of biofunctionality. When amino acids are purified to their singular form, they are in many respects similar to other chemical monomers, with a specific chemical structure and the ability to form polymerized chains of many amino acids under the appropriate conditions. These single amino acids can be studied in much the same way as any other common monomer can be studied via PECVD

deposition. This is significant since the ability to work with this class of materials has the potential to significantly broaden the applications of PECVD and other CVD coating methods to include biofunctional surfaces and interfaces.

While many different polymeric thin films can be fabricated with PECVD, the topic of biological molecules deposited via PECVD and their interface with different material systems is one which provides a significant area for development. Beginning with the simplest of biological materials, the deposition of various amino acids shows the potential use of PECVD as a compatible deposition process which can be used to readily deposit biomolecules on a surface which retains the original functionality of the material, capable of mineralizing nanoparticles from solution. This deposition method is extended to many different surfaces and structures enabling biofunctionalization on many surfaces where it was not previously available.

Table 1.2: List of monomers studies including biological molecules.

Name	Chemical Structure	Properties
Acrylonitrile	C_3H_3N	Small monomer easily plasma polymerized
Ferrocene	$C_{10}H_{10}Fe$	Iron containing molecule/optical modifier
Pyridine	C_5H_5N	Reduction of silver NPs
HEMA	$C_6H_{10}O_3$	Biocompatible/hydrogel
NIPAAM	$C_6H_{11}NO$	Temperature responsive
Titanium Isopropoxide	$C_{12}H_{28}O_4Ti$	Liquid precursor for Ti depositions
Tyrosine	$C_9H_{11}NO_3$	Amino acid for gold reduction
Histidine	$C_6H_9N_3O_2$	Amino acid for TiO_2 reduction

Biological monomers of interest are often in a powder form, presenting a unique set of challenges for plasma depositions of these monomers. Some solid monomers can be deposited through various sublimation methods whereby the monomers are pre-heated in the plasma chamber while under vacuum and vaporized into a gas phase.[73,90,91,92,93] The reaction proceeds akin to any gas-phase monomer. It has been shown that

sublimation PECVD is compatible with a range of materials, from organometallics to amino acids providing robust and stable films.[41,54,73,94] The utilization of heating and sublimation allows solid materials, which are not volatile, to be plasma polymerized, opening a new range of solid material precursors for study.

Examples from literature have demonstrated the viability of vapor deposition methods to form amino acid strucutres.[36,37] The example developed by Lee and Frank uses a heating method under vacuum to deposit a range of poly amino acids which were firmly grafted to a substrate and preserved their composition and functionalities. These films were limited to ~80 nm in thickness due to the surface modification necessary for adhesion to the substrate which was covered and negated as the deposition progressed. The major disadvantage to this deposition method is that the substrate requires prior preparation with a surface grafted initiator to allow the deposited of the amino acid on the surface. The use of PECVD allows us to effectively eliminate the initiator surface modification step and provides the possibility of coating a wide range of different and in many cases, rough substrates with surface features. The use of a surface grafted initiator also limited the total thickness of the film to typically less than 80 nm since once the depositing material can no longer interact with the initiator, the film will cease to grow. This is a major advantage of PECVD in that surface initiation continuously occurs with the formation of new radicals by the plasma on the deposited surface which provide reactive sites for further film growth. Thus PECVD allows films of much greater thickness to be constructed. PECVD allows more rapid deposition rates as well, usually 1-2 orders of magnitude larger, measured in nanometers per minute rather than per hour. This study provides excellent detail regarding the reactions occurring among the deposited amino acids and the structures they are capable of forming on the surface.

Single amino acids deposited via sublimation PECVD are excellent candidates for further investigation based on their unique functionalities and fundamental biological characteristics.[45,95,96] There is also a significant and growing interest for the use of PECVD in biological applications and for the synthesis of biological films. Direct synthesis of raw amino acids into well-defined coatings is a critical component of understanding the full potential of PECVD for biological applications. One major advantage that will be explored in this thesis is the ability of PECVD to copolymerize multiple monomers in a single reaction. PECVD lends itself well to co-polymerizations of two or more chemical species in order to facilitate complex and stable, functionalized mixed coatings. However, this adds a layer of complexity to the deposition process given the different reactivities of the precursors used. For instance, co-polymerization has been previously reported using benzene and octafluorocyclobutane (liquid and gaseous) monomers which are copolymerized in the plasma simultaneously to fabricate films with controllable refractive indices.[97]

One challenge with this fabrication process, though, is determining the appropriate deposition conditions, which allow a controlled reaction of different organic materials simultaneously. This challenge is magnified when using one monomer, which is solid and must be sublimed into the plasma stream since flow rates are not as easily controlled as they are with conventional liquid and gas phase monomers. The deposition rates of each material must be matched based on the desired end ratio of the final film's composition. As the monomers are mixed in the plasma stream they form highly randomized structures, which when deposited, exhibit characteristics of both components.[97,98] Despite the utility of sublimation PECVD procedures for biological molecules, examples of robust and uniform binary plasma polymerized films utilizing them are very rare. Developing the capability of simultaneous deposition with different

monomers, including bioactive compounds, of any important material highlights the versatility offered to the composition of the resulting plasma polymerized films.

1.3 Biological Applications of PECVD

As such a versatile deposition technique, both in terms of materials deposited and substrates deposited on, CVD and PECVD coatings are finding uses in many applications that demand a responseive film. This requires scientists and engineers to develop not only an understanding of the CVD processes used for the depositions, but also an understanding of functional film properties capable of being harnessed with these films. Development of processes and materials in the realm of biological applications, which requires a decidedly different area of expertise compared to traditional CVD, is an expanding area where many opportunities for new studies are being pursued.

1.3.1 Biomaterials

PECVD as it relates to applications in biology and biomedicine have been a topic of discussion in literature.[14] This is a field with many challenges to address as it requires the combination of expertise of several different fields, namely CVD, biological/biomedical engineering and materials science. There are many potential applications though as a rapid, dry and uniform deposition method for biological coatings on devices such as implants and bio-active surfaces and for the direct synthesis of proteins and peptides. PECVD has tremendous potential to offer this branch of materials science as it is a deposition technique which is compatible with many different types of materials including amino acids and peptides, allowing them to be deposited on and adhere to a variety of surfaces. PECVD can be used as a method to functionalize surfaces with biological material which can then be modified or implanted into a body or

it can facilitate the integration of biological and non-biological materials into a single integrated structure.

Directly depositing biological molecules such as amino acids, proteins and peptides is an area of study which is quickly gaining interest.[14,35,37,38,39] Previous examples of these types of depositions have used vapor deposition polymerization where the short peptide sequence is heated under vacuum to undergo polymerization into various ordered structures such as tubes or spheres on surfaces. Unique structural formations have also been observed to self-assemble from solution cast diphenylalanine dipeptides and can control surface wetability.[99] In this instance the amino acid or peptide is heated under high vacuum and deposited on a heated substrate. Some examples utilize a silicon surface modified with an initiator to allow adhesion of the peptide sequence. This seems to have only a limited effect on the film formation as the maximum thickness reported using this method is around 80 nm. The formation of peptide nanostructures by a similar method can produce much larger features of up to tens of microns in size, large enough to affect the surface properties such as wettability.

The surface characteristics of vapor deposited (physical, not chemical deposition) materials are seen to be very featured with a markedly high roughness as compared to many CVD deposited materials.[37] When beginning with pure monomers, PECVD allows the formation of much more uniform and flat films on the target substrate. PECVD also does not require the use of surface treatments prior to deposition of the monomer since the plasma itself causes radicals to form on the target substrate and act as initiating site for the attachment of monomer units. This type of mechanism repeats itself allowing for the formation of films of variable thickness from a few tens of nanometers to over a thousand. PECVD also provides a method to create very smooth and uniform films in

comparison to the large, rough tube structures formed. This is a critical advantage when considering conformal coatings of intricate structures for further modification through particle mineralization.

PECVD films find use in bio related fields not only in the direct deposition of biological materials, but also through coatings of other polymers for biological and biomedical applications as they relate to topics such as protein binding, cell adhesion, anti-fouling, antibacterial and biocompatibility.[14,100,101,102,103] Using different polymers to modify surfaces for these types of applications is becoming an increasingly relevant use for PECVD, which coats materials quickly and easily in a single step. Most films for biological and biomedical applications are required to be stable in aqueous environments, sometimes for extended periods and this must be designed into these films during their deposition. By adjusting the plasma conditions, films vary from robust to unstable in fluid even if they are composed of the same material as previously discussed with the pNIPAAM example. Films also require good adhesion to the substrate and this becomes critical in cases when the film is expected to exhibit functional post-deposition behavior.

One example of plasma polymerized thin films studied for bio-related applications are the plasma coatings of simple amine, hydroxyl and fluorinated compounds polymerized onto substrates to significantly alter the surface chemistry.[104] Adsorption of fibrinogen was observed to be highest on the amine surface coating with hydroxyl and fluorinated surfaces adsorbing significantly less than the poly(ethylene terephthalate). This study indicates surfaces and characteristic compositions which are observed to be anti-fouling and to be adhesion promoters, both of which are important in future applications. A related study investigated the adsorption of immunoglobulin G (IgG) on plasma

polymerized hexamethyldisiloxane (HMDSO) and acrylic acid (AA).[105] The HMDSO film showed good adsorption of the IgG, but poor adhesion upon rinsing. The retention of IgG on the surface was observed to be much higher with the AA films through covalent coupling with a polyethylene glycol-polyethyleneimine (PEG-PEI) copolymer even after rinsing with buffer and the addition of bovine serum albumin, making these films of interest in immunoassay roles due to the fact that any type of surface may be used.

In addition to IgG, AA films have also been observed to support the growth of human fibroblasts.[106] Allylamine is another material that has been investigated through plasma deposition as a means of fabricating surfaces for cellular adhesion.[107] These plasma polymerized surfaces were observed to be robust through autoclaving and stable enough to be used for several cell culture cycles. The allylamine films were very effective a promoting the growth and adhesion of central nervous system cells in the study by Gross et al. The fact that the plasma coating can be applied to almost any surface is noted as a key advantage over other chemical surface modification methods and is a fact which is observed repeatedly in many of the studies and papers reviewed.

1.3.2 Biomineralization

One specific bio-application of PECVD films that will be a recurring theme in this dissertation is that of biomineralization. Biomineralization is a process which many organisms in nature use to construct rigid structures either as means of bodily support in the case of bones or for protection as in the case of shells.[108,109,110] Biological molecules, such as amino acids, peptides and proteins are used to precipitate inorganic nanoparticles directly from a precursor solution onto a surface. The variety of mineralizable materials and mineralizing agents has been extensively studied using a

variety of techniques and cataloged according to which amino acid sequences best bind certain ions from solution.

While the actual mechanism is still a subject of debate, the results of the biomineralization process, the formation of rigid inorganic structures, is repeated many times in the laboratory and in nature.[111] Molecules such as amino acids, proteins and peptides act as precipitating agents for specific inorganic materials base on their chemical functionality. The inorganic precursor solution is typically one which contains ions in a dilute solution of the material to be mineralized. It is theorized that small pre-nucleation clusters of these ions form and de-form in solution and begin to aggregate around active surface sites which leads to the formation of larger clusters (Figure 1.5).[112] These clusters give rise to nanoparticles on the surface and continue to grow, eventually becoming more ordered deposits which can show a crystalline structure when reaching a larger size.

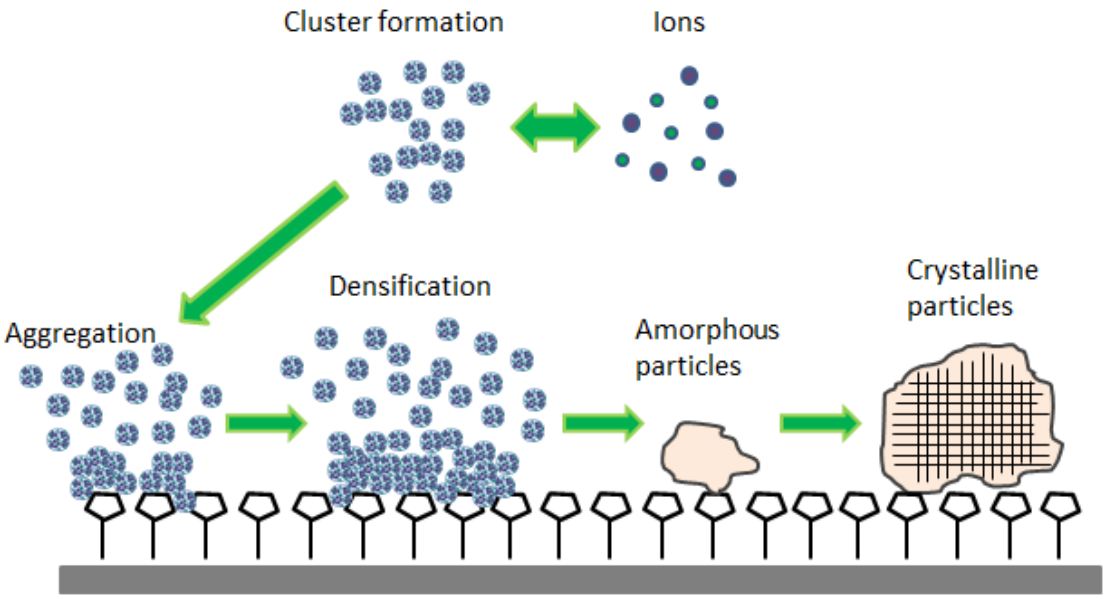

Figure 1.5: Proposed mineralization pathway from ions to clusters to particle formation. Adapted from Sommerdijk et al.[112]

Typically this type of mineralization occurs in solution and any attempt at surface mineralization must include a reliable method of binding the mineralizing amino acid sequence to the surface. Difficulty can arise in creating reliably grafted coatings to certain surfaces that are resistant to modification. By employing the use of PECVD with dry amino acid monomers, the formation of single amino acid peptide sequences leads to a viable method of surface modification by which the film is bound to the surface while still maintaining the necessary functionality to induce mineralization of inorganic particles from solution.

Mimicking a naturally occurring biomineralization process has promising implications for biomimetic engineering. A variety of different metal-binding synthetic macromolecules, proteins and peptides have been demonstrated to effectively form inorganic nanoparticles from precursor solutions and bind them to functionalized surfaces where an excess of the protein or amino acid is properly tethered.[113,114] Functionalized polymeric materials, such as poly(ethyleneimine) and multifunctional hyperbranched molecules, have been demonstrated to be effective in the reduction of silver and gold nanoparticles as well.[115,116]

Many examples of this bioenabled approach have been demonstrated, including but not limited to the use of biological and synthetic macromolecules containing tyrosine, tryptophan and cysteine groups for the controlled formation of gold nanostructures; tyrosine, AG3 and AG4 peptides for the reduction of silver nanoparticles; and cysteine for obtaining platinum nanostructures.[95,117,118,119,120,121,122] As known, proteins and peptides with higher concentrations of charged amino acids (e.g., arginine, lysine) are effective in the reduction of titania nanoparticles.[123,124,125,126] Additionally, histidine amino

acids with their high concentration of amine groups, are considered to be potential precursors for titania reduction, enabling nanoparticle formation from aqueous solution onto surfaces.[95,127] The rSilC protein is one such class which has been demonstrated as being effective at functionalizing surfaces for the formation of large titania structures and nanoparticles.[128,129]

1.4 Complex topological architectures in PECVD

While 2D structures provide excellent model systems for the fundamental characterization of plasma polymerized materials, there are many applications which require the use of non-planar, non-ideal surfaces. Analysis of plasma polymerization on different types of 3D structures is an essential study in the development of understanding functional limits of plasma coatings. One limit of PECVD is that it is a line-of-sight technique whereby the material is coated most prominently on sections of the substrate which are perpendicular to the plasma stream. For this reason coating on surfaces parallel to the monomer flow direction will produce much thinner films leading to growth rates which have a strong directional component to them. However, plasma polymerization is highly compatible with many different substrate materials and can coat highly featured surfaces easily and uniformly, offering a major processing advantage in many cases.

1.4.1 Non-planar coatings

Non-planar and complex surface topologies represent a unique challenge to many CVD methods. It is particularly important that any deposition method be compatible with non-planar substrates if it is to see eventual application in any process outside of the laboratory setting. PECVD provides adept coatings on non-uniform and rough surfaces on a small scale of less than 10 μm. Any part of the substrate which is exposed to the

plasma is capable of generating radicals and securing monomers on the surface. This allows many small features to be coated and for small surface roughnesses of the substrate to have little effect on the final film and quality of the coating. This also makes PECVD useful for modifying small features constructed on a substrate. The coating and filling of mesoporous titania films for dye sensitized solar cell applications has also been demonstrated where iCVD is used to deposit a polymer, such as PHEMA, into the small pores of the surface.[130] This is one example of how very rough surfaces can be intimately coated with a polymer layer.

The line-of-sight limitation of PECVD means features on the surface that run parallel to the plasma stream see much less coating than those running perpendicular as previously stated. Other CVD methods such as iCVD have been shown to provide a much more reliable method of coating non-line-of-sight features such as the walls of high aspect ratio trenches.[19] Selective coating is made easy using PECVD in the case where the top of a pillar is to be modified with a coating while leaving the sides uncoated. This arrangement can be used advantageously in many coating scenarios and becomes more pronounced with larger feature sizes which will show less of a bleeding effect.

1.4.2 Anisotropic coatings

Fabrication of anisotropically coated particles and structures, such as Janus particles, is an area that has seen rapid development in recent years as new fabrication techniques and applications are applied to these systems (Figure 1.6).[131,132] One challenge that is ever-present in the fabrication of anisotropic particles is scalability and the ability to produce a large number of modified particles in a quick facile manner. While PECVD does not address all known fabrication issues associated with these types of particles, the rapid, conformal coatings provide a reliable means with which to build coatings on

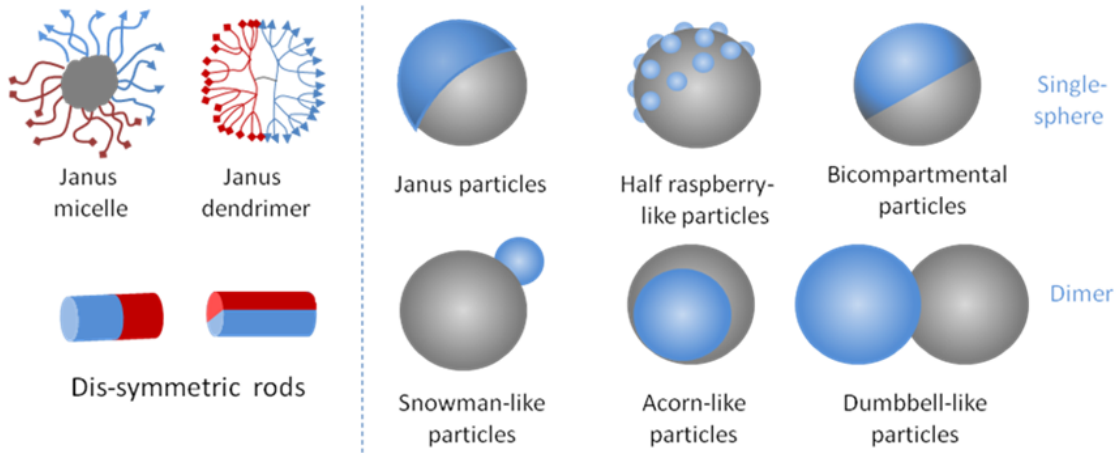

Figure 1.6: Various configurations possible with anisotropic and Janus-like particles.

very fine structures. One area of non-planar substrates where PECVD has seen success is that of micron sized curved spheres. The plasma process is able to easily coat micro particles to create Janus-type structures with a solid supporting sphere capped by plasma deposited polymer. Janus structures represent a unique structure which exhibits two different surface contained on one structure.[131] This has been an area of great interest in recent years focusing on different fabrication methods to create particles from a variety of material combinations and in ever increasing amounts. PECVD lends itself well as a coating technique to deposit a range of monomers directly on one half of silica microparticles embedded in a protective layer. The masking is essential and provides a very definitive protection layer for the particle. Since this type of method allows many particles to be modified during a single plasma deposition, it is seen as having potential for larger scale production of coated microparticles. These types of surface modifications could be used to easily apply coatings which can promote protein adsorption, cellular attachment and growth along with other biofunctional enhancements or can promote several different objectives in the case of multiple or mixed material coatings.

1.5 Conclusions

There is a broad range of materials and applications for not only PECVD and films fabricated with this method, but also many different types of CVD and CVD polymers in general. The distinct advantages offered by each of these processes will become a major factor in their growing use, both in research and in industrial applications since the processes are simple, robust, solvent-free, green and readily scalable especially through the use of off the shelf commercial monomers, which can be applied equally well to many different kinds of surfaces on a larger scale without the need to change the deposition process significantly. The sheer variety of materials and applications possible make CVD-based film fabrication an attractive method for many studies, especially ones that may have previously required complex chemical methods of surface modification. Biocompatible and bio-responsive coatings are a growing area of interest for CVD films as they provide robust films with tailored chemistries for promotion of cellular growth or prevention of microbial growth and may help facilitate implants. Overall, the continued study of the combination of CVD and soft matter will allow films to be designed quicker, easier and more tailored for future applications.

CHAPTER 2 : Goals and Objectives

2.1 Goal

The goal of this study is to understand the plasma deposition process used to form ultrathin functional films which can serve as biological, optical and responsive surface coatings. This goal is achieved through the elucidation of novel chemical and optical properties of highly cross-linked films from plasma polymerized amino acid and synthetic monomers. PECVD is established here as a solvent-less coating technique, including for the conformal deposition of biological materials, since it possesses the ability to modify surfaces rapidly and uniformly through a robust, one-step dry chemical process and can be broadly applied to diverse monomers and substrates. This research further addresses the key challenges associated with the sublimation plasma polymerization of important biological and synthetic molecules including proper vaporization and deposition rates, chemical cross-linking control, monomer functionalization and retention of vital functional groups after polymerization.

This work takes an interdisciplinary approach to developing sublimation PECVD methods targeted for biologically active coating applications by using elements of material science, biochemistry and chemical synthesis in an engineered manner to address functionalized film fabrication as summarized in Figure 2.1. Uniform ultrathin films of both amino acids and synthetic monomers are plasma polymerized through a dry process on a variety of practical polymeric and inorganic surfaces such as silicon wafers, Teflon, negative photoresist (SU-8), nitrocellulose, silk fibers, silica microspheres and polystyrene films. The insight developed from these plasma polymer coatings may

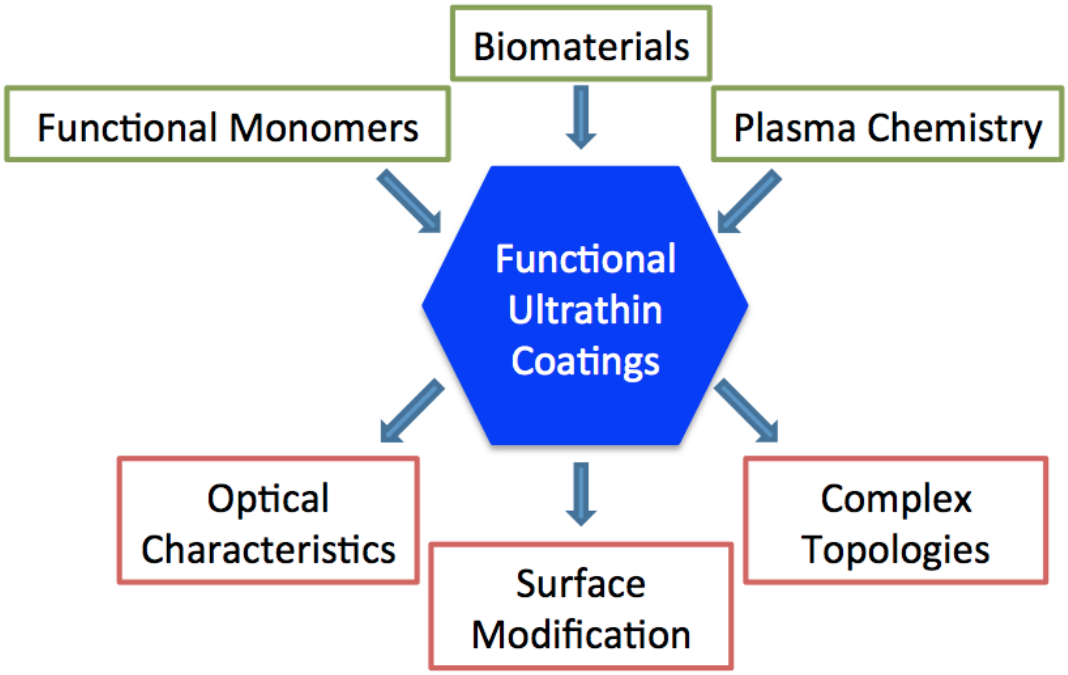

Figure 2.1: Overview of the approaches and materials selected as well as target applications of PECVD ultrathin film polymerization.

serve to enhance many practical surfaces with biological, optical and responsive coatings.

2.2 Key technical objectives

The key technical objectives that are pursued in this work are summarized as follows:

- Investigate the sublimation PECVD process as a facile method for the reactive formation of smooth, uniform, conformal, stable and robust ultrathin films of various functional materials including amino acids and synthetic organic monomers on a variety of substrates.
- Optimize plasma deposition conditions for both sublimed amino acid monomers and vaporized liquid phase synthetic monomers for stable plasma polymerization and film fabrication with controllable physical and chemical characteristics.

- Perform comprehensive characterization of the plasma polymerized ultrathin film surfaces for chemical bonding and changes along with cross-linking, surface morphology, domain structures and functionalities using a variety of surface sensitive analytical, spectral and microscopy tools.
- Design co-polymerization plasma deposition methods to combine amino acid and synthetic monomers, resulting in robust nano-composite films of controlled, mixed composition and tunable properties.
- Assess plasma polymerized amino acid coatings as biomineralization promoters for the reduction of inorganic nanoparticles from solution on uniformed and patterned substrates and analyze nanoparticles fabricated on these plasma polymerized biofunctional surfaces.
- Explore PECVD as a means to modify surface optical properties through the addition of mineralized nanoparticles with different refractive indices and co-polymerized plasma polymerized films.
- Fabricate conformal plasma coatings on complex micro-fabricated topologies which can serve as templates for further material modification via nanoparticle reduction in solution.
- Design and investigate polymeric/inorganic two-faced Janus micro structures by plasma coating microspheres embedded in a masking layer and subsequently modifying and releasing the plasma polymer cap from the underlying support, creating free-standing anisotropic structures.
- Explore PECVD co-polymerization as a method of fabricating optically enhanced and environmentally responsive ultrathin polymer films exhibiting a rapid response to relative humidity.

In this study, we will demonstrate that Plasma polymerized films with proper functionalities allow mineralization of specific inorganics, such as gold and titania, to occur rapidly and repeatedly on 2D and 3D templates. Further chemical modification of surfaces can be achieved through the co-polymerization of multiple monomers used simultaneously with the PECVD method. Co-polymerization introduces a facile method of integrating amino acids with other biocompatible polymers to construct tailored interfaces for specific integration applications. Application of these films to complex topological systems, such as patterned and curved surfaces, demonstrates the versatility of PECVD as a coating method for real-world modifications of engineered and implantable structures.

2.3 Overview of Thesis Composition

Generally, this work deals with the fundamental study of the synthesis and comprehensive characterization of plasma polymerized biological and synthetic monomers as fabricated by PECVD on planar and complex topologies. Special attention is paid to the chemical composition of the resulting films to determine their chemical structure, morphology and composition following the plasma deposition. The retention of chemical functionality of the initial monomers is a critical focus of the study since these coatings are intended to augment the surfaces they are applied to. Surface enhancement is demonstrated through mineralization, conformal coating and altering responsive optical films on both 2D and 3D substrates, highlighting the versatility of the plasma polymerization regime used.

A comprehensive critical review of CVD methods employing organic monomers, covering a range of functionalized materials, with specific attention paid to various

PECVD techniques and how these relate to key areas of current research in the related literature is presented in **Chapter 1**.

Chapter 2 provides a brief summary of the dissertation including the general goal and technical objectives of all related research efforts conducted in support of this study. Also provided is an overview of the dissertation itself and a guide to its general organization.

The experimental techniques and approaches used in these studies are briefly summarized in **Chapter 3.** Monomer and target surface selection and preparation are also discussed. Both the materials fabrication and characterization methods are detailed including various PECVD polymerization approaches, biomineralization of nanoparticles and the Janus micro particle fabrication and release technique. The characterization techniques introduced here include atomic force microscopy (AFM), scanning electron microscopy (SEM), energy-dispersive X-ray spectroscopy (EDS), transmission electron microscopy (TEM), Fourier transform infrared spectroscopy (FTIR), variable angle spectroscopic ellipsometry, X-ray photo electron spectroscopy (XPS), confocal fluorescent microscopy, optical microscopy, and Raman spectroscopy.

The following individual chapters discuss the specific experimental details related to those particular topics as **Chapter 3** is intended to provide a general overview of the experimental techniques used.

A novel method for the facile fabrication of conformal, ultrathin, and uniform synthetic amino acid coatings on a variety of model and practical surfaces by PECVD is introduced in **Chapter 4**. L-tyrosine amino acid, which can be utilized as an agent to

reduce gold nanoparticles from solution, is sublimed into the plasma and directly deposited on a variety of substrates to form a homogeneous, conformal and robust polyamino acid coating in a one-step, solvent-free process. This approach is applicable to many practical surfaces and allows surface-induced biometallization while avoiding multiple wet-chemistry treatments that can damage many soft materials. By placing a mask over the substrate during deposition, the plasma polymerized tyrosine coating can be micro-patterned. Upon the films exposure to a dilute gold chloride solution, gold nanoparticles form on the PP-Tyr surface and concentrate on the micro-patterned areas containing the polymer. This method of templated biometallization is adaptable to a variety of practical inorganic and organic substrates, such as silicon, glass, nitrocellulose, polystyrene, polydimethylsiloxane, polytetrafluoroethylene, polyethylene, and woven silk fibers. No special pretreatment is necessary, and the technique results in a rapid, conformal polymerized amino acid coating that can be utilized for further biometallization.

Building on the previous chapter, **Chapter 5** focuses on the conformal synthesis of ultrathin films from the amino acid, histidine, on flat silicon substrates and 3D periodic polymer structures via plasma enhanced chemical vapor deposition. A demonstration of the efficient utilization of this functional amino acid nanocoating for the formation of individual titania nanoparticles with dimensions from 2 to 15 nm, depending upon reduction conditions, is shown. The titania nanoparticles were grown directly on histidine-functionalized 2D and 3D polymer substrates by a wet-chemistry method which showed uniform surface coverage reaching 70%. This approach demonstrates the potential for modifying the optical properties of periodic porous polymeric structures via direct conformal growth of titania nanoparticles.

The use of PECVD for the simultaneous co-deposition and co-polymerization of amino acids with synthetic monomers is discussed in **Chapter 6**. This study serves as a model system to study the feasibility of a direct, facile method for integrating biocompatible and synthetic materials into biofunctional films. The ability to copolymerize a biological molecule (L-tyrosine) with various monomers such as acrylonitrile, HEMA and titanium isopropoxide in a dry, one step process to form thin films of mixed composition films. Mineralization has been previously used to create hybrid organic/inorganic structures and co-polymerization of L-tyrosine with titanium isopropoxide provides an alternate method of fabricating hybrid ultrathin films. The fundamental aspects of plasma co-polymerization of different materials with tyrosine are evaluated and PECVD is investigated as a possible method to integrate biological and non-biological (organic and inorganic) components in a single, stable, mixed, uniform film. This process may lead to a method of interfacing biological systems with synthetic materials as a way to enhance the interface between an implant surface and biocompatible coatings.

Chapter 7 is focused on the universal fabrication of Janus microparticles from a wide variety of organic and inorganic components compatible with PECVD. The Janus particle fabrication described in this study details the synthesis of the highly cross-linked polymer coatings on the exposed half of the partially embedded particles via PECVD. Plasma polymerization of different functionalized, reactive, responsive, organic and biomolecular materials ranging from acrylic compounds to organometallic molecules and amino acids is done directly on silica and titania microspheres. A masking technique is used to ensure that only a controlled fraction of the total particle surface area will be covered. This facile, fast, and scalable plasma polymerization approach allows for single-face polymerization, generating organic-inorganic Janus particles which are robust and can be further converted into a variety of interesting anisotropic mesoscale

structures. Half-fluorescent, half-metal decorated and half-shelled structures were all demonstrated here as particular representative examples.

Chapter 8 reports on the plasma co-polymerization of poly(NIPAAM), a well know temperature and water responsive polymer, which has previously been observed to retain its responsiveness after undergoing polymerization through various chemical vapor deposition processes. In this study the expected responsiveness of the plasma polymerized NIPAAM films to moisture is verified through spectroscopic ellipsometry of film swelling. A comparison of this ultrathin film response is made to PP-NIPAAM films plasma co-polymerized with titanium isopropoxide, which significantly increase the refractive index of the final mixed film, leading to a coating with a tunable thickness and refractive index. By maintaining a response after doping with an optically modifying material, the PP-NIPAAM film provides a facile method for creating rapidly humidity responsive and optically tunable ultrathin film.

A general discussion of the major results, new and significant findings, research impact and overall significance of this study are presented in **Chapter 9** along with concluding remarks and discussion of broader impacts and future directions.

CHAPTER 3 : Experimental Techniques

This chapter will provide a summary of procedures, experimental techniques and analytical tools used throughout this work. Specific details regarding individual experiments will be provided locally in the corresponding chapters. A general summary explaining sample preparation and characterization will be provided here.

3.1 Synthesis and Fabrication

Two major fabrication methods, plasma polymerization for film fabrication and biomineralization for film modification, are described here. Specific fabrication procedures are detailed in their respective chapters.

3.1.1 Substrate and materials preparation

All monomers were purchased from Sigma-Aldrich and used as received, without further modification. Typical monomer purity was >98% unless otherwise noted. Depositions performed on highly polished single crystal silicon substrates {100} were acquired from University Wafer and cleaned in piranha solution (3:1 conc. H_2SO_4 & 30% H_2O_2). Wafer cleaning was done by scoring and cleaving the silicon into approximately 1 cm x 2 cm area and then rinsing with water and sonicating for 10 minutes. The wafers were placed in a wafer holder containing 24 pieces and were then immersed in piranha solution by adding 100 ml of 30% H_2O_2 to a large beaker followed by 300 ml of concentrated H_2SO_4.[133] The reaction was run for 45 minutes and then the wafers were removed and rinsed six times with copious amounts of Nanopure (18MΩ•cm) water. The wafers were stored under Nanopure water in individual containers and dried with dry nitrogen just prior to use. All solvents used were purchased from Aldrich and used as received. All

other substrates for use in the experiments described were used as received from the vendor unless otherwise specified. Details relating to each material are discussed in the corresponding chapter

Table 3.1: List of all monomers used for PECVD depositions.

Name	Structure	Characteristics	Source
Tyrosine	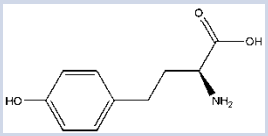	Amino acid for sublimation	Sigma-Aldrich
Histidine	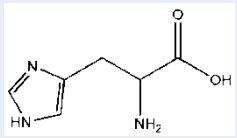	Amino acid for sublimation	Sigma-Aldrich
Acrylonitrile	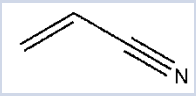	Liquid monomer for facile film formation	Sigma-Aldrich
Pyridine	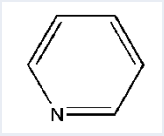	Liquid monomer for facile film formation	Sigma-Aldrich
Ferrocene	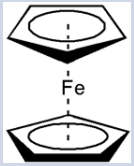	Organometallic sublimation compound	Sigma-Aldrich
Titanium Isopropoxide	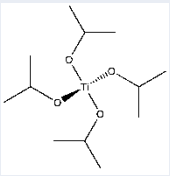	Liquid monomer for high refractive index film fabrication	Sigma-Aldrich
NIPAAM	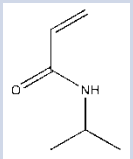	Temperature and moisture response	Sigma-Aldrich
HEMA	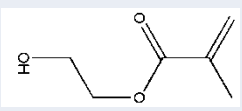	Biocompatible swellable hydrogel	Sigma-Aldrich

3.1.2 Plasma Reactions

All PECVD was done at Wright-Patterson Air Force Base in collaboration with Dr. T. J. Bunning's and Dr. R. Jakubiak's research groups. The plasma chamber used was custom built and used two primary configurations: gas phase and sublimation (Figure 3.1).[1,73] RF power at 13.56 MHz was used to generate a plasma under vacuum conditions between two parallel aluminum electrodes. All cases utilized argon (Ar 99.999%) carrier gas unless otherwise noted. Other carrier gases used include oxygen and nitrogen or a mixture, depending on the specific reaction. The variables monitored during the deposition were applied power, chamber pressure, carrier gas flow rate,

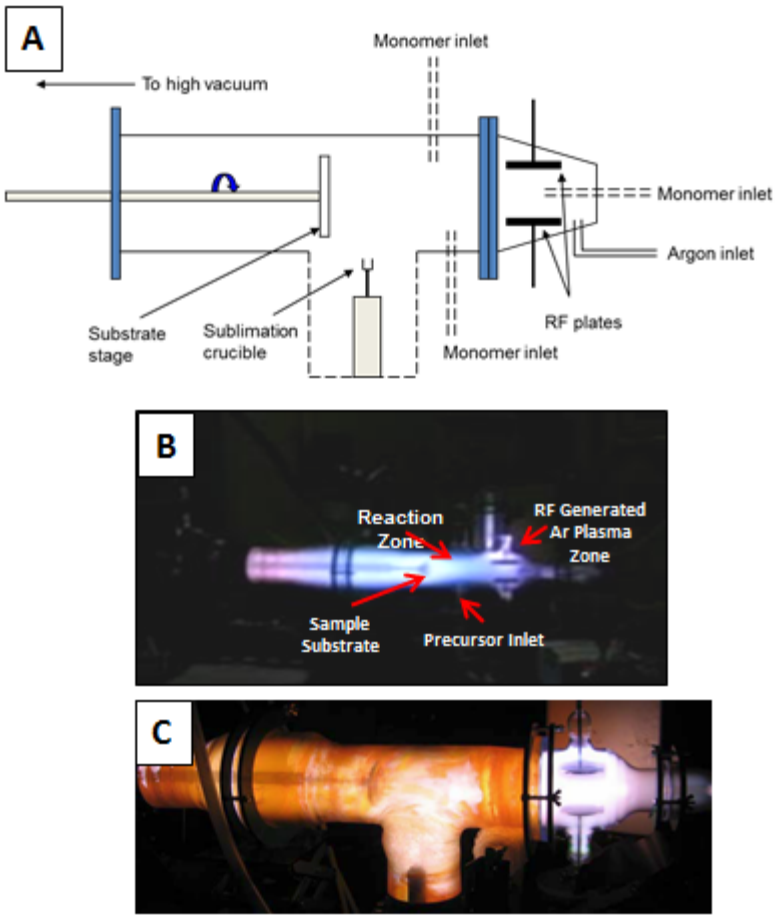

Figure 3.1: Plasma enhanced chemical vapor deposition reactor design. A) schematic of reactor showing optional placements of precursor inlets used through the study. B) Gas phase monomer configuration with Ar plasma being run. C) PECVD chamber in the sublimation configuration with Ar plasma being run.[1,73]

sublimation temperature and time of deposition. The typical power setting used for organic monomer depositions range on the order from 20 to 60 Watts of applied RF power. The second major variable is the chamber pressure. The depositions studied utilized chamber pressures between 0.05 torr and 0.2 torr. The chamber pressure affects the deposition rate of the monomer with lower pressures typically showing higher deposition rates. Closely related is the carrier gas flow rate which partially determines the chamber pressure and the rate at which the monomer is incident upon the target. Typical flow rates of 10-20 sccm were used for the carrier gas.

All monomers were introduced to the plasma downstream in the flowing afterglow except in the case of co-depositions, where the liquid monomer was flowed directly through the plasma zone due to limitations in the reactor set up. The sublimation crucible was a resistively heated tantalum crucible which was located about 15 cm downstream from the plasma generating zone. Power was applied to the heating boat to heat the monomer through electrical resistance up to a temperature of 300ºC, subliming the monomer for induction into the plasma. The liquid monomer inlets had different positions on the chamber ranging from 10-15 cm downstream from the plasma generating zone. The target substrate was placed another 5-10 cm downstream from the monomer inlet and was oriented orthogonal to the plasma flow. The substrate was mounted on a rotating arm, which facilitated a more even coating of the plasma film during the deposition, by slowly rotating the sample at approximately 10 rpm. The largest silicon wafer substrate coated was two inches in diameter compared with a five inch diameter glass reaction chamber allowing ample area for exhaust flow from the reaction chamber. Typical deposition times ranged from 3 to 15 minutes, depending on the rate of deposition of a given monomer under specific conditions. Only ranges of conditions are listed as opposed to specific chamber settings since there can be

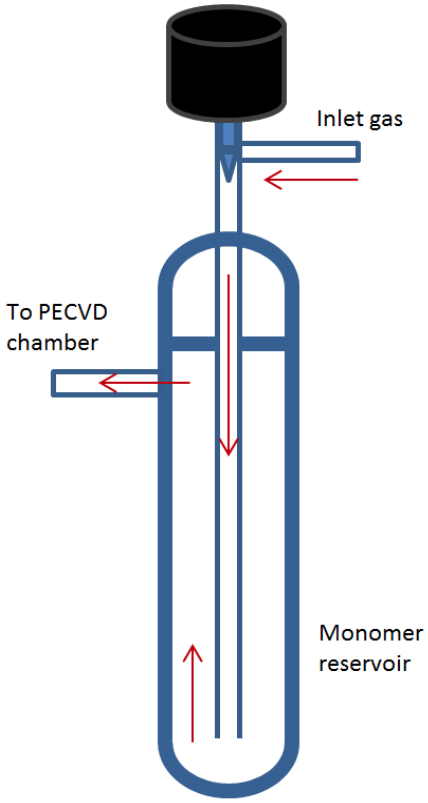

Figure 3.2: Schematic showing the vaporizing apparatus used with liquid monomers for PECVD and direction of flow.

variation in films of the same material deposited under identical conditions due to changes in the plasma reactor geometry, ambient atmospheric conditions and previously deposited polymer on chamber components which builds up after extended use. Factors such as these lead to variations, which must be dealt with experimentally during each deposition session.

3.1.3 Biomineralization

Biomineralization was carried out for two different inorganic materials, gold and titania. The mineralizations were carried out by diluting the precursor solution in Nanopure water or borate buffer (pH 10) to low concentration. The gold solution was made using gold chloride ($HAuCl_4$, 30% Sigma-Aldrich) to a concentration of 0.1 M. The dilute solutions were then placed onto the plasma polymerized amino acid films and allowed to sit for 1

to 5 days. After completing the mineralization, the samples was gently rinsed in Nanopure water and dried under dry nitrogen. The titania mineralizations were done using a diluted titanium(IV) bis-(ammonium lactate) dihydroxide (TiBALDH) (Sigma-Aldrich) solution which was diluted from a starting concentration of 2M to a final concentration of 2 mM in Nanopure water or 0.5 M phosphate citrate buffer prepared at pH 7. Both solutions (water and buffer) were mixed at a 3:500 volume ratio and mixed thoroughly before the histidine coated wafers were immersed. The PP-His coated samples were exposed from 1-24 hours. These procedures were followed regardless of the substrate utilized.

3.2 Characterization

A variety of characterization techniques were employed to elucidate the properties of the plasma polymerized materials both before and after modification. Determination of the chemistry of the plasma polymerized films was paramount to understanding the type of reaction which occurred the deposition process and the resulting surface chemistry available. Chemical characterization (FTIR, XPS) was needed to determine the functional group retention and the presence of reduced inorganic materials. The surface morphology was determined using AFM and SEM and optical properties were measured using spectroscopic ellipsometry.

3.2.1 Atomic Force Microscopy

The surface morphology and roughness for all samples was evaluated using atomic force microscopy (AFM). The instruments included in this dissertation are: Dimension 3000 (Nanoscope IIIa), Multimode (Nanoscope IIIa) and Icon (Nanoscope V) systems (Bruker, Santa Barbra). Tapping mode was primarily utilized in the surface characterization of all materials.[134] Non-contact silicon cantilevers (MicroMasch) with

aluminum backside coatings and a nominal spring constant of 40 N/m (resonance frequency 330 kHz) were used for all tapping mode scanning. Typical tip radii were in the range of 10-20 nm as calibrated by gold nanoparticle standards according to established procedure.[135,136] After collection of the images, a flattening procedure was typically employed to remove curvature effects, which are artifacts of scanning, with a 1^{st},2^{nd} or 3^{rd} order flattening regime. Image scan sizes range from 0.4 x 0.4 μm^2 to 10x10 μm^2.

Tapping mode utilizes a cantilever, which is driven near its resonance frequency just above the surface. Interaction of the tip with the surface occurs causing a deflection in the cantilever that is measured by the photodetector producing topographical information. The phase channel is collected by measuring the difference between the drive frequency of the cantilever in free space, as applied by the direct drive piezo, and the measured oscillation frequency in the photo detector. Interactions with the surface will cause a dampening in the oscillations, changing the wavelength and amplitude from that measured in free space, thus giving rise to the phase channel.

AFM images collected on the Icon system used a new imaging technique developed by Bruker known as PeakForce® Quantitative Nanomechanical Analysis mode. The cantilever used is typically much softer, with a spring constant of 0.4 N/m as opposed to the tapping mode cantilevers with a spring constant of 40 N/m. The cantilever is driven at a constant 2 kHz, far below its resonance frequency. In this sense, the cantilever is tapping the surface, but very lightly. PeakForce® QNM mode collects topographical information in a similar manner to classic tapping mode, but additionally collects information such as the surface adhesion and DMT modulus by using a calibrated cantilever to collect force v. time curves at each pixel.[137] All QNM mode images were

collected over scan sizes from 20 μm to 500 nm at an optimized scan rate of 1 Hz. The surface distribution of relative mechanical properties were collected in the peak-force mode and the DMT model was used to calculate elastic modulus.[138,139] A force v. time curve is collected and analyzed "on the fly" allowing real-time mapping of surface mechanical properties. All surface (rms) microroughness measurements were conducted over six 1x1 μm^2 area and averaged over several locations.

Prior to collecting quantitative nanomechanical data, the system was calibrated by first determining the sensitivity of the cantilever/photodetector system. This was done by making a single force curve with the tip in contact with a sapphire substrate. The substrate approximates an infinitely hard surface into which the cantilever will not penetrate, but only deflect. The photodetector measures this deflection by the change in the laser position which is measured in voltage. By matching the distance moved in nanometers to this voltage change, the sensitivity of the system is then calibrated in nm/V. This will allow all subsequent measurements to be done in units of meters and Newtons giving precise control over the system. Next, the spring constant of the cantilever is determined by using the thermal tune regime in the V8.10 software.

Finally the tip radius is measured by scanning a gold nanoparticle standard with an optimal particle diameter of 5 nm. The tip radius can then be calculated by[134]:

$$R = \frac{w^2}{8h} \quad (1)$$

where R is the tip radius, w is the apparent width of the gold nanoparticle and h is the height of the gold nanoparticle, which is assumed to be spherical. Upon completion of this calibration procedure, the system is capable of collecting quantitative nanomechanical data. The data is analyzed on-the-fly to produce the mechanical

property channels from rapidly collected force curves. The individual force curves are not saved as in classic force volume mode for further analysis. This can be a potential drawback of the system as the only model available for calculating modulus is the DMT model, which may not be ideal for all systems, but is generally widely applicable.

3.2.2 Ellipsometry

Ellipsometry is a widely used indirect method to determine the thickness of a thin film as well as the optical properties, refractive index (n) and absorption (k). Ellipsometry is also an absolute method in that it does not require standards for comparison. Ellipsometry relies on the analysis of the changing polarization of an incident light wave reflected off a surface to obtain data which is then modeled to determine the properties of the film. The values measured using ellipsometry are Ψ and Δ, parameters of the ellipse of the light wave which change with surface interaction, and are used to describe the complex reflectance ratio ρ. This parameter is constructed from the Fresnel coefficients of reflection R^P & R^S that are present at each layer interface. These coefficients are derived from the parallel (P) and perpendicular (S) light polarizations with respect to the plane of incidence.

$$\rho = \frac{R^P}{R^S} = \tan(\Psi)\, e^{i\Delta} \tag{2}$$

Ellipsometric measurements were carried out using a JA Woollam M-2000U variable angle spectroscopic ellipsometer in reflection mode. Angles of 65º, 70º and 75º were used over the wavelength range from 245 to 1000 nm. All model fitting was done using the WVASE32 or CompleteEASE software. Typical models were constructed with a silicon substrate layer followed by a native oxide SiO_2 layer. Standard optical constants were used for the native oxide layer and a nominal thickness value of 2 nm was used in

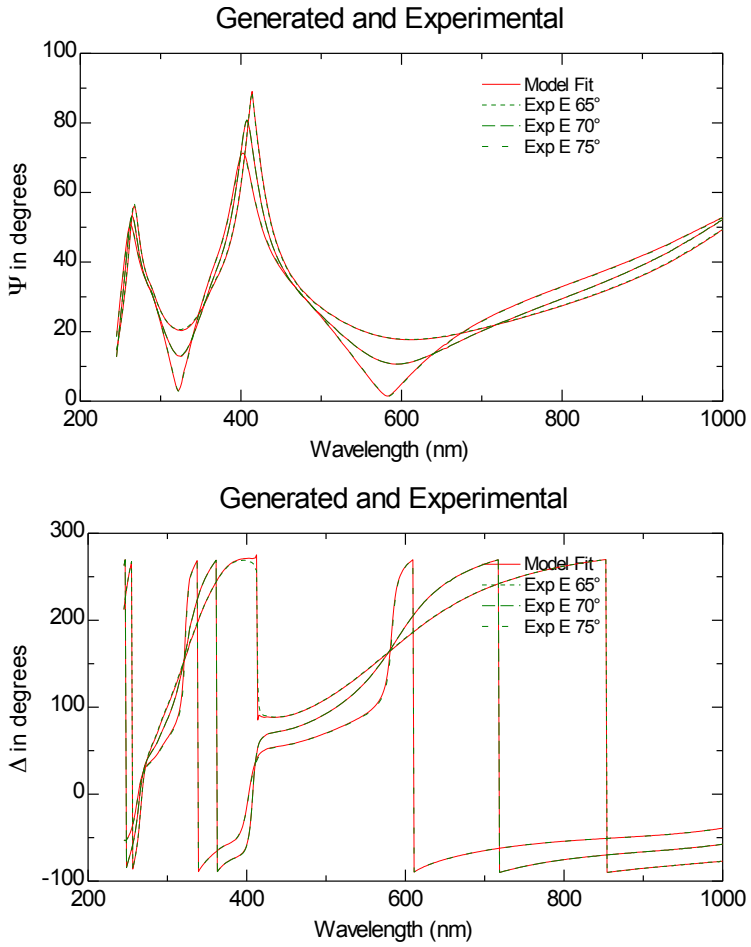

Figure 3.3: Examples of ellipsomtry fitting of Psi (top) and Delta (bottom) from the WVASE32 software.

all cases. All data were fit using a Cauchy model or Effective Medium Approximation (EMA) except where noted. Psi and Delta plots along with the fitted model are shown as examples of standard ellipsometric data collected (Figure 3.3).

3.2.3 XPS

X-ray photoelectron spectroscopy (XPS) determines elemental composition of a materials surface by measuring the kinetic energy of electrons ejected from the surface by incident X-rays.[140] The typical penetration depth is no more than 10 nm, making this a very surface sensitive technique, which can be augmented by sample etching to obtain data at different depths of the film. XPS measurements were performed under high

vacuum using an M-PROBE Surface Science XPS and a Thermo K-Alpha XPS (Al K_α source) system utilizing charge neutralization. Spectra were collected from 0 - 1300 eV at 1 eV steps at a spot size of between 300-800 μm and averaged over 5-15 scans for standard resolution. High resolution scans were performed over the range of interest, 270-300eV for carbon and 450-470 eV for titanium at 0.1 eV steps and averaged over five scans.

3.2.4 FTIR

Fourier transform infrared spectroscopy (FTIR) utilizes near and far IR radiation to excite the chemical bonds in a molecule which produce characteristic vibrations and certain wavelengths. These can then be used as indicators of the type of chemistry present in a material. FTIR measurements were conducted on a Perkin-Elmer SPECTRUM 2000 FT-IR spectrometer in transmission mode and a Bruker FTIR spectrometer (Vertex 70) equipped with a narrow-band mercury cadmium telluride detector in reflection mode.[141] Samples for transmission FTIR were prepared on double sided polished silicon wafers to minimize the background signal. Spectra was collected over the range of 500cm^{-1} to 4000 cm^{-1} at 1 cm^{-1} resolution and averaged over repeated scans (typical 16 on the Bruker system and 1000 on the Perkin-Elmer system). Background, baseline and atmospheric corrections were applied to the spectra.

3.2.5 Electron Microscopy

Measurements of film morphology and Janus particle structures were carried out on either a LEO 1530 field-emission or S-3400 N Hitachi thermal-emission scanning electron microscope (SEM) with operation voltage of 5-10 KeV. All the samples were sputtered (5-10 nm) with gold and mounted on SEM stubs with conductive carbon or copper tape. INCA energy dispersive X-ray spectroscopy (EDX) was used in

conjunction with the S-3400 SEM scans to determine the chemical composition with collection times of 300 seconds.

Transmission electron microscopy (TEM) was also used to image gold nanoparticles and measurements were taken on a Phillips CM200 transmission electron microscope operating at 200 kV. The samples were prepared by pipetting a single drop of nanoparticle precursor solution onto a 3 mm diameter copper grid previously coated with a carbon film prior to PECVD deposition of monomer (Electron Microscopy Sciences or Ted Pella, Inc.).

3.2.6 Contact Angle

All contact angle measurements were done with a KSV CAM 100 goniometer system. A single drop of water (~2 µl) was placed on a thin film surface coating and observed optically. The angle formed by the water drop relative to the surface was measured to assess the wettability and surface energy of the film.

3.2.7 Quartz Crystal Microbalance

Quartz Crystal Microbalance (QCM) measurements were carried out on a Masscal G1 systems with nanocalorimetry enclosure. Plasma polymeric coatings were deposited directly on QCM disks which were then placed in the QCM chamber. The chamber was sealed and flow controllers used to adjust the inlet of water vapor to the system. The profile was preprogrammed to automatically adjust the flow rate of wet nitrogen. The change in mass of the polymer film was recorded as the atmosphere was adjusted from dry to wet and reported in micrograms.

CHAPTER 4 : Facile Plasma Enhanced Deposition of Ultrathin Cross-Linked Amino Acid Films for Conformal Biometallization

4.1 Introduction

Bioenabled methods are used to form inorganic coatings and nanoparticles composed of gold, silver, platinum, titania, silicates, calcinates and iron through the reduction of corresponding ions with biomolecules (DNA, amino acids, proteins and peptides), which act as nucleation sites, templates, and reduction agents.[95,122,142,143,144,145,146,147,148,149] A wide range of applications makes the method extremely useful for directed assembly, in which a targeted surface can be coated with the biomolecules and exposed to a solution containing the desired ions to be deposited. Reduction to form nano- and microparticles or even uniform coatings will only occur at activated sites on the deposited biorelevant layer.[108,150,151,152] This coating method allows a directed placement of inorganic nanoparticles on a surface through direct nanoparticle formation on materials that may be otherwise difficult to coat. Additionally, nanoparticles can be directed to form at specific locations on the surface by pattering the biomolecular layer during plasma deposition or by microprinting.[153] This method of nanoparticle formation allows for more functional and diverse uses of hybrid nanomaterials in applications such as optical sensing and responsive materials.[154]

It is well known that amino acids such as lysine, tyrosine, and dopamine are effective agents for the reduction of noble metal nanoparticles from solution, due to the amine and

hydroxy groups in the molecule that reduce gold directly from an ionic precursor solution.[155,156,157] By coating a substrate surface with polytyrosine (pTyr), gold nanoparticles can be reduced directly from solution to a desired surface coverage density.[114] Traditional techniques for fabricating these types of coatings include simple solution- and dip-casting, spin-casting, spin-assisted layer-by-layer (LbL) assembly, self-assembled monolayer formation and Langmuir-Blodgett (LB) film formation.[158,159] To achieve uniform coverage of inorganic nanoparticles on the surface, the substrate to be coated would have to be immersed in an aqueous amino acid solution for prolonged times or chemically modified with an additional LbL coating on an existing Langmuir monolayer.[116,156,160,161,162,163,164] Such polyelectrolyte-assisted deposition of silaffin proteins was demonstrated to be an effective method for surface growth of monodisperse titania nanoparticles.[129,141] Several inherent drawbacks of this approach stem from the extensive exposure of the substrate to salt solution which can potentially leading to swelling, partial dissolution, corrosion, or additive leaching. In addition, prolonged exposure to aqueous solutions may lead to particle aggregation, non-uniform coverage, and surface defects. By developing a rapid, one-step, solvent-free, conformal method for depositing, templating or mineralizing inorganics on surfaces, substrate materials not amenable to the traditional wet chemistry approaches may be utilized for mineralization.

Polymerization of amino acids, including tyrosine, as well as the formation of synthetic polyamino acids has been readily demonstrated through wet chemical means.[165,166] The method of *in situ* polymerization of tyrosine coatings proposed herein focuses on the utilization of plasma-enhanced chemical vapor deposition (PECVD) as a potential method to polymerize the tyrosine monomer in the plasma stream and directly deposit the pTyr on the surface. This type of plasma polymerization reaction has been

previously demonstrated with various organic molecules and amino acids to form thin films that can also be easily patterned through the use of a mask secured on the substrate.[31,167,168,169,170,171,172]

A major advantage of PECVD is that it allows dry tyrosine powder to be sublimed into the plasma stream and coated onto a variety of substrates, making the technique an alternative method to depositing tyrosine coatings through a wet chemistry approach. Another key advantage of PECVD is the dense, highly cross-linked conformal coatings over sharp corners, textured surface and patterns as opposed to direct film transfer or casting from solution which can result in delamination and defects in film coverage on such non-ideal surfaces. Biometallization on PECVD modified surfaces demonstrates a bio-enabled coating method which has potential applications in the modulation of surface conductivity and catalytic properties through inorganic nanoparticle deposition. The addition of inorganic nanoparticles can be used for the mediation of optical properties, micropatterning, fabrication of selective surfaces and other thermal and microsensing applications.[173,174]

In this study, the plasma polymerization of tyrosine and formation of ultrathin conformal coatings on a variety of practical materials was demonstrated, making them capable of selectively binding and reducing gold nanoparticles onto various surfaces. This method of tyrosine-coating formation allows the utilization of readily available L-tyrosine monomer to form highly cross-linked, robust, conformal and functionalized pTyr coatings in a simple, rapid one-step process that can be applied to a variety of substrates. This type of coating method will allow virtually any object to be uniformly coated with a functional bioenabling layer, yielding an unlimited number of prospective applications

where nanoparticle reduction is needed and providing a universal fabrication method to achieve this.

4.2 Experimental Details

Materials. Standard silicon wafers were used as substrates. Additional substrates used for deposition were cut from stock sheets of poly(tetrafluroethylene) (PTFE), polyethylene, polydimethylsiloxane (PDMS), polystyrene, woven silk fibers, glass, and nitrocellulose.

The PECVD vacuum chamber was setup for plasma enhanced coatings by sublimation according to the established procedure [73,175] For best tyrosine film results, the chamber plasma was run at 60 W with an argon flow rate of 10 cm^3/min (99.99% purity) at a pressure of 0.05 Torr for all tyrosine sublimation depositions. Patterning of the tyrosine was done by securing a 1000 mesh (10 μm) copper TEM grid to the silicon wafer. The deposition was carried out according to the listed procedure and the grid was removed upon completion. Generally, the most influential parameters in this study were the applied power, monomer heating and chamber pressure. A matrix of testing was done over the range of 20-80 W power, 0.05 – 0.2 Torr chamber pressure and 150 - 350 °C monomer heating.

Gold chloride ($HAuCl_4$) (30% Aldrich) was diluted in borate buffer (pH10) to a concentration of 0.1M. This solution was then placed onto the PECVD-coated tyrosine film and allowed to absorb for a specified length of time between 1 and 5 days. After deposition the sample was rinsed with Nanopure water (18.2 MΩ•cm) and dried under nitrogen.

4.3 Results and Discussion

4.3.1 Film deposition

In general, PECVD coatings have the advantage of being uniform across the surface with a minimum of defects and non-uniformities: the tyrosine films exhibited here were no exception. PP-Tyr films deposited onto clean silicon wafers showed a uniform surface morphology over a 10 x 10 μm^2 area (Figure 4.1 A). Higher resolution imaging at 1x1 μm^2 showed surface features of a distinctive morphology composed of many small, distinct needle-like domain structures (~50-100 nm in length and diameter below 10 nm) (Figure 4.1 B). These features correspond to the PP-Tyr films shown in Chapter 6 as well. No dewetting of the films was seen after removal from the deposition chamber, indicating that the deposited tyrosine is stable on the substrate and not prone to delamination owing to internal stresses.[176,177] The PECVD tyrosine films were robust and were not easily removed from the silicon mechanically or in solution. The films performed well under a tape test as they did not show significant change when tape was applied to the film and removed. The PECVD tyrosine films were also observed to be very smooth as indicated by a surface roughness of 0.4 nm over a 1 x 1 μm^2 surface area (Figure 4.1 B). Under PECVD conditions, any part of the substrate that is facing perpendicular to the plasma stream was seen to be uniformly coated.

The tyrosine monomer was directly sublimed from the solid phase, with no modification, into the plasma stream, and is deposited on the substrate surface while undergoing considerable chain growth and cross-linking, both of which help to create stable, robust, and conformal ultrathin films on the surfaces. Monomers that are exposed to the high-energy plasma field under an inert atmosphere form reactive species, as previously described, allowing the radicals to react chemically with each other as they are polymerized and cross-linked into a network during deposition.[26,178,179] These films

frequently exhibit unique physical properties that are controlled through the variation of system parameters such as chamber pressure, power, argon flow rate and deposition time.[1,29,51,180,181] Many samples were made under different deposition conditions to optimize thickness and uniformity of the films. The thickness of the film was controlled through the variation of the deposition time (typically 8-12 min) at the optimized temperature, pressure and argon flow rate listed. This gives a degree of control over the film formation, but it is still subject to the random nature of the plasma stream. The same deposition conditions were maintained for different deposition times and characterized thickness and microroughness. Typical film thicknesses were measured

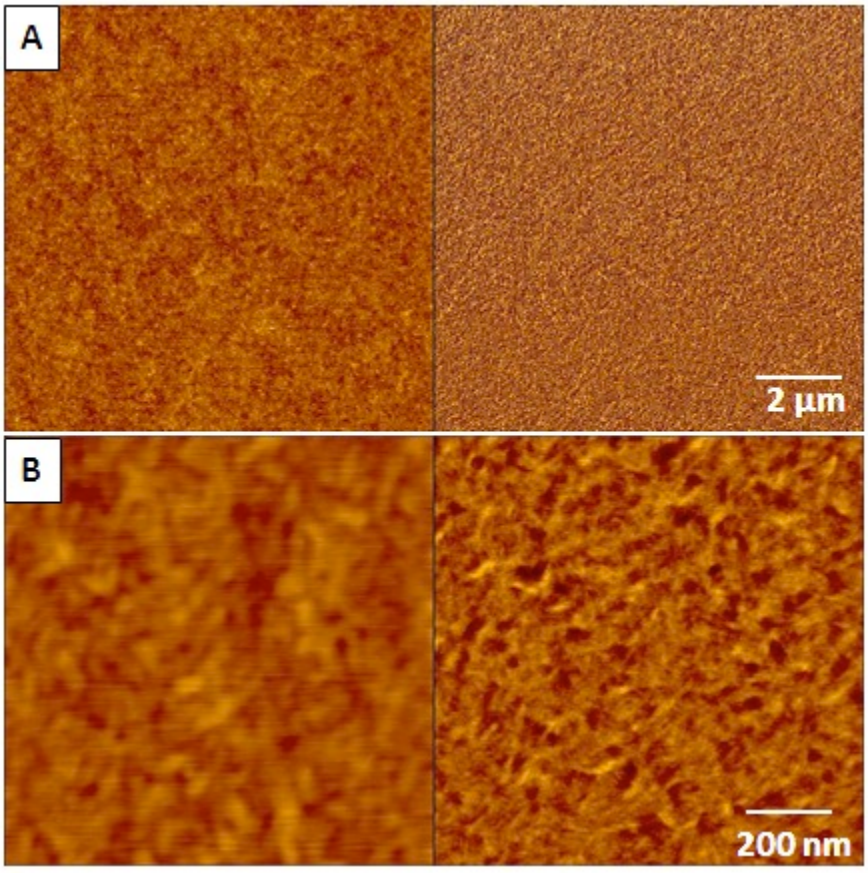

Figure 4.1: A) 10x10 μm^2 and B) 1x1 μm^2 AFM topography (left) and phase (right) of PECVD tyrosine film on silicon substrate prior to exposure to $HAuCl_4$. Z = 5 nm for topography and 5º for phase in both images. Typical thickness and microroughness for the samples was 120 nm and 0.4 nm, respectively.

by ellipsometry to be between 100 and 150 nm with the microroughness from 1 x 1 μm^2 images varying from 0.4 to 1 nm, depending on the particular sample.

The tyrosine coatings that were created were observed to be robust and resistant to mechanical wear and exposure to aqueous gold chloride solution. Preliminary observations of the films showed that they were stable under mild rubbing and not easily dissolved, even in solutions with high pH values. It is essential that the film be stable during the reduction of gold and that it remains intact for the duration of the exposure to solutions. Film stability is critical to the subsequent biometallization process, so that the film will not delaminate from the substrate or dissolve in the solution when exposed to aqueous gold chloride. Delamination and film instability were seen in some films made under non-optimized chamber pressure conditions.

4.3.2 Composition of PECVD films

During deposition of the tyrosine monomer it was critical to determine what, if any, changes occurred in the chemical structure of the molecule as a result of heating and interaction with the plasma field followed by deposition onto a solid substrate. As the reduction of gold is dependent on key functional groups, such as the amine and hydroxy groups of the tyrosine molecule, these components must remain active on the surface of the film after plasma deposition for the effective reduction of the gold nanoparticle.[182,183] If critical functional groups were cleaved or rendered nonfunctional, the ability of the film to reduce gold nanoparticles may be diminished or negated.

FTIR measurements on the solution-cast tyrosine film, plasma deposited tyrosine film, and spin-cast pTyr film were conducted to elucidate the similarity of their chemical composition (Figure 4.2, Figure 4.3). The absorption peaks were assigned to key

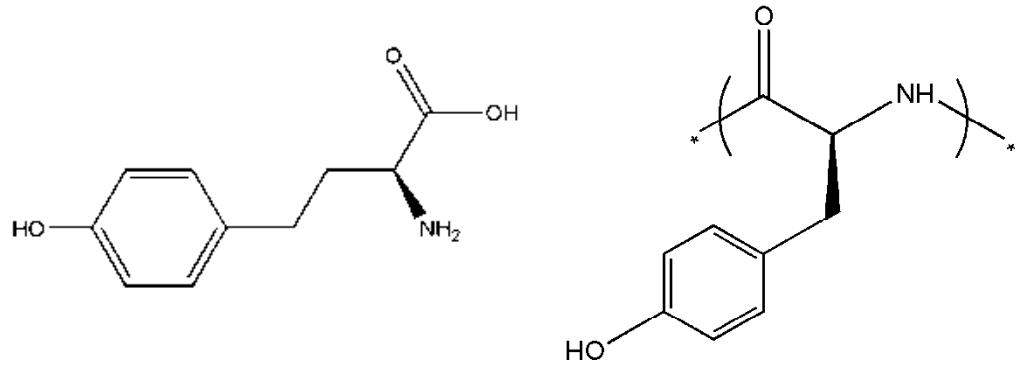

Figure 4.2: Chemical structure of L-tyrosine monomer and pTyr.

chemical groups of the plasma polymerized tyrosine using ACDLABS peak assignment software as well as comparison of known literature data.[26,184,185] For instance, NH_2 out-of-plane bending is seen at 829 cm^{-1}, in conjunction with a C-H stretch from the aromatic ring. The spectral shift from 876 cm^{-1} of this peak in L-tyrosine closer to the 826 cm^{-1} seen in pTyr, is a key marker that polymerization of the tyrosine monomer is indeed occurring. This shift is most likely caused by the amide bond formation, which occurs as the monomer polymerizes, and is similar to that observed in pTyr (Figure 4.2).

This observed peak also leads us to infer that the amine group was retained in the plasma polymerized tyrosine and is present on the surface coating. The presence of bands for aromatic rings in the FTIR spectrum is another strong indication that tyrosine remained, to great extent, intact during deposition and did not undergo significant decomposition upon heating and exposure to the plasma. The peak seen in the PECVD tyrosine spectra at 1246 cm^{-1} corresponds to the bending OH vibration in the ring structure while the 1332, 1515 and 1614 cm^{-1} peaks arise from the C-C double- and single- bond vibrations found in the aromatic ring. The peak for the alcohol group of the ring structure is seen at 3205 cm^{-1}, and a broad amine peak is seen at approximately 3000 cm^{-1}. These peaks remain for the most part consistent between the three different

spectra, indicating no dramatic changes and main bond cleavage in the structure of the tyrosine monomer. The structural determinations of the different tyrosine samples using FTIR were consistent with the chemical structure of pTyr known from the literature.[165] The spectra indicate that the monomers did not undergo complete dissociation during the plasma deposition. Much of the same chemistry was seen between each spectra as expected with several changes as noted, indicating slight changes in the molecules as

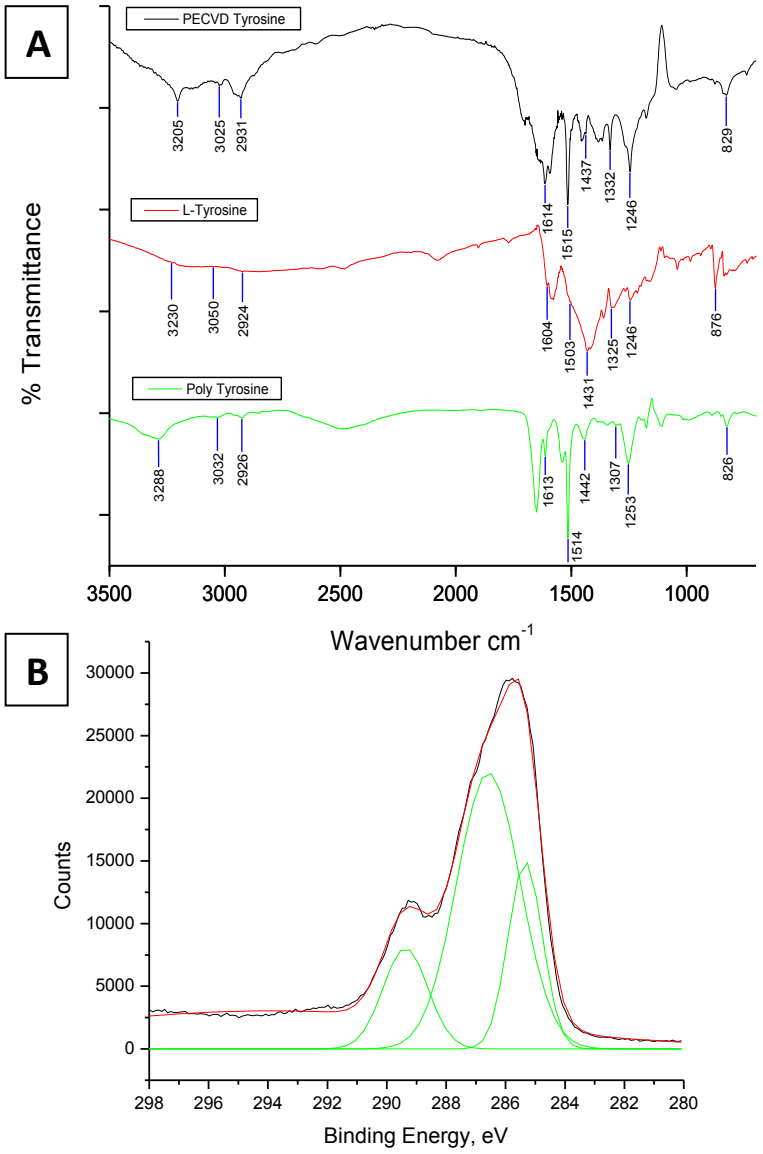

Figure 4.3: A) FTIR of films from PP-Tyr (top), L-tyrosine (center), and pTyr (bottom). B) High resolution XPS of carbon bonding in PP-Tyr.

they undergo radicalization and cross-linking. Differences were generally seen most often in portions of the spectra associated with different end groups on the monomer, which may tend to radicalize more easily. From this it is inferred that the L-tyrosine monomer undergoes random cross-linking and network formation as the film is polymerized on the substrate, yet still maintains the chemical functionality needed for the reduction of gold. Monomers become reactive after exposure to the plasma stream through the formation of ions and free radicals. The statistical majority of ions and free radicals are formed from the most reactive functional groups in the system. Owing to the random nature of the plasma, cross-linking becomes a statistical phenomenon, and a single reaction mechanism does not encompass the scope of the reactions that can occur at any radicalized, available site on the growing PP-Tyr network.[26] This process leads to a network formation in the PP-Tyr film which consists of many random cross-links and monomer fragments that do not always occur as predicted in theoretical models.

High resolution XPS spectroscopy (Figure 4.3 B) of the PP-Tyr film shows the expected presence of carbon-carbon (285.2 eV), carbon-nitrogen (286.5eV) and carbon-oxygen (289.0 eV). These peaks are determined through de-convolution of the high resolution carbon peak. These peaks indicate that the general integrity of the monomer is maintained, specifically with the presence of a signal representative of C-N, which is expected to be a bonding site as the polymer network is formed. If no evidence of C-N bonding had been seen, this may have been an indication of the dissociation of the monomer, but its presence indicates that this site remained in the system and is likely a key bonding location as evidenced by FTIR. Additionally, the evidence of C-O presence further indicates the intact nature of the monomer as the OH group remains attached to the ring structure. The use of the plasma is intended to catalyze the formation of

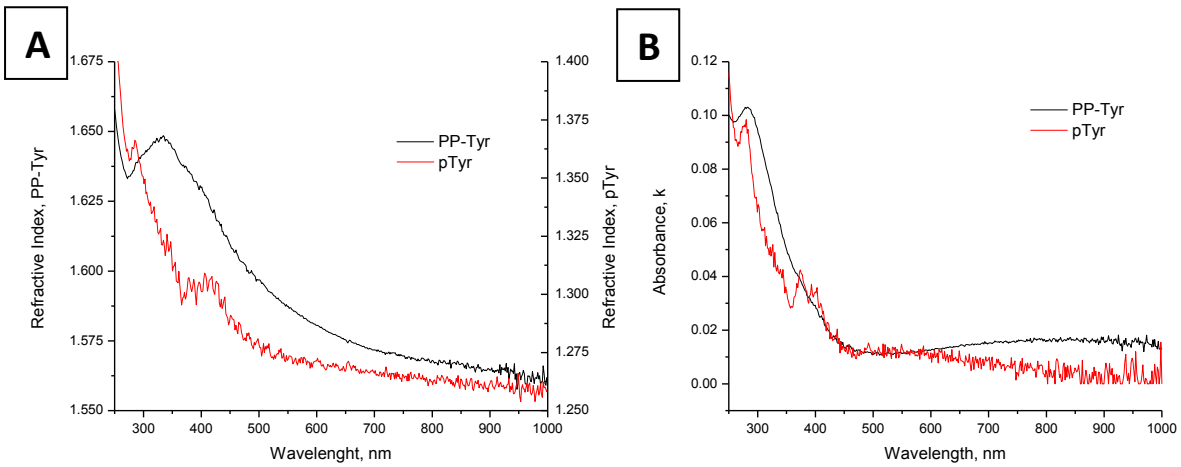

Figure 4.4: A) Refractive index n and B) absorbance coefficient k of PECVD tyrosine coating and spin-cast pTyr films from 245 to 1000 nm.

radicals on the monomer while at the same time preserving the structure. At lower power settings this is possible and is critical to the construction of the final films. If these bonds were not observed, it would be an indication that the power applied during the plasma deposition was too high and was destroying a majority of the bonding in the monomer.

Optical characteristics of the PECVD tyrosine film were measured by spectroscopic ellipsometry and modeled with a Cauchy fit. The measured real refractive index, *n*, for a PECVD film of 120-nm thickness showed conventional behavior decreasing from 1.65 in the UV range to 1.55 at longer wavelength close to near-IR (Figure 4.4). At a wavelength of 543 nm the refractive index was relatively high, *n* = 1.59 (Figure 4.4). This value is much higher than traditional values for conventional synthetic polymers and corresponds to reported values of the refractive index for tyrosine crystals with a high packing coefficient.[184] This confirms dense local molecular packing of tyrosine residues within the PECVD coatings. Notably, the PP-Tyr film showed a higher refractive index than the spin-cast pTyr film with similar wavelength-dependent dispersion which decreased at longer wavelengths. This difference confirmed the PECVD tyrosine film

was more densely packed and cross-linked than the spin-cast film of pre-polymerized monomer.

The optical absorbance coefficient, *k*, which represents the imaginary component of the complex refractive index, is also found to be very low for both spin cast and PECVD tyrosine films, but much more so for the PECVD film (Figure 4.4 B). This indicates that at wavelengths greater than 400 nm, the films possess little optical absorption and are highly transparent. For example, at wavelength 542.7 nm, k=0.011 for the PECVD film and k=0.012 for the spin-cast pTyr film. Significant absorption is detected only in the UV region and can be associated with the presence of the phenyl ring with a UV-absorption band at around 250 nm.[186,187] At λ= 250 nm, *k* is significant, reaching 0.10 for the

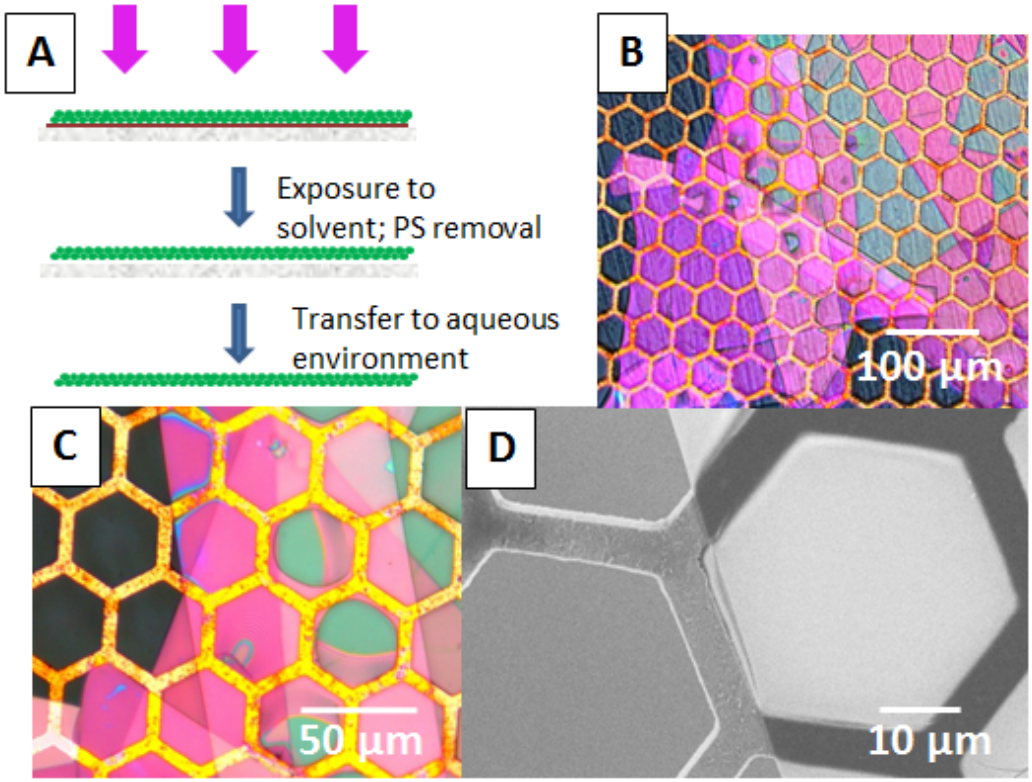

Figure 4.5: A) Diagram of free-standing film fabrication process B) Large scale optical image of free-standing film on Cu TEM mesh C) Free-standing PP-Tyr on Cu TEM mesh D) SEM micrograph of PP-Tyr film on Cu mesh at high magnification showing freely suspended material.

PECVD film and 0.12 for the spin cast pTyr film. Because of this low absorbance in the visible wavelength regime, these PP-Tyr films can be used in optical applications that require optical transparency. The results presented herein demonstrate that the formation of polymerized, highly cross-linked tyrosine networks readily occurs under the deposition conditions utilized. The plasma stream will impart enough energy to activate reactive sites (NH_2 and CO groups) on the L-tyrosine monomer and allow reactive species to form in the plasma which will polymerize and crosslink as they are deposited on the target substrate.

In addition to the stable PP-Tyr films deposited on silicon wafers, the same films show remarkable robustness as they are capable of forming free-standing structures. The fabrication of free-standing PP-Tyr films has been demonstrated by depositing the monomer on a sacrificial PS layer which is then dissolved in toluene releasing the pure PP-Tyr film (Figure 4.5 A). This is an excellent demonstration which shows that the films are robust and survive washing and transfer from one substrate to another. While the example shown looks at films transferred to clean silicon wafers and copper TEM grids, it is also very easy to transfer these films to any number of other substrates, such as PDMS. The films are observed to be freely suspended over the copper mesh and to have undergone folding during the release and transfer (Figure 4.5 B, C, D). This evidence implies that the films are mechanically robust yet flexible enough to support a high degree of folding. The mechanical stability of free-standing PP-Tyr films is believed to be a result of the high degree of cross-linking, which creates a self-supporting network in the plasma polymer film.

AFM comparison of the free-standing PP-Tyr films to the films deposited directly on silicon showed similar characteristics of smooth, uniform films indicating that the films

did not experience significant change or degradation upon exposure to toluene. Both films show very similar surface morphologies and low surface roughness, which indicates that very little effect of the solvent rinse is seen on the film. The surface roughness was measured at 0.4 nm over a 0.5 x 0.5 μm^2 area for the PP-tyr deposited

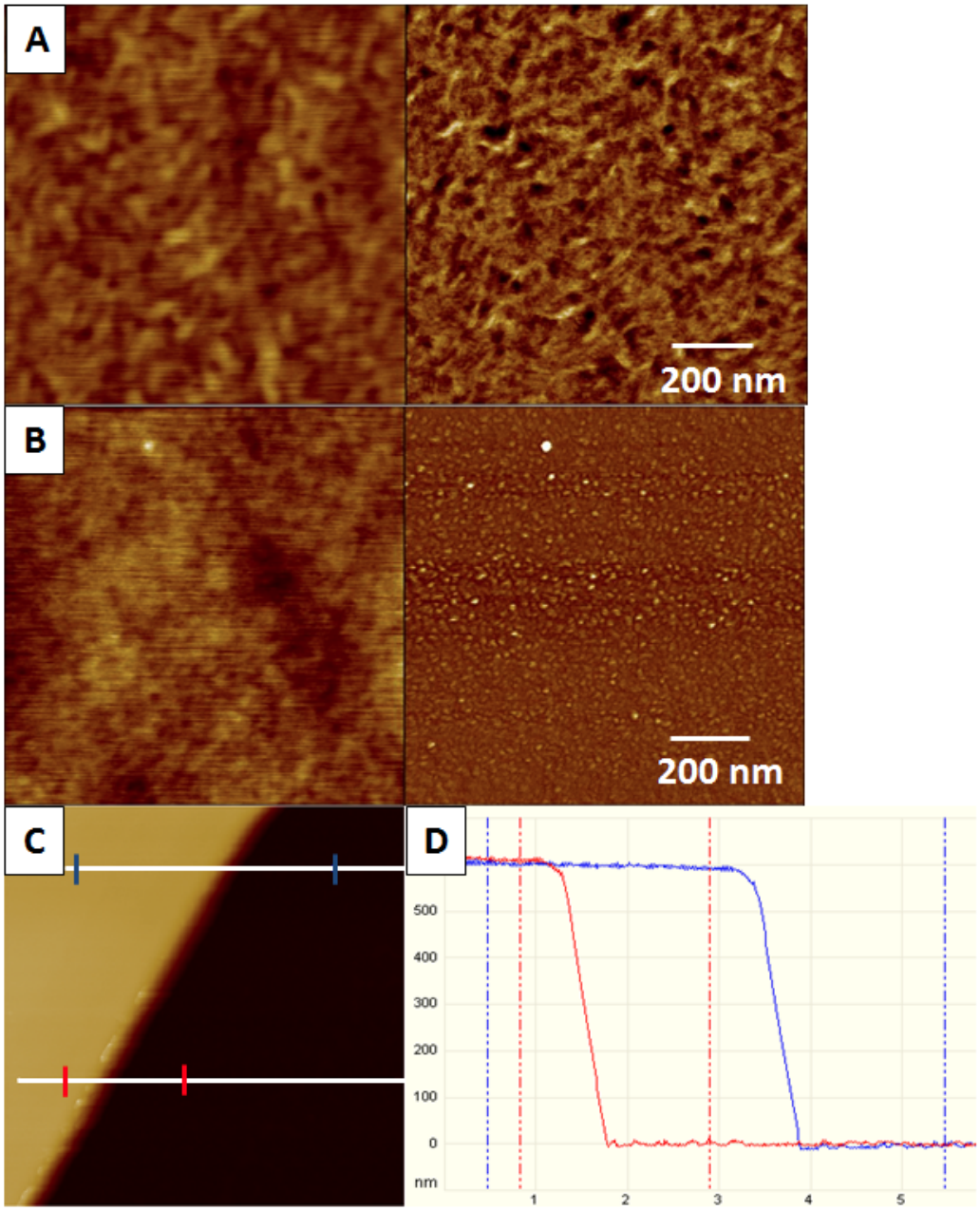

Figure 4.6: A) 1x1 μm^2 AFM topography (left, Z= 5 nm) and phase (right, Z= 5º) of PP-Tyr on silicon and B) PP-Tyr (Z= 4 nm, 15º) after release from PS sacrificial layer and transferred to a new silicon surface. C) Cross-section of free-standing PP-Tyr after transfer showing the thickness of the film (Z= 1.1 µm).

directly on silicon and is comparable to a roughness of 0.3 nm over a 0.5 x 0.5 μm^2 area for the free-standing PP-Tyr film after transfer to a new substrate (Figure 4.6 A, B). The evidence that little change is seen in the films morphology and structure will become important in Chapter 7 as well, with the washing and releasing of plasma coated microparticles. This experiment aims to analyze the proof of concept that plasma polymer films are robust, able to be processed in a solvent environment and mechanically robust after dissolution of the supporting layer with little change observed in the PP-Tyr film itself. The ability to fabricate free-standing films of amino acids could have potential applications in biological sensors, filters or coatings of devices and implants.

The film thickness as measured by AFM height measurements was approximately 600 nm in the example shown (Figure 4.6 C, D). The thickness appears to be consistent over several measured locations on the film. The PP-Tyr film shows a distinct difference in the AFM phase channel from the silicon substrate it was transferred to after being released from the sacrificial PS layer. The cross-section analysis shows an accurate measurement of the thickness of the film. It was observed that thicker films were typically more robust and easier to transfer from one substrate to another. Films that were very thin (<100 nm) would sometimes lose structural integrity during the transfer. Increasing the films thickness was the easiest way to create more stable films; however, the plasma conditions could be adjusted to increase the cross-linking which would also serve to make the free-standing films more stable.

4.3.3 Biometallization on PECVD tyrosine

Gold nanoparticles were reduced on the PP-Tyr film by placing a solution of gold chloride ($HAuCl_4$) diluted in borate buffer on the film and allowing reduction to occur over

a time period of 1-5 days. Two distinct sizes of gold nanoparticles were seen on the surface. The small gold nanoparticles were typically within a 1-5-nm diameter range and were uniformly distributed on the surface at a high density (Figure 4.8 A, B). These small particles corresponded to the beginning stages of the formation of larger structures as detailed previously. These images show the stark contrast between the unmodified PP-Tyr surface and the surface after gold nanoparticle reduction. While the changes in the surface morphology are indicative of the formation of gold nanoparticles, the phase image provides further information (Figure 4.8 A, B right). It is clearly evident in the phase image that the features on the surface have different mechanical characteristics than the surrounding background area as they clearly stand out from the surface. If the

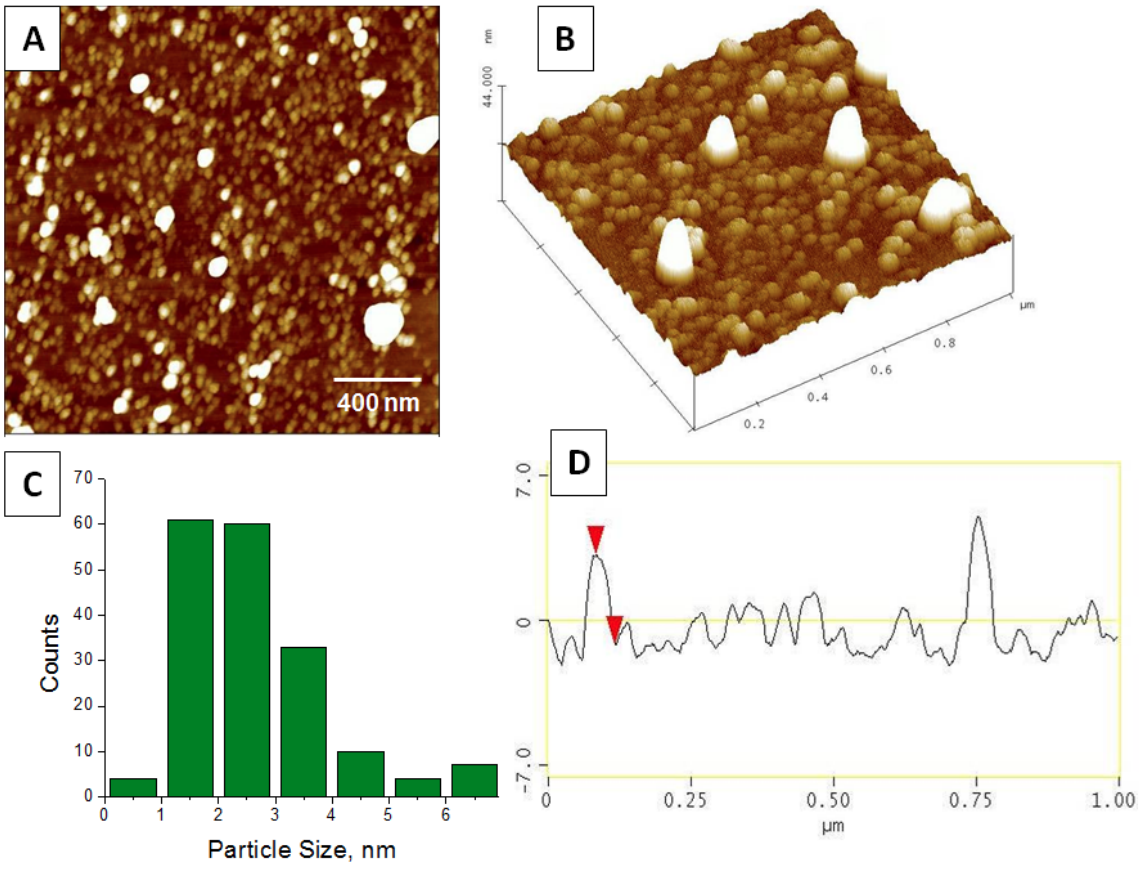

Figure 4.7: Analysis of gold nanoparticles after reduction on PECVD tyrosine film. AFM images A) 2x2 µm^2, Z=15 nm and B) 3D 1x1 µm^2, Z=15 nm. C) Histogram of particle size distribution on tyrosine surface. D) Sample of cross-section analysis from AFM image showing measured height of the nanoparticles.

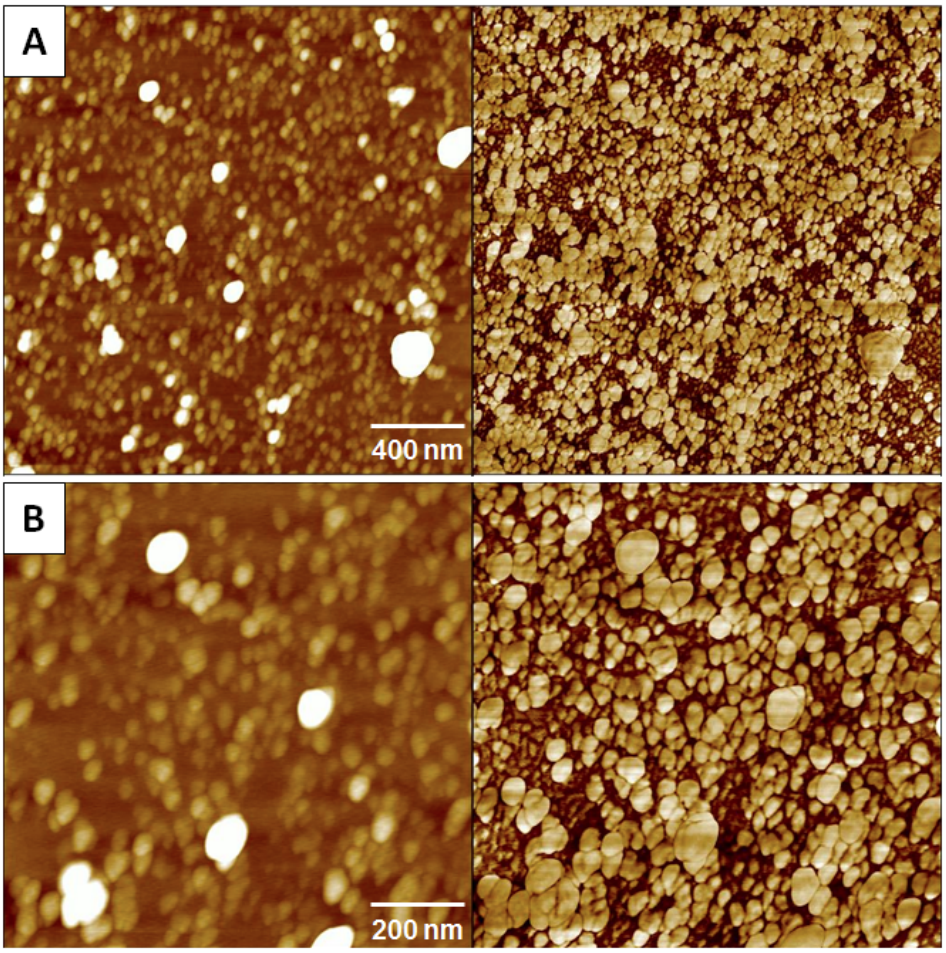

Figure 4.8: AFM of gold nanoparticles reduced on a PP-Tyr surface. A and B) Topography (left) Z=15 nm, Phase (right) Z=50°.

features seen were simply occurrences of PP-Tyr, it is expected that there would be little to no change in the phase image, but since a distinct contrast is seen, it is likely that the change arises from the gold nanoparticles on the surface. From this, it is inferred that the small particles are composed of gold, however, direct measurement of a single particle composition by EDX or XPS was not possible due to the size of the features.

AFM cross-section analysis of the nanoparticles was used to determine the average nanoparticle diameter. This method was applied to the entire area to determine the number and average size of nanoparticles on the surface (Figure 4.7 A and B). The

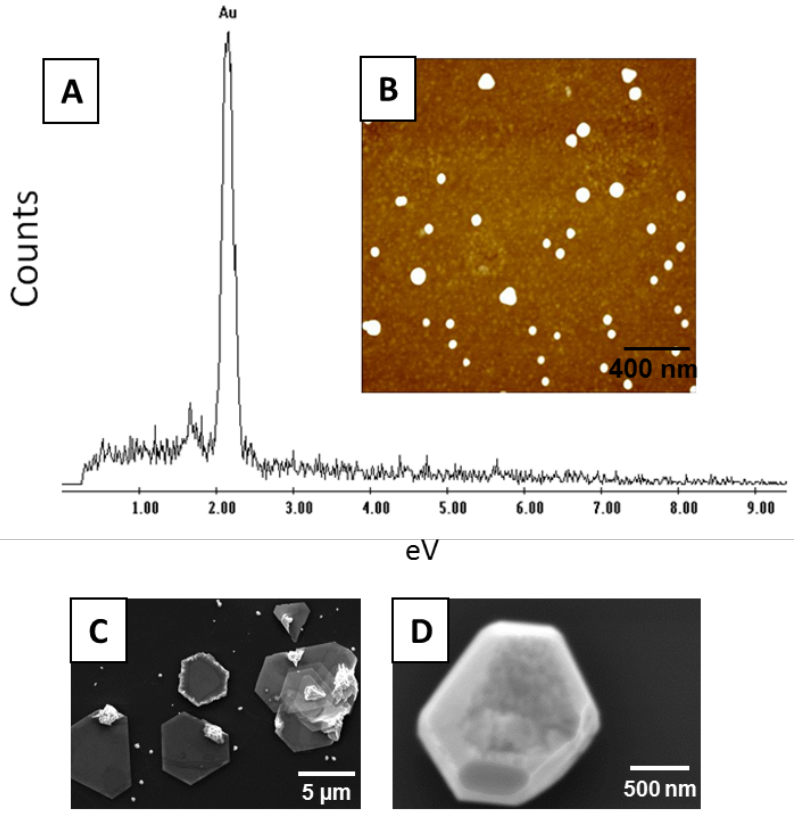

Figure 4.9: Compositional analysis of gold nano particles and plates. A) EDX spectra showing the presence of gold on the surface. B) AFM of gold nano plates on a PP-Tyr surface. C and D) SEM micrographs showing larger gold structures on the PP-Tyr surface in addition to nanoparticles.

particle size of the small gold nanoparticle distribution obtained from cross-sections was relatively narrow, yielding an average diameter of 2.2 ± 1 nm (Figure 4.7 C and D), tracked over about 200 particles on six different samples. Larger gold clusters were observed on the surface occasionally, with sizes up to 30 nm (Figure 4.7 B). These larger clusters represent the agglomeration of many small particles on the surface and may eventually become more ordered as the mineralization process progresses. These larger geometric gold shapes were imaged via AFM and SEM and were capable of providing compositional information via EDX. EDX spot analysis of the particles reduced on the surface confirms gold (Figure 4.9). A representative AFM image shows the gold nanoparticles and platelets on the PP-Tyr surface (Figure 4.9 B). These particles are also clearly seen via SEM, which allows them to be targeted for EDX sampling. No gold

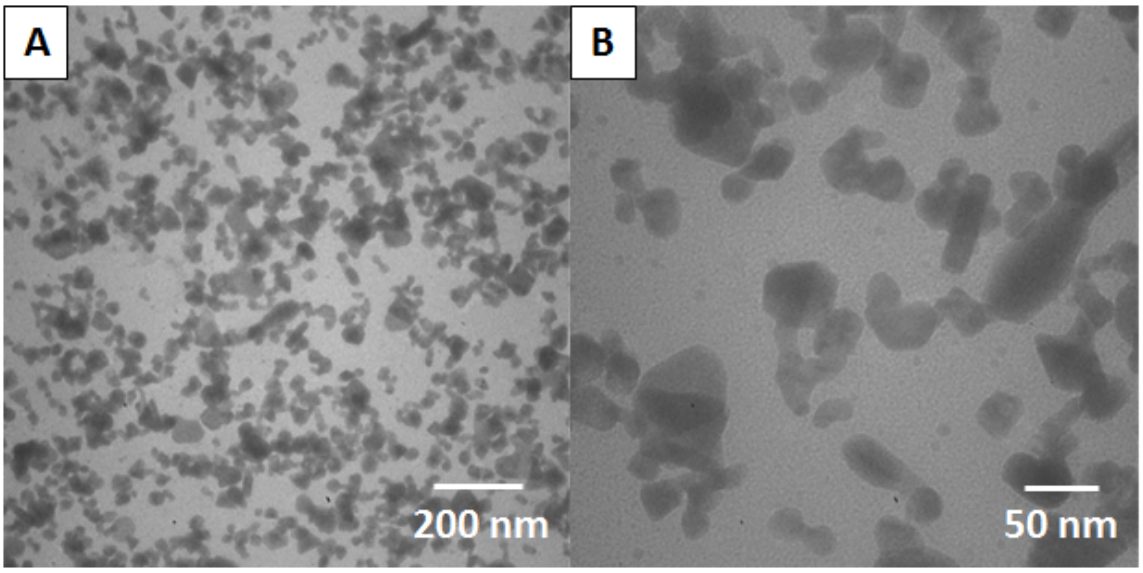

Figure 4.10: TEM micrographs of gold nanoparticles on PP-Tyr after mineralization. A) low and B) high magnification images.

signal is observed in areas surrounding the gold nanoparticles indicating that the only deposition of gold is occurring at specific sites and not at every point across the surface. Examples of these features seen in SEM show clearly that the platelets can form larger features on the surface, up to approximately 5 microns in size (Figure 4.9). This is typically the final phase of mineralization where many small aggregates cluster to form larger, ordered structures (Figure 4.9 C and D). The examples shown represent the entire range of possible surface formations following this type of mineralization process.

Additional imaging of the gold nanoparticles was done via TEM which showed a high density of gold nanoparticles on the PP-Tyr surface (Figure 4.10). These samples were prepared by directly plasma polymerizing tyrosine on TEM grids coated with a carbon film to support the polymer deposition. The visible gold nanoparticles ranged in size from 5 nm for individual particles to over 100 nm in size for larger, agglomerated particles. Distinct shapes were observed as the particles grow in size and begin to form a more ordered long-range structure. A high density of particles was observed over the larger area image which shows that particles tend to form broadly across the surface of

the PP-Tyr film and have a large variation in size distributions, which is in agreement with the AFM and SEM studies previously conducted.

4.3.4 Micropatterning of Tyrosine Coatings

Patterning of the tyrosine during plasma deposition was done by securing a 1000-mesh TEM grid with 10 x 10 μm^2 square openings to the substrate to act as a mask during the PECVD deposition. This method allowed regular patterns to be created on the silicon surface across the entire masked region (Figure 4.11 A and B). AFM section analysis of the patterned area shows that the peak height of the square tyrosine regions was 80 nm

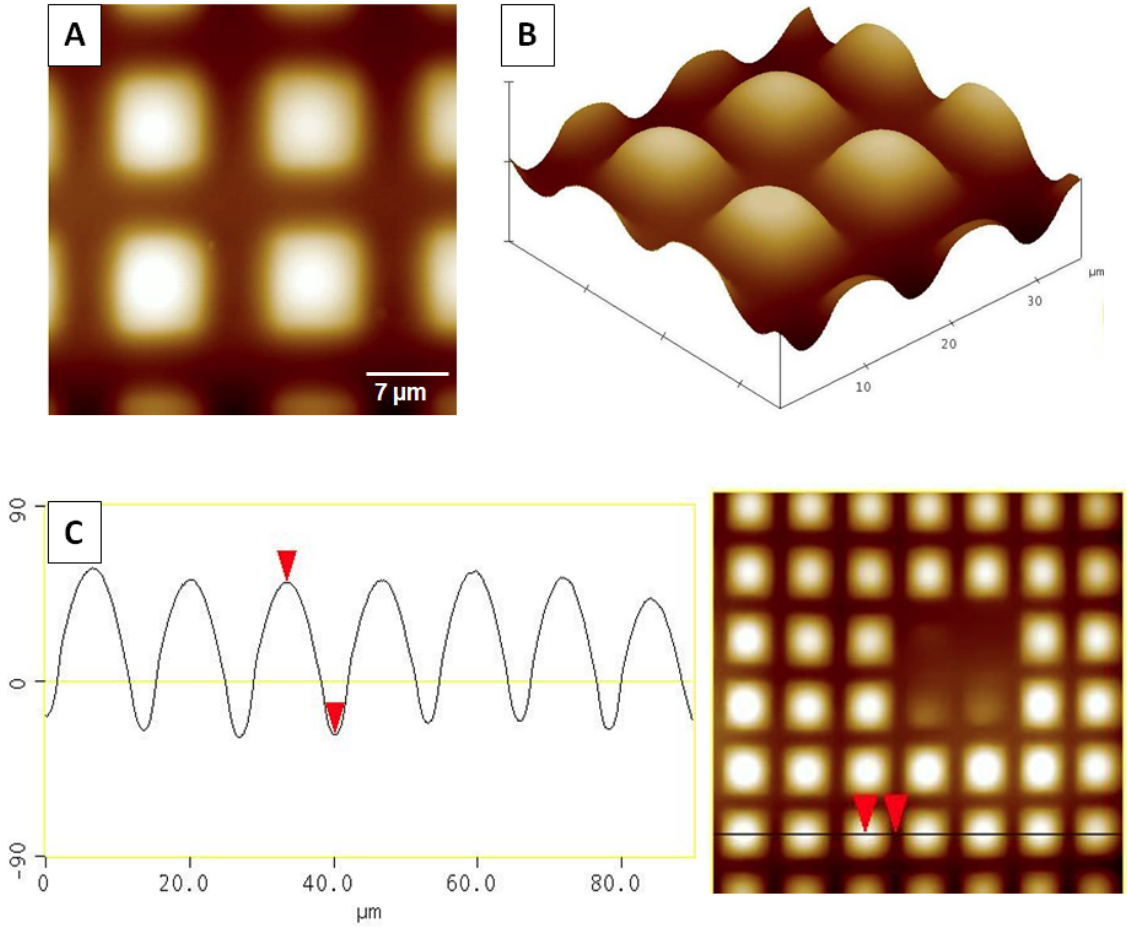

Figure 4.11: Micropatterned tyrosine films: A) patterned tyrosine 35 x 35 μm^2 scan Z = 230 nm. B) 3D scan of patterned area shown in A). C) Cross-section analysis of patterned area showing heights of regions.

(Figure 4.11 C). The four missing squares were caused by defects in the grid that prevented polymer deposition. This selective deposition demonstrates the ability to introduce, control, and reproduce changes to the patterned system with the mask during deposition (Figure 4.11 C).

After exposure of the patterned tyrosine substrate to the gold chloride solution, it was seen that these patterns are capable of selectively reducing gold nanoparticles on the tyrosine-coated regions while leaving the areas of exposed silicon relatively clean and free of nanoparticles, which creates density controlled regions of gold nanoparticles selectively reduced on the surface of the square PP-Tyr coated areas (Figure 4.12 A and

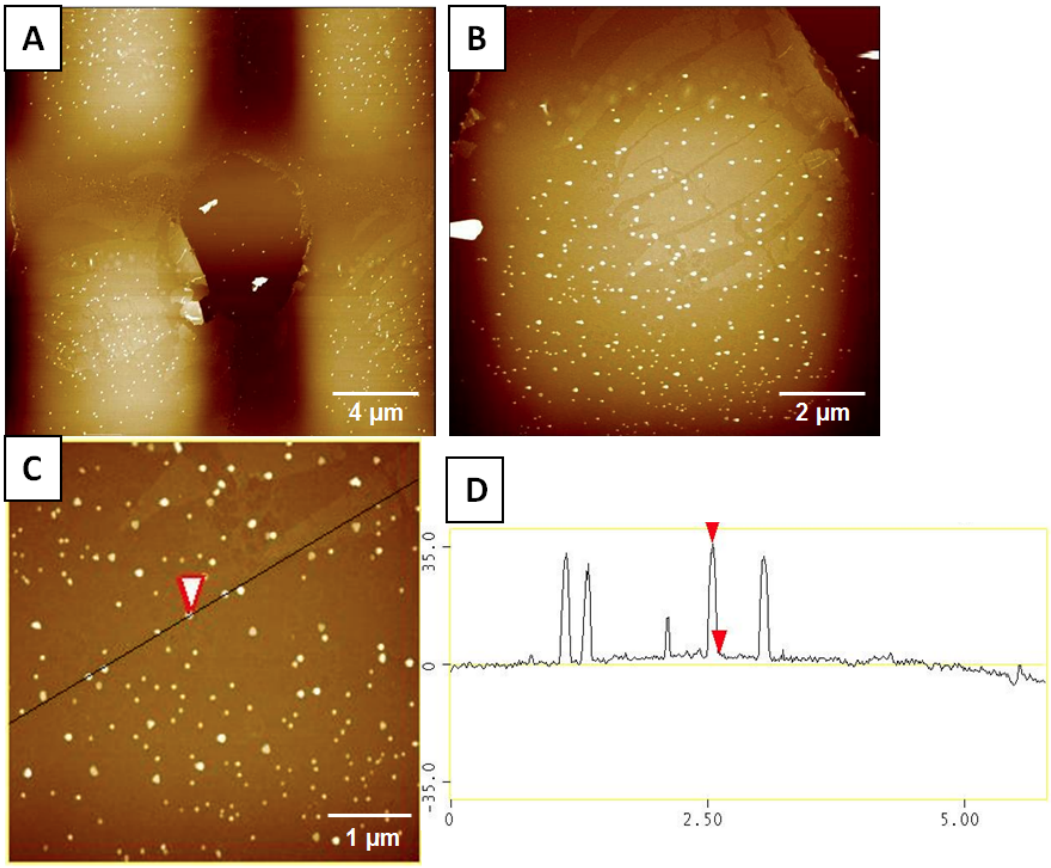

Figure 4.12: AFM images of gold nanoparticles grown on micropatterned film: A) Z = 60 nm, B) Z = 90 nm, C) Z = 60 nm. Height of gold nanoparticles measured is 33 nm.

B). The nanoparticles observed in these regions were 20-30 nm nanoparticles which match the results seen on the uniform tyrosine films along with larger gold aggregates which were also present (Figure 4.12 C).

The small feature sizes of the patterning resulted in some delamination of the tyrosine film during removal of the mask and exposure to the gold chloride solution (Figure 4.12). This delamination primarily occurred at the edges of the squares and was evidenced by the non-uniformity of the coating between the squares. As the TEM grid was secured only around the edges to the substrate, there was some tyrosine that permeated under the masked area leaving a thin residual film in the valleys between the raised areas with a thickness of less than 10 nm. These are weaker regions that are prone to de-lamination.

4.3.5 Alternative substrates for PECVD tyrosine coatings

By using PECVD to deposit tyrosine, functional coatings were fabricated on not only on atomically flat silicon wafers, but also on specimens of commercial PTFE and nitrocellulose (discussed here) along with PDMS, polystyrene, glass, woven silk and polyethylene. The specimens coated represent a wide range of conventional plastics. The results for these materials were favorable and warrant further study into their specific coating and reduction potential, which would be valuable. Through further study, a determination of where the limits of this coating technique lie may be made. It has been observed that PECVD is a faster coating method and offers more complete coverage than solution treatment with pTyr as seen in comparative experiments. While all samples tested supported stable plasma coatings and gold reduction, PTFE and nitrocellulose are characterized here for preliminary studies since they proved promising

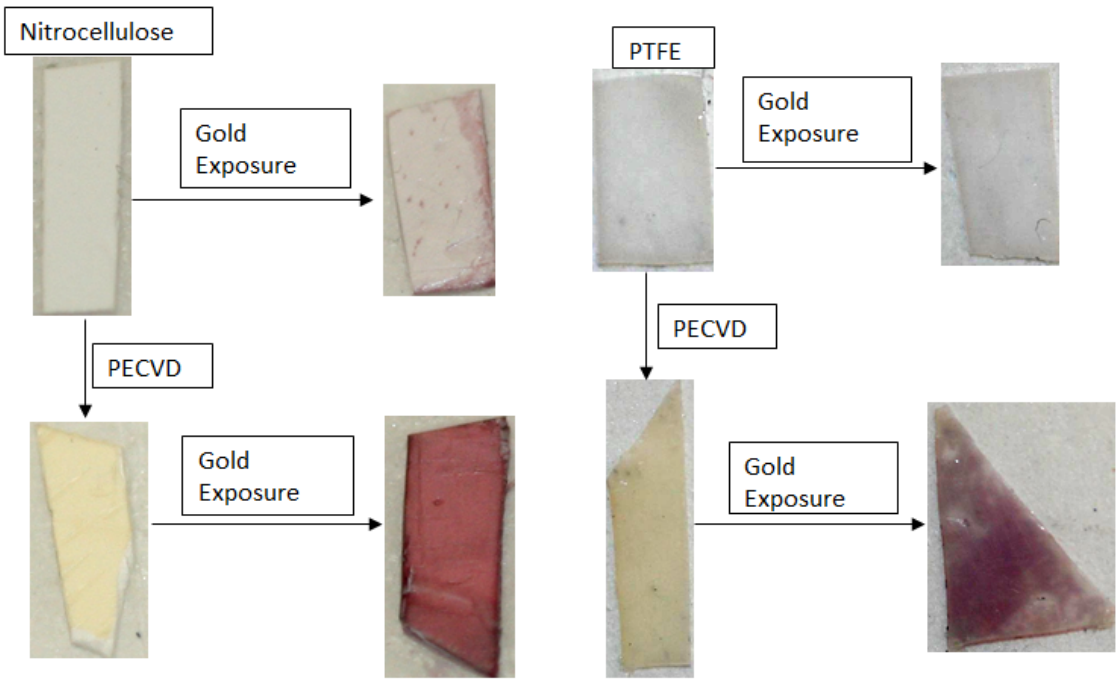

Figure 4.13: Optical images of nitrocellulose (left) and PTFE (right) coated with tyrosine coating and exposed to gold chloride. The unmodified substrate is first exposed to the gold solution with no tyrosine coating. A PECVD coating of tyrosine is placed on the blank substrate and exposed to gold chloride. This visibly highlights the reduction of gold nano- particles on the surface by the tyrosine.

and provided the clearest optical images of the coating and reduction process (Figure 4.13).

By demonstrating the ability to make robust PP-Tyr coatings and gold nanoparticles on different surfaces, there exists the potential for the reduction of metal nanoparticles on surfaces not previously seen to support such types of growth and attachment. Four samples were prepared including: a bare substrate, a bare substrate exposed to a solution of gold chloride, tyrosine deposited on the substrate, and the tyrosine coated substrate exposed to gold chloride. The reduction of gold chloride resulting in gold nanoparticles on the surface by the tyrosine is evidenced by a color change between the samples of tyrosine coated and uncoated nitrocellulose exposed to gold chloride. A

drastic change in color is seen in the tyrosine-coated surface, where a deep red color is observed, in contrast to almost no color change on the uncoated sample (Figure 4.13). Differences are also evident on the samples that have not been exposed to gold chloride. Both the tyrosine-coated nitrocellulose and PTFE were seen to be a light yellow, whereas the uncoated samples were white. This is a striking example of the effectiveness of plasma deposited tyrosine at reducing gold nanoparticle across an entire surface.

To confirm the presence of the tyrosine film and gold nanoparticles on the PTFE, nitrocellulose and silicon substrates, XPS analysis was also conducted. Examples of spectra obtained from the tyrosine coating with reduced gold nanoparticles on silicon and PTFE clearly show distinct peaks for gold and nitrogen (Figure 4.14 A and B, Table 4.1). The essential marker from the tyrosine is the nitrogen indication from the N 1s peak which is derived from the amine group of the tyrosine. Au 4f and Au 4d are seen on the samples only after tyrosine has been deposited and the sample exposed to gold chloride. The blank substrates exposed to gold chloride show no gold except in the case

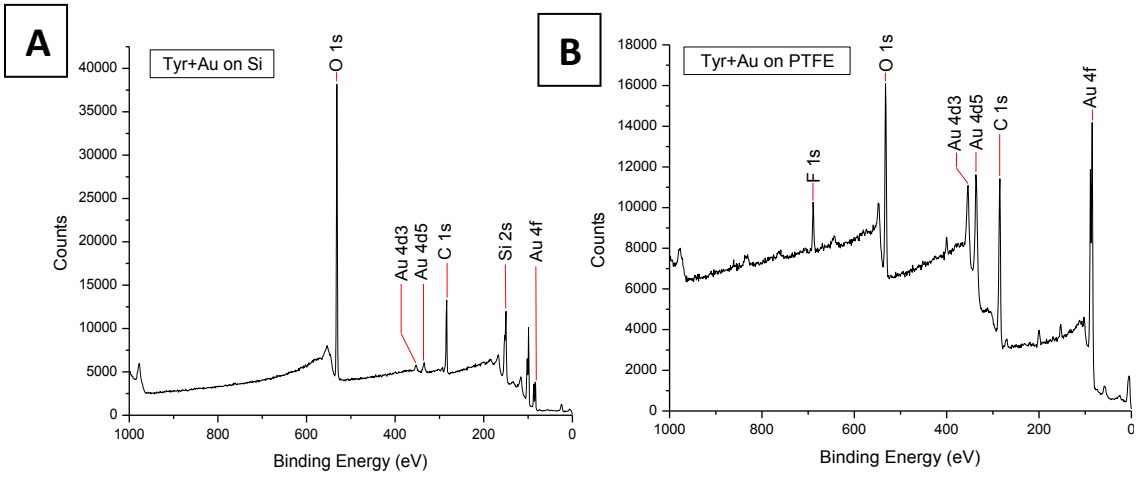

Figure 4.14: A) XPS of PP-Tyr after reduction of gold on silicon. B) XPS of PP-Tyr after the reduction of gold on a PTFE substrate.

of nitrocellulose, which is capable of a small amount of reduction on its own (Table 1). However, gold chloride reduction is much more pronounced after the addition of the tyrosine. The control samples of the other blank substrates exposed to gold chloride do not show the presence of gold, which indicates that reduction of gold chloride and formation of nanoparticles is a direct result of the tyrosine present on the surface and not only the substrate functionality. The small amount of chlorine detected was a result of the exposure to the gold chloride solution.

Table 4.1: Atomic percentages showing composition of films on PTFE, nitrocellulose and silicon by XPS. The spectra of the uncoated substrate, the uncoated substrate exposed to gold chloride solution (+Au), the substrate coated with tyrosine via PECVD (+Tyr) and the tyrosine-coated substrate after exposure to gold chloride solution (+Tyr+Au).

	Si 2p	Si 2s	C 1s	O 1s	N 1s	Au 4f	Au 4d5	Au 4d3	Au 5p3	F 1s	Cl 2p
PTFE	-	-	42.6	4.2	-	-	-	-	-	53.0	-
PTFE + Au	-	0.3	32.3	2.8	-	0.1	-	-	-	63.6	-
PTFE + Tyr	4.7	4.3	47.1	16.5	4.1	-	-	-	-	-	-
PTFE + Tyr + Au	-	3.7	38.4	29.4	2.7	4.4	3.6	5.3	3.7	3.5	1.6
Si	-	36.7	17.7	32.5	-	-	-	-	-	-	-
Si + Au	-	31.7	17.5	30.7	-	-	-	-	-	-	-
Si + Tyr	-	5.4	70.1	19.7	3.4	-	-	-	-	-	-
Si + Tyr + Au	-	28.7	21.5	27.5	-	0.5	0.4	0.5	-	-	-
Nitrocellulose	-	-	53.0	38.8	7.3	-	-	-	-	-	-
NC + Au	-	-	46.6	40.6	8.5	0.6	0.4	1.3	-	53	-
NC + Tyr	0.9	0.7	52.2	17.0	5.6	-	-	-	-	-	-
NC + Tyr + Au	-	-	53.7	24.0	6.4	2.0	2.0	2.4	-	-	3.0

This analysis demonstrates the effectiveness of PECVD for tyrosine deposition and shows that the resulting film has good adhesion to many substrates, enabling the reduction of gold nanoparticles on these surfaces. This type of coating-reduction system allows simple surface modification and has many potential applications in tunable optical coatings and chemical detection. It is suggested that tyrosine plasma coatings can potentially be applied for gold reduction to many other substrates as well, offering a wide range of surfaces suitable for applications involving plasma coating and the reduction of gold nanoparticles.

4.4 Conclusions

This study shows that PECVD provides a facile method for the deposition of PP-Tyr for biometallization. Smooth, conformal and uniform films were created quickly and reliably with this method. Additionally, PECVD is a one-step coating process that completely eliminates the need for any wet chemistry in the fabrication of the tyrosine film since the solid monomer can be heated and sublimed directly into the plasma stream during deposition. The plasma deposition method described results in a highly cross-linked tyrosine coating on the substrates, which contributes significantly to the stability and robustness of the films.

The PP-Tyr films show excellent robustness when exposed to gold chloride solution for biometallization, demonstrating the versatility and durability of this surface coating technique for biometallization on a variety of substrates from silicon to PTFE. Patterning of the tyrosine films demonstrates that the PECVD-mask system combination is an effective method to create patterned regions on the substrate that are capable of selectively reducing gold nanoparticles on the surface. These results demonstrate the potential for precisely directing the areas of gold nanoparticle growth that can be controlled simply by the mask. While only square patterns were created and studied herein, there is a much larger range of potential shapes and patterns that can be created and this method could possibly be extended to such complex shapes as seen in micro- and nano-scale photolithography patterning.

This type of inorganic reduction can be extended from gold nanoparticles to other minerals and metals by using different amino acids and peptides to make PECVD films. Robust PECVD films can potentially be made from a number of different monomers and

even short peptides, each selected for a specific function and binding ability. Mixtures of amino acid monomers or selective patterning during deposition can potentially be used to deposit several different types of inorganic material on or in close proximity to one another, allowing different metal nanoparticles and bimetallic materials to be precisely placed to tune optical or conductive properties. Plasma polymerized polyamino acid coatings have a great potential for tunable organic/inorganic composite material fabrication since the inorganic reducing amino acid monomer can be conformally coated onto many substrate. Functionalized PECVD films that allow biometallization may see applications in tunable optical device layers, wavelength-specific filters and selective surfaces for optical and sensing applications such as stacked layers that act as broad-spectrum filters for electromagnetic radiation.

CHAPTER 5 : Plasma Deposited Amino Acid Coatings for a Conformal Growth of Titania Nanoparticles

Reprinted with permission from Anderson, K. D.; Marczewski, K.; Singamaneni, S.; Slocik, J. M.; Naik, R. R.; Bunning, T. J.; Tsukruk, V. V. "Plasma Amino Acid Coatings for a Conformal Growth of Titania Nanoparticles" *ACS Applied Materials and Interfaces* 2010, 2, 2269-2281.

5.1 Introduction

Surface functionalization is frequently used to alter or enhance the desired response in organized organic and inorganic structures in order to tailor their optical properties, reactivity, mechanical strength, surface wettability, biocompatibility, sensing ability, and photovoltaic capability.[188,189,190,191,192,193,194,195,196,197,198,199,200,201,202,203,204,205] Some systems currently studied make use of the active sites on biological molecules, which supports the reduction of inorganic compounds directly from solution onto the surface.[44,141,206,207,208] This approach allows the direct modification of surface properties through tailored wet-chemistry nanoparticle reduction from precursor solutions on properly functionalized substrates. On the basis of these systems, new bottom-up techniques can be developed for material fabrication or surface enhancement via surface protein and peptide mediated synthesis.[95,209,210,211,212]

Mimicking a naturally occurring biomineralization process has promising implications for biomimetic engineering. A variety of different metal-binding synthetic macromolecules, proteins and peptides have been demonstrated to effectively form inorganic nanoparticles from precursor solutions and bind them to a functionalized surfaces where an excess of the protein or amino acid is properly tethered.[113] Functionalized polymeric

materials, such as poly(ethyleneimine) and multifunctional hyperbranched molecules, have been demonstrated to be effective in the reduction of silver and gold nanoparticles as well.[115,116]

Many examples of this bioenabled approach have been demonstrated, the use of biological and synthetic macromolecules for the controlled formation of gold nanostructures; tyrosine, AG3 and AG4 peptides for the reduction of silver nanoparticles; and cysteine for obtaining platinum nanostructures.[95,122,117,118,119,120] As is known, proteins and peptides with higher concentrations of charged amino acids (e.g., arginine, lysine) are also effective in the reduction of titania nanoparticles.[123,124,125,126] Additionally, histidine amino acids with their high concentration of amine groups, are considered to be potential precursors for titania reduction, enabling nanoparticle formation from aqueous solution onto the surfaces.[95,127] The rSilC protein is one such class which has been demonstrated as being effective at functionalizing surfaces for the formation of large titania structures and nanoparticles in both bulk solution and at surfaces. [128,129]

This study focused on developing the direct growth of an inorganic phase as a method to modify the optical properties of a polymeric substrate and periodic structures by the in-situ growth of high-refractive index materials. This may enable polymeric thin films, both single and multi-layer, which will potentially possess a high contrast in refractive index. Using an active layer for the nanoparticle reduction enables the prospective high-refractive index material to be grown directly on the final configuration. Many previous studies have used high refractive index materials, such as titania, in one-dimensional photonic structures due to the large refractive index it affords compared with many other materials.[16,27,213,214,215] Various methods including atomic layer deposition, chemical vapor deposition and sol-gel processes have all been employed to create the inorganic

conformal nanocoatings.[94,216,217] However, most of these techniques require high temperatures, result in incomplete filling or clogging of the structures or promote their disintegration and collapse.

In this study, a histidine monomer for the fabrication of robust and uniform nanocoatings capable of forming titania nanostructures on different substrates. The sublimation PECVD technique is used in this study. It has proven to be a reliable method for creating ultrathin robust coatings quickly and over a large area while retaining functionality.[12,26,218] Our recent work has shown that PECVD is well-suited for the sublimation of powdered amino acids and their deposition on target substrate in the form of cross-linked nanocoatings.[33,44] Using a similar process, the capability of the plasma polymerized histidine for the reduction of titania nanoparticles onto both flat substrates and periodic porous polymeric structures is shown here.[219,220,221] The formation of uniform individual titania nanoparticles on plasma deposited histidine (PP-His) nanocoatings on both smooth substrates and in a highly conformal manner on periodic porous polymer structures fabricated by interference lithography is demonstrated.

5.2 Experimental

Synthetic amino acid monomer, L-histidine (Sigma), was purchased and used without further modification for all plasma depositions. A temperature of approximately 200 ºC was applied to the L-histidine monomer and then slightly reduced, once sublimation had begun in order to sustain the heating while giving the monomer a longer time to sublime. The histidine amino acid was in powder form and was placed in a tantalum heating boat in the PECVD chamber and kept under high vacuum for 20 minutes prior to deposition. All histidine sublimation procedures were carried out according to the well-established

routine with a chamber pressure of 0.02 torr, Argon (99.99% purity) flow rate of 10 cm^3/min and RF power applied at 50 W.[44,51,73]

The fabrication process is shown along with chemical structures of the compounds used in this study (Figure 5.1). The dry histidine monomer was deposited in a custom built plasma chamber through the direct sublimation of the solid monomer into the plasma stream.[44] As the dry monomer was heated and sublimed into the plasma stream, smooth, conformal films were formed on the substrates. All substrates were placed perpendicular to the plasma stream and were rotated to ensure uniform coverage during the deposition. Upon removal from the plasma chamber, the plasma polymerized histidine (PP-His) coated substrate was immersed in a titanium(IV) bis-(ammonium lactate) dihydroxide (TiBALDH) solution to allow mineralization to occur. After removal of the substrate from the TiBALDH, it was rinsed with Nanopure water and dried under nitrogen.

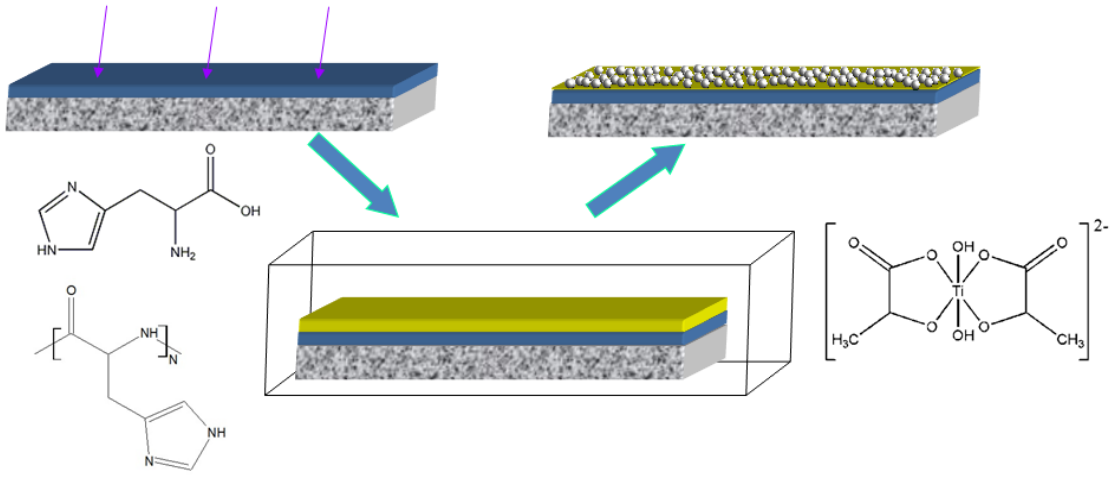

Figure 5.1: The fabrication process beginning with sublimation of histidine amino acid, followed by immersion into precursor solution, and resulting in growth of titania nanoparticles. The chemical structures of L-histidine (left top), pHis (left bottom) and TiBAHLD precursor (right) are shown as well.

A 2 M TiBALDH (Aldrich) was used for all particle reduction experiments. The TiBALDH solution for mineralization was prepared by diluting this into two separate solutions, one with buffer and one with Nanopure water. 0.5 M phosphate citrate buffer was prepared and used at pH 7 to dilute the TiBALDH to a final concentration of 2 mM. Both solutions (water and buffer) were mixed at a 3:500 volume ratio and mixed thoroughly before the histidine coated wafers were immersed. Samples were exposed to the solution for different lengths of time ranging from 1 to 24 hours and then removed, rinsed twice, and dried under a stream of dry nitrogen. In some cases, reduce film thickness may result from washing due in part to unbound monomer being removed form the surface during this step. The exposure of the film to the TiBALDH solution was used as the washing step in these procedures. Periodic porous polymer SU8 templates (epoxy based negative photoresist) fabricated using multi-beam IL according to published procedures have been supplied by the Thomas lab.[219] The materials platform consisted of Epon-SU8 (Miller Stephensen) as a photoresist (a multi-functional epoxy derivative of a bisphenol-A Novolac) and H-Nu 470 (Spectra group) as a photosensitizer. [222,223]

5.3 Results and Discussion

5.3.1 Plasma Polymerized Histidine Films

The PP-His deposited film was smooth and pinhole free with a surface microroughness of 0.3 nm over a 1 x 1μm^2 surface area (Figure 5.2). This histidine film morphology is similar to plasma polymerized ultrathin films from various monomers showing smooth, defect free structures which uniformly coat the target surface. At higher magnification, a very fine grainy texture is observed which is characteristic of plasma polymerized films with a random cross-linked network of polymerized segments.[33,51] The thickness of the film was typically 150-200 nm and was controlled through the deposition time and the amount of material used. The films did not delaminate from the substrate upon removal

from the plasma chamber and subsequent exposure to air. The plasma polymerized histidine films were also stable under light mechanical abrasion and showed good adhesion to the substrate. However, the PP-His films did not show the same robustness when immersed in water as they tended to partially dissolve, indicating there may not be complete network formation occurring. A very thin (few nanometers) residual surface layer of histidine is preserved after exposure to the precursor solution thus facilitating further titania forming routines.

After plasma deposition of the histidine, the resulting chemical structure was compared

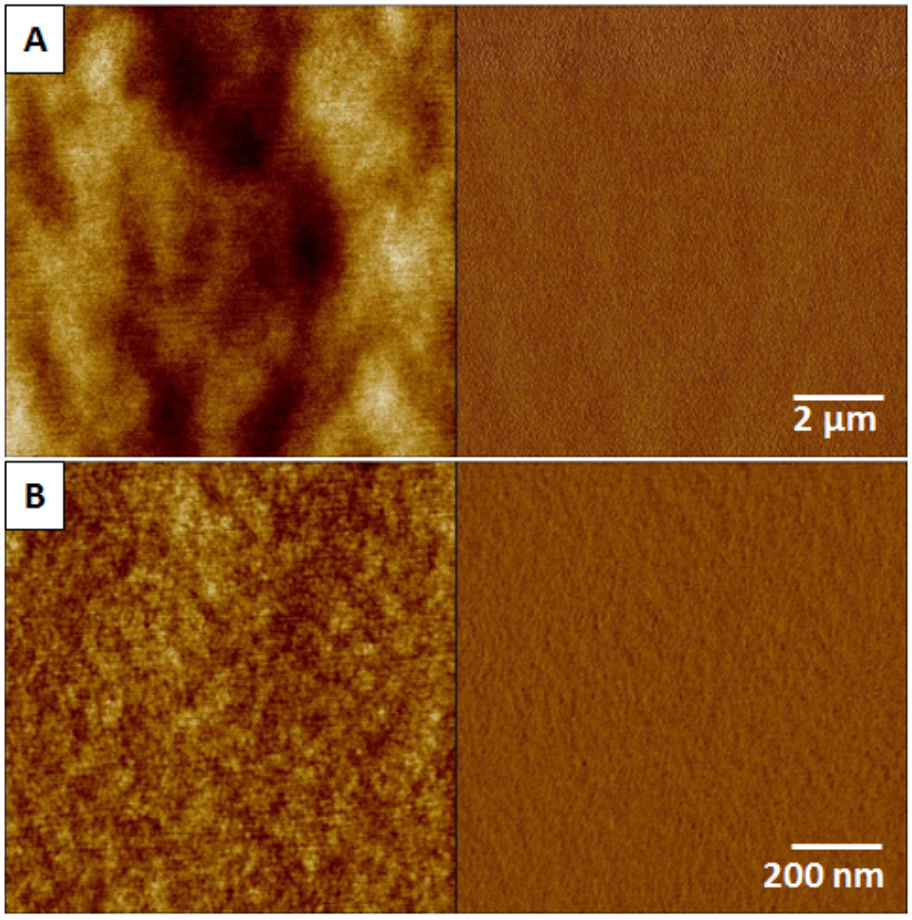

Figure 5.2: Plasma-polymerized histidine films deposited on silicon wafers show smooth and uniform surface morphology. AFM images show topography (left) and phase (right) at different magnifications (both images) with (a) Z = 5 nm height and 10° phase and (b) Z = 3 nm height and 10° phase.

to a solution-cast film of histidine to verify that the PP-His film retained functional groups necessary for titania formation, namely the amine functional groups (Figure 5.3).[114] FTIR spectra show that key functional groups are retained after the polymerization process but there are some notable differences indicating that significant chemical changes occur (see peak positions and assignments in Table 5.1).[224,225,226,227] Although most major peaks of the initial histidine monomer can be found in the FTIR spectrum of PP-His, they are much broader and less intense, indicating significant polydispersity in chemical composition due to random polymerization and limited ordering.

Specifically, the peak at 3273 cm^{-1}, indicative of the NH_2 group in the L-histidine, is shifted as this nitrogen becomes part of the backbone structure. The amine backbone

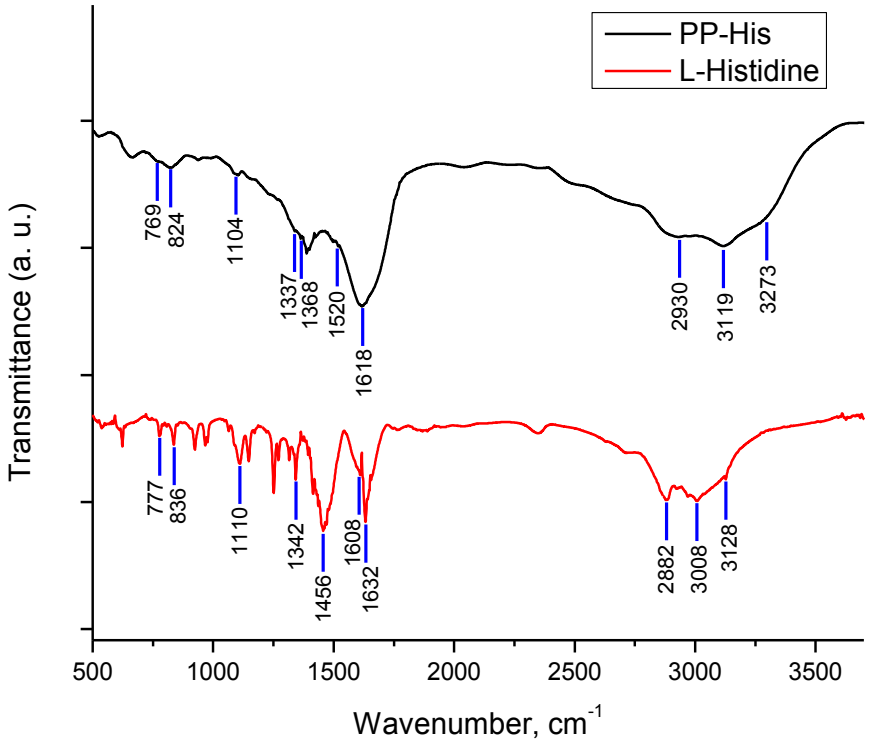

Figure 5.3: FTIR spectra of L-histidine monomer and plasma-polymerized PP-his films.

peak of polyhistidine (pHis) is usually reported at 3282 cm^{-1}.[228] Also observed is the decrease of peak intensity around 2800 cm^{-1}, indicative of the similar loss of O-H groups during PECVD. This is also affected by the changes in the N-H stretching, as polymerization occurs as well as the C-H aliphatic stretch mode seen in L-histidine at 2880 cm^{-1}.[227] Strong peaks seen at 1632 cm^{-1} and 1608 cm^{-1} indicate C=C, C=O or C=N bonds and that the ring structure is intact. From these observed changes it can be inferred that the O-H group is lost and a new bond is formed via the nitrogen, creating the backbone of the polyamino acid network. Peak positions were determined through deconvolution of the FTIR spectra.

Furthermore, L-histidine shows a strong peak at 1456 cm^{-1} with no peak seen in the plasma polymerized film at that position. This is likely due to the OH group being removed from the L-histidine during polymerization, as it is present in the L-histidine molecule, but not the linear synthetic pHis material (Figure 5.1, Figure 5.3). Additional peaks seen at 1368 cm^{-1}, 1342 cm^{-1}, 1337 cm^{-1}, 1110 cm^{-1} and 1104 cm^{-1} correspond to the different modes of the C-N, C=N, N-C-H or C=C bonds present in both the L-histidine and linear pHis.[228] The 767 cm^{-1} peak in the PP-His spectra corresponds to the C=O or N-H in the backbone structure. The 777 cm^{-1} peak of the L-histidine corresponds to the C-C, CH_2 or NH_2 bonds in the intact monomer. The spectral shift seen from 836 cm^{-1} in the L-histidine to 824 cm^{-1} in the PP-His (and to 827 cm^{-1} in pHis) is an indicator of polymerization likely occurring at the NH_2 site in the same manner previously explained with the PP-Tyr polymerization. From this analysis it is seen that the plasma polymerized histidine film is comparable to the L-histidine monomer and corresponding linearly polymerized histidine, with several changes in chemical composition due to random polymerization, but with the retention of essential components of initial monomer unit needed for further titania nanoparticle formation.

The PP-His spectrum is lacking a peak around 1550 cm^{-1}, typically seen in pHis due to C-N bond formation in the backbone (Table 5.1). This may indicate that there is not a clearly defined polymerization occurring, but rather a random network formation of chemical linkages happening between the molecules as they are deposited on the surface.

Table 5.1: FTIR Peak Positions and Assignments for PP-His and L-Histidine Films. Peaks reported in literature for synthetic pHis are included for reference from (228).

	PP-His		L-histidine	pHis
3273	N-H backbone			3282
3119	N-H	3128	OH-O hydrogen bond, N-H	3075
		3008	C=C aromatic	2972
2930	C-H			
		2882	C-H aliphatic stretch	2895
1618	C=O, C=N backbone	1632	C=O stretch, NH_2	1642
		1608	NH_2, C=N	
1520	H-N-C backbone			1510
		1456	COOH stretching	1446
1368	H-N-C, C-N, C=C, H-N=C, N=C-H, C-N			1362
1337	H-C=C, H-N-C, N-C-H, C-N, H-N-C, H-N=C	1342	CH_2 twist	1330
1268	C=N, H-C-C, C=O, C-C-H, N-C, H-C-C,C-C			
1232	C=N, H-C-C, C-C, C-C-H, C=O, C-C	1251	COOH	1230
1104	C-N, H-C-C, C-C, N-C-H, C=N, C-N,C-C=C	1110	O-H…O in plane bend	1112
		966	ring sym stretch	988
824	C-C, C-N, C=C, C-N=C	836	ring sym stretch, H wag	827
769	C=O, N-H backbone	777	C=O	767
667	C-N-C, N=C-N, H-N-C, C-N, C-N=C,C=C-N	623	ring deformation	662

5.3.2 Titania Nanoparticle Formation

Two different routes were used for the formation of titania nanoparticles on the plasma polymerized histidine surface. The first route used a TiBALDH/water solution (Figure 5.4 A,B) and the second used a TiBALDH /phosphate buffer solution at pH 7 (Figure 5.5, Figure 5.6). Along with a change in topography, the phase images of the particles show a distinct morphological change from that of the plasma deposited thin films, indicating the presence of numerous titania nanoparticles on the surface. It was observed that there is a high level of titania particle surface coverage measured up to approximately

75% in both cases.[229,230] Particle coverage of the surface is typically not seen to be higher than this in part because the particles do not follow a close packing regime, as they simultaneously form at many reactive sites on the surface and are dispersed in a more random fashion. It is noted however, that when the solution is reduced in the water solution, there appear to be more large voids on the surface than when the particles are reduced from the buffered precursor solution. It can be seen that in Figure 5.4 a second layer of titania particles appears to be forming on top the first layer, resulting in areas of double layers of particles on the surface.

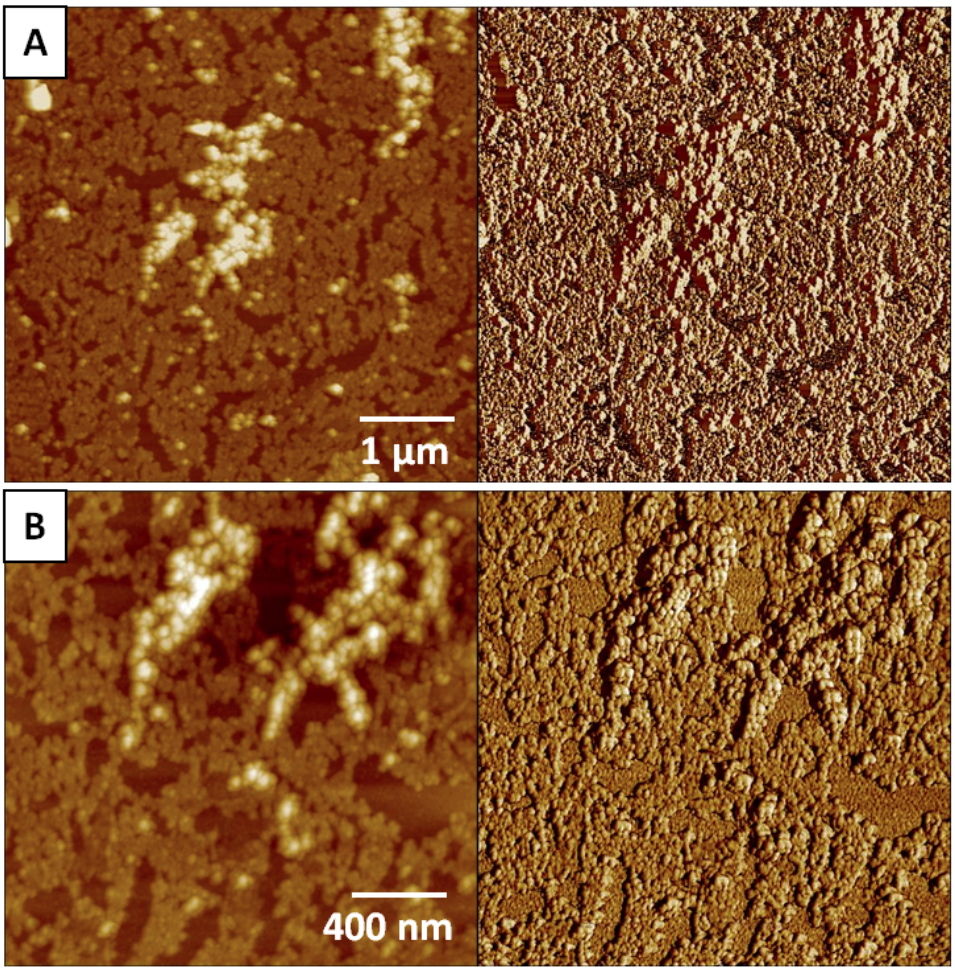

Figure 5.4: AFM images (topography, left; phase, right) of plasma polymerized histidine film with titania nanoparticles formed from aqueous precursor solution; z = 75 nm height and 40° phase for all images.

Although both routes were successful with mineralization, the primary difference between the two methods was the size of the titania nanoparticles. The diameter for nanoparticles formed in buffer was an average of 3.5 ± 1 nm, while the average diameter of titania nanoparticles obtained from the water-based precursor significantly increased to 13 ± 4 nm (Figure 5.7). It is thought that this size difference is related to the exposure of an active histidine site in the phosphate buffer. As is known, under different conditions, competitive inhibition occurs differently, which modifies the catalytic activity of the histidine-rich enzymes.[231] Additionally, as has been shown, the activity of

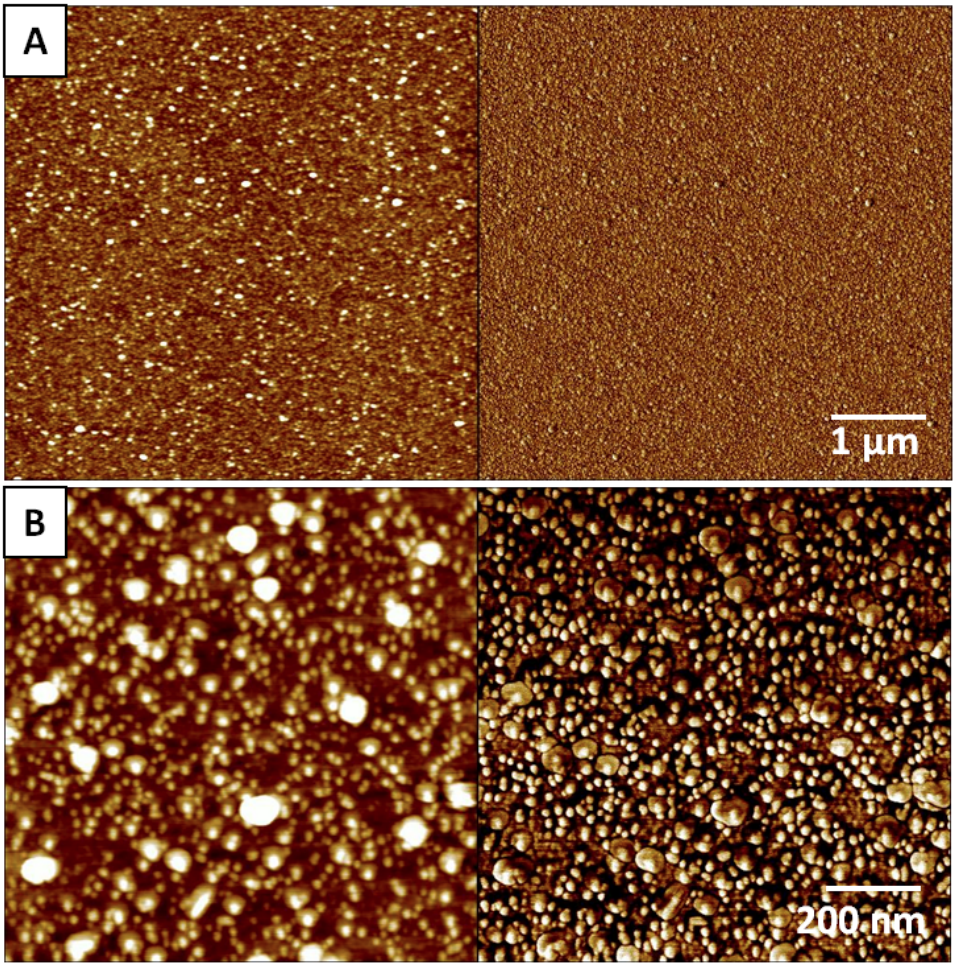

Figure 5.5: AFM images (topography, left; phase, right) of histidine film with titania nanoparticles formed on PP-His in phosphate citrate buffer for 24 h; (a) *z* = 10 nm height and 30° phase. (b) *z* = 6 nm height and 10° phase.

histidine-serine dipeptides is inhibited by selective interaction with a citrate buffer.[232]

These observations indicate that the phosphate citrate buffer may effectively modify the reactivity of histidine sites available for precursor binding thus influencing the size of mineralized nanoparticles. If more nucleating sites exist on the surface, then a higher number of smaller particles can be expected to form simultaneously. This effectively limits the size of the particles that can be formed. When fewer nucleating sites are present on the surface, there are fewer opportunities for new particles to begin formation

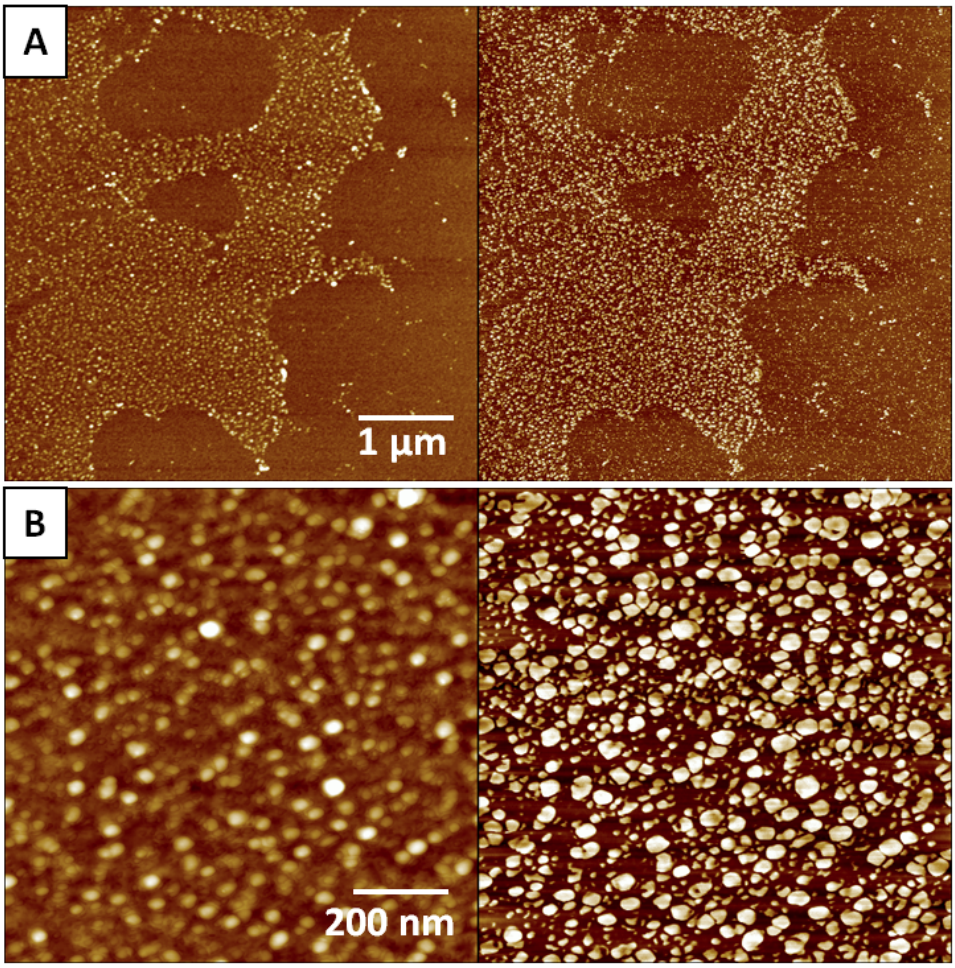

Figure 5.6: AFM images (topography, left; phase, right) of histidine film with titania nanoparticles formed on PP-His in phosphate citrate buffer for 2 h; (a) *z* = 20 nm height and 100° phase. (b) *z* = 15 nm height and 70° phase.

and more of the precursor is consumed as the existing particles grow. While the exact chemical mechanisms of mineralization are still a matter of debate, it is observed that compounds containing NH_2 and OH functional group are seen to be effective at inducing nanoparticle formations. Plasma polymerized materials such as HEMA, which contains an OH group was seen to reduce gold chloride, while PP-TTIP did not. Other studies looking at functional groups and their role have been presented in detail elsewhere.[95]

It is also observed that exposure time of the plasma coated surface to the precursor has an effect on the particle formation as well. The PP-His films exposed for 24 hours showed a greater surface coverage of particles than the films exposed for a shorter period (Figure 5.5 A, Figure 5.6 A). Over longer exposure times, there exists a greater tendency for larger particles to begin to form on the surface as smaller particles continuously grow. This was seen in the case of the gold particles on PP-Tyr as well where structure from gold nanoparticles to large geometric plates were observed. Being able to define and control the size and shape of the mineralized particles remains an area of challenging study. For the case of the PP-His and formation of titania particles, formation was typically complete in about five hours. Longer precursor exposure, typically did not further modify the surface.

AFM scratch test shows that there are two distinct heights in the final film cross-section after titania nanoparticles formation (Figure 5.8). A distinct ultrathin residual layer of PP-His under the titania nanoparticles was observed. This residual PP-His layer was typically measured at a thickness of 3.5 ± 1 nm. This indicates that during the exposure to the precursor solution, most of the initial PP-His film is dissolved with the exception of an ultrathin surface layer, which remains firmly tethered to the silicon dioxide surface. The PP-His film likely dissolves due to low or less stable cross-linking between the

molecular chains, which leads to a less robust structure on the surface. The film instability can possibly be attributed to excess internal stresses built into the film during the plasma deposition which typically occur as a result of the plasma conditions used. Generally, faster deposition rates contribute to increased stresses and this can be especially prevalent in sublimation depositions where the deposition rate can be difficult to control. Resistively applied heating of the monomers is more difficult to control, especially at the lower temperatures used for histidine as compared to tyrosine. The dissolution of the PP-His film may also be partially attributed to incomplete polymerization of the monomer, whereby a thin layer adheres to the surface, but further polymerization is not sustained and the monomer is only physically deposited on the surface and easily rinsed away. Even if a small amount of polymerization occurs and there is a significant amount of unreacted monomer, this can lead to film dissolution

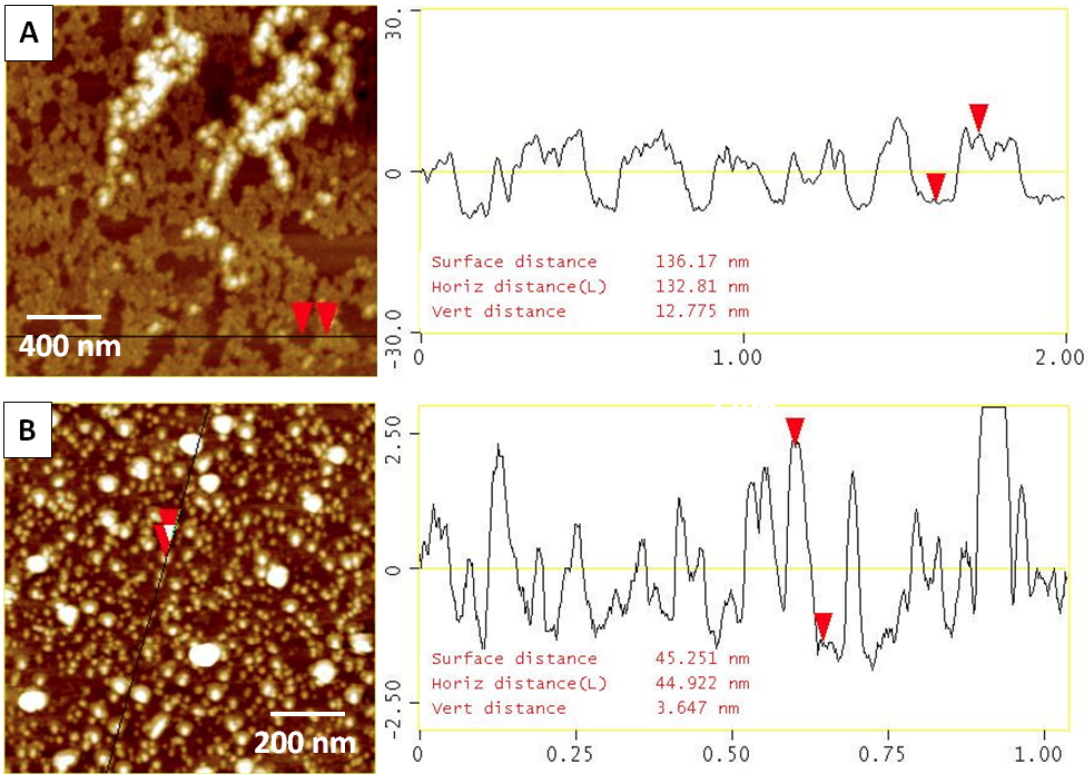

Figure 5.7: Surface topography cross-sections showing the size of titania nanoparticles mineralized on the surface with TiBALDH in (a) water and (b) phosphate citrate buffer solution.

since after the free monomer is rinsed, the remaining part of the film is not self-supporting.

XPS measurements confirmed the presence of titanium on the PP-His surface after exposure to the TiBALDH solution (Figure 5.9 A). The presence of elemental titanium is indicative of titania on the surface. The presence of the characteristic titania peaks are seen in contrast to the pure histidine plasma deposited film, which shows only carbon, oxygen and nitrogen-related peaks as expected (Figure 5.9 C). Additionally, the high resolution XPS spectra show two distinctive peaks of titania which appear as expected for Ti $2p_{1/2}$ and $2p_{3/2}$ at 463.9 and 458.2, respectively, and agrees well with values previously determined in the literature (Figure 5.9 B).[233,234] A comparison of the observed shape and position of major peaks to those in the literature confirm the

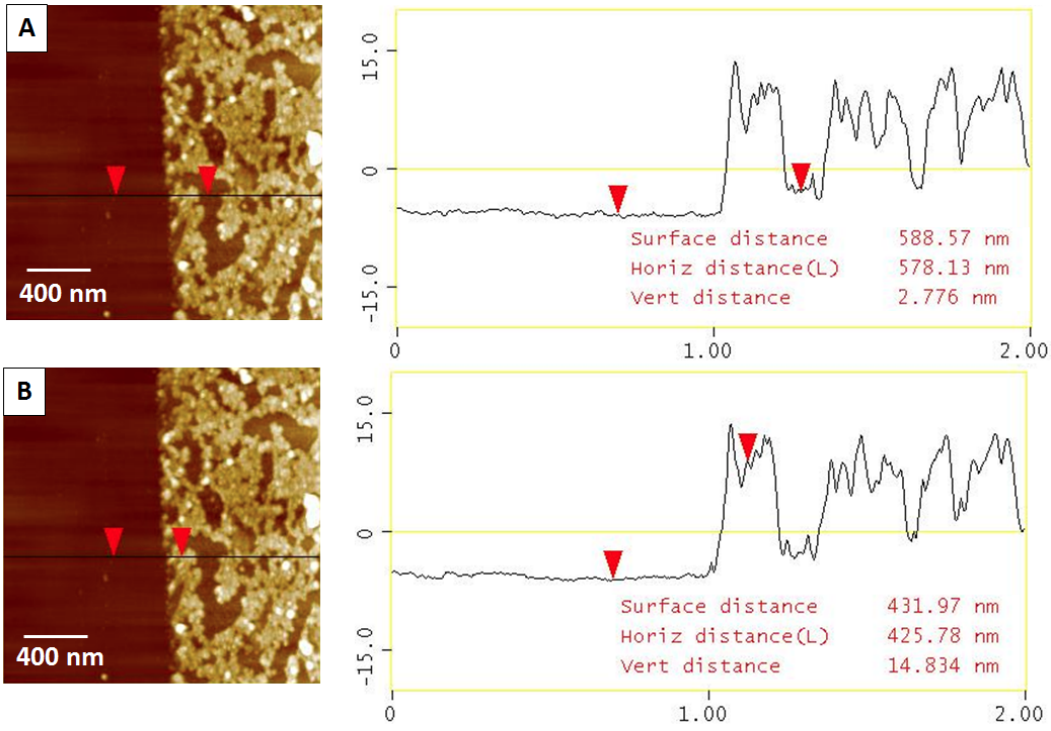

Figure 5.8: AFM scratch test showing the height of (a) the thin residual histidine film present after mineralization on a silicon substrate and (b) the typical particle size in relation to the substrate and residual histidine film. Typical particles sizes ranged from 10-13 nm, as reduced in nanopure water. Topography image, *z* = 40 nm.

presence of titania and indicates that the Ti^{4+} surface species are predominant as seen by the clear and symmetric peaks.[235,236]

Several attempts to determine the crystal structure of the mineralized titania were made, but the results were inconclusive as to whether there was a definitive crystalline phase. Because the layer of titania was thin (<10 nm), X-ray diffraction measurements could not detect a discernible signal to confirm the presence of a crystalline titania phase. A second attempt at determining the crystal structure was carried out by plasma depositing histidine on silver particles to perform surface enhanced Raman scattering (SERS) measurements on the subsequently mineralized titania. It is known that the Raman spectrum of anatase titania exhibits characteristic bands at 143 cm^{-1} (E_g), 197 cm^{-1}(E_g), 396 cm^{-1} (B_{1g}), 515 cm^{-1} (A_{1g} or B_{1g}), and 638 cm^{-1} (E_g). On the other hand, for rutile titania, Raman bands from are located at 439 cm^{-1} (E_g), 611 cm^{-1} (A_{1g}), and 805 cm^{-1} (a weak shoulder, B_{1g}).[237,238] The Raman spectra obtained here showed several peaks which could be indicative of either rutile (440 cm^{-1}, 230 cm^{-1}) or the brookite (405,630 cm^{-1}) phases of titania (Figure 5.9 E, F). Therefore, it remains open as to which phase is dominant via this mineralization technique, and mixed crystalline structures are probably formed under these conditions. It is also possible that amorphous or anatase structures are likely in the nanoparticles as there can be considerable challenges in reducing rutile via mineralization which usually requires heating to induce a phase change as conversion to rutile at room temperature is relatively rare. To further address this question, larger sample sizes of mineralized material, possibly using multi-layer depositions will need to be investigated to more accurately assess the crystalline phase of the mineralized particles.

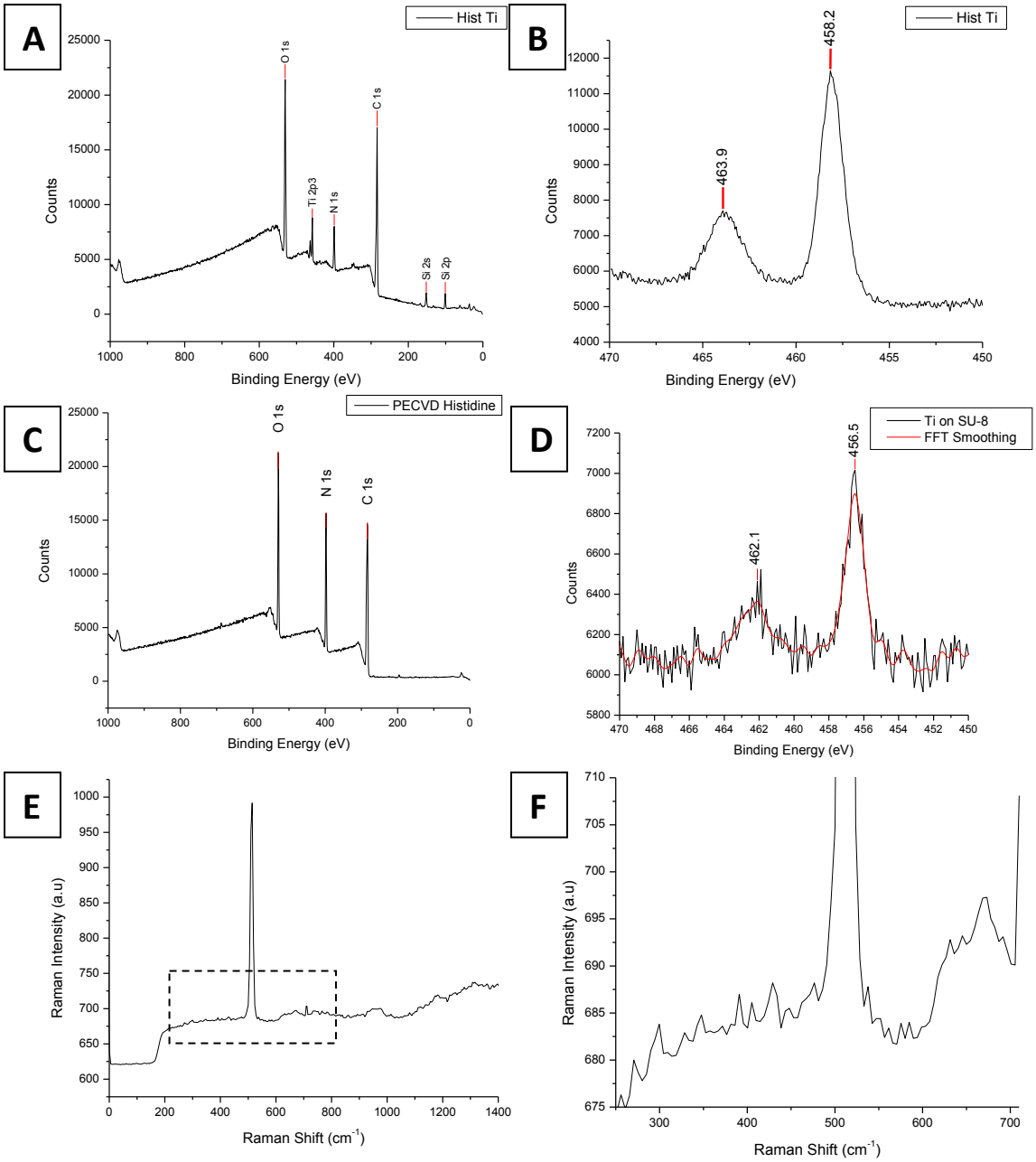

Figure 5.9: XPS spectra of (A) PP-His spectra after titania mineralization; (B) high-resolution XPS scans show distinction between Ti 2p1/2 and 2p3/2 for initial PP-His film; (C) XPS spectra of PP-His prior to mineralization; (D) high-resolution spectra of titania mineralized on an SU-8 periodic structure; (E) Raman spectra of mineralized titania on silicon; (F) detailed Raman spectra showing peaks indicative of different titania crystalline phases.

5.3.3 Optical Properties of Films

A direct determination of the optical properties of amino acid- and titania-containing films was obtained by exploiting a bi-layered model during analysis of spectroscopic ellipsometry data. At least six individual samples were fabricated independently under identical conditions and also were independently measured and analyzed. Ellipsometric measurements were conducted for the polymerized histidine film and for the histidine film with the topmost titania layer. For full analysis of the titania-containing films, independently measured optical properties of the pure PP-His film were utilized. Since AFM measurements indicated that the titania nanoparticle layer showed only partial surface coverage, an effective medium approximation was used to model this layer which accounts for the incomplete surface coverage of the particles (Figure 5.10 F).

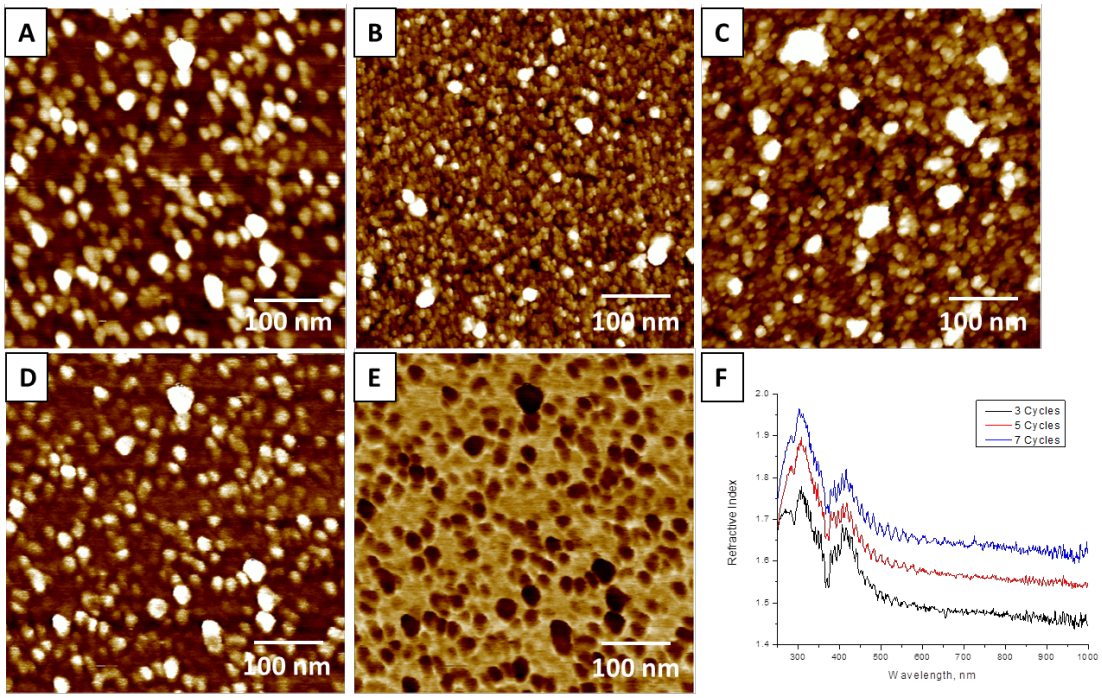

Figure 5.10: A-C) AFM height images showing the changing surface and increasing particle coverage through multiple deposition and reduction cycles of A) 1, B) 3 and C) 7 deposition and reduction cycles. Z= 4 nm, 10 nm and 10 nm respectively. D) relative DMT modulus channel and E) relative adhesion channel. F) Optical analysis from ellipsometric data: refractive index of multiple deposition cycles of titania nanoparticles. PP-His is shown for comparison.

This partial surface coverage, after a single reduction cycle, is also noted through the relative DMT modulus and adhesion channels which show a distinct difference between the particles and the substrate surface (Figure 5.10 D,E). It is expected that the titania nanoparticles will have different mechanical and adhesion properties when compared to the silicon surface coated by PP-His. By depositing multiple layers of PP-His and titania on the same surface, the surface coverage was eventually increased enough to be modeled as a single layer. The two models used in determining the optical constants were the Cauchy and effective medium approximation (EMA) and both models produced consistent results.[218,229] The EMA model was used to verify the results of the Cauchy model since the layer of titania particles was not complete and included some small voids, which can be effectively accounted for when using EMA analysis.

The values for the thicknesses of the PP-His and titania layers determined from ellipsometry closely matched those measured by AFM which was considered as verification of the optical analysis routine. The refractive index, measured over a wavelength range of 250 nm to 1000 nm, shows the change observed in the profile as more layers are added (Figure 10F). The index is seen to increase as the particle density on the surface increases and forms a more complete layer. The intact PP-His film, for comparison, showed a normal dispersion with a gradually decreasing refractive index, *n*, from 1.68 at 350 nm down to 1.59 in the near-IR region (1000 nm). The PP-His film is much thicker than the titania particles at around 240 nm and shows a higher index than a modified surface with fewer than 5 reduction cycles. However, surface modifications with titania particles of around 15 nm in thickness, showed a higher index film, providing a means of creating higher index, ultrathin films on the target surface.

The minor shoulder around 300 nm is caused by the strong absorption of double bonds in the histidine structure (Figure 5.10). The overall value of refractive index is slightly higher than that for traditional polymers (usually within 1.5-1.6) likely due to the higher concentration of intermolecular and cross-linking bonds in plasma polymerized film which result from the network formation.[239] The absorption coefficient, *k*, is relatively high in the near-UV range due to the presence of double bonds and the five-membered ring structure. But the k-value decreased to below $2x10^{-3}$ in the visible and near-IR range indicating low light absorption and good optical transparency in comparison to conventional, covalently cross-linked polymers with localized ordering.[186,187]

A significant increase in the refractive index value is observed upon titania nanoparticle formation across the whole wavelength range (Figure 5.10). The refractive index increased to 1.74 from 1.67 in the UV region and to near 1.65 at 1000 nm. The titania nanoparticle formation also increased the optical absorbance to 0.025 in the visible range indicating some optical loss likely due to additional scattering or absorption by the dense surface coverage of titania nanoparticles and their aggregates (Figure 5.10). The effect of refractive index adjustment is further seen through a series of multiple deposition and mineralization cycles. As the number of depositions increase, a clear change in thickness occurs and the refractive index of the nanoparticle film becomes much more defined and grows higher with each additional layer. This type of cyclic deposition allows for precise control of refractive index and particle coverage depth. This presents a similar deposition method to surface sol-gel, but without the need for modification with hydroxyl groups on the surface.

Although the measured value of the refractive index increased significantly due to the presence of titania nanoparticles, it is still much lower than that of crystalline titania

phases (about 2.7 at λ=500 nm).[240,241,242] For example, the reported literature values for atomic layer deposited (ALD) titania range from about 2.3 to 2.8 at λ = 500 nm, depending on the deposition conditions.[243,244] However, for titania films of less than 20 nm thickness, the refractive index was reported at 1.8 at 500 nm, thus demonstrating a trend similar to that observed for reduced refractive index for ultrathin titania layer without further high-temperature annealing.[245]

Finally, the measured refractive index of the titania nanoparticles formed on the bio-surface appears lower for two primary reasons. First, the titania nanoparticle layer is incomplete, having both voids and organic matter between the nanoparticles which contribute to the lowering of the refractive index even within EMA analysis which is not accounted for by current modeling. This is addressed by completing multiple depositions of PP-His and reductions of titania particles on the surface filling the voids and contributing to a noticeable increase in the refractive index. Second, titania nanoparticles formed via a bio-enabled wet-chemistry approach typically show an amorphous phase that has a characteristically lower refractive index than common crystalline titania phases, which have proven to be difficult to obtain using room temperature synthesis routines.[246] Additional treatment of the titania phase and increasing surface coverage might be required to boost the absolute values of the refractive index for potential high refractive index properties. However, even for the values observed here, a significant contrast in refractive indices can be achieved in the visible range if the titania layer is combined with low index polymer materials.

5.3.4 Titania formation on periodic 3D templates

Periodic photonic structures with a square lattice of cylindrical pores of periodic spacing 830 nm served here as the basic template to demonstrate the highly conformal nature of

such depositions.[247] Prior to the plasma depositions and subsequent particle reduction the surface morphology of the pristine SU-8 microtruss was observed to be clean and free of defects or nodes, which were subsequently seen after mineralization (Figure 5.11 A). Plasma polymerization of histidine and the following formation of titania nanoparticles on the surface through mineralization resulted in a visible change in the surface morphology (Figure 5.11 B). The AFM images clearly demonstrate the highly conformal nature and uniform coating layer of PP-His and reduced titania nanoparticles after a single coating and reduction cycle. The nanocoating is observed to be uniformly distributed across the microtruss surface and the presence of titania nanoparticles over the surface of periodic structures shows how this method is used to easily modify complex structures. The surface coverage density of titania nanoparticles can be increased by repeated plasma polymerizations of histidine and exposure to the TiBALDH precursor solution. This layered buildup of particles is performed in the same manner, with multiple deposition and reduction steps, as described in the optical study.

The titania nanoparticles show a trend of significant agglomeration after multiple treatment cycles forming large nodes on the SU-8 microtruss as demonstrated in the corresponding AFM images (Figure 5.11 C). This method could be further adapted to provide an effective means of modifying the optical properties of photonic structures. The titania-coated structures exhibit the same periodic pattern over a larger surface area

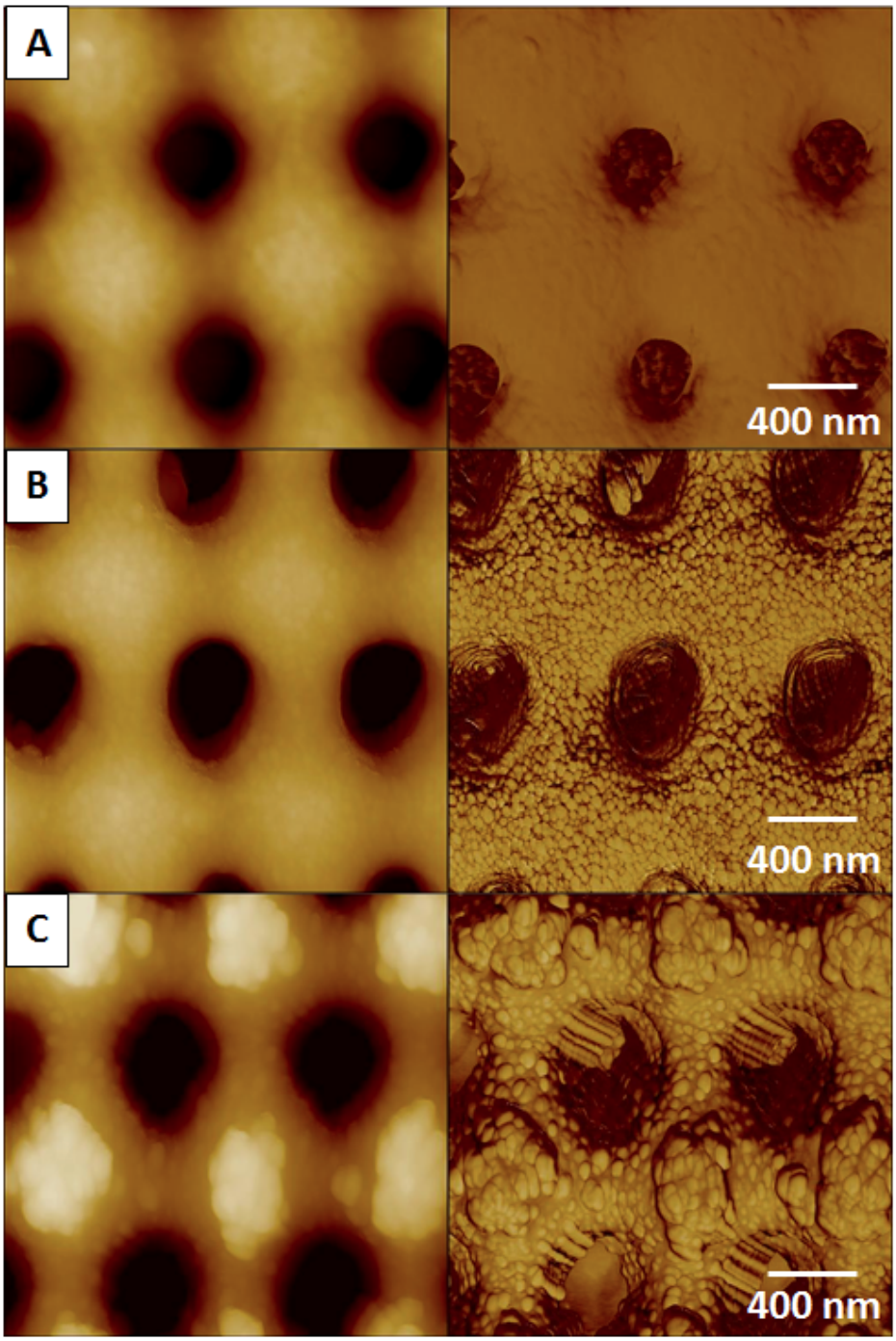

Figure 5.11: AFM images demonstrating the conformal titania nanocoatings on periodic porous structure (topography, left; phase, right; all images): (A) pristine periodic structure before modification, *z* = 300 nm height and 170° phase; (B) periodic structure after one PP-his polymerization and titania formation showing significant change in the phase image, *z* = 500 nm height and 40° phase; (C) periodic structure after three titania formation cycles. Large agglomerations of particles are easily visible on nodes, *z* = 600 nm height and 60° phase.

with a very repeatable local morphology of the polymeric nodes (Figure 5.12). Local microroughness of these nodes after histidine polymerization indicates the presence of the additional plasma coating. Although the square pattern of nodes remains unchanged after titania formation, the local morphology of nodes changed significantly due to the presence of the titania nanoparticles localized at nodes of the squared lattice.

The addition of surface and optical modifying agents in this manner to microtruss structures is of interest primarily because of the gentle process used, with no harsh

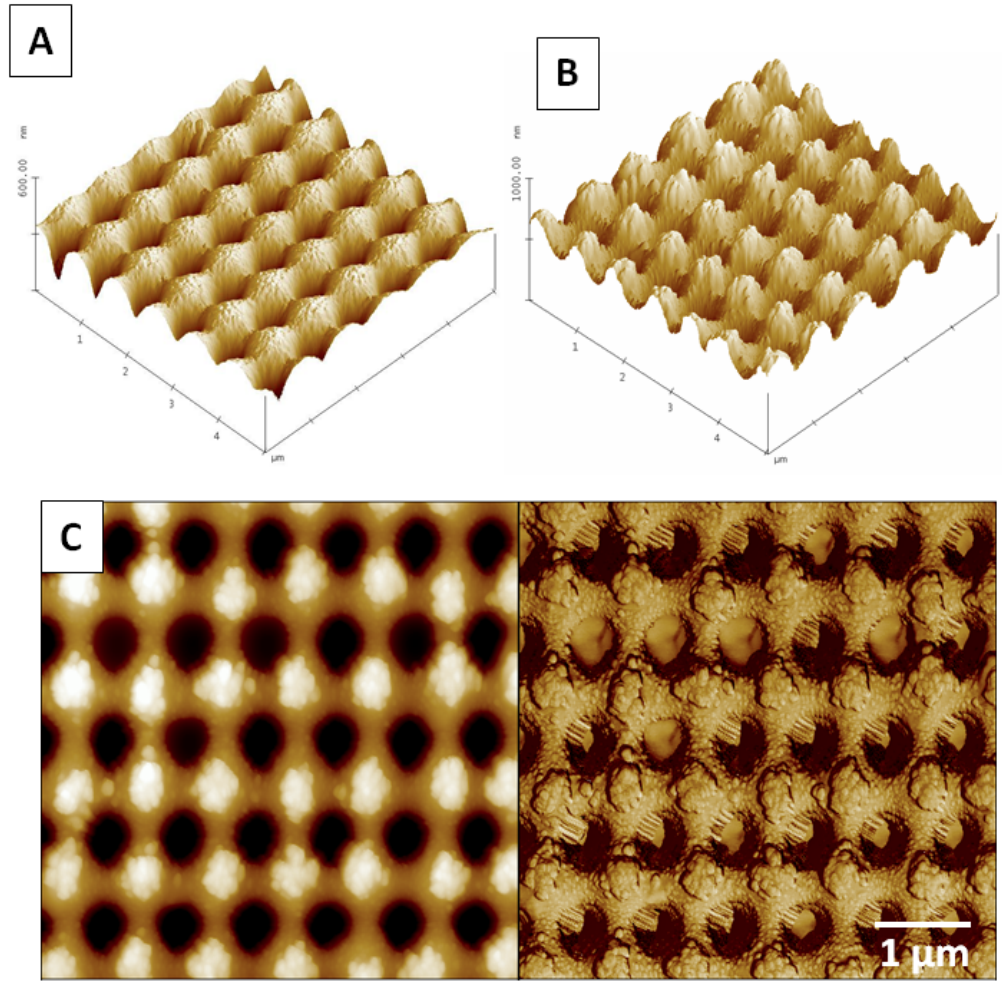

Figure 5.12: 3D AFM (topography) images at large scale showing pristine squared periodic porous pattern (A) *z* = 600 nm height and the same structure after titania nanoparticle formation on lattice nodes (B), *z* = 1000 nm height. C) AFM images showing node formation of titania after multiple reductions on IL truss structures.

solvents or treatments. Using gentle (room temperature, aqueous, neutral pH solutions) conditions for modification of polymeric structures is essential since they may not be robust under other processing methods, either melting under heating or dissolving/degrading in solvent. This type of modification also allows complex surface patterns to be fabricated and then modified to achieve the desired properties (optical, catalytic, etc.) rather than having to shape materials, which may be less amenable to micro- and nano-fabrication techniques.

5.4 Conclusions

The implementation of plasma-deposited amino acids as functional surface coatings for the conformal formation of titania nanoparticles is demonstrated. This is a rapid and non-destructive method for the formation of a functional histidine layer which can then be utilized for forming individual and uniform titania nanoparticles under mild, environmentally friendly conditions, enabling the modification of the surface properties of the original templates. These titania nanoparticles, possessing a higher refractive index, were demonstrated on both smooth substrates and on complex 3D periodic porous polymers such as interference lithography structures. This coating and in situ titania growth may be useful in the creation of high-contrast periodic photonic-related structures formed under mild conditions. By directly reducing the titania onto or into a prefabricated periodic porous structure, this approach might allow full construction of a hybrid organic-inorganic system to be fabricated.

This type of bio-enabled modification highlights a very interesting technique, which can be used to modify these structures and warrant further study into the optical and catalytic properties. For instance, the periodic polymeric structures are prone to mechanical instabilities even under moderate compressive stresses.[248,249] Under mild processing

conditions suggested in this study, there was no degradation and collapse in the periodic polymer structure. By creating a method to embed titania nanostructures onto periodic polymer templates, a means of tailoring photonic structures and their refractive properties in a nondestructive way is demonstrated. This approach can also be used in the stepwise construction of multilayered systems where the PP-His layer alternates with a polymer layer, thus creating high contrast in refractive index. Further development of the optical and catalytic properties of the titania replicas obtained here will be addressed in future investigations.

CHAPTER 6 : Plasma Enhanced Co-Polymerization of Amino Acid and Synthetic Monomers

Reprinted with permission from Anderson, K. D.; Young, S. L.; Jiang, H; Jakubiak, R.; Bunning, T. J.; Naik, R. R.; Tsukruk, V. V. "Plasma Enhanced Co-Polymerization of Amino Acid and Synthetic Monomers" *Langmuir* 2012, *28*, 1833-1845.

6.1 Introduction

CVD methods have been widely used to polymerize materials directly on a variety of surfaces.[7,12,14,15] CVD processes have been designed to allow organic monomers to undergo *in situ* polymerization during the deposition process resulting in stable films of polymerized material on the surface. Polymerization is initiated by a range of different stimuli including RF plasma radicalization, oxidation or injection of an initiator into the reaction chamber.[17,18,19,20,21,22,26,27] Each deposition method has the effect of creating a polymerized film on a target substrate with different variations in the cross-linking density and morphology depending on the CVD method used and the reaction mechanisms.[28] This leads to films with a wide range of unique surface properties that can be tailored for many specialized applications.

PECVD is a specific form of CVD which has been adapted from its common use to deposit dielectrics to successfully deposit a wide range of monomers covering many traditional polymers, ranging from styrene, acrylonitrile and benzene to responsive materials such as poly(2-vinyl pyridine) and poly(N-isopropylacrylamide) to functional amino acids.[40,41,42,43,44,45,46,47,48] PECVD represents a versatile "dry" chemistry fabrication method which is capable of utilizing precursors in solid, liquid or gas form for facile, rapid

and solvent free fabrication of ultrathin coatings for use in many systems.[29,49,50,51] There is a growing interest in the deposition of biological molecules via PECVD which can potentially be used to enhance surface functionalities and structures for cell viability and can also help bridge the interface between inorganic and biological components of integrated systems and biomedical applications.[14,36,53,54,55]

Biological monomers of interest are often in the form of a solid, presenting a unique set of challenges for plasma depositions of these monomers. Some solid monomers can be deposited through various sublimation methods whereby the monomers are pre-heated in the plasma chamber while under vacuum and vaporized into a gas phase.[73,90,91,92,93] The reaction proceeds akin to any gas-phase monomer. It has been demonstrated that sublimation PECVD is compatible with a range of materials, from organometallics to amino acids providing robust and stable films.[44,45,73,90] The utilization of sublimation allows solid materials which are not easily vaporized to be plasma deposited opening a new range of solid material precursors for study.

Amino acids might be deposited via sublimation PECVD and are excellent candidates for further investigation based on their unique functionalities and fundamental biological characteristics.[44,45,95,96] Lee and Frank demonstrated vapor deposition of a wide range of amino acids which were firmly grafted to a substrate and preserved their composition and functionalities.[36] PECVD lends itself well to co-polymerizations of two or more chemical species to facilitate complex and stable functionalized mixed coatings. However, this adds a layer of complexity to the deposition process given the different reactivities of the precursors used. For instance, co-polymerization has been previously reported using benzene and octafluorocyclobutane (liquid and gaseous) monomers

which are copolymerized in the plasma simultaneously to fabricate films with controllable refractive indices.[97]

One challenge with this fabrication process though is determining the appropriate deposition conditions which allow a controlled reaction of different organic materials simultaneously. This challenge is magnified when using one monomer which is solid and must be sublimed into the plasma stream since flow rates are not as easily controlled as they are with conventional liquid and gas phase monomers. In this regard, the deposition rates of each material must be matched based on the desired end ratio of the final film composition. As the monomers are mixed in the plasma stream they form highly randomized structures, which when deposited, exhibit characteristics of both components.[97,98] Despite the utility of the sublimation PECVD procedure on biological molecules, examples of robust and uniform binary plasma polymerized films utilizing them are very rare. Developing the capability of simultaneous depositions with different monomers, including bioactive compounds, highlights the versatility offered to the composition of the resulting plasma polymerized films.

In this study, the PECVD co-polymerization of sublimed amino acid (L-tyrosine) with vaporized liquid monomers, which results in stable and uniform ultrathin coatings with unique surface morphologies and characteristics is examined. PECVD co-polymerization of L-tyrosine (tyr) was carried out with several different monomers such as acrylonitrile, (ACN), 2-(hydroxyethyl)methacrylate (HEMA) and titanium tetraisopropoxide (TTIP). The organic and inorganic functional monomers used were chosen to demonstrate the feasibility of the integration of an amino acid with other synthetic materials which have been extensively studied to date. L-tyrosine was chosen for this study due to its important bioactive function in peptides, the expected

compatibility with sublimation PECVD, and the previously understood plasma deposition parameters.[44,96] It is hoped that L-tyrosine provides insight to the co-polymerization of biological molecules with other materials for many bio-interfacial applications.[14]

ACN was utilized due to its compatibility with our plasma deposition process. Many previous studies have evaluated this polymer and its deposition characteristics.[26,33,198] This fact allowed the focus of this deposition to be centered on controlling the tyrosine deposition rate for proper material mixing in the plasma. The HEMA is an example of a material which has been previously characterized and demonstrated as biologically compatible with its use in implants.[250,251] Previous studies have further characterized CVD HEMA as a swellable material.[42,43,74,252] Any future integration of biological materials to form composite films must include a second component which has been well characterized and is understood to be biologically compatible, such as HEMA.[253] In this study HEMA serves as a biocompatible material for co-polymerization as it has been previously combined with tyrosine through radicalization via peroxide and UV polymerization.[254] Finally, titanium tetraisopropoxide was used since it provides a facile method of introducing an inorganic component to the amino acid film. Creating such an interface on the micro- to nano-scale in this manner is potentially useful as an interface, which more easily allows the integration of implants with biological systems. The different materials selected here were simultaneously reacted during the plasma deposition to a) determine their ability to form ultrathin stable, robust, uniform coatings with chemically mixed composition and b) to determine the co-polymerization characteristics of biological molecules with organic and inorganic materials for fabrication of bioactive plasma polymerized coatings.

6.2 Experimental

Materials: All monomers, L-tyrosine (98%), acrylonitrile (99%), 2-(hydroxyethyl) methacrylate (97%) and titanium tetraisopropoxide (97%) were purchased from Sigma-Aldrich and used as received for all plasma processes described (Figure 6.1).

The sublimation of tyrosine in the PECVD chamber was run according to established procedure and utilized both downstream and plasma zone monomer inlets, where the sublimation boat was placed downstream of the plasma generating zone.[4,44,255] The specific configuration used in this study utilized the modified sublimation chamber with a heating crucible and an end cap containing a second inlet for the liquid monomer delivery (Figure 6.1).

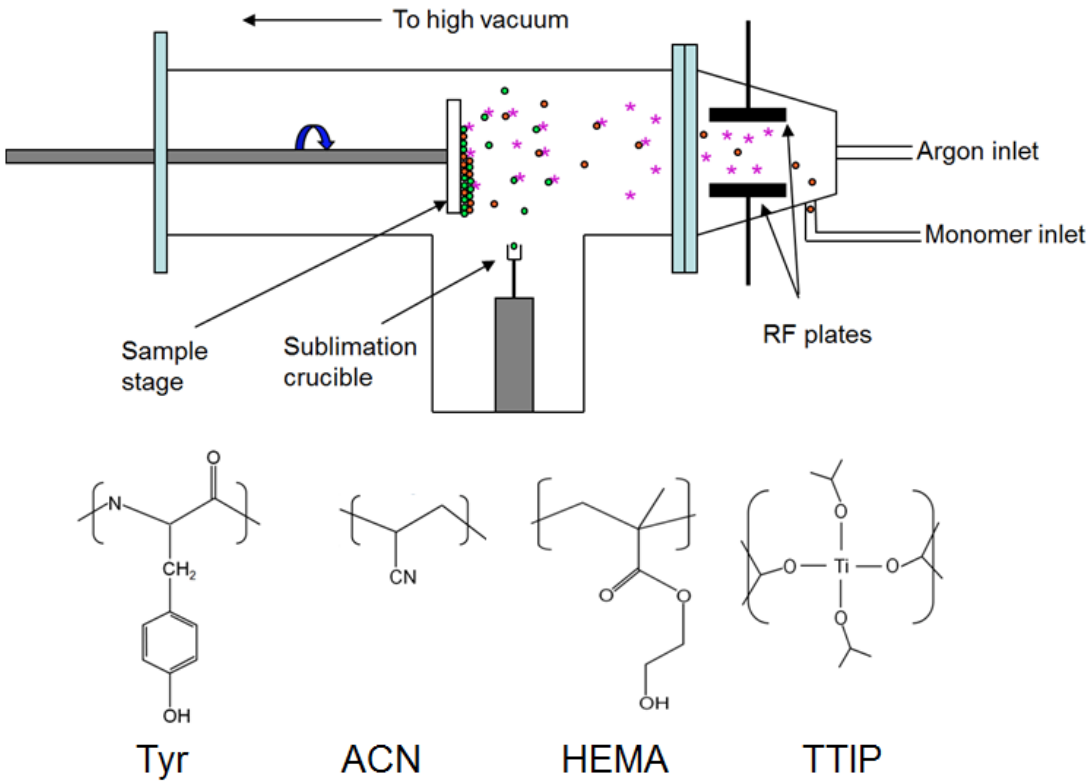

Figure 6.1: Chemical structures of compounds studied and diagram of sublimation PECVD chamber set up for co-polymerization with inlet for additional monomers showing flow of monomers to the surface in a random configuration. Circles represent monomers in the PECVD chamber while stars represent radicals.

The solid L-tyrosine monomer was placed in a restively heated tantalum crucible and heated to approximately 200ºC to begin the sublimation and then subsequently reduced to approximately 140ºC after sublimation had begun and held at this temperature for the remainder of the deposition. The monomers deposited in liquid form (ACN, HEMA, TTIP) were placed in a custom built vaporizing tube connected to the reaction chamber and heated to 60ºC in a water bath. The lines running from the vaporizing tube to the chamber were also heated to 60ºC to prevent condensation of the monomer in the tubes. The depositions of tyrosine, ACN, HEMA and all associated co-polymerizations were run under varying sets of conditions which were in the ranges listed: 20-45 W power, 0.05-0.1 Torr operating pressure, 20-50 sccm Ar carrier gas flow rate and 6-12 minute deposition time. The variation in conditions allowed for control of the cross-linking density of the film.[84] The TTIP depositions were run under identical conditions with the addition of an oxygen carrier gas at 20-50 sccm instead of argon. This was used for both pure PP-TTIP and PP-Tyr/TTIP films.

6.3 Results and Discussion

6.3.1 Single Material Depositions

Prior to beginning co-polymerization PECVD experiments, each monomer was plasma polymerized and characterized independently to evaluate the quality of ultrathin films formed. All monomers were deposited on clean silicon substrates and characterized by AFM to determine the morphology of the PECVD films and the mechanical stability of each coating. All films were deposited to a thickness of between 200-300 nm as measured by spectroscopic ellipsometry and were characterized with FTIR and XPS to determine the composition in addition to AFM. Significant differences were noted in the morphology between the four materials evaluated here.

AFM imaging shows the resulting depositions of all materials on clean silicon surfaces (Figure 6.2, Figure 6.3). The dry L-tyrosine (PP-Tyr) powder was sublimed for deposition (Figure 6.2 A, Figure 6.3 A). The liquid acrylonitrile (PP-ACN) monomer was plasma polymerized by the standard vaporization method (Figure 6.2 B, Figure 6.3 B) and the liquid HEMA (PP-HEMA) monomer was heated to 60ºC and deposited as a standard vapor deposition (Figure 6.2 C, Figure 6.3 C). Large-scale AFM images show very uniform surface morphology of all films indicating highly homogeneous composition with low surface microroughness that is indicative of uniform cross-linking and wetting. These films are free of pinhole defects as well. This observation is in good agreement with previous studies of tyrosine and published literature regarding HEMA.[42,44] The surface microroughness of each sample was measured to be 0.6 nm, 0.3 nm and 0.4 nm for PP-Tyr, PP-ACN and PP-HEMA, respectively, which correspond to values usually reported for PECVD films.[85] These values correlate well with our previous data for microroughness of the various polymer and amino acid films obtained via PECVD.[33,44]

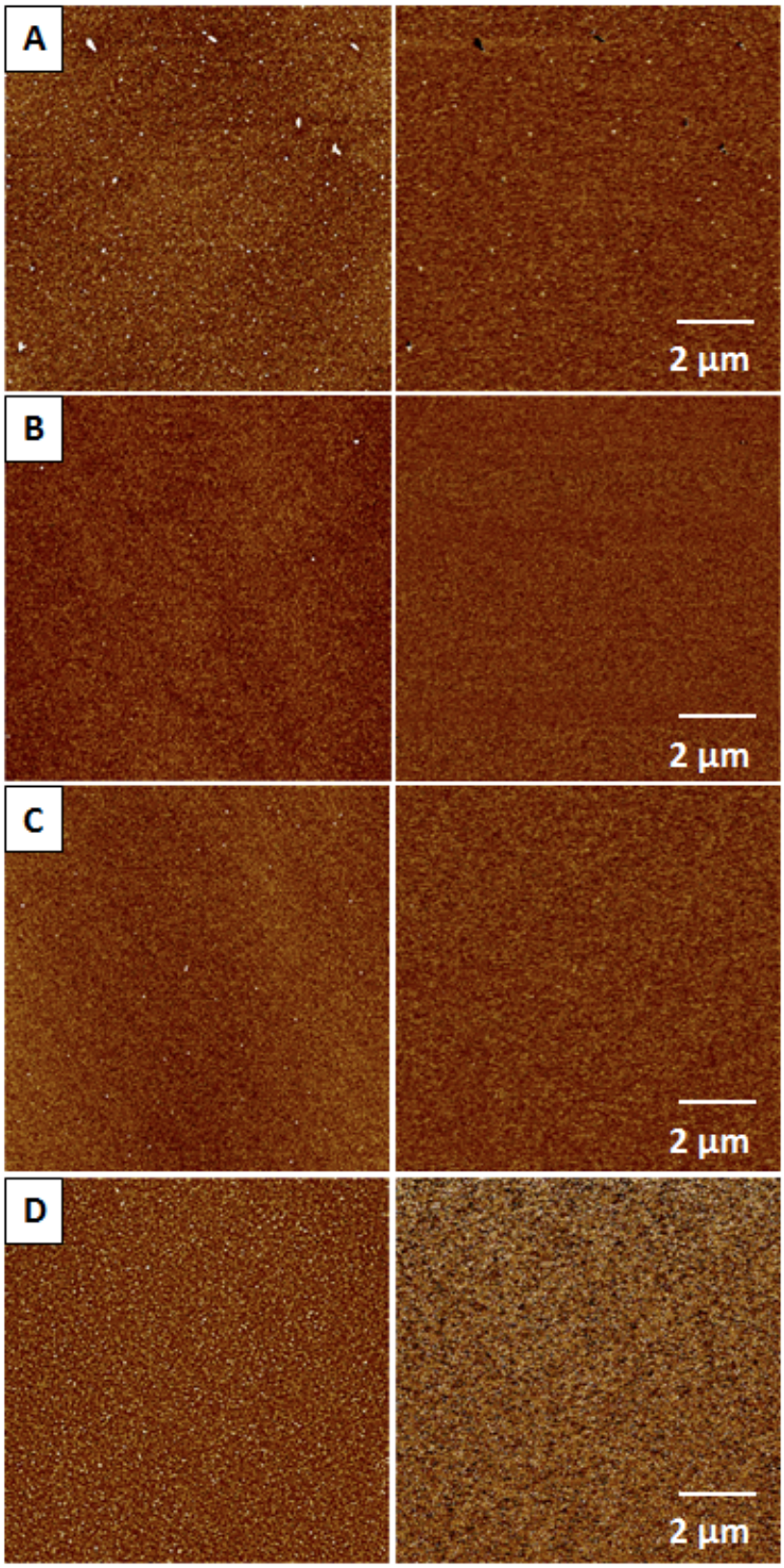

Figure 6.2: AFM images of A) PP-Tyr, B) PP-ACN, C) PP-HEMA and D) PP-TTIP coatings. The left images show the topography (z (A,B,C) = 4nm, z (D) = 24nm) and the right images show the relative surface stiffness (arbitrary z scales).

High magnification AFM images show the differences in the fine morphologies of the plasma polymerized films of each coating (Figure 6.3). The PP-Tyr film shows a distinctive morphology composed of many small, distinct needle-like domain structures

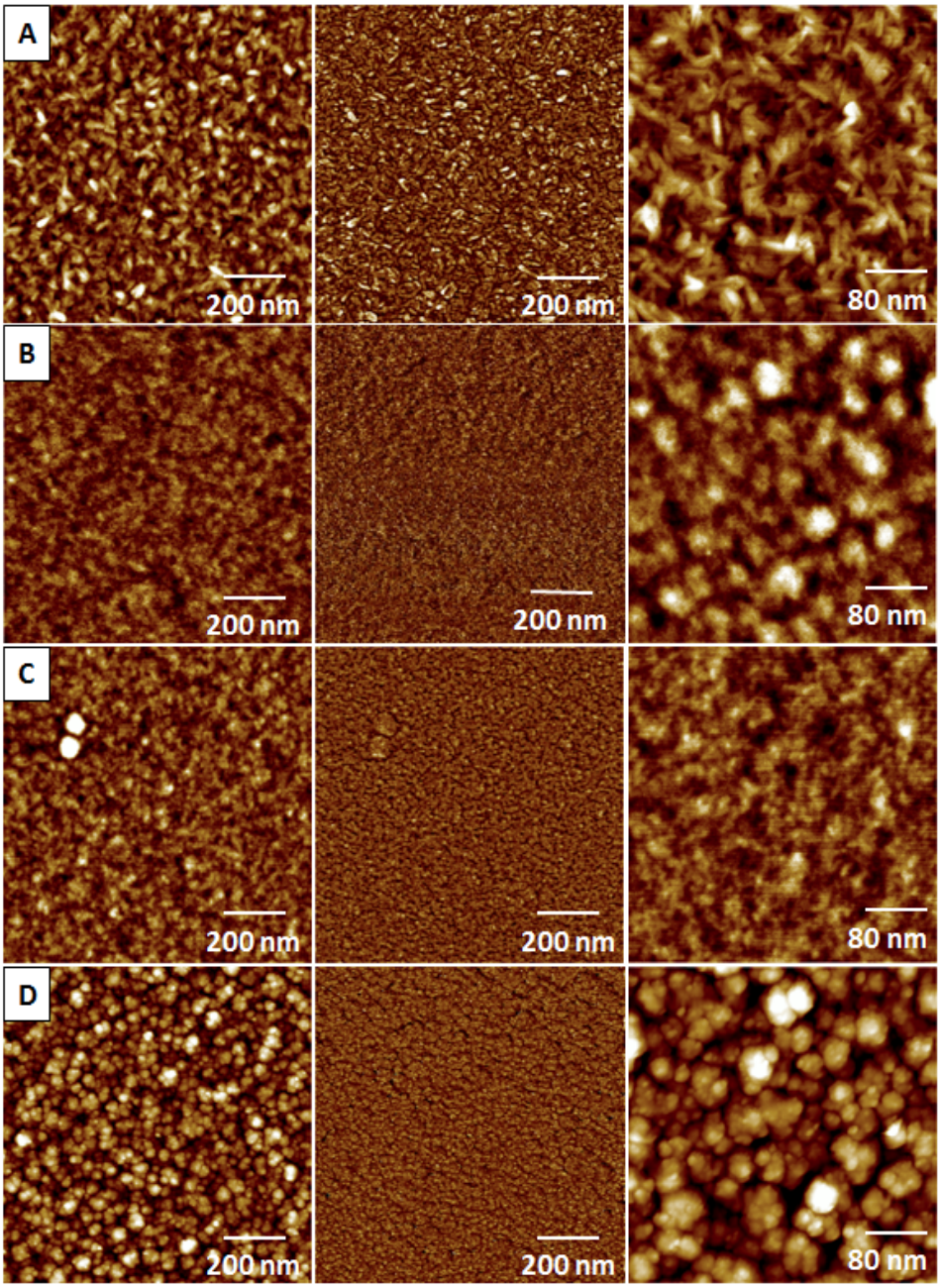

Figure 6.3: High resolution AFM images of A) PP-Tyr, B) PP-ACN, C) PP-HEMA and D) PP-TTIP coatings. Left: topography (z (A,B,C) = 4nm, z (D) = 24nm). Center: relative surface stiffness (arbitrary z scales). Right: High resolution topography (z = 4nm (A), 6nm (B), 3nm (C), 24 nm (D)).

(~50 - 100 nm in length and diameter below 10 nm) which differs from the more uniform texture features of PP-ACN and PP-HEMA films where dimensions of isolated round grains are within 20 - 50 nm. The PP-Tyr structure becomes clearly evident under the highest resolution scanning (300 nm x 300 nm) where it is observed that the domains are in fact individual tubular structures in random orientations on the surface (Figure 6.3 A, right image). Three organic films show significant differences in morphology, structure and roughness when compared to the much rougher PP-TTIP inorganic coating. These distinctions in film morphology are important to note, as they govern properties such as microroughness and show that each material will deposit in a unique manner, even under similar deposition conditions.

The PP-TTIP film was deposited in an oxygen rich atmosphere as a homogenous film on a larger scale and showed a coarse grainy surface with a high porosity composed of aggregated and coarser features with cluster dimensions above 40 nm which are composed of 10-20 nm round grains (Figure 6.3 D). Such morphology results from the plasma deposition in the presence of oxygen as previously reported.[256,257] According to previous studies, the resulting porous surface is a product of the deposition in an oxygen rich environment in which the titanium atom of the TTIP will completely radicalize to a Ti^{4+} state. This is in contrast to the partial radicalization (Ti^{3+}) which occurs in a pure argon environment and is resistant to complete oxidation upon removal from the vacuum.[93,258,259] The surface microroughness of the PP-TTIP film was measured at 3.6 nm, which is much larger than that measured for the organic and biological plasma deposited films and larger than that of a PP-TTIP film deposited under an argon atmosphere. The oxygen rich deposition was used as a method to promote the highest possible valence state of the titanium atom allowing for an increased number of bonding sites for oxygen which creates titania molecules with a 2:1 oxygen:titanium

stoichiometry. In some instances, the introduction of oxygen may provide a non-ideal deposition regime for the second material as oxidation can occur. However, it was observed that the resulting co-polymerized films were stable when deposited with oxygen present in the chamber and were not significantly affected by this change in the atmosphere. Some reports have recently demonstrated that crystalline titania can be formed on the surface through O_2 plasma depositions at low temperatures, but the mechanism behind this remains under investigation.[260]

The AFM images of each of these materials show the topography and the surface DMT modulus distribution (in relative units) obtained from peak force mode scanning (Figure 6.2, Figure 6.3).[261] In addition to smooth topography, all coatings exhibit a uniform surface stiffness across the surface with very modest variation indicating that there are no local surface regions of dramatically different mechanical properties and thus the uniform distribution in cross-linking density of the plasma deposited films can be suggested. When compared to the traditional spin cast films of the same materials (both monomer and polymer coatings), the plasma deposited films were seen to be much more stable, have greater adhesion to substrates and be more uniform, albeit ultrathin coatings.

6.3.2 Chemical composition of single material films: FTIR studies

Chemical composition of plasma polymerized films was evaluated from FTIR spectra with several characteristic peaks detectable for each monomer (Figure 6.1, Figure 6.4, Table 6.1). The PP-Tyr film shows key absorption peaks around 3200 cm^{-1} which corresponds to the O-H stretch, and around 3000 cm^{-1} representing an amine peak (Figure 6.4 A).[185] The preservation of the ring structure during plasma-assisted polymerization is confirmed by the presence of peaks at 1610 cm^{-1}, 1514 cm^{-1} and 1332

cm^{-1} which correspond to the intact aromatic ring C-C double and single bond vibrations.[184] The peak seen at 1257 cm^{-1} confirms the presence of O-H groups attached to the aromatic ring. The NH_2 bending vibration peak occurring at 829 cm^{-1} in the PP-Tyr film has been previously observed to be a marker present in poly-tyrosine which shifts during cross-linking from an original position of 876 cm^{-1}.[44] This band is a key indicator of the cross-linking that is occurring in the film as it is deposited.

The FTIR spectrum for the PP-ACN film shows several intense peaks indicative of a high degree of cross-linking (Table 6.1, Figure 6.4 B). The first is seen as a large, broad peak around 3270 cm^{-1} present from the N-H stretching and the second is the C=N stretching mode seen around 1675 cm^{-1} along with the peak at 1092 cm^{-1} from the C-N

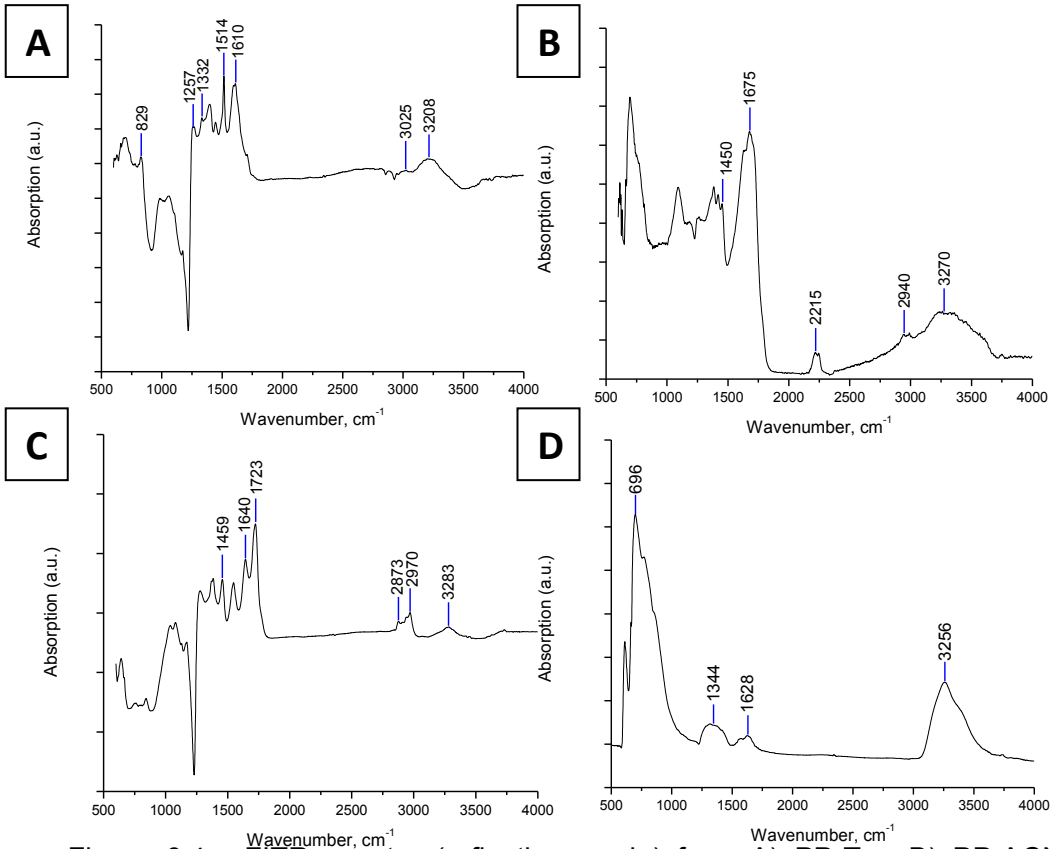

Figure 6.4: FITR spectra (reflection mode) from A) PP-Tyr, B) PP-ACN, C) PP-HEMA, D) PP-TTIP coatings.

which results from the cyano group dissociation and cross-linking.[33] The observed peaks of CH_2 stretching at 2940 cm^{-1} and C-C stretching at 1450 cm^{-1} are also indicators of the preservation of backbones. The C≡N stretch seen around 2215 cm^{-1} is characteristic of the cyano group, indicating its presence in the plasma deposited film.

The PP-HEMA spectra exhibits several characteristic peaks including a broad O-H stretch around 3283 cm^{-1} and a C=O stretch at 1723 cm^{-1} (Figure 6.4 C).[74] Both of these groups are seen in the side structure and their presence indicates that they remained intact during the plasma deposition. Additional side chain peaks also seen are a CH_2 asymmetric stretch at 2970 cm^{-1} and CH_3 symmetric stretching at 2873 cm^{-1}, CH_2 in plane bending at 1459 cm^{-1} and C-O-C asymmetric and symmetric stretching vibrations at 1079 cm^{-1} and 1037 cm^{-1}. As indicated by Pfluger *et. al.* the absence of a peak in the range of 3060-3010 cm^{-1} and at 1600 cm^{-1} indicates that no H-C=C structure is present in the PECVD film indicating no residual monomer, as this double bond structure is not expected in a polymerized HEMA film. Also, the OH peak around 3300 cm^{-1} is expected to be minimized with higher cross-linking, which is the case in the sample measured, indicating that significant cross-linking is occurring in the PP-HEMA film.[252] This agreement of the measured PP-HEMA films with established literature values provides strong evidence of efficient polymerization occurring under given plasma deposition conditions.[42,89]

Finally, the PP-TTIP film exhibited a characteristic Ti-O peak near 700 cm^{-1} (Figure 6.4 D). The peak seen is expected to contain minimal contributions from the silicon substrate as these peaks were carefully accounted for during the measurements and result primarily from the convolution of the Ti-O and residual carbon peaks indicating polymerization reactions in accordance with known mechanisms.[262] In this case,

additional carbon peaks are seen at 1628 cm^{-1} and 1344 cm^{-1} that correspond to the C=C and CH_3 bending vibrations, respectively.[258] The O-H stretching peak at 3256 cm^{-1} is also consistent with the predicted reaction products as well as a result of the silicon substrate used where surface hydroxylation occurs during the cleaning process. This spectrum confirms the presence of the titania as well as expected by-products from the dissociation of the TTIP monomer during the plasma deposition.

Table 6.1: List of polymerized films with FTIR peak assignment.

	PP-TYR	PP-ACN	PP-HEMA	PP-TTIP	PP-TYR/ACN	PP-TYR/HEMA	PP-TYR/TTIP
NH stretching		3270				3263	
OH stretch	3208		3283	3256	3204		3200
Amine peak	3025				3024		
CH_2 asymmetric stretch		2940	2970		2962	2935	
CH_3 symmetric stretch			2873			2875	
C≡N stretch (cyano)		2215			2220		
C=O stretch			1723			1725	
C-C stretch	1610	1675	1640	1628	1611	1611	1612
C-C/C-H (ring)	1514				1515	1516	1515
CH_2 inplane bending		1450	1459		1452	1456	1447
C-C stretch	1332			1344	1331	1330	1330
ring OH vibration	1257				1244	1247	1250
NH_2 backbone bending	829				840	839	857
Ti-O				696			697

Overall, FTIR results discussed above confirm that the PECVD coatings contain key functional groups intact and are not structurally compromised. The data also indicates that chain formation and cross-linking are occurring among the monomers as they are deposited.

6.3.3 Chemical composition of single material films: XPS analysis

XPS analysis of the plasma polymerized coatings confirms the expected presences of the chemical elements corresponding to the monomers original chemical structures (Figure 6.1, Figure 6.5). PP-Tyr and PP-ACN showed the expected carbon, nitrogen

and oxygen peaks whereas the PP-HEMA shows only the carbon and oxygen peaks (Figure 6.5 A,B,C; Table 6.2). The PP-TTIP film shows a strong Ti peak as well as significant oxygen with some residual carbon content in the film (Figure 6.5 D). The residual carbon in the PP-TTIP film results from the number of methyl groups attached to the oxygen atoms, which react to form a separate carbon system that was deposited on the surface as detailed elsewhere.[258]

The measured compositions generally correspond to theoretically calculated ones based on the chemical structures of the monomers (Table 6.2), but with some notable differences. This correlation indicates that the plasma deposited films are maintaining roughly the same atomic composition of the monomers, except for a few cases, notably PP-HEMA which shows an excess of carbon, likely resulting from surface carbon

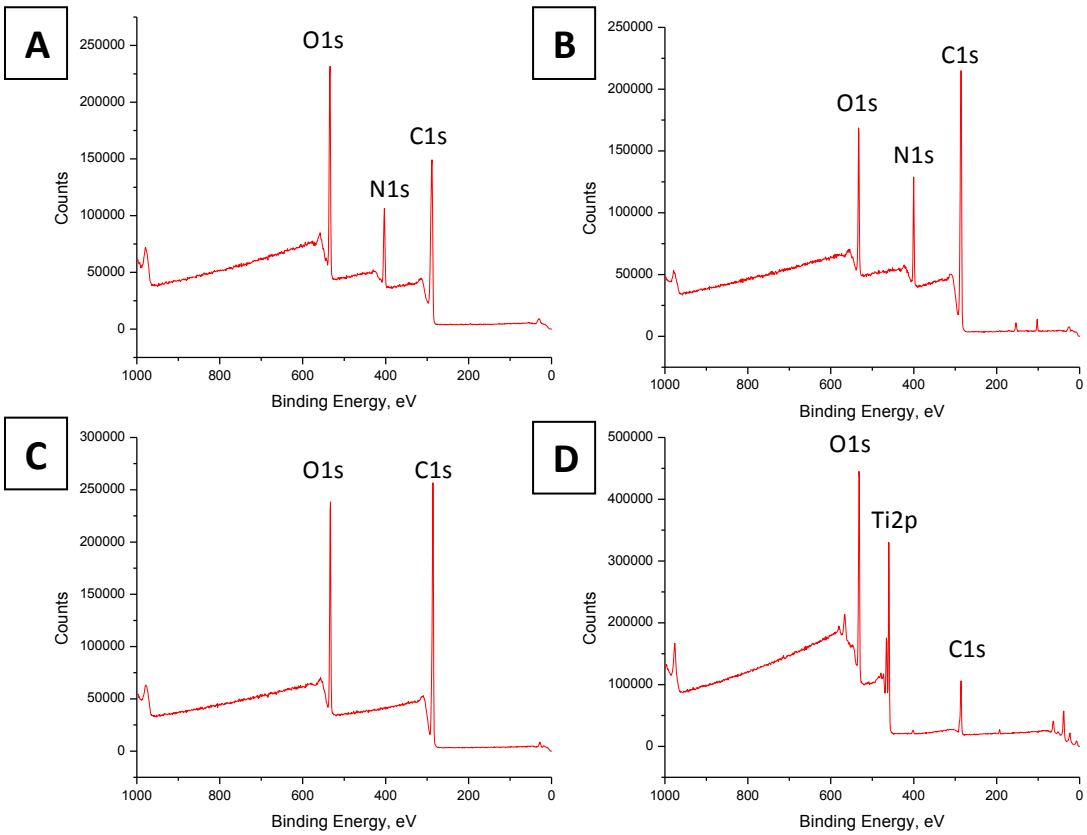

Figure 6.5: XPS plots for A) PP-Tyr, B) PP-ACN, C) PP-HEMA, D) PP-TTIP coatings.

contamination. Both the PP- TTIP films shows less carbon and more oxygen than expected which is likely due to the loss of the carbon as a byproduct of the deposition which is aimed at capturing the titanium and oxygen on the surface. Since this deposition was done in an oxygen rich plasma, contributions to the oxygen content of the film could also be present from this source as well as absorption from the atmosphere, as is likely the case with PP-ACN.[259] Another likely reason for discrepancies is that theoretical compositions are assumed to have an equal portion of each monomer. In reality, it is unlikely that this is the case as flow rates of the co-polymerized monomers were not monitored closely enough to confirm this.

Table 6.2: Atomic percentages of key elements from XPS data.

	Theoretical composition					**Experimental results**			
Compound/composition	C	O	N	Ti		C1s	O1s	N1s	Ti2p
Tyr	59.6	26.5	7.7	0.0		68.5	21.8	9.7	0.0
ACN	67.8	0.0	26.4	0.0		71.0	13.5	12.8	0.0
HEMA	55.3	36.9	0.0	0.0		77.6	22.4	0.0	0.0
TTIP	50.7	22.5	0.0	16.9		34.1	48.2	2.0	15.9
Composite films									
Tyr/ACN	61.5	20.5	12.0	0.0		69.6	21.2	7.5	0.0
Tyr/HEMA	57.8	30.8	4.5	0.0		75.4	21.6	3.0	0.0
Tyr/TTIP	54.1	24.1	3.0	10.3		69.2	22.9	6.8	0.0

6.3.4 Co-polymerizations of different compounds

The first co-polymerization of L-tyrosine and ACN was carried out with simultaneous use of the sublimation apparatus and vapor bubbler to introduce both materials to the plasma reactor. Care was taken to match the deposition rates of the two materials so as to minimize non-uniformity of mixed films and deposit approximately similar amounts of each monomer. Similar deposition rates helped keep the film at controlled composition ratios and also made the films much less likely to delaminate from the surface after removal from the chamber. Matching the deposition rates was done by first depositing

the PP-Tyr on a clean silicon wafer and measuring the thickness, giving a deposition rate calibration for a particular set of conditions. These conditions were then verified as

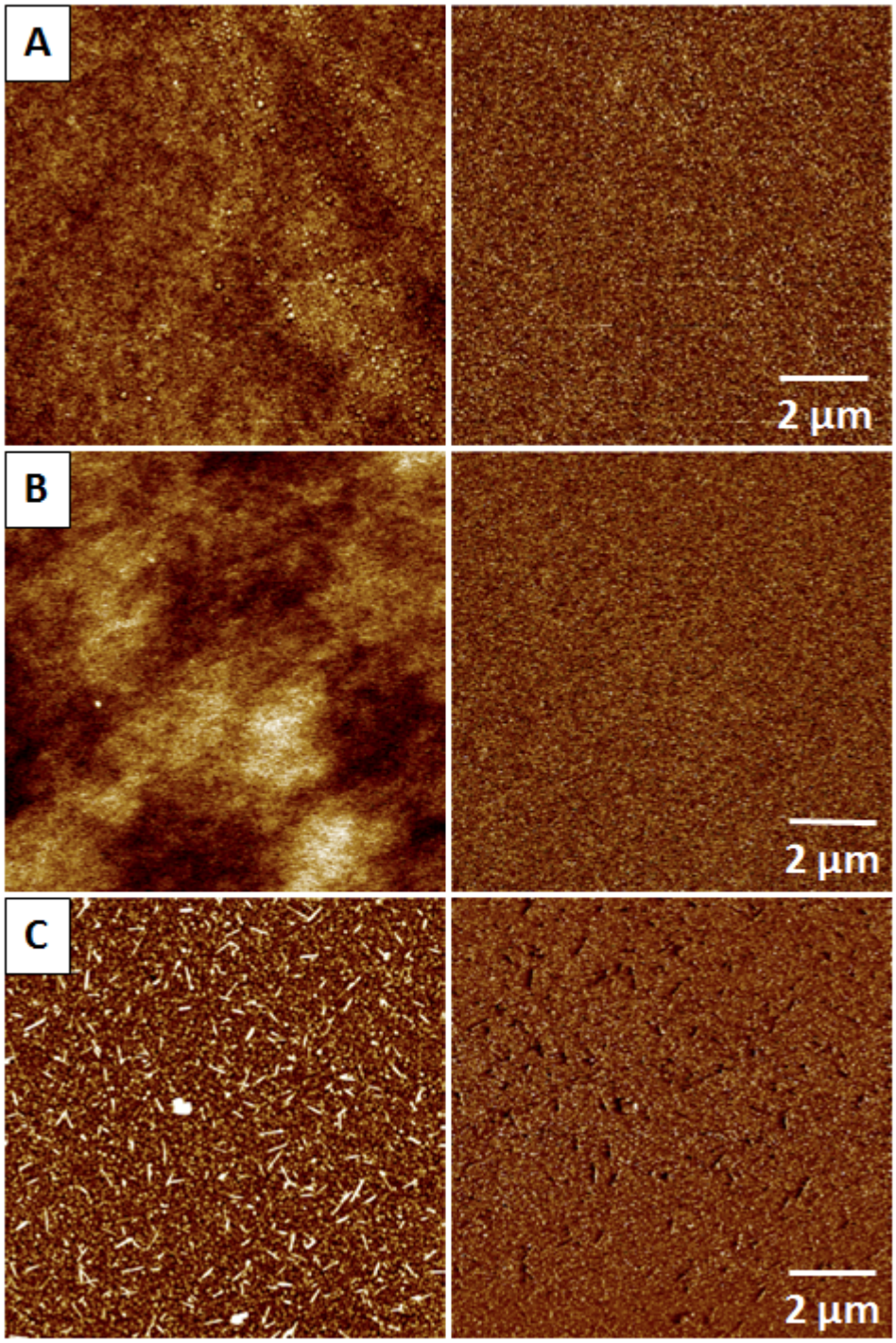

Figure 6.6: AFM images of co-polymerized films: A) PP-Tyr/ACN, B) PP-Tyr/HEMA and C) PP-Tyr/TTIP. Left: topography A (z=14 nm), B (z=8 nm), C (z=24 nm). Right: surface stiffness (arbitrary z scales).

viable for the deposition of the second monomer and an appropriate monomer flow rate for the second monomer was then calibrated so the two monomers could be simultaneously deposited.

At large scale, the resulting composite films from two different monomers are relatively smooth and defect free showing relatively few features (Figure 6.6). An increase in the surface microroughness was observed when compared to the two single material depositions. The microroughness was measured at 1.4 nm which represents a three-fold increase over that of the single monomer films. Mixing two monomers results in the network having local variations in the chemical structure and a grainy morphology which increases the overall roughness of the film. This can happen if the monomers aggregate or in the case of the PP-Tyr/TTIP, form unique structures upon plasma polymerization. The typical surface feature size ranges from 5-10 nm in height and approximately 10-50 nm laterally, depending on the films composition. Overall surface stiffness remains relatively uniform on a large scale confirming the absence of microscopic dewetting and aggregation.

Next, L-tyrosine and HEMA monomers were deposited on the silicon surface simultaneously while under an argon atmosphere. The deposition rates of the L-tyrosine and HEMA were matched so that the deposition occurred with a deposition rate of approximately 20 nm/min. Heating of the L-tyrosine monomer was begun prior to engagement of the plasma so that the material would be subliming as soon as the plasma was activated and HEMA introduced to the system. Both the ACN and the HEMA monomers deposited similarly with the L-tyrosine but produced dissimilar features in the final film.

An interesting and distinct microstructure was observed in the composite film that is not seen in either of the monomer films under high resolution AFM imaging (Figure 6.7 A,B,C). The surface stiffness distribution shows some inhomogeneities which are also seen in the topography. These variations of topographical features are measured to be less than 4 nm in height and are only clear at the highest magnifications. The PP-

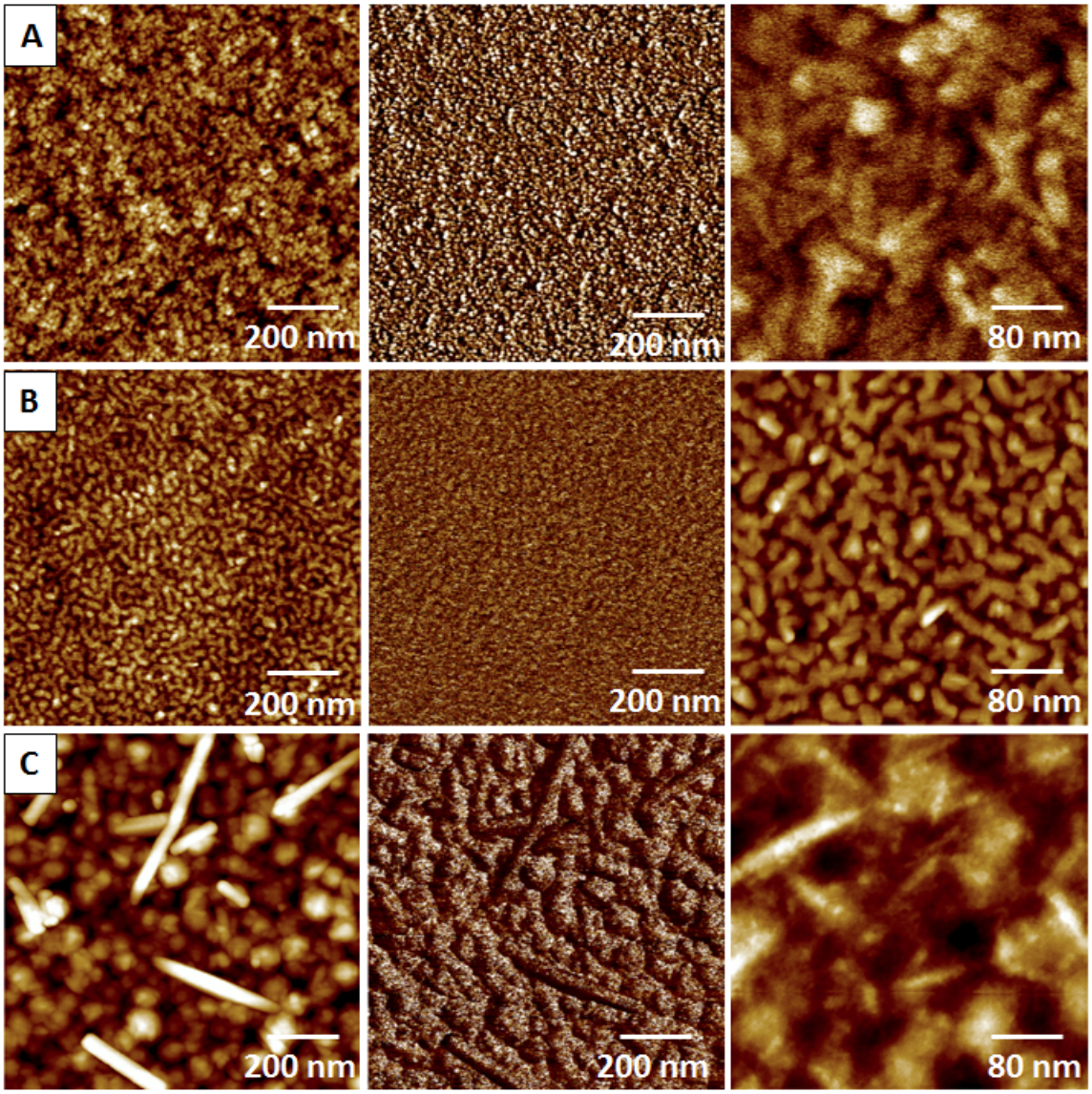

Figure 6.7: High resolution AFM images of composite films: A) PP-Tyr/ACN, B) PP-Tyr/HEMA and C) PP-Tyr/TTIP. Left: topography A (z=14 nm), B (z=8 nm), C (z=24 nm). Center: surface stiffness (arbitrary z scales). Right: High resolution topography (z = 8nm (A), 8nm (B), 16nm (C)).

Tyr/ACN film shows tubular-like structures very similar to that observed for the PP-Tyr film but in a much more diluted version. A distinctive morphology also seen in the PP-Tyr/HEMA film is reminiscent of the appearance of a microphase separated system at the nanoscale, but is not necessarily an indicator of this phenomena occurring and may be a product of a reaction during polymerization or other structural formation similar to the tyrosine nanotubes of the PP-Tyr/TTIP. It is apparent that there are no tubular-like PP-Tyr morphological structures seen in the PP-Tyr/HEMA film. These structures are are seen in both the PP-Tyr/TTIP and high resolution PP-Tyr/ACN AFM images. A more uniform weakly phase separated surface is seen in the PP-Tyr/HEMA. The co-polymerized PP-Tyr/HEMA film was seen to be defect free with a measured surface microroughness of 0.8 nm, an increase over the pure PP-HEMA film.

The final co-polymerization study utilizing the liquid inorganic component, titanium isopropoxide and the solid L-tyrosine was conducted with the two monomers being vaporized and exposed to the plasma simultaneously. The titanium isopropoxide was heated in a liquid state to facilitate vaporization, while the L-tyrosine was sublimed in the same manner used for the single monomer depositions. The combination of these two materials showed a highly unique microstructure consisting of large needle-like structures embedded in a uniform matrix. This structure has not been observed in any of our previous plasma deposition studies (Figure 6.6 ,Figure 6.7 C). These needle-like structures are prominently visible in the adhesion channel and typically measured 200-600 nm in length and 20-25 nm in height (Figure 6.8). These needle-like structures are likely composed of PP-Tyr structures, which have grown to larger sizes as compared to the nanoscale features seen on the PP-Tyr film. These features are much more reminiscent of the amino acid nanotubes formed under vapor deposition as reported in the literature and could be forming through a similar route.[39,263]

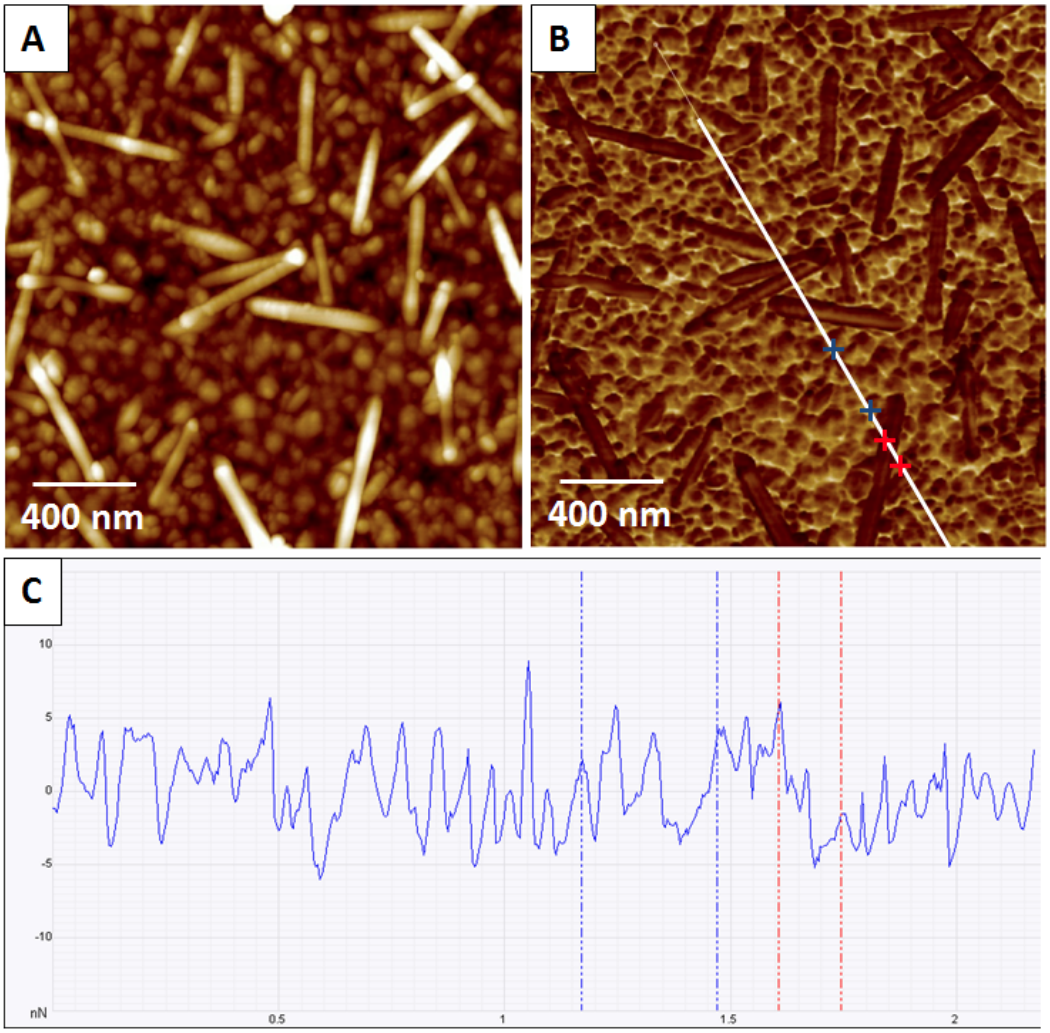

Figure 6.8: AFM image showing A) height image of needles B) relative adhesion of the PP-Tyr/TTIP needle structures and C) topography cross-section (along white line in (B)) detailing the height and width (nm) of the needles.

These studies suggest that the formation of tubular structures based upon tyrosine is possible under vacuum deposition conditions.[37] These structures are likely seen on the surface of the film as sublimation will continue for a short time after the heating crucible and plasma are switched off while the crucible cools. Tubular structures from amino acids are well documented under this type of physical vapor deposition and will cover the surface with pure tyrosine, masking the titanium signal when evaluated via XPS. Any large scale or repeated microphase separation in the system is unlikely due to the

rapid step growth mechanisms, as there is thought to be insufficient time for such a phase separation to occur before the layer is immobilized by more monomer polymerizing on top. Local inhomogeneities may well exist in the film as the plasma deposition process is subject to a degree of monomer mixing and randomness during the deposition and a truly homogenous film would require perfect distribution of the vaporized monomers. Additionally, some radicals go unreacted and are held in place through the cross-linked network which is formed and do not permeate from the film. This would imply that any phase separation occurring after the deposition is unlikely and the patterns seen in the mixed films are forming during the plasma deposition and the monomers are not simply separating after the removal from the plasma.

These needle-like structures are dramatically different in comparison to the shapes reported for titania structures deposited under oxygen at 298 K.[256] Previous studies have shown titania structures with the round and pitted features seen on our films by AFM (Figure 6.3 D). No needle-like, lateral features across the top of the film were reported, only vertical features running though the depth of the deposited layer were of prominence. Second, the surface stiffness map shows some relative change in the mechanical properties of the features (Figure 6.7 C). This is an indication that while features are forming in the film during deposition, they are of a varied composition and some stiffness contrast is observed as would be expected for titania-based structures, with the tubes being slightly less stiff. Third, needle-like structures show low adhesion when compared to the rest of the surface which should be expected for a crystal surface in comparison with disorganized surrounding surface (Figure 6.8 B). Finally, the absence of clear titanium signal in the XPS scan indicates that the upper surface structure is not composed of titanium containing material.

6.3.5 Chemical composition of composite films: FTIR, XPS, and spectroscopic ellipsometry

Common characteristic peaks on FTIR spectra are seen for the composite films and the single material films (Table 6.1, Figure 6.9). PP-Tyr/ACN showed major absorption peaks from each monomer including the C≡N stretch of the cyano group seen near 2220 cm^{-1}, the broad O-H peak of tyrosine centered near 3200 cm^{-1} combined along with broad amine peaks and C-H peaks near 3000 cm^{-1} and 2960 cm^{-1}.[33,185] Additional peaks correspond well with the remaining PP-Tyr peaks seen in the single material film, especially those of the aromatic ring at 1611 and 1515 cm^{-1}. The C=N stretch seen in the PP-ACN film is still present near 1675 cm^{-1}, but is convoluted with the aromatic ring peak of the PP-Tyr and not readily visible. The PP-Tyr/HEMA composite film shows all of the characteristic FTIR peaks of the PP-Tyr film in addition to the C=O stretch seen in PP-HEMA at 1725 cm^{-1}.

Peaks were also seen near 1160 cm^{-1} indicating C-O bonding, the C-O-C asymmetric and symmetric vibrations seen at 1079 cm^{-1} and 1037 cm^{-1} and the characteristic amide bonding near 1247 cm^{-1}. The PP-Tyr/TTIP film is seen to retain the Ti-O peak at 697 cm^{-1}, indicating the presence of titania. The peak is shifted and obscured from Si-C bonding, which occurs as the deposited material attaches to the substrate. Previous studies of tyrosine/HEMA grafting have reported radicalization of the –OH group on the tyrosine via peroxide exposure which served as an attachment site for HEMA.[254] Similar bonding characteristics were observed with the co-polymerization of tyrosine and HEMA. Literature reports that previous studies were carried out on tyrosine attached to a collagen surface and directly modified through peroxide exposure and surface radicalization to bond to free HEMA monomer.

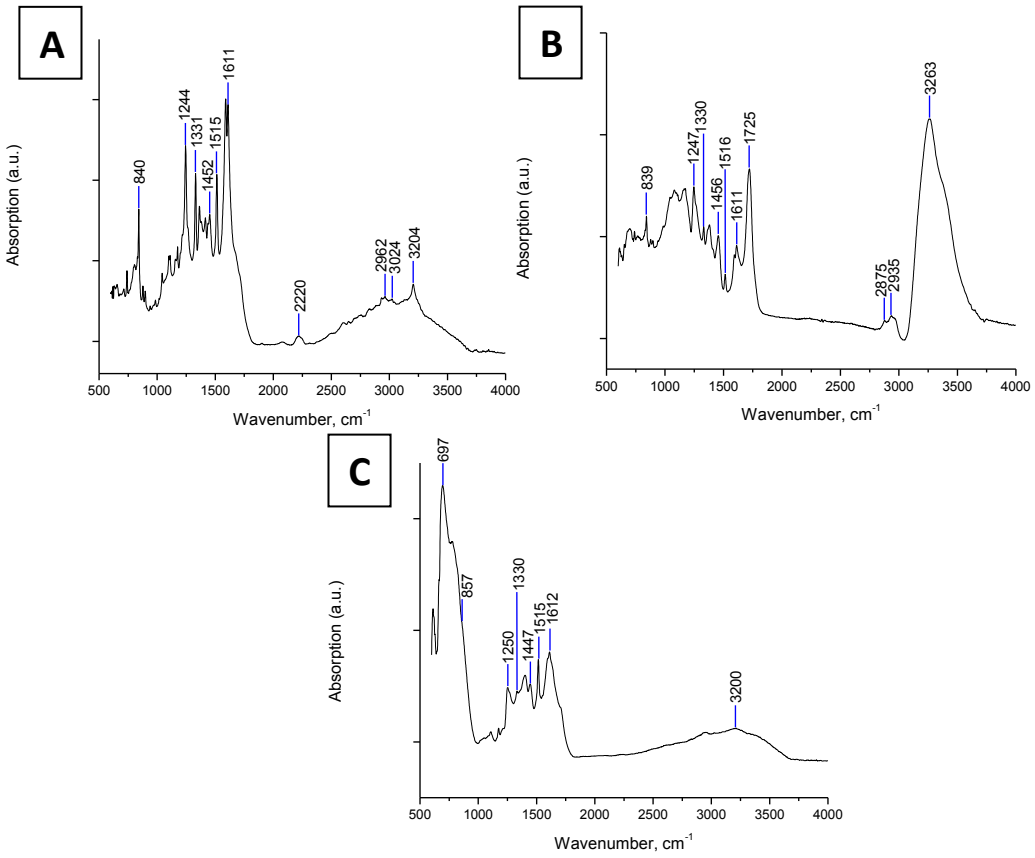

Figure 6.9: FTIR spectra (reflection mode) of composite films: A) PP-Tyr/ACN, B) PP-Tyr/HEMA, and C) PP-Tyr/TTIP.

All of the co-polymerized films show peaks that are consistent with the tyrosine ring structure remaining intact and selected marker peaks from the second component indicating that co-polymerization is occurring and resulting in a cross-linked film with a mixed composition. This shift from the L-tyrosine position of 876 cm^{-1} is seen in all the composite films at 840 cm^{-1}, 839cm^{-1} and 857 cm^{-1} for PP-Tyr/ACN, PP-Tyr/HEMA and PP-Tyr/TTIP respectively. The PP-Tyr/TTIP peak at 857 cm^{-1} is determined through de-convolution of a single larger peak seen and represents our best estimate. All the peak shifts of this NH_2 peak in the co-polymerized films are less than that of the L-tyrosine to PP-Tyr which indicates that the monomers are forming bonds near this position in the molecular structures. The shift shows that this is occurring between the two monomers

and they are not solely polymerizing as isolated monomers. It is noted that this NH_2 peak does not appear in the PP-ACN film and is a characteristic peak of the tyrosine. These results indicate the presence of tyrosine and the consistent shift seen in the co-polymerized films likely results from the NH_2 acting as a bonding site leading to the conclusion that true co-polymerization of the monomers is occurring during the plasma deposition.

XPS of the co-polymerized films shows the expected characteristic peaks of the PP-Tyr/ACN, PP-Tyr/HEMA and PP-Tyr/TTIP with strong peaks of carbon, nitrogen and oxygen as demonstrated in a representative observational XPS plot (Figure 6.10 A). The atomic percentage distributions show the presence of the expected elements in the films and generally correspond to the theoretical predictions of composition (Table 6.2). The theoretical atomic percentages were estimated assuming a 1:1 ratio of the mixed monomers. While the PP-Tyr/ACN and PP-Tyr/TTIP have values that are in general agreement to the expected values for 1:1 mixture, the PP-Tyr/HEMA shows an increased carbon (and thus decreased oxygen) content in the co-polymerized film similar to the PP-HEMA film. The expected nitrogen signal from the tyrosine is present in the PP-Tyr/HEMA film but not in the PP-HEMA film which indicates the presence of both monomers in the PP-Tyr/HEMA film. The excess carbon seen in all samples is likely carbon contamination which commonly occurs on the surface of plasma polymerized films.

High resolution XPS spectra of the carbon content in the PP-Tyr/ACN and the PP-Tyr/HEMA films show a shift of the carbon peak shoulders consistent with combining the two monomers (Figure 6.10 B,C). The primary peaks corresponding to C-C and C-H bonds are present in all single material films. De-convolution of all carbon peaks was

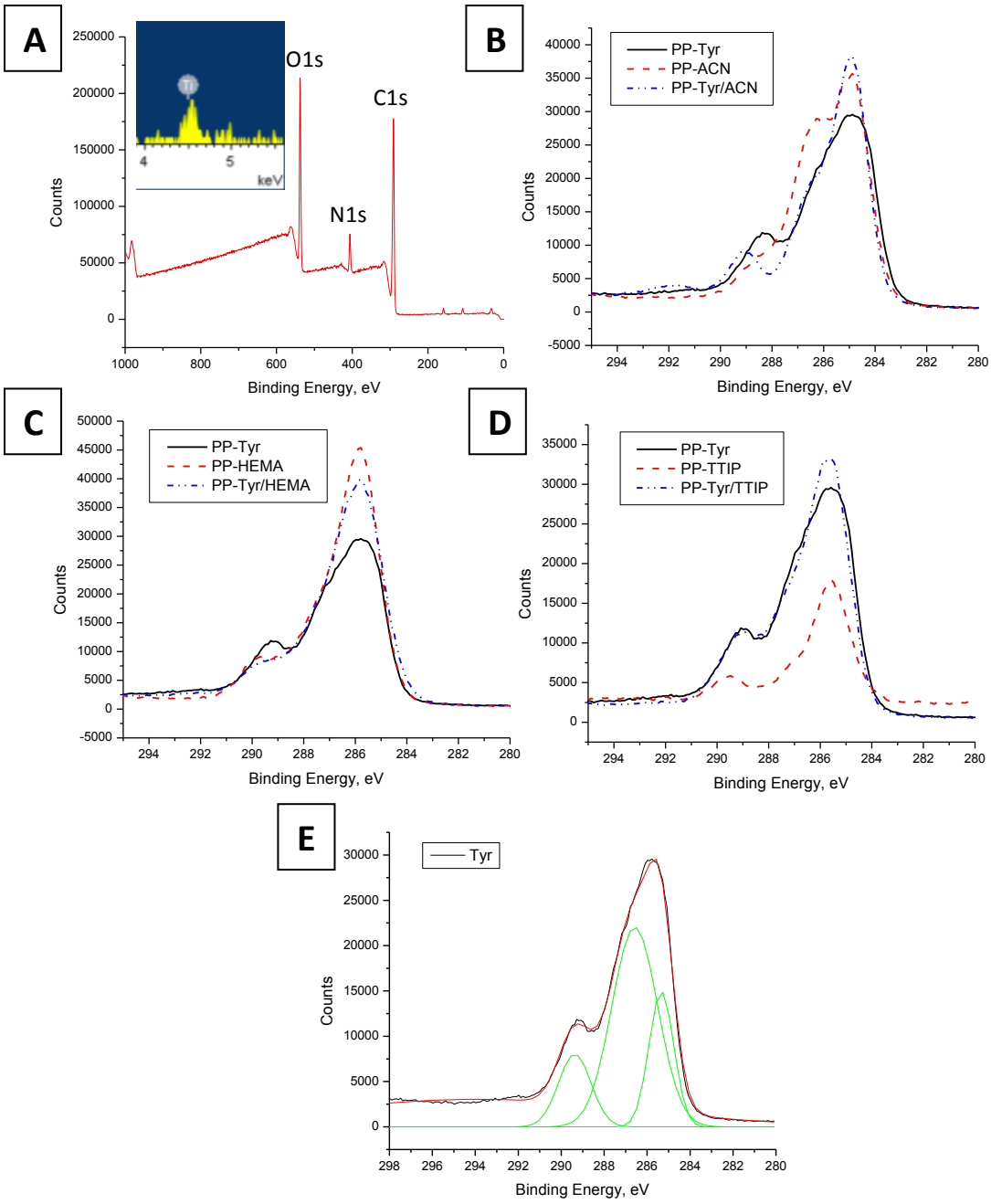

Figure 6.10: XPS of composite films A) PP-Tyr/TTIP (inset: EDS spectrum). High resolution XPS scan of Carbon region: B) PP-Tyr and PP-ACN films, C) PP-Tyr and PP-HEMA films D) PP-Tyr and PP-TTIP films E) representative plot showing peak de-convolution of the PP-Tyr film.

performed to determine the exact position of all the peaks (see one example in Figure 6.10 E). The PP-Tyr/ACN films shows C=O bonds (289.1 eV) not present in the PP-ACN film and a reduced presence of the C-N (286.3 eV) with the addition of the C-C

(284.5 eV) bonds from tyrosine.[264] The same C=O shoulder is seen in the PP-HEMA films (289.6 eV) as well and is expected based on its chemical structure. The PP-Tyr/TTIP XPS spectrum shows clear C-C, C-H (285.6 eV) and C-O (289.0 eV) peaks with a broadening of the primary peak from the addition of C-N (287.1 eV) containing tyrosine (Figure 6.10 D). These results indicate that the original molecular carbon architecture remains mainly intact during the plasma polymerization.

The PP-Tyr/TTIP XPS scan shows the carbon, oxygen and nitrogen peaks as expected, but does not show a clear signature of titanium. This indicates that the titania is buried in the film and is not present at the surface. As is known, a common XPS probing depth is around 10 nm for carbon-based materials.[265] A titanium signal is clearly seen, however, at around 4.5 keV in the EDS spectrum (Figure 6.10 A inset). Additional evidence of the presence of titanium is seen in both FTIR and ellipsometry data refractive index. While the amount of titanium seen via EDS is relatively small (~2 atomic %), it confirms the presence of this element in the film; an indication that the co-polymerizations are occurring as described and corroborating the FTIR and ellipsometry assertions that titanium is present in the films.

The refractive indices of mixed films fall between those of the two indices of the individual PP monomers as is usually observed for mixed films without significant heterogeneities (Figure 6.11). [97,266] The refractive index of the mixed film can be adjusted by varying the composition of the films by controlling the feed rates of the monomers into the plasma, although this is somewhat more of a challenge to control with a sublimation process. This allows the relative ratios of each monomer in the film to be controlled to a degree. The possibility of variable refractive index is highlighted in three different examples for PP-Tyr/HEMA composite film which shows a lower refractive

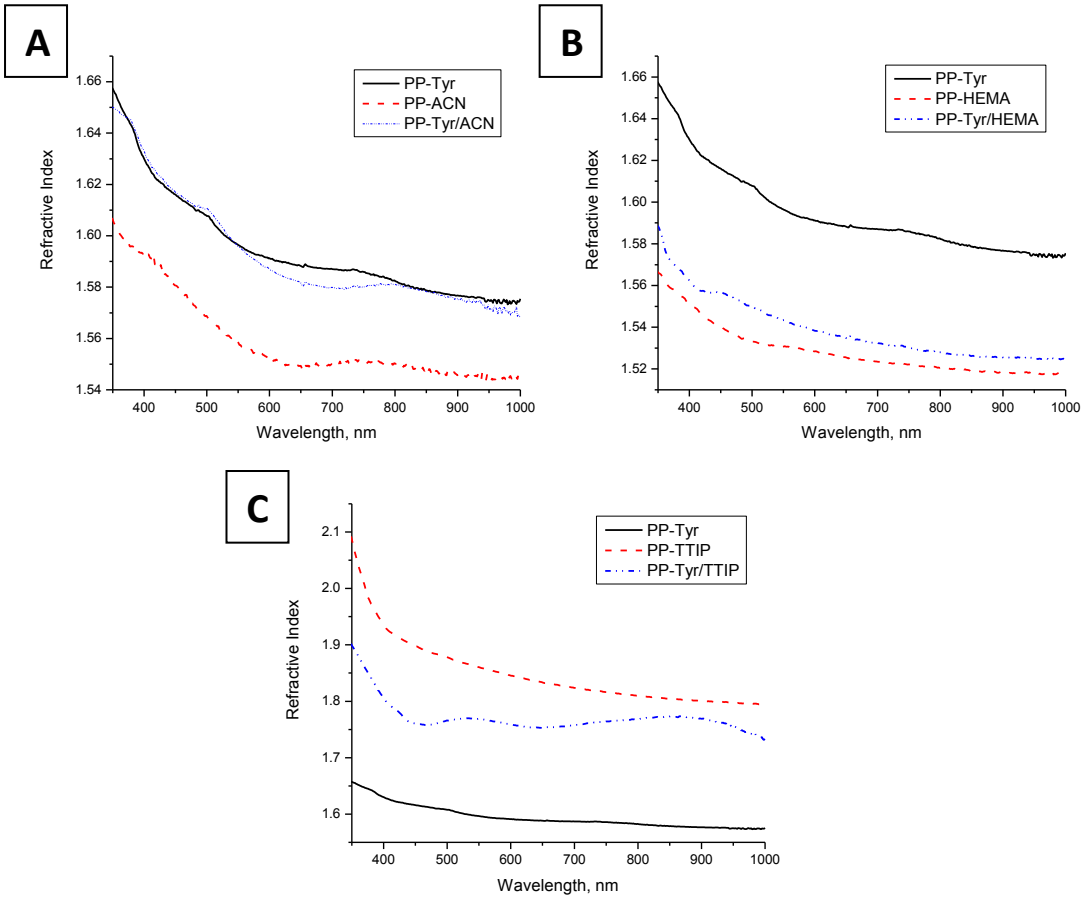

Figure 6.11: Refractive index of: A) PP-Tyr/ACN, B) PP-Tyr/HEMA, C) PP-Tyr/TTIP coatings.

index after increasing HEMA supply (Figure 6.11 B). The PP-Tyr/TTIP film clearly shows a higher refractive index than the PP-Tyr film, but lower than that of the PP-TTIP film (Figure 6.11 C). The change in refractive index to a higher value is a strong indication of the presence of titania and its role as an optical modifier of the films. It is worth noting that refractive index variation is an important feature which can be adapted to many other plasma deposited systems as well. Finally, all composite films exhibited a low absorption (k) value of less than 0.04 over the visible spectra, indicating relatively low absorption, important for optical coatings. Once deposition parameters are established, it may be possible to design a process to yield a specified refractive index, based on predictive modeling, although this would be practical challenge.

Lastly, contact angle measurements were carried out on surfaces of all plasma polymerized films to assess the hydrophobicity of the samples. The organic materials showed typical values ranging from θ = 60-75° indicating surfaces of moderate hydrophobicity. The PP-TTIP film though showed a much higher contact angle around θ = 112°, which was considerably higher than values seen for the PP-Tyr, PP-ACN and PP-HEMA films. The co-polymerized films of PP-Tyr/ACN and PP-Tyr/HEMA were relatively unchanged from the single monomer films, showing values in the range of θ = 60-75°. However, the PP-Tyr/TTIP film showed a dramatic decrease to around θ = 38°. This is significantly lower than the PP-Tyr film or the PP-TTIP film. This dramatic change can be a result of the unique surface morphology seen, with the formation of the needle-like structures. This presents an interesting application of these plasma co-polymerized films for use in modification of fluid flow devices. It is possible that other combinations of material co-polymerized in this manner can expand the range of surface chemistries available which can be tailored to specific applications.

While these data offer glimpses into the composition and structure of the films, they are not the basis for a final conclusion of the film structure. Further detailed chemical analysis to precisely determine the structure and specific compositional details of the plasma polymerized film must be done via techniques such as NMR. This however, has proven difficult due to the insolubility of the films but future experiments are being designed to address these concerns.

6.4 Conclusions

A selected amino acid, L-tyrosine, was able to be co-polymerized with other synthetic organic and inorganic monomers via PECVD to form a stable and robust partially cross-

linked composite coating with fine morphology formed by microphase-separated individual components which to great extent preserve their individual chemical composition and morphological features. Co-polymerization of materials via sublimation PECVD demonstrates the ability to combine biological and non-biological molecules into a single uniform coating of several hundred nanometers thickness in a rapid, facile, solventless, one step procedure. This co-polymerization method can be used to form biologically-active and biofunctionalized robust coatings by adding amino acids and short peptides for organic and inorganic matrices. Amino acids used in this study can serve as a proxy for other biological molecules (such as short-chain peptides) which can potentially be co-polymerized in a similar fashion with other polymers and inorganic materials to produce robust films with desired compositions and enhanced surface functionality and compatibility. Since the plasma polymerization fabrication approach can be widely applied to many different surfaces, this technique has the potential to applicable for designing enhanced biological interfaces.

CHAPTER 7 : Robust Plasma Polymerized-Titania/Silica Janus Microparticles

Reprinted with permission from Anderson, K. D.; Luo, M.; Jakubiak, R.; Naik, R. R.; Bunning, T. J.; Tsukruk, V. V. "Robust Plasma Polymerized-Titania/Silica Janus Microparticles" *Chemistry of Materials* 2010, 22, 3259-3264.

7.1 Introduction

Janus particles result from the assembly of two different components combined into a single unit along an interface which allows the design of multifaceted microparticles with unique directional interactions.[267,268,269] The dual nature of the particle's surface chemistry allows for their use in hierarchical assembly and is currently the subject of many experimental studies which exploit Janus–guided assembly.[270,271,272,273] Many methods for creating Janus particles have been explored, covering a wide range of fabrication techniques from wet chemistry to microstamping.[274] These methods include both chemical and physical means of construction utilizing both self-organization and top-down fabrication. Some of the recent fabrication methods include deposition of modification layers to substrates via grafting to/from polymerization, self-assembly of co-polymer and micelllar systems, vapor deposition techniques, layer-by-layer assembly, microfluidic co-flow, wax emulsion and microcontact printing, all of which are capable of creating a wide variety of Janus particles in different sizes and chemical compositions.[272,275,276,277,278,279,280,281,282]

Additional types of particles, such as amphiphilic Janus particles, can be obtained via ligand-exchange reactions.[283] These particles can spontaneously assemble in solution as a result of interactions between their functional groups.[284] Reversible self-

aggregation into regular monodispersed supermicelles has also been observed in amphiphilic Janus particles.[285] Another example involving the self-assembly of zwitterionic Janus particles in aqueous solutions showed the formation of charge-equilibrated aggregates caused by the charge asymmetry of individual particles.[286] Asymmetric functionalization was applied to polystyrene particles coated with multilayered films and stamped with polycations on the negatively charged particles. After dissolution from the polystyrene core, this yielded zwitterionic hollow Janus microcapsules.[278] In addition to spherical Janus particles, discs, cylinders, and other biphasic structures have also been fabricated.[287,288] Other intriguing examples of complex, structured particles and "patchy" microparticles decorated with gold nanodots have been assembled by Grzybowski and Möhwald.[289,290]

Janus particles with a distinct biphasic chemistry combined in a single structure, are of interest since they possess both the physical and chemical properties of each phase present and thus display interesting assembling behavior not only in mixed solutions but also at interfaces.[283,275,291,292,293] Assemblies of Janus particles result in minimized interfacial energy and corresponding spontaneous aggregation of particles into clusters with well-defined aggregation numbers and symmetries, not just simple strings.[286,294] These unique anisotropic interactions and assembly properties offer Janus particles great potential in a wide range of applications which require mesoscale ordering of microparticles such as prospective drug carriers, emulsion stabilizers, electronic paper matrices, anisotropic plasmonic materials and anisotropic imaging probes for both diagnostic and therapeutic purposes.[282,295,296,297,298,299,300,301]

Toposelective modification methods have been previously used to coat microparticles, and are commonly used with a surface masking technique to prepare Janus

particles.[280,281,302,303,304] While all of these techniques are able to create bifunctional particles of a variety of sizes, some processes suffer from tedious multistep fabrication, low yields of functional particles, and problematic stability of these particles. It is our aim to provide a toposelective method for the facile fabrication of Janus particles. Certain inherent material characteristics may result in a limited range of applicable chemistries and surface functionalities, which can limit the general applicability of a specific fabrication technique.

Generally, chemical vapor deposition gives access to a host of different functionalities that can be used on solid microspheres, not available with traditional wet-chemistry approaches.[305] Using a more sophisticated version, PECVD, the surface modifying material can be deposited across the entire substrate, coating the microparticles and masking layer. The plasma polymerized coatings are usually chemically grafted to the particle surfaces with a properly selected composition.[14,26] PECVD has been shown to rapidly create robust polymerized coatings of many different materials on a variety of surfaces and thus can be extended as a universal method in the fabrication of many types and compositions of Janus particles simultaneously without tedious prior surface modification, multiple functionalization steps, or a slow buildup of the "second face".[12,74,98,198,306]

Here, the universal fabrication of Janus microparticles from a variety of organic components is described. Specifically, plasma polymerization is utilized to deposit different monomers onto the exposed surfaces of the partially embedded microspheres of titania and silica to demonstrate facile and robust preparation of organic-inorganic Janus particles. Highlighted examples of acrylonitrile, pyridine, HEMA, NIPAAM and ferrocene materials, all of which are readily able to be deposited by plasma deposition

and represent examples of functional nanocoatings with the ability to further covalently graft or tether other materials to the particles and to act as redox-active and responsive coatings.[307,308] This study is based on previous experience on planar PECVD polymerization, which can be applied to a range of surfaces and generate unique robust conformal coatings.[44] This allows different physical and chemical properties to be imparted to the surface of the inorganic microparticles and microstructures.[29,33,51,198,259,309]

7.2 Experimental Details

Polystyrene (PS, M_w=250,000) and toluene were purchased from Janssen Chimica and J.T. Baker. SiO_2 particles with diameter of 3 μm and TiO_2 particles with diameter of 3 μm were purchased from Microspheres-Nanospheres Corpuscular Inc. The PS was dissolved in toluene at low concentration and spun coated onto a silicon substrate. Variations in the concentration of the PS solution and spin coating speed were used to prepare sacrificial layers of different thicknesses. A spin speed of 1500 rpm at solution concentration of 12 wt% was used to fabricate layers from 1.4-1.6 μm in thickness. The thicknesses of the spin-cast PS films were measured using ellipsometry and an AFM scratch test. The microparticles were suspended in ethanol to form a dilute solution concentration (approx. 1 mg/mL) which was then cast on the PS film. A drop of the solution (100 μl) was placed on the PS coated wafer and allowed to dry. After casting of particles on the PS film, the system was heated to 135ºC for 3 hours and then slowly cooled to room temperature. This process allowed the particles to partially sink into the PS layer (Figure 7.1). To embed them further in a controllable manner, additional calibrated hydrostatic pressure must be applied uniformly to the particles. This was done by placing a clean 5 x 5 cm^2 silicon wafer with a small weight on top of the specimen to distribute force evenly. In this instance a 150g mass was evenly distributed

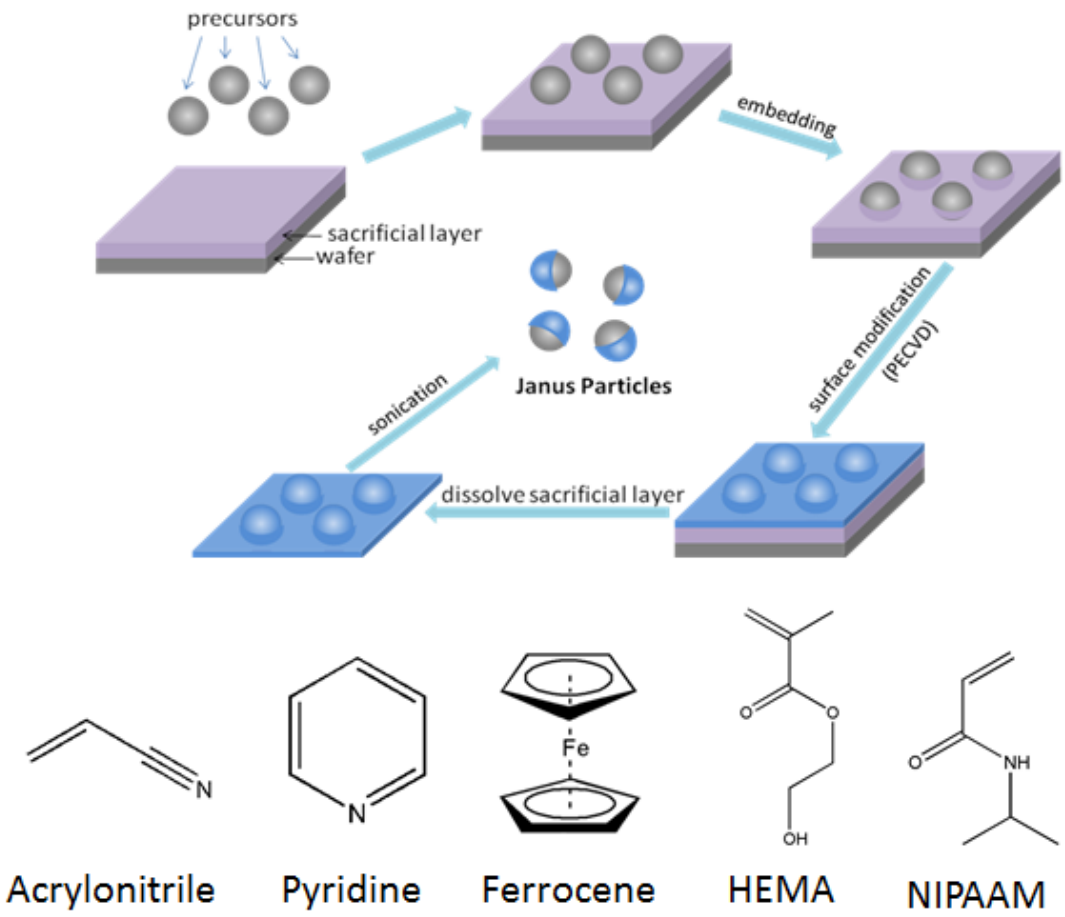

Figure 7.1: Janus particle fabrication using a sacrificial layer to embed the particles prior to plasma polymerization. Upon dissolution of the PS layer, the particles are released with a characteristic half coating. Chemical structures of selected monomers are presented as well.

through a plate to the particle surface, where the particles were dispersed on a 2x1 cm^2 silicon wafer. The amount of pressure applied must be determined experimentally for each case as it is highly dependent on the viscosity of a particular PS solution, the size of the particle and the temperature at which it being heated. Typically higher heat and pressure will cause the particle to be embedded further in the masking layer.

The monomers acrylonitrile, ferrocene, HEMA, NIPAAM and pyridine were purchased from Aldrich and used as received. Plasma depositions were carried out in a custom built PECVD vacuum chamber according to established procedure.[1] Liquid monomers

were placed in a sealed tube connected to the reaction chamber and vaporized directly into the plasma stream. Solid monomers were directly sublimed into the plasma stream by heating the monomer in a tantalum crucible in the reaction chamber.[44,73] The pyridine and acrylonitrile were deposited under identical conditions at a chamber pressure of 6.7 Pa, 30W of power applied to the plasma and an argon flow rate of 10 cm^3/min. The plasma was run for 5 minutes. The ferrocene was deposited under modified conditions since it was done via sublimation. A pressure of 2.7 Pa was used with an applied power of 45W. The argon flow rate was 20 cm^3/min and exposure time was 12 min. The ferrocene was heated to approximately 120°C for sublimation.

After the plasma polymer coating is applied, the microparticles were washed with hot toluene (50 ºC) and centrifuged six times, each time removing the supernatant, to remove all PS from the particles. The particles were then sonicated to help separate particles which may have agglomerated. Upon completion of the sonication, the particles were suspended in toluene and cast on a clean silicon wafer substrate for characterization. Some particles were subject to an etch with 8% hydrofluoric acid while sitting on the silicon wafer to remove the central silica particle. The etch lasted for 2 hours and then the sample was gently rinsed with copious amounts of Nanopure water and dried under dry nitrogen.

The fluorescent dye Fluorescein isothiocyanate (FITC) was purchased from Fluka, which was then dissolved in ethanol and used as the dying solution. The SiO_2-ACN Janus particles were placed in the dye solution for 8 hours and then washed with ethanol several times. The solution was sonicated for 30 seconds before washing with ethanol. The silver nanoparticles, with an average diameter 30 nm, were prepared according to the literature.[310] The TiO_2-pyridine Janus particles were placed in a solution of silver

nanoparticles for 3 hours to assure selective adsorption on pyridine surface and washed with Nanopure water several times. The solution of particles was then drop-cast on the surface of a silicon wafer for characterization.

All AFM, SEM and EDX characterization was done according to the procedures outlined in Chapter 3. The confocal fluorescent microscope images were recorded via a Carl Zeiss Laser Scanning Microscope LSM 510 with FITC reflector and objective of Fluar 40*/13 and plan-Neofluar 63*/1.25 oil.

7.3 Results and Discussion

7.3.1 Fabrication and Coatings

The masking technique utilized in this study was adapted from a previous fabrication process (Figure 7.1).[302] By varying the thickness of the PS layer, the masked areas of the spheres can be tailored to cover varying portions of the particles surface. After the silica and titanium dioxide microparticles were embedded in the PS layer, selected materials could be effectively plasma polymerized on open surface areas. The residual PECVD film was removed during rinsing and sonication since the free-standing film is not tethered to a surface. Because the film is thin, the particles can easily break from the free-standing film after the sacrificial layer is dissolved.

These selective plasma polymerized coatings remain firmly attached to the particles as the sacrificial polystyrene layer was dissolved and the Janus particles were released (Figure 7.2). The coverage areas of the particles with the polymerized coatings can vary over a wide range: from a high ratio of up to 75% of the area coated (Figure 7.2 C) to an equal ratio with approximately 50% coated area (Figure 7.2 D), down to 25% coated (Figure 7.2 E). The protect-and-release method proves to be a critical step and can be

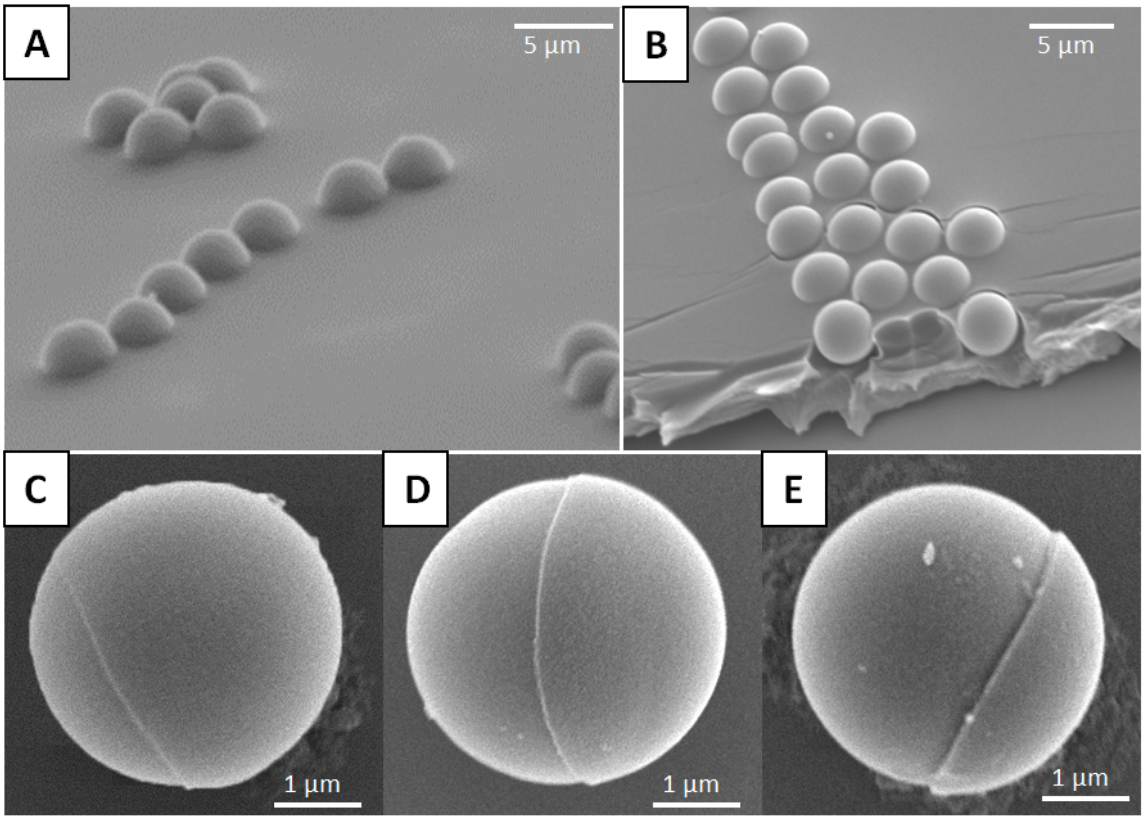

Figure 7.2: A) SEM image of 3 µm silica particles half embedded in a PS layer. B) Embedded particles at typical depth in the PS layer. C-E) Janus particles with controlled coating coverage: ¾, ½, ¼ coverage of particles with acrylonitrile on silica microspheres.

applied in a number of different fabrication scenarios. Embedding the microparticles into an easily removable sacrificial layer facilitates the protection of the embedded portion while allowing further modification to the exposed portion. This leaves the protected portion of the particle clean for further modification later. By utilizing easily dissolvable polymer layers of different thicknesses, the microparticles can be easily coated to a controlled degree of surface coverage through toposelective modification before final release of the modified particles through dissolution of the masking layer.

Additional studies also investigated the viability of monomers such as NIPAAM and HEMA with the anisotropic particle fabrication process. Both monomers are well known to undergo plasma polymerization from literature and from previous experiments. These materials were deposited on 3 μm silica particles and processed according to the standard processing metrics for other particles. Both materials showed excellent half coatings with very clearly defined sections when observed under SEM (Figure 7.3). The PP-HEMA coating on the microparticle had a very clear and distinct boundary, which was visible in an orientation that provides a means of estimating the coating thickness at

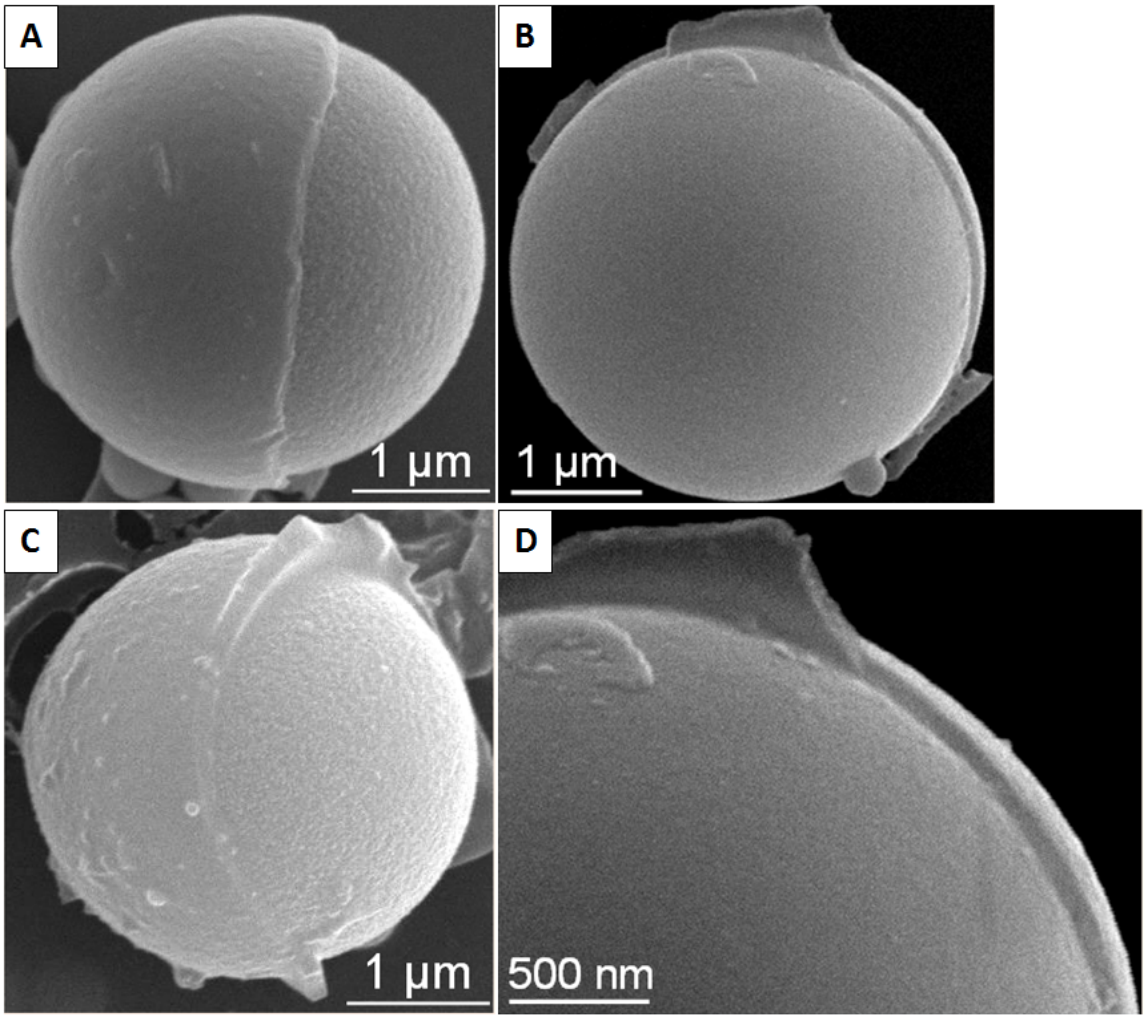

Figure 7.3 A,C) SEM images of PP-NIPAAM half coatings. B) PP-HEMA on silica particle. D) High magnification of PP-HEMA showing fine detail of the coating.

approximately 100 nm. These are excellent examples of conformal coatings, which are nicely cleaved at the edge of the particle, and show generally smooth and uniform surface morphologies confirming again that this process can be broadly applied. By applying and processing these monomers to the microparticles, it is hoped that further experiments will be able to investigate the responsive nature of these coatings.

7.3.2 Composition and Morphology

The materials selected in this study show the compatibility of the PECVD process on complex topologies with both liquid phase monomers and sublimation depositions. SEM imaging of individual microparticles shows selective, one-face deposition on their surfaces with a clear delineation of polymer coated/non-coated. Images of PECVD-fabricated ferrocene, acrylonitrile and pyridine on 3 μm silica spheres show a PP coating covering approximately 50% of the total surface area of the particle with a well-defined boundary (Figure 7.4 A, B, C). The same monomers were deposited with similar results on 3μm titania microparticles as well (Figure 7.4 D, E, F). On both types of particles explored here, the plasma polymerized coating was seen to be conformal to the surface with a sharp delineation between the plasma polymerized region and the bare silica/titania region that was masked. Estimation of the thickness of the plasma polymerized layer on the microparticles from the images was 200-300 nm, which was consistent with the expected film thickness of a typical plasma deposition of the same material on a flat substrate under similar conditions.[31,73,259]

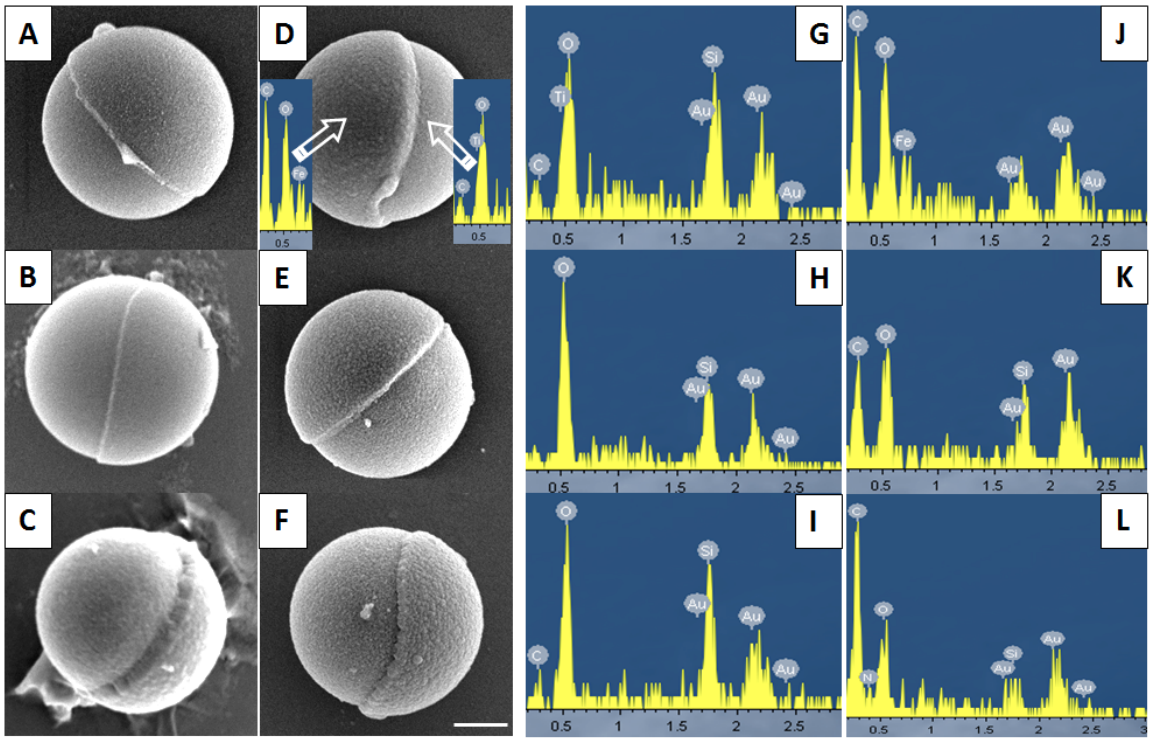

Figure 7.4: A-C) SEM images of various coatings on silica and D-F) on titania microparticles via plasma polymerization: A & D) ferrocene; B & E) acrylonitrile and C & F) pyridine coatings. G-L) shows EDX of the particles in D-F with G-I being the signal from the uncoated side and J-L being from the coated part. The inset in D) clearly shows the presence of iron and carbon on the coated portion of the particle. Scale bar = 1.0 µm for all images.

Compositional analysis of the PP coatings on the Janus particles shows the polymerized materials were deposited as expected. EDX shows iron was present on the coated side, along with an increase in carbon from the ferrocene material (Figure 7.4 D). Full EDX spectra from each particle coating show a similar trend with more carbon and certain trace elements seen in the section with the coating as opposed to the uncoated half of the particle (Figure 7.4 J,K,L). In the case of pyridine, both nitrogen and an increased carbon signal were present. Acrylonitrile coating also showed an increased carbon content for the polymerized region.

AFM topography and phase images of a 1x1 μm^2 area show the polymerized regions on the apex of the silica microparticles (Figure 7.5 A, B, C). All images show a uniform surface morphology of the different PP coatings with a fine, grainy surface morphology free of microscopic defects.[33,44,51] This indicates the presence of a complete, uniform layer, which conformally coats the designated highly curved surface areas of the microparticles. These images were obtained prior to the release of the particle from the PS sacrificial layer due in large part to the significantly more stable configuration of the particles. In this instance, the particles were immobilized on the surface as opposed to one after washing which are cast upon the substrate, but free to move. The immobilization of the particles allows for greater ease in collecting the data from the surfaces even with the limited area available for scanning. The limitation of the scanning area is evidenced by the characteristically dark edges seen in the images as the surface drops away due to the curvature of the microparticle.

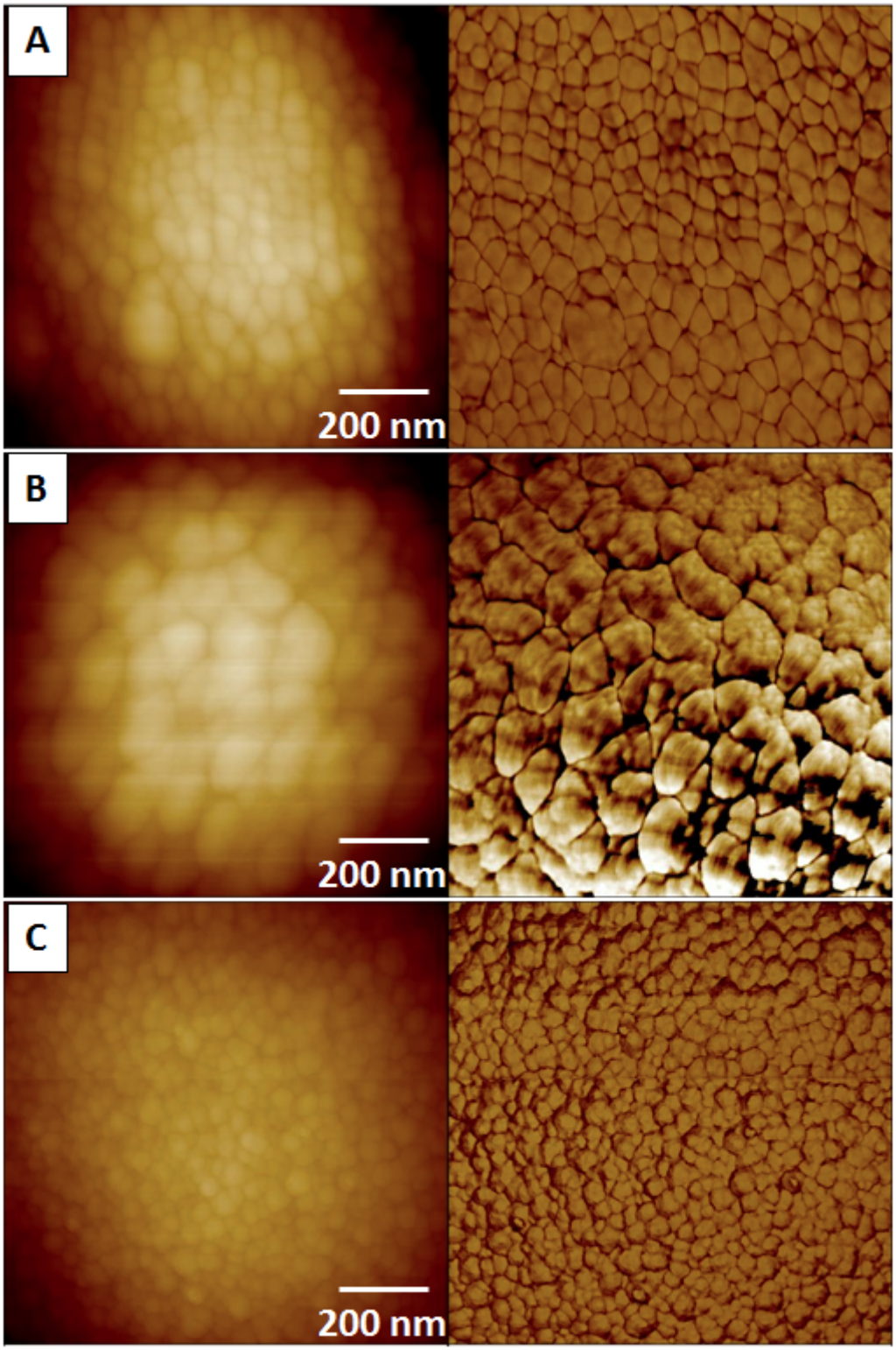

Figure 7.5: AFM topography (left) and Phase (right) of plasma coatings on microparticles. A) Ferrocene (z= 200 nm, 50°); B) acrylonitrile (z= 100 nm, 50°); C) pyridine (z= 130 nm, 60°).

7.3.3 Particle Coating Modification

Different plasma polymerized coatings can be employed for the selective adsorption of metal nanoparticles, site-selective grafting, potential biological activity, and generation of distinct optical responses as briefly discussed below. The Janus particles with the ACN coating were placed in a fluorescent dye solution and were seen as half particles under confocal fluorescent microscopy due to the selective grafting of the fluorescent dye molecules to the highly reactive polymer coating (Figure 7.6 A, B). This was seen as regions of bright and dark green on the particles, where the brighter regions fluoresce under the incident light more readily when located on a surface in a higher concentration. The darker region has subsequently less fluorescent dye present and was not illuminated to the degree which the polymer coated regions were.

Pyridine coated micro particles can serve as templates for further modification with citrate-modified silver nanoparticles which selectively were adsorbed to the plasma polymer and firmly grafted to the reactive pyridine surface in greater numbers in contrast to the uncoated silica portion of the Janus particle (Figure 7.6 C,D). This method of fabrication was compared to a conventional layer-by-layer (LbL) (Figure 7.7 B) and encapsulation assembly approach. Both approaches showed a strong EDS signal indicating the presence of silver nanoparticles on the surface. The use of XPS for this and other studies of the detailed composition on the coated microparticles was an experiment that would be useful to help determine differences in the particle coating resulting from the 3D geometry of the film and the solvent washing. XPS is limited however, in the area that can be seen and collected (30 μm spot size) making the analysis of these Janus structures by this technique not currently possible. Plasma coating is generally perfered to LbL assembly in this case as it is a more rapid process offering a wider range of choices of materials that can be coated on the particles.

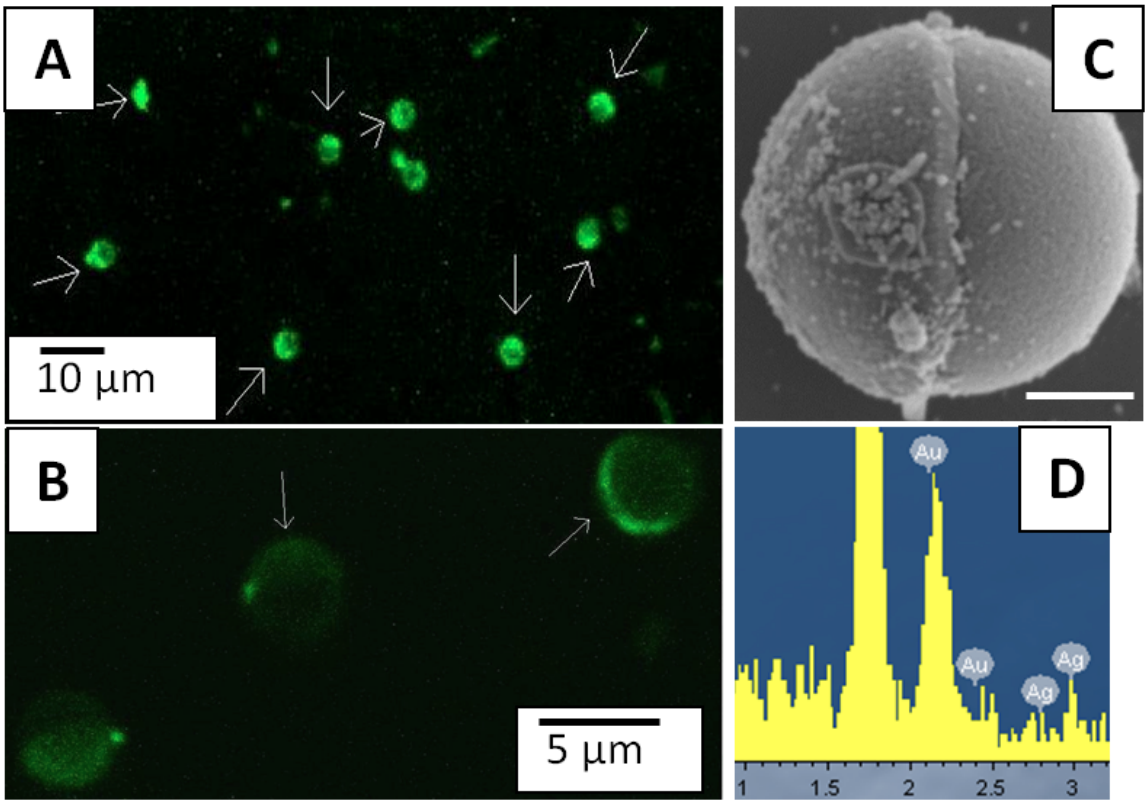

Figure 7.6: A and B) Half-fluorescent Janus particles with selectively grafted dye molecules. Arrows indicate fluorescently labeled regions of the particles. C) Pyridine-coated Janus particle with selectively tethered silver nanoparticles. D) EDX spectra confirming the presence of silver from (C).

The micro particles modified with PECVD were compared to the same microparticles coated with films from conventional spin coating to provide a comparison between different fabrication methods. Spin coating was used to compare not only the polymer coatings, but specifically the ability for metallic nanoparticle retention on the microsphere surface. Using the same particles embedded in a PS masking layer, alternating layers of polystyrene sulfonate (PSS) and poly(allylamine hydrochloride) (PAH) (0.2% wt. conc. solution) were spun coat on to the microparticles and released using the same toluene rinsing method. The LbL microparticle coatings fabricated by LbL showed a very clear and stable coating on the silica spheres and were also capable of supporting the

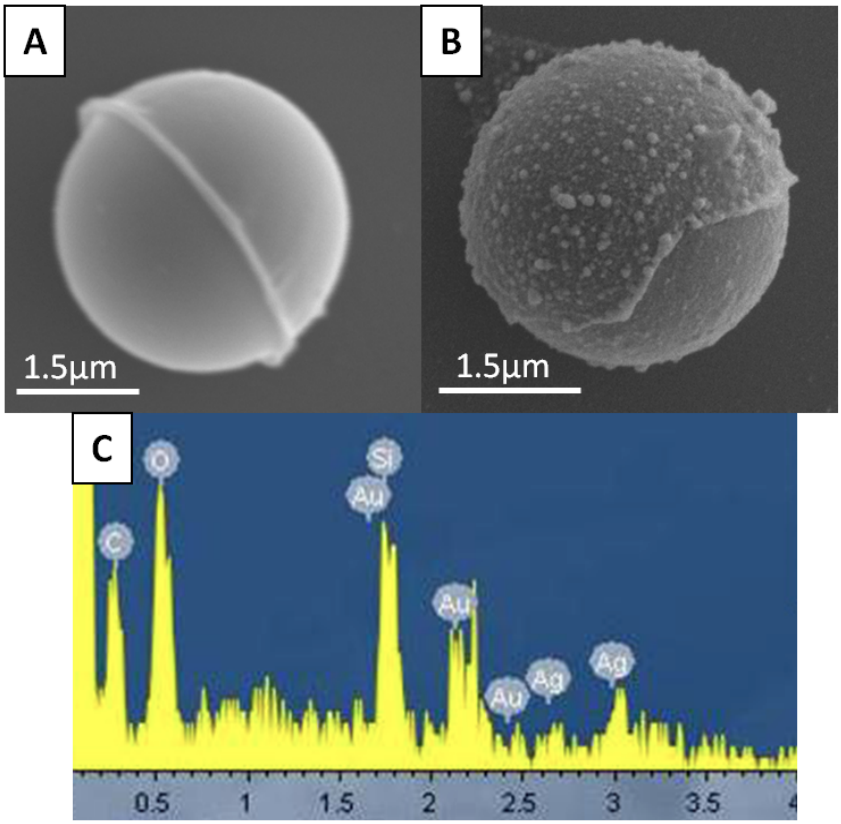

Figure 7.7: A) Layer by Layer PSS-PAH construction on silica microsphere. B) Silver nanoparticles encapsulated in LbL film. C) Corresponding EDX spectra show presence of silver.

addition of metallic nanoparticles in the LbL film in a similar manner to the ones reduced on the surface (Figure 7.7 A, B).

The presence of silver encapsulated in the polymer coating is confirmed via EDX spectra (Figure 7.7 C). This provides a demonstration of a multi-step wet chemical means to fabricate a similar system to what PECVD allows for in a single deposition. The PECVD deposition also has the advantage of being compatible with many different materials. A similar type of spin coating was much more limited in the number of material systems that it is compatible with and takes a significantly longer time to complete than the PECVD version due to the spin coating process. Spin coating still produces high quality

coatings on the microspheres and may act as an alternative means of fabricating particle half-coatings with modifying materials in certain situations.

7.3.4 Free-Standing Half Shells

Robust half-shell, free-standing polymerized structures can be obtained upon the release or dissolution of the inorganic cores. These anisotropic free-standing structures demonstrate that the plasma polymerized coatings covering the microspheres can be released, without damage, as robust half-shells which can undergo release, drying and

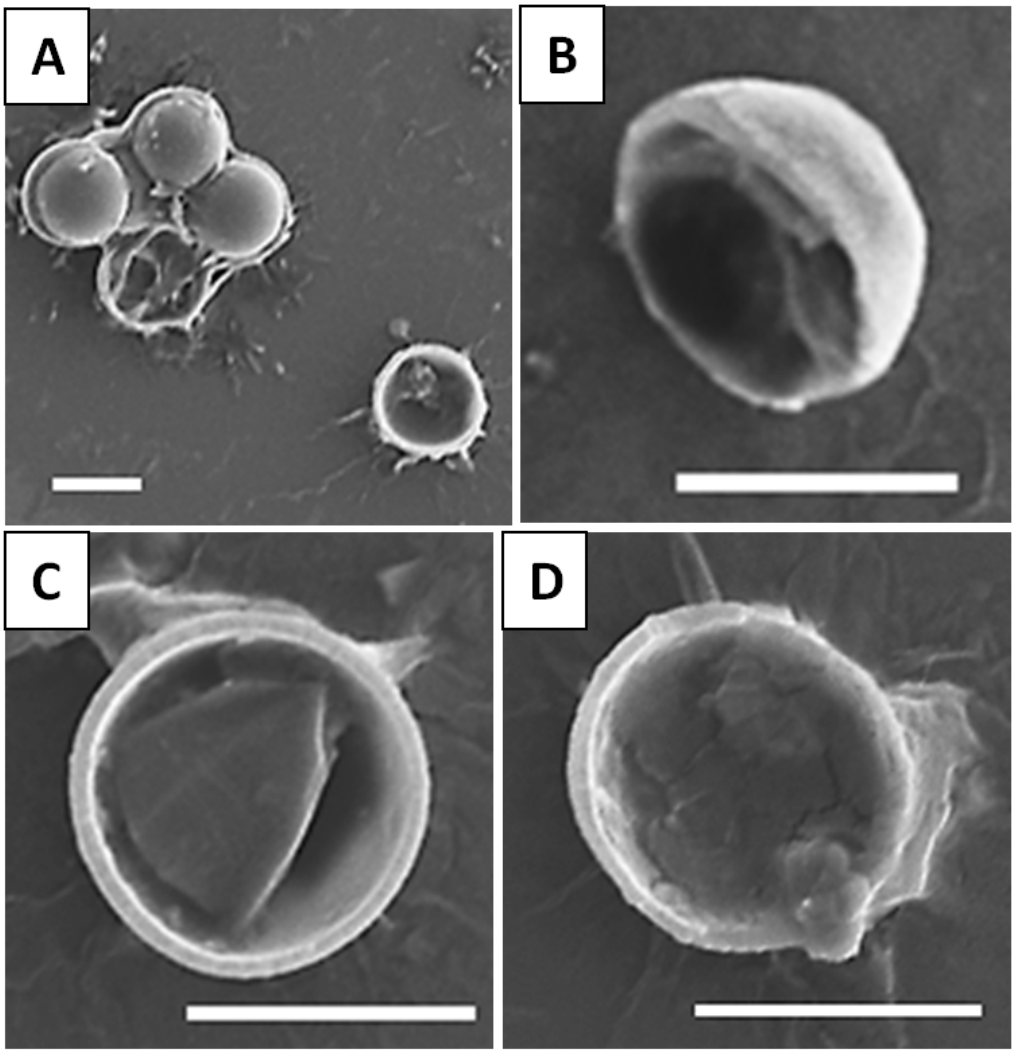

Figure 7.8: Pyridine coatings A) released shells along with some containing cores B, C, D) pyridine anisotropic caps. All scale bars 3 μm

transfer to high vacuum without losing their original shape. The first method of producing these anisotropic structures was through extensive sonication of the polymer coated silica spheres. This method was demonstrated using pyridine, which was the material coating it worked most reliably with. It is theorized that PP-Pyridine may also have lower adhesion to the silica particle surface, facilitating the release of the cap. These half-shelled structures demonstrate the robust nature of plasma polymerized films, showing their ability to be self-supporting and stable through ultrasonication cycles and during release. This type of stability was generally thought to be a result of the high degree of cross-linking in the plasma polymerized films. In addition to the free-standing curved structures, two-dimensional free-standing films were also routinely observed from many different materials including PP-Tyr. Free-standing films are seen after incomplete washing of the particles and tend to be smaller with the more sonication cycles that film has been subjected to. The stability of the half shells was one demonstration of the mechanical robustness possible with plasma polymerized materials.

While the sonication method of releasing pyridine caps worked well for that specific material, other materials, such as PP-NIPAAM caps, did not behave the same way and were not easily released through an extended sonication regime. Extended sonication tended to destroy the polymer coating completely leaving no cap. Thus, a different release method was employed using HF to dissolve the silica cores away from the plasma polymerized coating. The dissolution method showed excellent compatibility with PP-NIPAAM, producing many free-standing structures after complete dissolution of the core (Figure 7.9). The PP-NIPAAM was also robust against the low pH of the acid, which has been observed to readily dissolve PP-P2VP films below a pH of 3. After the dissolution of the silica core, two very distinct types of caps were seen. The first caps observed showed the PP-NIPAAM collapsed and wrinkled on the surface, as it was

unable to support itself after being recast on a clean silicon wafer. This was likely due to either the coating layer being too thin or the film having insufficient cross-linking to become fully self-supporting. The next set of PP-NIPAAM caps showed that after core

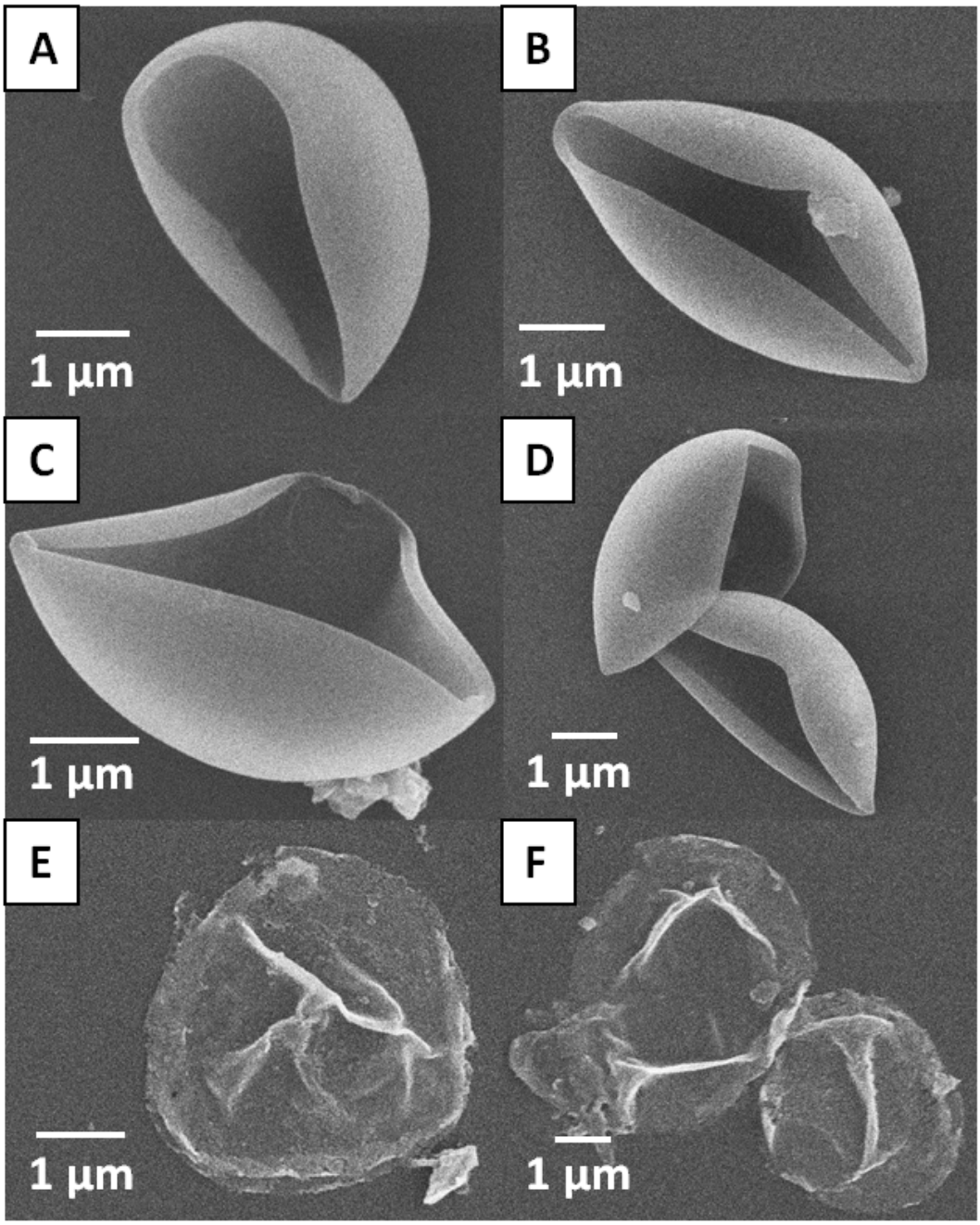

Figure 7.9: SEM micrographs of PP-NIPAAM caps after dissolution of the silica core. A, B) released self-supporting caps with a single folding axis. C) released cap with multiple folding points. D) Nested caps. E, F) released caps after collapse.

dissolution, excellent self-support and retention of the rounded shape of the microsphere was possible. The caps show some curling near the edge and were observed to have both single and multi-folding axes', but were robust and stiff enough to remain self-supporting and not undergo collapse upon rinsing, casting and drying. The PP-NIPAAM caps are in contrast to the PP-Pyridine caps which tended to hold their shape better and did not show folding or collapse when washed and recast on a surface.

7.3.5 Biomaterial Coatings

Selective particle absorption and reduction may be extended to include many different inorganic materials mineralized via biological molecules such as amino acid and peptide coatings on the Janus particle. To this end, different amino acids have been attempted to be polymerized onto silica microspheres, creating biomolecular Janus particles (Figure 7.10). These types of coatings, especially ones of certain functional peptides, could play a key role in facilitating the interface of biological systems with these sorts of engineered structures. The demonstration of amino acid coating conformally to 3D surfaces shows that PECVD can be used as a method to create such complex

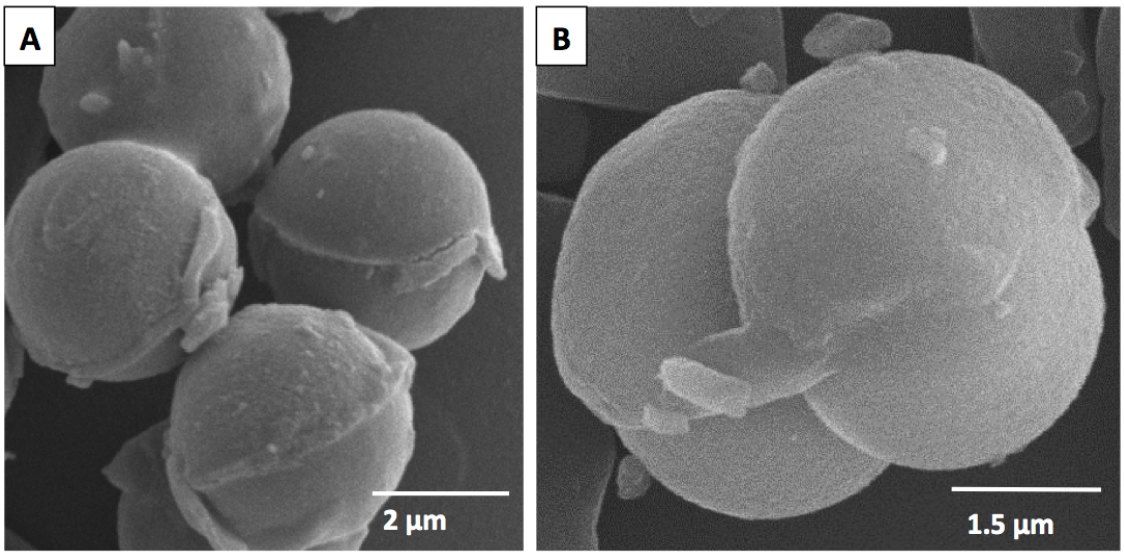

Figure 7.10: A) PP-His coated microparticles and B) PP-Tyr coated microparticles.

topologies of biological functionality. However, these coatings do not exhibit the same uniform and sharp surface coatings as other materials, leading to rougher and less well defined boundaries on the surfaces of the microparticles. This may be a result of variations with the sublimation polymerization process of the amino acid monomers.

The PP-His coated particles were seen to exhibit a more uniform coating on the surface of the microparticles with some distinct coated and uncoated areas. The PP-Tyr coated particles showed a similar type of coating clearly visible on the microparticles, but not as clearly defined as synthetic monomers. The surface of the coatings appear somewhat smoother and more conformal to the microparticle's surface than the PP-His coating. Both the PP-Tyr and PP-His coated microparticles showed instances of stable and unstable coatings as a result of the plasma deposition process. Some microparticles showed Janus structures and other particles put through the same post-processing did not. Some particles were rinsed and sonicated and showed no film degradation while others showed microparticles with no coatings. The choice of solvent is highly important as toluene exposure had a vastly different effect when compared to water. This highlights the need for careful design and deposition of the plasma polymerized films in conjunction with curved geometries, which can significantly affect the integrity of the film. The deposition of these materials onto microparticles is an ongoing area of research and the improvement of the uniformity, conformality and robustness of the coatings is critical in allowing these types of particles to be fabricated in large numbers.

7.4 Conclusions

The Janus particles detailed here represent a selected portion of many systems tested and have thus far, shown the highest potential for further utilization. Other monomers including dopamine, methylamino ethanol, 2-vinyl pyridine, hexafluorobenzene, and

polyethylene glycol were tested, but did not yield as promising results for microparticle coatings as the monomers shown. With further development, these and other monomers may prove to be viable microsphere coating materials. This highlights the universal nature of the plasma polymerization approach to the fabrication of robust organic/inorganic Janus particles covering a broad range of functionalized and biological materials. While this fabrication method is limited to the surface (2D) fabrication regime, it is estimated that the simultaneous construction of up to 10^8 particles is possible, based on the size of the particles, substrate and the density with which the particles are coated on the surface. This shows a significant increase in the number of particles over other methods, which are usually used on a smaller or even single particle scale. The mask and release coating systems demonstrates a facile, fast, and scalable approach that allows selective polymerization on embedded particles, generating functionalized organic-inorganic robust Janus particles. PECVD neatly accommodates the coverage of a relatively large surface area with complex topologies when compared to conventional microprinting with planar stamps. PECVD also does not require any post deposition treatment of the particles for curing, cross-linking or stabilization.

Many Janus particles can be rapidly fabricated in a single plasma deposition cycle on hard inorganic spheres through the use of PECVD. The process described uses silica and titanium dioxide microspheres (~3 μm diameter) and can be applied to a wide range of other substrates. The coatings used cover a wide range of monomers readily deposited in a single step, which can be further diversified in future studies. The Janus particles were fabricated without the need for extensive and tedious wet chemical synthesis, electrostatic assembly or microprinting to modify the microparticles' surfaces. Using the plasma deposition technique, a wide variety of material systems can be used to create Janus particles with a large range of surface chemistries for different

applications. Examples of five different reactive organic monomers ranging from conventional acrylic compounds to organometallic molecules and amino acids all were utilized successfully. Finally, half-fluorescent, half-metal-decorated, and half-shelled structures all were demonstrated as examples in the current study of further unique structure which fan be fabricated using PECVD.

CHAPTER 8 : Responsive Plasma Polymerized Ultrathin NIPAAM/Titania Films

8.1 Introduction

Material systems capable of autonomous, self-actuating response to specific stimuli are desirable in a wide range of applications including thermal and chemical sensing, tunable optics, targeted drug delivery, switchable surfaces and micro actuators.[16,199,202,311,312,313] Designing materials which are capable of generating a response from the stimulus itself eliminates the need for additional and complex triggering and control mechanisms as the response process will be fully contained within a layer of material integrated into the larger system. Polymeric thin films are one responsive system which have been utilized in an array of applications through a variety of synthesis methods and materials. Responsive thin films, such as poly(N-isopropylacrylamide) (pNIPAAM), exhibit a response, typically as a change in thickness, under appropriate conditions as has been widely reported in recent literature, including examples with UV-photografting and chemical vapor deposition (CVD).[49,314,315,316,317,318] This type of switching behavior can be used to drive mechanical changes in systems, actuate folding behavior, alter surface mechanical properties or enhance switchable cell scaffoldings.[32,87,319,320]

Plasma enhanced chemical vapor deposition (PECVD) is a specific deposition technique in the wider CVD family, which has been used extensively to polymerize a wide variety of materials directly onto target substrates, both planar and textured for numerous surface modification applications.[7,12,19,21,46] PECVD polymerization is a unique thin film fabrication method which allows the direct deposition and polymerization of a wide

variety of monomers directly on a target substrate through a one step, robust, solvent-less deposition process.[14,18]

This technique has been adapted for use with soft matter and allows facile, rapid and solvent free synthesis of highly cross-linked polymer networks which are typically very stable on the substrate. The range of monomers available for deposition using PECVD covers many traditional monomers such as polystyrene, polyethylene glycol and benzene to responsive materials like poly(2-hydroxyethyl methacrylate), poly(2-vinylpyridine) and pNIPAAM to biological monomers such as functional amino acids.[3,40,41,44,45,321] PECVD allows deposition of many monomers under "dry" conditions meaning that only the pure monomer and no additional solvents, surfactants or reactants are needed in the synthesis of the film. This becomes especially useful for depositions of materials which may otherwise require complex wet chemical procedures to firmly attach to some surfaces. Radicals formed by the plasma on the surface of the substrate help bind the monomer to the surface regardless of the specific chemistry.

Many of the CVD techniques used for fabrication provide a facile method to coat materials onto any surface rapidly in a single step, which is considered an advantage over the use of bulk polymers synthesized by other wet chemical methods in some scenarios. Bulk polymers and hydrogels typically show a greater response, on the order of 100% greater, much more than plasma polymerized films. Crosslinked hydrogels have much lower cross-linking densities and more regular polymer networks than plasma polymerized films allowing hydrogels to exhibit a greater swelling response.[88] PECVD offers the advantage of creating ultrathin films which are compatible with almost any substrate, even without prior modification. PECVD also readily allows the addition of a second material to the PP-NIPAAM when co-polymerized during the same

deposition. In this study, titanium isopropoxide is co-polymerized to construct a thin film, which exhibits a higher refractive index than the PP-NIPAAM while still maintaining some of the responsiveness of the PP-NIPAAM. This provides an effective means of fabricating rapidly responsive films with tailored high refractive indices. Previous studies have addressed pNIPAAM as a plasma polymerizable material, which retains its well-known and characteristic response.[40,41,314]

Hess et. al. have conducted extensive investigation into different plasma deposition conditions of PP-NIPAAM looking at temperature and pressure effects on the cross-linking during film deposition via FTIR.[40] Changes in the surface were observed under contact angle, which was altered significantly upon heating and cooling indicating that plasma polymers exhibit the same LCST behavior of bulk materials. Measurements of water uptake in the films by QCM also provided evidence as to the swellable nature of plasma polymerized NIPAAM films.[41] Ratner et al. has also investigated the LCST effects in plasma polymerized NIPAAM showing AFM mechanical data which correlates a change in response of the film with a change in temperature confirming the switchable nature of these films.[314,72] A significant demonstration of control of the LCST has been recently shown by Gleason et al. using iCVD. It can be shifted significantly (16-28 °C) depending on the relative amount of co-monomer added to the film during deposition.[322] These films also showed a similar rapid response compared to other reports, further indicating NIPAAM thin films potential use in rapid, responsive microactuators or MEMS devices. Optical characterization of co-polymerized materials demonstrates swtichability of responsive ultrathin films. A demonstrated capability of rapid switchability of PP-NIPAAM and co-polymerized PP-NIPAAM/TTIP films and the accompanying change in the refractive index and thickness is shown here. Rapid and robust substrate adhesion

provided by PECVD is a major advantage when applying optically responsive coatings to surfaces as well as reversible switching as demonstrated here.

8.2 Experimental

All monomers, *N*-Isopropylacrylamide (97%) and titanium(IV) isopropoxide (99%) were purchased from Aldrich and used as received for all subsequent plasma processes (Figure 8.1). pNIPAAM (M_w = 19000-26000) was purchased from Sigma-Aldrich and dissolved in Nanopure water at a 2% concentration. The solution was then spin-cast on a clean silicon wafer at 3000 rpm for 30 seconds.

Samples utilizing the TTIP monomer used an additional carrier gas of oxygen at a flow rate of 40-70 sccm filtered through the liquid monomer to assist with vaporization of this monomer. The deposition times ranged from 2-10 minutes depending on the desired thickness of the final film. The solid NIPAAM monomer was heated in a water bath to 80° C to liquefy it for vaporization into the plasma. This allowed the NIPAAM monomer to melt and vaporize into the plasma chamber when the flow valve was opened. Careful control of the monomer flow was needed to ensure that the flow rate was kept low for a slower deposition rate. It was observed that films deposited under very high deposition rates of over 100 nm/min generally lead to films that were unstable and either

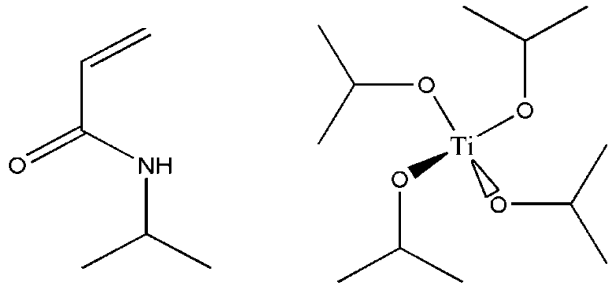

Figure 8.1: NIPAAM (left) and TTIP (right) monomers used in all plasma polymerizations.

delaminated from the surface or were otherwise compromised, most likely due to internal stresses. The monomer inlet was downstream of the plasma generating zone. The titanium isopropoxide monomer was placed in a custom-built bubbling apparatus for vaporization and heated to 60ºC in a water bath. The tubing connecting the bubbler to the plasma chamber was also heated to prevent condensation of the monomer before entering the plasma chamber. After plasma polymerization, the films were removed from the chamber and stored under normal atmosphere for a minimum of 48 hours before further testing was carried out to allow any residual internal stresses in the films to equilibrate.

8.3 Results and Discussion

8.3.1 Surface Morphology

Large scale AFM images of PP-NIPAAM films show a uniform surface coverage of the polymer with no visible pinholes or defects in the film deposited on a clean silicon surface (Figure 8.2 A). It was also observed that there are no major changes or features in the surface morphology. The surface microroughness of the PP-NIPAAM film measured by AFM is less than 0.4 nm over a 1x1 μm^2 area, indicating a very smooth and uniform plasma deposition of the polymer close to literature.[27,325] The uniform surface creates a more ideal system for responsive testing, theoretically with less variation among various locations, providing a more indicative picture of the films actual response.

Corresponding high resolution AFM imaging of the PP-NIPAAM film shows a uniform film without many unique features as compared to the PP-TTIP film (Figure 8.2 B). This type of film morphology matches uniform polymerization and is important as it governs the surface roughness and wetting characteristics of the films. The PP-TTIP film was

deposited under an oxygen enriched argon atmosphere in the plasma chamber and showed a surface morphology with many fine, round features which form a much

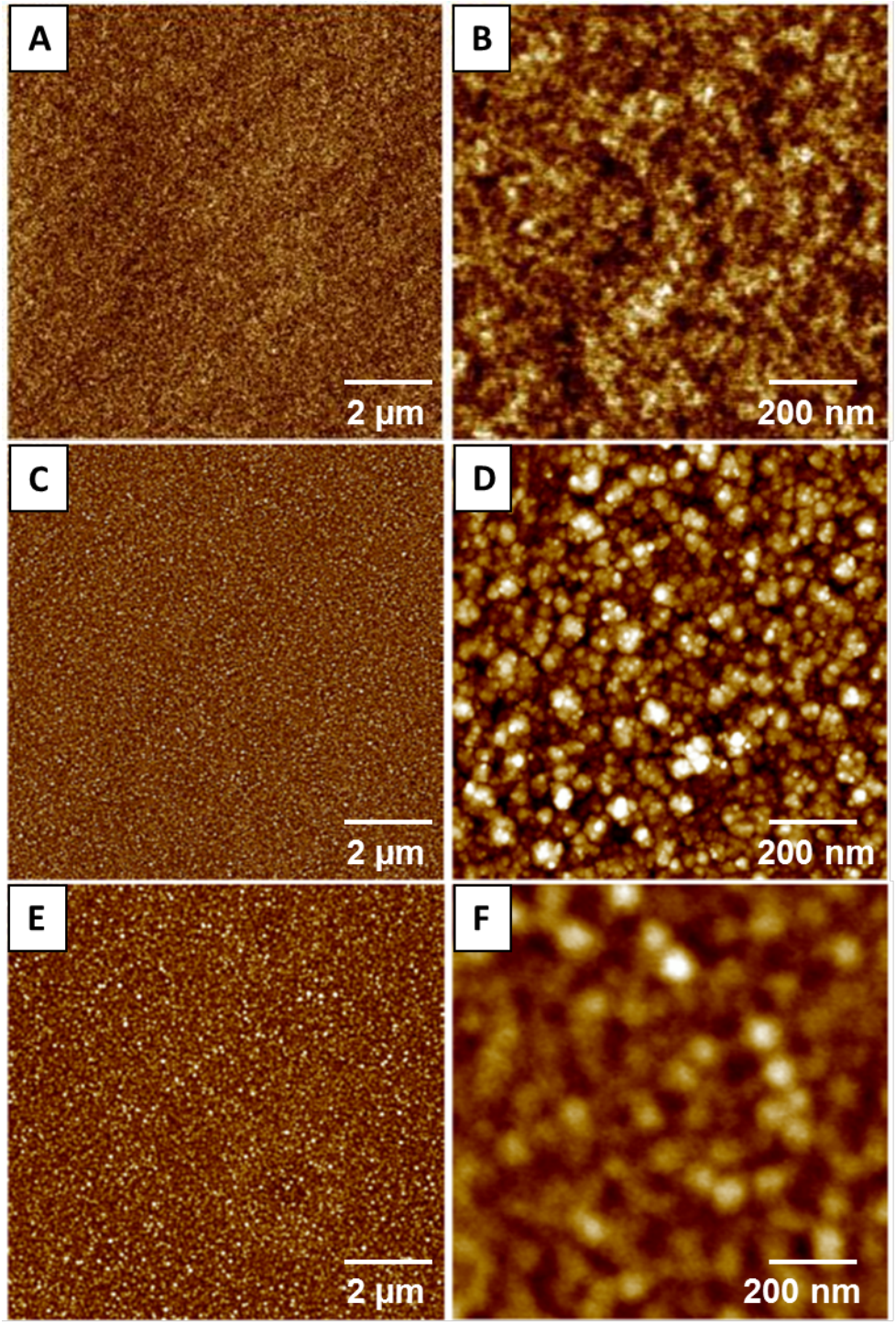

Figure 8.2: AFM of A, B) PP-NIPAAM (Z=2 nm), C, D) PP-TTIP (Z= 16 nm), E, F) PP-NIPAAM/TTIP (Z=14 nm) at low and high magnification.

rougher surface (Figure 8.2 C,D). Previous studies have detailed the use of different deposition atmospheres with titania precursors and found that oxygen rich atmospheres will allow for more complete oxidation to the Ti^{4+} state to occur. This promotes the most complete conversion of the precursor to titania versus an argon atmosphere and produces more stable films.[258] The surface roughness was measured at 2.6 nm, a marked increase from the PP-NIPAAM film and results directly from these characteristic features.

AFM of the PP-NIPAAM/TTIP film shows a surface morphology composed of features of both pure material films (Figure 8.2 F). Some larger, distinct circular features were visible on the surface, but which appear to be coated and not as distinct as the pure PP-TTIP. No fine surface structures were seen in the PP-NIPAAM film was visible on the copolymerized surface, which was likely a result of film mixing and residual methyl group reactions from the TTIP monomer. The surface microroughness was measured at 1.8 nm The film appears to be uniform and free of defects, indicating the plasma deposition process uniformly coats the substrate surface.

8.3.2 Chemical Composition of Thin Films: FTIR & XPS Analysis

FTIR and XPS measurements of the PP-NIPAAM, PP-TTIP and PP-NIPAAM/TTIP films confirm their composition and determine if any major structural changes were occurring during polymerization. The peak assignments for PP-NIPAAM spectra show an N-H (secondary amide) stretch at 3272 cm^{-1} and a C-H asymmetric stretch at 2973 cm^{-1}. Carbon bonding in PP-NIPAAM side chains include a C=O (amide I) stretch at 1645 cm^{-1}, C-H bending at 1463 cm^{-1} and two final peaks at 1390cm^{-1} and 1366 cm^{-1} which are indicative of the methyl groups in the structure. N-H (amide II) stretching is also seen at 1548 cm^{-1} (Figure 8.3, Table 8.1).

Table 8.1: FTIR peak assignments for plasma polymerized films.

	PP-NIPAAM	pNIPAAM	PP-NIPAAM/TTIP	PP-TTIP
N-H stretch	3272	3275	3272	
O-H stretch				3252
C-H stretch	2973	2974	2973	
C=O stretch (amide I)	1645	1640	1646	
C-C stretch				1628
N-H stretch (amide II)	1547	1548	1548	
C-H symmetric bending	1463	1462	1454	
C-CH_3 methyl bending I	1390	1389	1384	
C-CH_3 methyl bending II	1366	1368		1376
Ti-O			697	699

The retention of these methyl groups was important as it is believed that they are contributors to phase transitions in the PP-NIPAAM film.[314] The same peaks were seen in the spun-cast pNIPAAM film with some slight shifting. This provides verification that the plasma polymerization process did not causes significant degradation to the NIPAAM monomer during the plasma process. The PP-NIPAAM spectra also showed excellent agreement compared to the spun-cast film of pNIPAAM and is in agreement with literature.[3,314,323]

The expected peaks of Ti-O at 699 cm^{-1}, residual carbon bonding at 1628 cm^{-1} and methyl groups at 1376 cm^{-1} were seen in the PP-TTIP film as previously noted.[325] The mixed PP-NIPAAM/TTIP film showed distinguishing characteristics of both materials with a Ti-O peak at 697 cm^{-1} and the characteristic peaks of PP-NIPAAM at 1646 cm^{-1}, 1548 cm^{-1}, 1454 cm^{-1} and 1384 cm^{-1} (Figure 8.3). Some broadening of these peaks was seen in comparison to the pure PP-NIPAAM film, which was likely the result of the excess carbon content in the TTIP monomer, deposited on the surface as a byproduct. Overall, the FTIR spectra indicate that the monomers are deposited intact, without significant

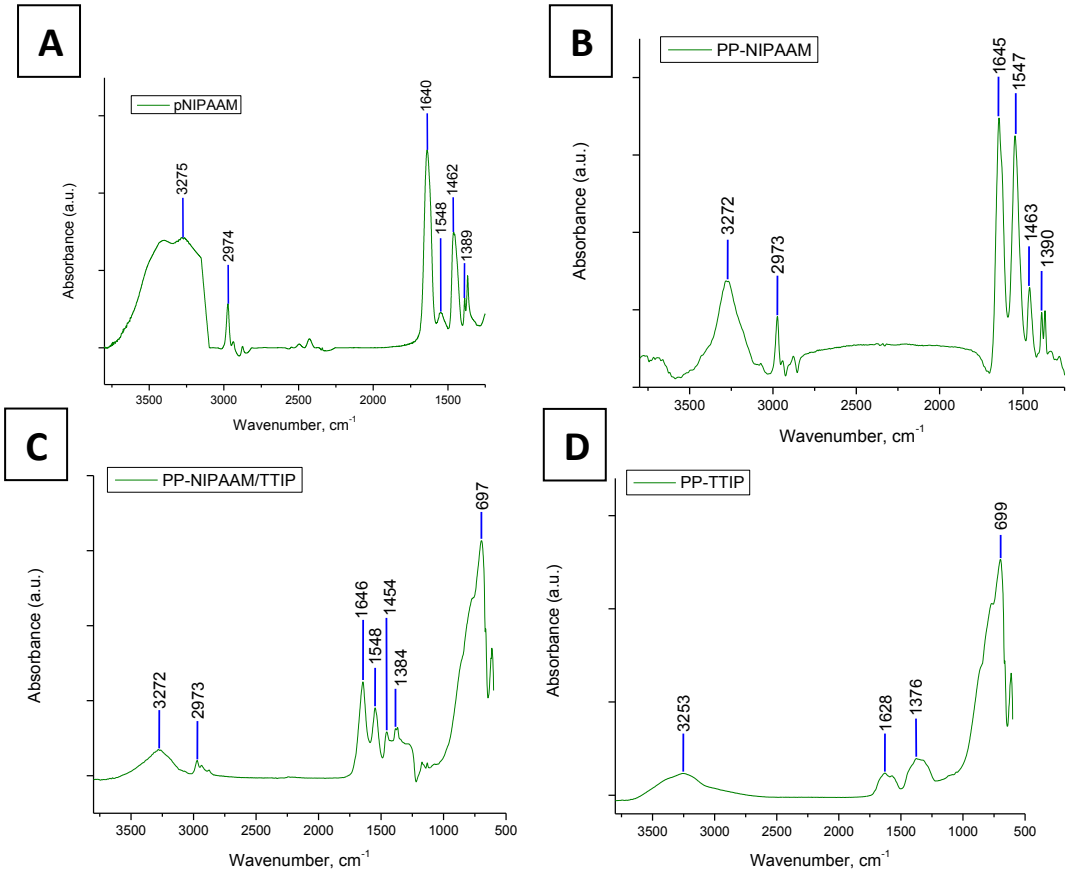

Figure 8.3: FTIR of A) Spun-cast PP-NIPAAM, B) PP-NIAAM, C) PP-NIPAAM/TTIP, D) PP- TTIP.

alteration and combine well to form a mixed film with strong characteristics of both precursor monomers.

XPS analysis of all plasma polymerized films verified the expected compositions which correspond directly to the chemical structures of the monomers (Figure 8.4). High resolution XPS of the carbon content of all three films showed the expected C-C and C-H bonding referenced at 285 eV.[3] The PP-NIPAAM film showed the presence of a carbonyl group (C=O) at 287.7 eV. This peak was also seen in the PP-TTIP film at 288.9 eV and through de-convolution of the PP-NIPAAM/TTIP film spectra at 287.6 eV (Figure 8.5). As the two materials were mixed, this peak shifts closer to that of the PP-NIPAAM due to the increasing number of carbonyl groups of NIPAAM. PP-NIPAAM

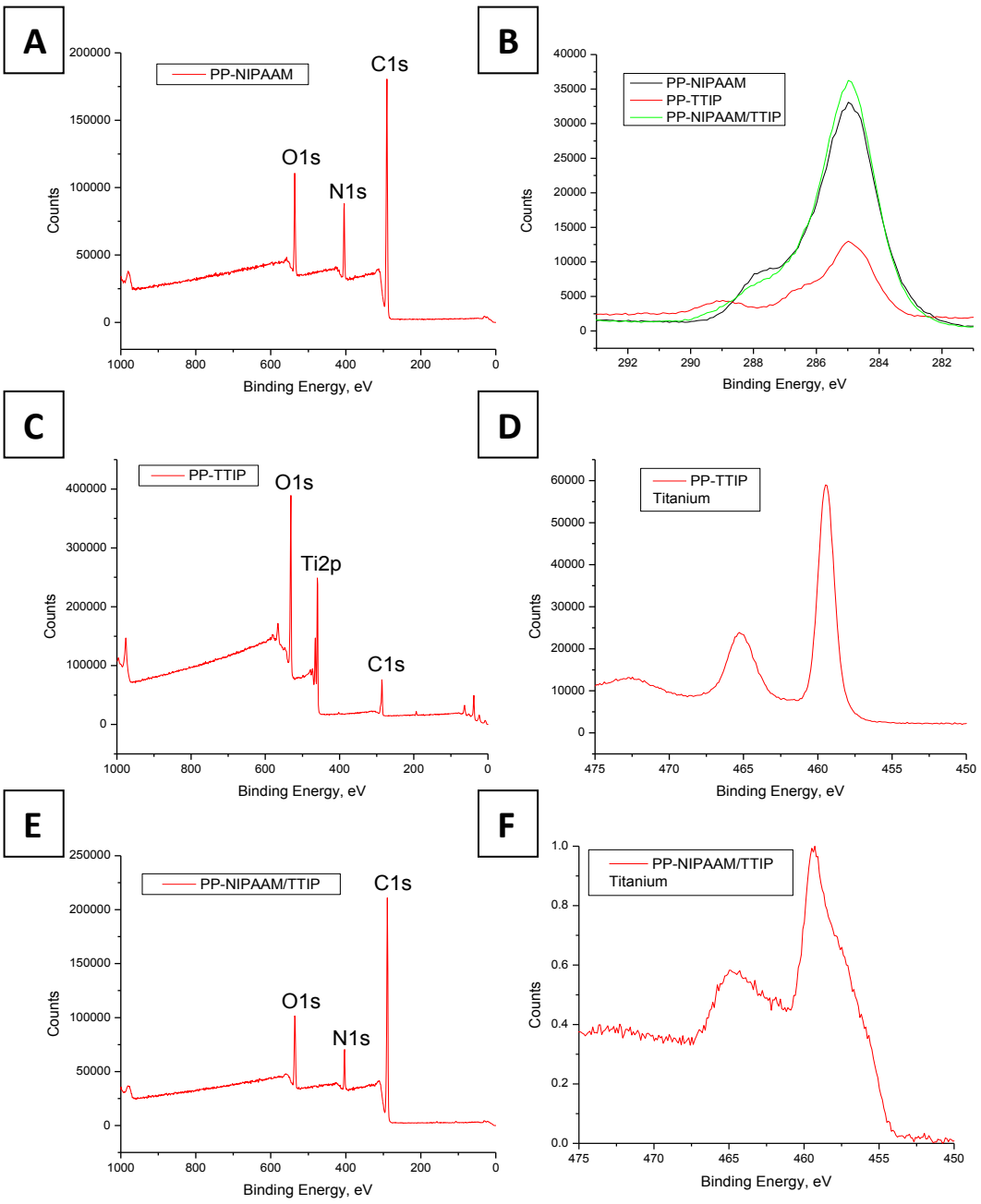

Figure 8.4: XPS of A)PP-NIPAAM, B)High resolution carbon signal of all three materials. C) PP-TTIP, D) High resolution of the titanium signal from the PP-TTIP film. E)PP-NIPAAM/TTIP and F) High resolution of the titanium signal from the PP-NIPAAM/TTIP film after surface etching.

films showed strong carbon, oxygen and nitrogen peaks and PP-TTIP films showed the expected titanium, oxygen and residual carbon peaks, which resulted from the methyl groups attached to the titanium atom in the monomer. Under appropriate conditions, these excess groups form polymerized methyl groups on the surface as well.[258] The

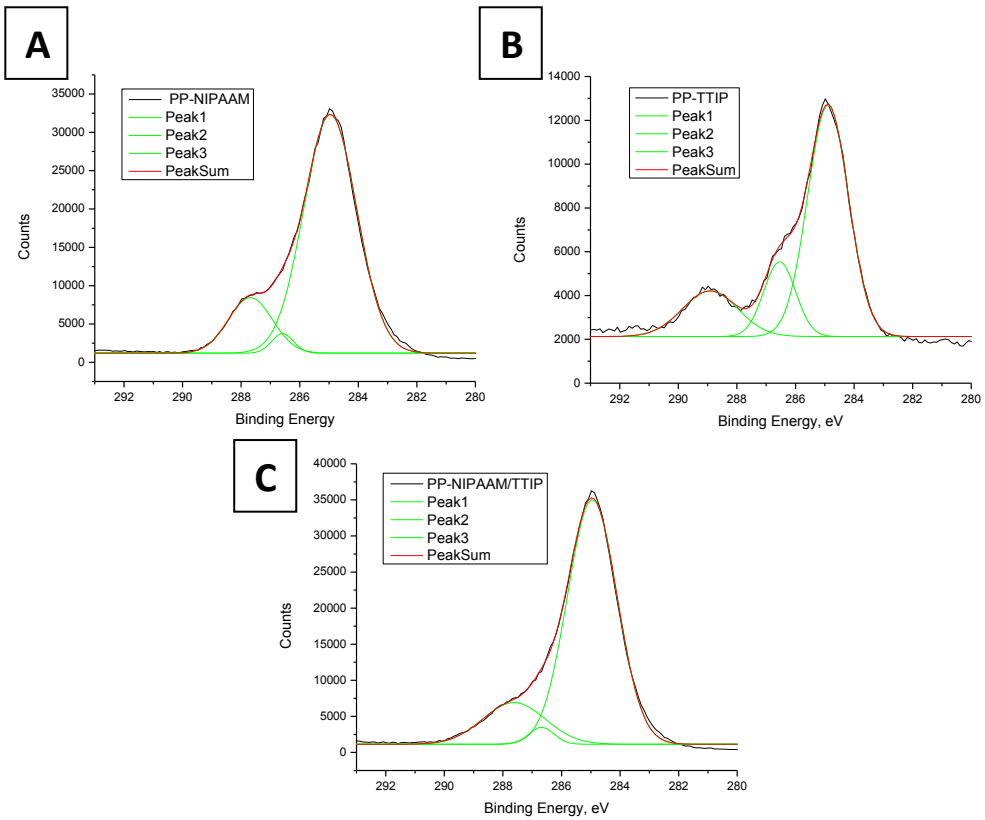

Figure 8.5: High resolution XPS of carbon for A) PP-NIPAAM, B) PP-TTIP, C) PP-NIPAAM/TTIP.

copolymerized film also showed the characteristic peaks of carbon, oxygen and nitrogen, but the surface scan did not reveal the presence of titanium. XPS surface scans only penetrate approximately the first 10 nm of the film and therefore only reveal the surface composition. However, upon etching of the film, a titanium signal emerges and becomes very distinct after ten etch cycles (Figure 8.4 F). This indicates that there is a layer of NIPAAM or residual carbon covering the film, which may occur as a by-product of the monomer inlet arrangement since the NIPAAM monomer was positioned closer to the substrate than the TTIP inlet.

8.3.3 Film Responsiveness

Both PP-NIPAAM and PP-TTIP films were deposited independently prior to co-deposition testing. This allowed for independent evaluation of each film to establish an

expected response magnitude prior to mixing the two materials. Nominal thickness values of all films tested were ~200 nm as measured via ellipsometry.

The PP-NIPAAM films fabricated here exhibit a response when exposed to a high humidity.[40,41,49] This is manifested as a change in thickness as measured by spectroscopic ellipsometry under varying environmental conditions. The high humidity in the atmosphere causes swelling of the PP-NIPAAM film in its hydrophilic state below

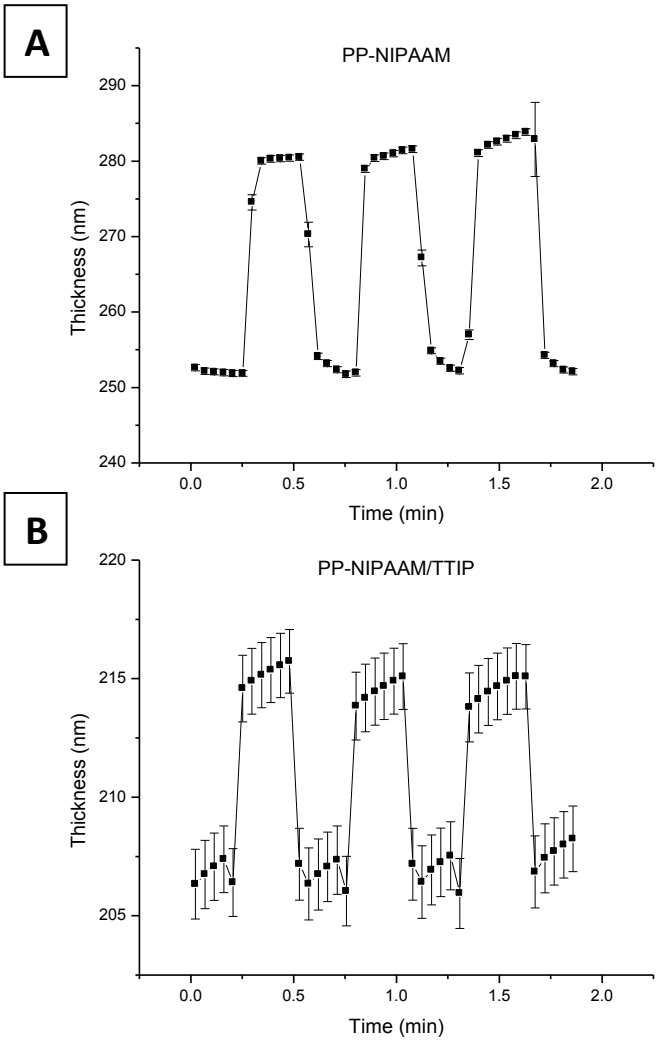

Figure 8.6: Responsive ellipsometry data plots showing on/off of moisture in thickness v. time comparing the rapid response of A) PP-NIPAAM and B) PP-NIPAAM/TTIP.

LCST as compared higher temperatures where swelling is much less pronounced. The response shown was obtained through the rapid switching of dry (1.5 % relative humidity) and moisture saturated nitrogen (95 % relative humidity) that was directly exposed to the film while it was on the ellipsometer stage under a continuous, dynamic measuring regime, which collected measurements at regular intervals. Both single, long moisture exposure and the short, rapid switching regimes were demonstrated (Figure 8.6, Figure 8.7). A full recovery to the initial state is observed in the cycling tests. Generally, the PP-NIPAAM film showed a 16 to 20 nm change in thickness (12%) and a response time on the order of two seconds at 25°C. This swelling ratio was smaller than traditional swollen hydrogel systems, which can range up to one hundred percent or more. This is due to the higher cross-linking density in these plasma polymerized films. UV-photografted pNIPAAM examples from the literature showed similar response times, but significantly larger swelling ratios given the lower cross-linking occurring in the films.[314] The single transitions profiles showed that even during longer exposures to moisture, the transition in thickness is rapid and stable at both high and low humidity conditions (Figure 8.7). One theoretical method for controlling the degree of the response is though the adjustment of the cross-linking density. Higher crosslinking typically will lead to less swelling as the film is more tightly constrained. The other possible method of controlling the response is via the LCST of the PP-NIPAAM. Tests at elevated temperature (50 ºC) show a significantly muted response when compared to ones at 20 ºC indicating that the polymer has passed the LCST. The actual boundary likely occurs around 30 ºC and can be verified through swelling response tests for each film as the actual temperature may vary depending on the polymerization of each film.

The PP-TTIP films were characterized in the same manner as the PP-NIPAAM films with moisture cycling between dry and high relative humidity nitrogen. Very little response

was observed (~1 nm) as expected. Any residual swelling that occurs in the TTIP films was likely the result of excess carbon compounds formed from the methyl groups of the TTIP precursor polymerizing independently on the surface. The reaction leading to this excess material is described in detail elsewhere.[262]

The PP-TTIP film was not responsive to stimuli and any response seen in the PP-NIPAAM/TTIP film came from the PP-NIPAAM component. This indicates that thickness changes of the films are dependent on the type of material used. Blank substrates of bare silicon also show no change in the thickness of the surface when tested under the same atmospheric regimes, indicating that the changes seen are occurring in the

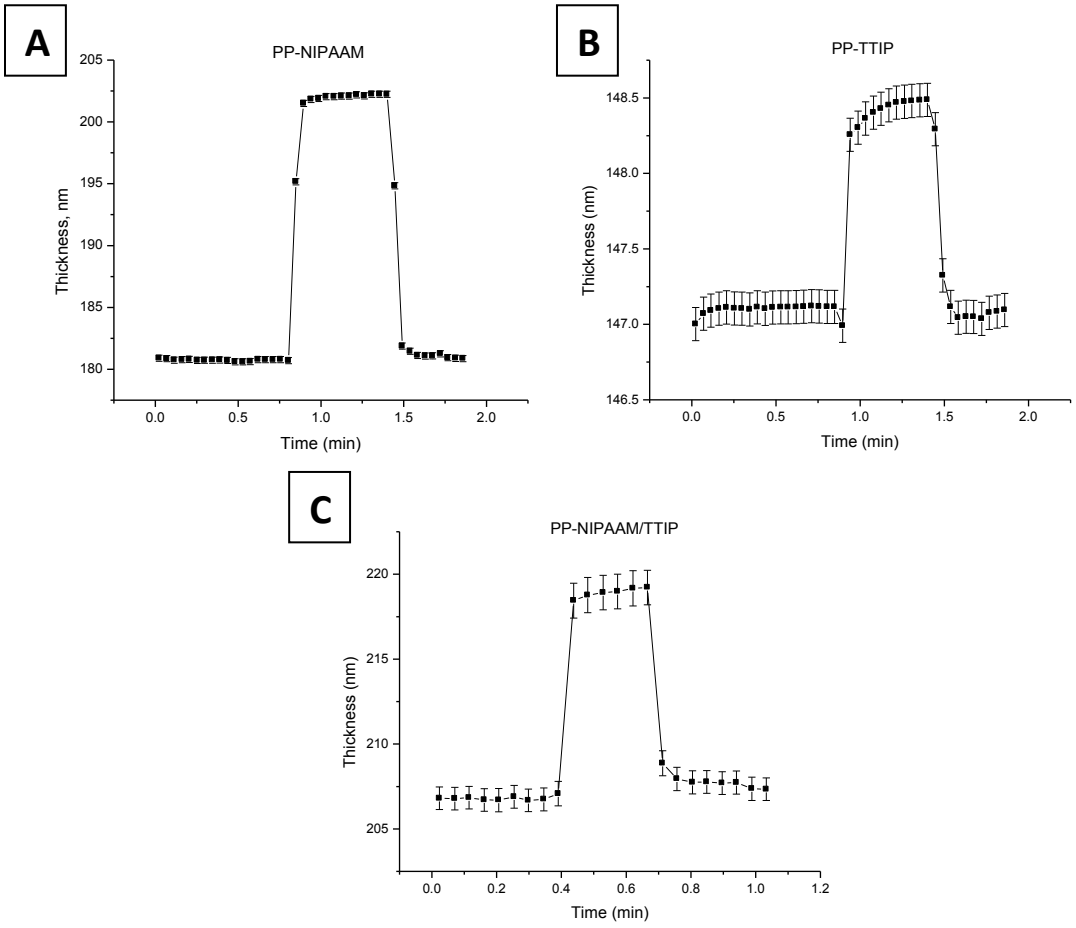

Figure 8.7: Responsive ellipsometry data plots showing on/off of moisture in thickness v. time comparing A) PP-NIPAAM, B) PP-TTIP and C) PP-NIPAAM/TTIP.

polymer layer. In this instance a silicon wafer with no coating was placed in the ellipsometer and subject to the same atmospheric switching used with the PP-NIPAAM films to verify that the thickness changes seen were not the result of moisture accumulation on the surface. Of several plasma polymerized materials tested, PP-NIPAAM showed the most significant response under these conditions.

While a responsive PP-NIPAAM film is interesting in and of itself, using co-deposition techniques where two or more materials are deposited simultaneously in the same plasma reaction, it becomes possible to introduce significant modifications to the original film. The introduction of TTIP to the PP-NIPAAM serves as an optical modifying agent, providing control over the refractive index of the film. The co-polymerized film of PP-NIPAAM/TTIP was subjected to the same moisture testing as the homogenous films. The observed response was similar overall to that of the PP-NIPAAM film (Figure 8.6 B). Even with the co-polymerization addition of the non-responsive titanium dioxide material, the PP-NIPAAM/TTIP showed a response to the humidity (~6% of total film thickness). These tests were repeated using much shorter on/off cycle times for the moisture exposure and the full range of the expected response was seen in the PP-NIPAAM/TTIP films. Each sample was tested for responsiveness many times and continued to show robustness in the response even after some wear from repeated mounting and moisture exposure. The transition (swelling) time in which the thickness change occurred was approximately between one and two seconds. More precise transition time measurements were limited by the time required between measurements on the ellipsometer. However, other swelling times of CVD polymers from literature indicate a swelling timescale of tenths to tens of seconds, depending on the specific film, putting our films well within standard expected response times for these types of films.[27,41]

To measure the mass of water vapor adsorbed on the surface, a QCM disk was coated with PP-NIPAAM and placed in the sealed chamber into which moist air was introduced at differing flow rates. This allowed monitoring of the mass of the water absorbing/desorbing from the plasma polymerized film and confirms a rapid adsorption/desorption was occurring on the film. As the relative humidity in the chamber was increased, there was a corresponding increase in the absorbed mass of the water on the plasma polymerized film. This measurement verified that water vapor was adsorbing to the film as an increases in mass was seen (Figure 8.8).

The moisture adsorption profiles shown indicate that the films rapidly respond to the change in moisture levels in the chamber and follow the programmed profile closely. Small changes in mass (0.01 μg) were easily detected using QCM. The films showed significant response when exposed to flow rates of high relative humidity nitrogen of 10,

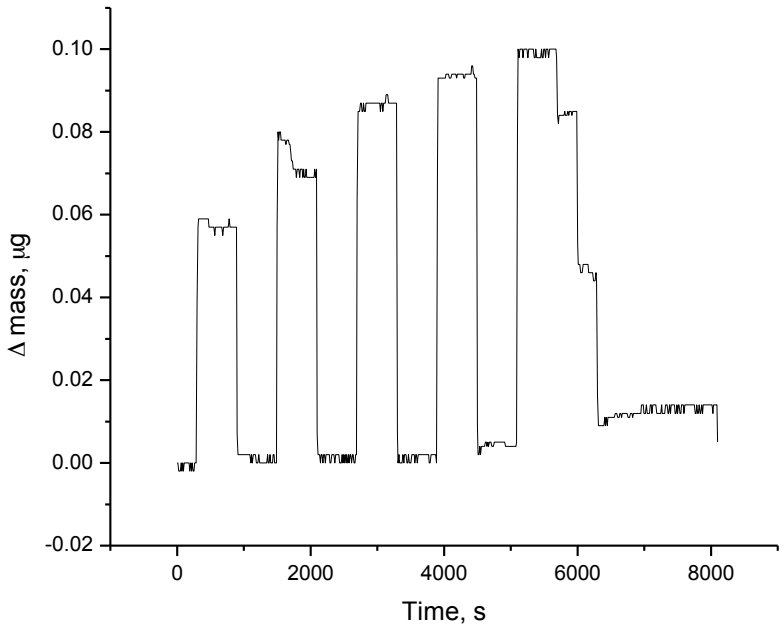

Figure 8.8: QCM measured mass of moisture absorbed by PP-NIPAAM film at various flow rates.

20, 30, 40 and 50 sccm. The final peak shows a gradual step-down of the moist nitrogen flow rate as the system was purged with dry nitrogen and indicates the precise control that can be exerted over the amount of water vapor adsorbed by the PP-NIPAAM film (Figure 8.8). Dynamic ellipsometry measurements and QCM experiments conducted at an elevated temperature of 50ºC showed a significantly reduced response due to the hydrophobic nature of the film seen above LCST. All samples showed a return to previous responsiveness levels when restored to 25°C, indicating a highly reversible and robust thermal transition. This provides another indication of where the LCST of the PP-NIPAAM film is and that behavior at temperatures above and below differ significantly. Since there is no phase separation below the LCST, the PP-NIPAAM system behaves in a much more miscible manner with the water vapor, allowing the film to undergo changes in thickness and adsorb the water onto the surface.

8.3.4 Tailored Refractive Indices

The refractive index was measured for each film composition at three different angles over a large spectral range. From previous experiments, it was expected that this type of material combination would yield a film with a refractive index between the upper and lower limits sets by the pure materials.[85] The upper limit was around 1.95 for PP-TTIP and the lower limit was just below 1.6 for the PP-NIPAAM. (Figure 8.9). The PP-NIPAAM/TTIP co-polymerized films showed a refractive index consistent with a mixture of the two starting monomers. By adjusting the deposition ratios of the monomers, the resulting refractive index of the composite film could be varied within the designated range. Several previous demonstrations have evaluated co-polymerization of distinct monomers for significant refractive index modification.[255,324] The addition of two or more monomers, each with a distinctive refractive index, can be used as a method to create films with precisely tuned refractive indices set at a desired value.[97,325] Additionally,

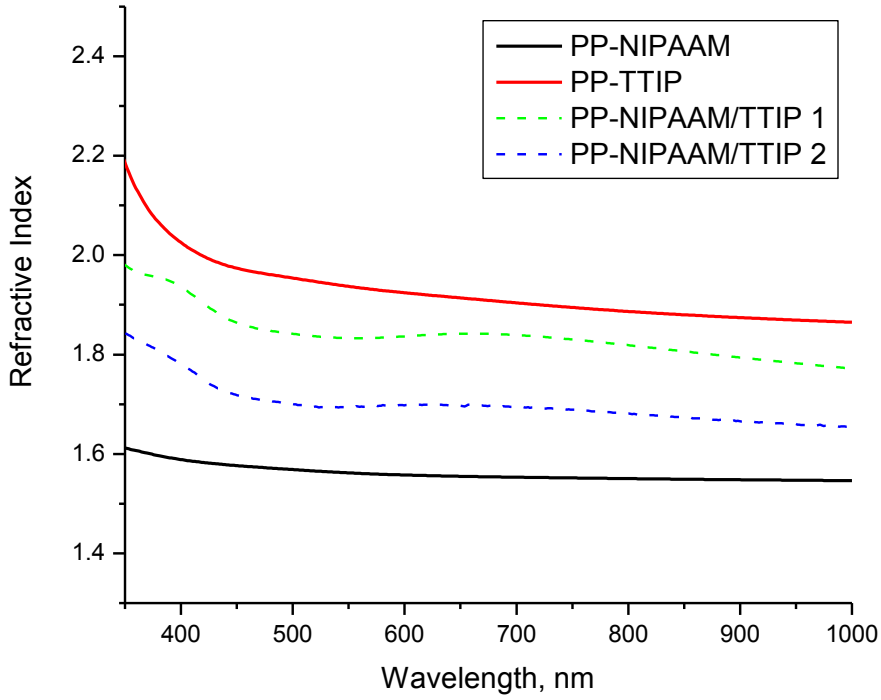

Figure 8.9: Ellipsometry measurements. Refractive index of PP-NIPAAM, PP-TTIP and PP-NIPAAM/TTIP showing mixed refractive index profiles. RI Δ = 0.35

optical stacks have been fabricated which show tunablility using swellable hydrogels sandwiched between high index layers which showed a shift in reflectivity upon activation.[27]

The co-polymerization of these two monomers (NIPAAM and TTIP) provides a facile method of creating a thin film with a higher refractive index than that of a pure polymer, while still retaining some of the moisture responsiveness seen in the pure PP-NIPAAM films as the thickness changes. Such a film could find potential use in many optical applications, especially detection and responsive scenarios. Fabrication of higher index layers with PP-TTIP may be possible at higher temperatures as suggested in the literature which details the formation of anatase phase titania from a TTIP precursor deposited at 300ºC.[326]

8.3.5 Tunable Refractive Indices

A small change in the refractive index was also monitored during the moisture exposure likely due to the change in thickness and the expansion/collapse of the internal cross-linked network in the film. This change was typically on the order 0.01 to 0.1 and is seen to be repeatable multiple times in both the PP-NIPAAM and PP-NIPAAM/TTIP films (Figure 8.10). The index change quickly switches between two states, remains stable for the duration of the applied conditions and then returns to the initial state. This type of rapid cycling demonstrates the rapid, reversible nature of the changing optical properties of the films and how this can be applied in applications where refractive index adjustments are of interest. By composing the film with a specific index of the mixture of the two monomers, tunable films could be applied over a wide range of indices.

Similar refractive index changes have been previously monitored in pNIPAAM hydrogel systems upon swelling and deswelling indicating that the plasma polymerized films are responding as expected when exposed to moisture.[312] The RI changes correspond to

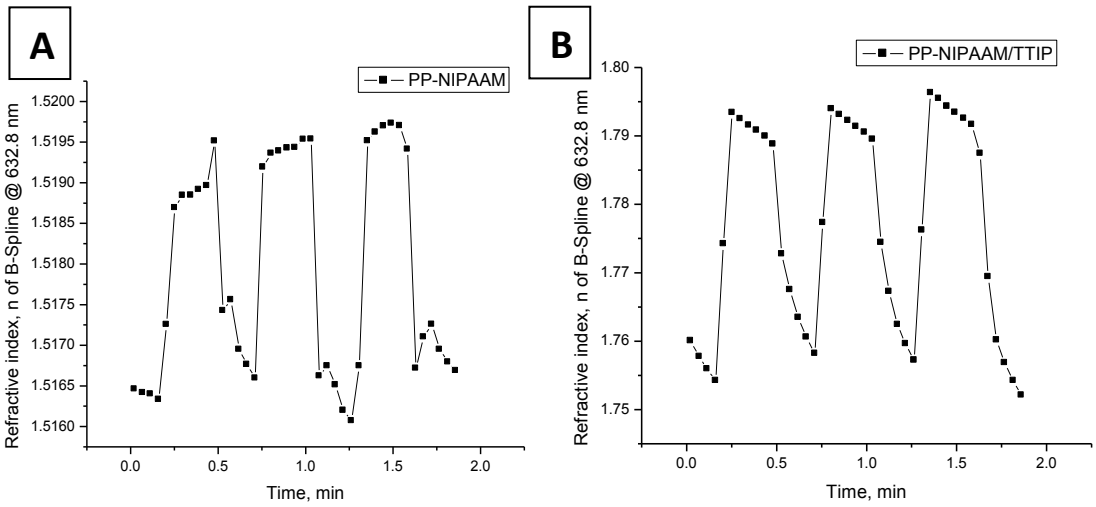

Figure 8.10: Changing refractive index values through moisture cycling. A) PP-NIPAAM and B) PP-NIPAAM/TTIP

the thickness changes of the film as measured by spectroscopic ellipsometry and the beginning refractive index can be adjusted to various levels by controlling the ratio of each monomer in the film. These refractive index variations are applicable in very sensitive applications and systems where this type of refractive index change would be truly effective. Finally, The optical absorption of all three films (PP-NIPAAM, PP-TTIP and PP-NIPAAM/TTIP) was noted to be very low, below 0.04 over the visible range for each of the materials, making these types of films ideal for application where optical transmission is of importance.

8.4 Conclusions

PP-NIPAAM films were shown to be responsive to humidity variation exposure by monitoring the change in thickness as the atmosphere is switched from dry to wet and back to dry with a very sharp on/off transition and a close adherence to the exposure profile of the moisture. This effect was preserved in films in which PP-TTIP has been added to greatly increase the refractive index while still showing a response to environmental stimuli. The response occurs very rapidly when the relative humidity conditions were changed and demonstrated a system that is ideal for responsive sensors, actuators and optical adaptation. The nature of the plasma deposition lends itself well to being able to apply this type of mixed, responsive coating onto a variety of surfaces for many different applications. The responsive PP-NIPAAM was able to be co-deposited with an optically modifying TTIP monomer and sees retention of the rapid and switchable response of the film. This type of switching could be valuable in optical and photonic applications requiring high refractive indices while still being able to exhibit a response as a sensor. The film responded with a change in thickness and refractive index at very low amounts of moisture, which would allow such a system to be used in

highly sensitive optical systems, where precise refractive index control and tunable optical properties are desirable.

This study demonstrated a high refractive index thin film system capable of rapid switching fabricated by a versatile technique that can be applied to a wide variety of surfaces. The rapid response time of the films was a critical component of the design. The design of the materials was a key factor in tailoring the responsiveness of the film to meet specific system design requirements. Future studies focusing on control of the film cross-linking have the potential to provide better control and higher degrees of response, which can be tailored to specific, responsive photonic or sensing applications.

CHAPTER 9 : General Conclusions and Broader Impact

9.1 General Conclusions

The use of PECVD, and the broader family of CVD soft matter deposition techniques, as a method for depositing biological, responsive, functional and unique ultrathin coatings is a growing field with many promising applications, especially in functional coatings, interfacial structures and sensing technologies. Many lessons learned from the PECVD of organic monomers can be applied to facilitate the deposition of biocompatible and biofunctional materials directly on surfaces, providing a direct, dry, one-step modification method which can be broadly applied and tailored to specific materials for various applications (Figure 9.1).

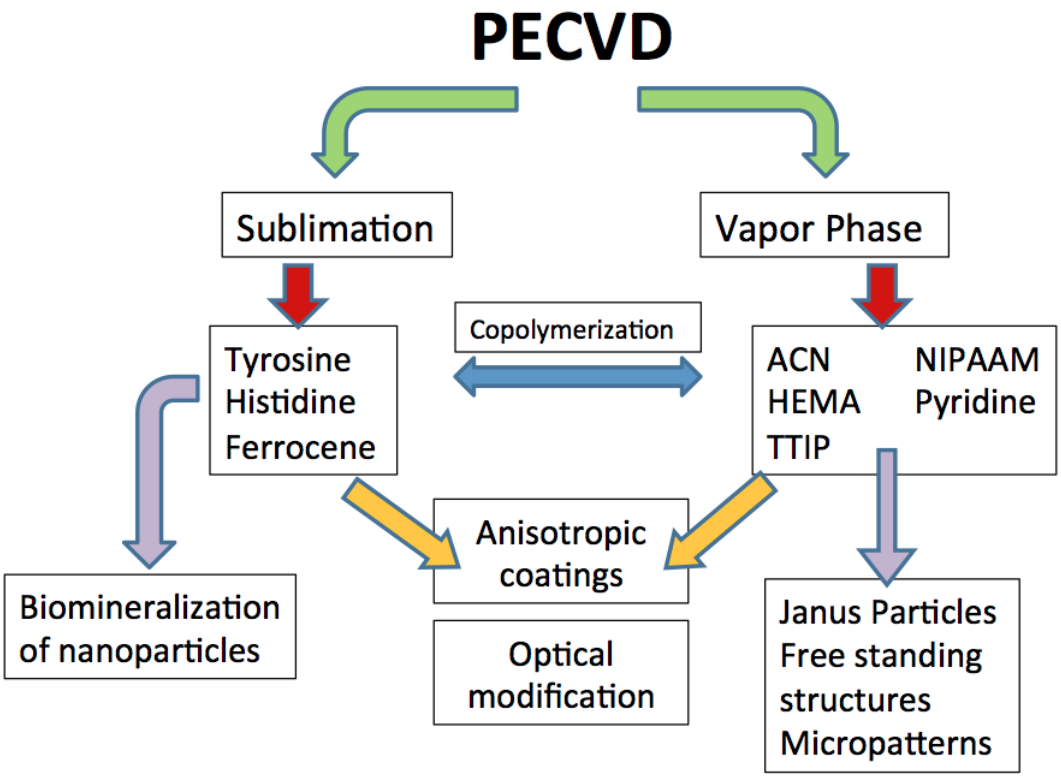

Figure 9.1: Summary of research program completed showing materials used and topics covered.

While this dissertation explores some of the possible materials for biofunctional coatings, specifically ones related to inorganic mineralization, there are many more that remain to be studied and fully characterized. By adapting a variety of modified PECVD techniques for use with specialized biological and complex topological coatings, tailored processes can be developed to meet specific needs in a variety of novel systems.

Ultrathin robust films of amino acids (PP-Tyr, PP-His) were successfully fabricated by PECVD on both smooth and non-uniform surfaces. These ultrathin amino acid films successfully retained their desired functionality. Mineralization of inorganic nanoparticles such as gold and titania directly from solution when exposed to an ionic precursor was fully supported by the plasma polymerized films. Typical mineralized nanoparticle sizes ranged from 3 nm at the smallest particles to over a micron for large aggregate plates. This deposition process demonstrates a unique method to polymerize amino acids directly onto surfaces for the specific purpose of reducing inorganics directly from solution. Plasma polymerization is a unique process, which expands traditional biologically driven mineralization studies to surfaces and systems where they may not be easily applied, such as Teflon, covering a range of practical substrates for use in engineered systems. The sublimation technique used with solid monomers has also proved to be a very effective method of heating powdered amino acids thus vaporizing them directly into the RF plasma stream where they undergo chemical cross-linking and form robust plasma polymerized ultrathin films on a target substrate.

The use of the plasma radical initiation addresses both the anchoring of the monomer to the substrate and the subsequent growth of the film and does not require the use of a surface bound initiator for film adhesion. For the monomer to adhere to the substrate

and growing film surface radicals supporting adhesion must be present and this was achieved by exposure of the substrate to the plasma at the outset of the reaction, allowing the PP film to build over time. This approach has advantages over a prepared surface initiator which limits the total thicknesses. Widespread activation of monomers by the plasma becomes especially important during co-depositions to facilitate facile bonding to the surface and other monomers. Plasma radicalization overcomes these issues allowing the formation of a very smooth and uniform film across the surfaces with typical roughness values below 0.5 nm.

Films formed from TTIP (inorganic compound) exhibit a higher surface microroughnesses (2-3 nm) depending on specific deposition conditions used. Key evidence supporting chemical changes that indicate cross-linking are seen in FTIR spectra, particularly in the 830-870 cm^{-1} range for the amino acid monomers. The shifting of this peak is related to changes in the NH_2 of the amino acid as polymerization occurs at this site. Another indicator of higher cross-linking of PP-Tyr is the refractive index which showed higher values around 1.6 for PP-Tyr compared to lower values of 1.3 and below for spin-cast pTyr films. Cross-linking density typically is correlated with higher indices.

In addition to the various monomers studied here with plasma polymerization, it is shown that a wide range of substrates were capable of supporting plasma polymerized films including polished silicon wafers, glass, nitrocellulose, PTFE, woven silk, SU-8 micro-trusses and silica micro particles. Plasma polymerized amino acids adhere well to these surfaces and they also support the mineralization of the gold and titania nanoparticles in these cases as well as was verified by XPS. This is shown in the case of PP-Tyr on

PTFE and nitrocellulose where a change in the color of the surface is seen from white to red after mineralization.

Modification of the coating's refractive index was demonstrated through multiple cycles of titania particle reduction as well to enhance the refractive index from 1.5 to 1.7. This surface coating nanoparticle reduction method provides a facile approach for tethering high index nanoparticles to many surfaces in a controlled, non-destructive process, which is beneficial for the modification of delicate surfaces, such as porous polymeric structures. Atomically flat {100} silicon surfaces offer an ideal characterization platform for plasma polymerized ultrathin films since they allow facile uniform coatings of the plasma polymers. Ideal surfaces, however, are not always encountered in practical applications of coating technologies and it is essential that the plasma coatings perform as well on other, more textured surfaces.

Co-polymerization of materials via sublimation PECVD demonstrates the ability to combine biological precursors (amino acids) and synthetic molecules into a mixed uniform coating of several hundred nanometers thickness in a rapid, facile, solventless, one-step procedure. This co-polymerization method can be used to form biologically-active and biofunctionalized robust coatings by adding amino acids and short peptides for organic and inorganic matrices. A combination of materials in this fashion could also lead to the formation of synthetic short chain peptide surfaces and could eventually be used in biofunctional and biocompatible coatings on an array of implantable devices.

Specifically, L-tyrosine was co-polymerized with other synthetic organic and inorganic monomers via PECVD to form stable and robust partially cross-linked nanocomposite coatings with a fine morphology formed by microphase-separated individual

components, which to great extent preserve their individual chemical composition and morphological features. The amino acid used in this study can serve as a proxy for other biological molecules (tri-peptides) which can potentially be co-polymerized in a similar fashion with other polymers and inorganic materials to produce robust films with desired compositions and enhanced surface functionality and compatibility. Additionally, the refractive index of mixed films was easily tuned anywhere between the index of the single material films by adjusting the mixing ratios. Since the plasma polymerization fabrication approach can be widely applied to many different surfaces, this technique has the potential for designing enhanced biological interfaces.

Co-polymerization of different monomers also demonstrated the ability to impart responsive characteristics to high refractive index films capable of adjustable thickness and refractive index under controlled humidity. Under moisture vapor exposure, a change in the thickness of the PP-NIPAAM/TTIP film occurred rapidly and reversibly and demonstrated a system ideal for rapidly responsive surfaces, actuators and optical adaptation. The PP-NIPAAM films showed approximately a 12% change in thickness. The composite refractive index of the mixed film was controlled in a wide range between 2.0 and 1.6 varying with monomer ratio of each film. Finally, a humidity responsive change in the PP-NIPAAM/TTIP refractive index was observed within a range of about 0.03. These transitions were typically measured to occur very fast over time scales of 1-2 seconds.

The responsive PP-NIPAAM film is able to be co-deposited with an optically modifying TTIP monomer and retain the same response seen in the pure PP-NIPAAM film. This type of switching could be valuable in optical and photonic applications requiring defined, high refractive indices while still being able to exhibit a fast response. The films show a

change in thickness and refractive index at very low amounts of relative humidity, which would allow such a system to be used in highly sensitive optical systems, where precise refractive index control and tunability are desirable.

The Janus structures demonstrated a unique approach to micro-scale coatings capable of supporting many materials on different substrates that allows the deposition of almost any modifying agent on the surface of a microparticle through a dry, one-step PECVD process. Typical fabrication methods of Janus particles utilize wet chemical synthetic methods and are performed one-by-one leading to a very limited number of particles fabricated. PECVD surface modification is unique in that it allows many particles to be fabricated simultaneously in a single process. It is much more suitable for large scale production and scale up than many single particle fabrication techniques.

Using the plasma deposition technique, a wide variety of material systems were used to create Janus particles with a large range of surface chemistries. The protect and release methodology used in conjunction with a rapid PECVD coating has the potential to be implemented on a larger scale for manufacturing of these types of multifunctional particles and could prove to be a viable method to create 0.1-1.0 g quantities of modified particles, something which is still considered a great challenge in microparticle manufacturing.

The toposelective modification method also demonstrated that free-standing anisotropic or “cap” structures can be reliably fabricated. Plasma polymerization allowed different monomers to be used for this purpose as was demonstrated with pyridine without the need for major changes to the fabrication processes. This method for creating free-standing structures is of interest since many materials can be made into a free-standing

meso-scale structure without the need of any additional supporting chemistries, reactions or modifications to the particles. These shape persistent structures can be produced in relatively high numbers through a process that shows scale-up potential and coated with a wide range of functional plasma coatings. Janus particles and caps of this variety have the potential to be scaled from 100's of nanometer diameter particles to larger ones above 50 μm diameter. Such structures benefit a wide range of emerging applications such as drug delivery, catalysts, sensors, photonic structures, drug delivery, various coatings technologies and micro and nanoelectronics and more uses are expected as these structures are more fully developed. Many structures in nature utilize highly featured meso-scale particles and indeed, cells are a prime example of compartmentalized systems. Plasma coating of microspheres is one method to mimic these highly unique structures for advanced applications.

Overall, the investigation of plasma polymerized amino acids showed remarkable promise as a means to coat, pattern and functionalize surfaces to support mineralization on a broad range of substrates. Complex co-polymerizations carried out have been proven to be a robust method of forming mixed monomer surfaces with biofunctional components. Further investigation of these types of dual coatings may lead to significant impact in the fields of biocompatible coatings, functionality, selective sensing and responsive applications. Plasma polymer coatings on micro particles represent an entirely new synthesis method open to further investigation to elucidate new potential functional coatings amenable to a range of applications that utilize patchy particles and free-standing half-shells.

9.2 Significance, Broader Impact and Future Directions

Our study suggests that PECVD holds an advantage as a synthesis and coating technique over many traditional wet chemical methods in several areas. PECVD is dry, meaning no solvents are needed and can potentially be used as a green manufacturing process in the future without excess chemical waste. PECVD also eliminates the need for complex chemical synthesis procedures for attaching polymers to surfaces, leading to simpler, cheaper coatings. Polymerization reactions are controlled by the plasma conditions allowing almost any functionalized monomer to be polymerized via this method. Due to the non-selective nature of the plasma, the monomer can be coated on to any substrate in the plasma chamber producing an infinite combination of monomer-substrate systems, which may be otherwise difficult to fabricate on a large, single process scale.

The advent of a broadly applicable deposition method compatible with biological monomers, including amino acids and peptides, which can be applied uniformly on many different substrates has potential use as conformal coatings for biomedical devices and implants as well as the direct coating of specific biological materials on a surface. The deposition of biological materials provides a unique opportunity to expand the application of PECVD to these specific types of materials. The ability of these types of films to be used as implant coatings, biosensors, surface enhancement agents and biocompatibility facilitating agents are some of the potential engineering applications of this coating technology. Plasma polymerized biomaterials address issues of surface compatibility and substrate adhesion while allowing direct modification of surfaces with no pre- or post-deposition treatments, a major advantage of plasma polymerization in future applications. Biocompatible implant coatings can be easily and robustly deposited on medical devices to facilitate integration into the body as well as promote cellular

attachment and growth by using compatible surface chemistries and even depositing key peptides such as RGD. The use of amino acids as plasma polymerizable monomers highlights the continued need for PECVD studies with extended peptide sequences as well as an in-depth investigation of in situ shorter oligopeptide formation from several single amino acid monomers.

Co-polymerization PECVD, as a method of reacting multiple monomers (biological and synthetic), has the potential to be the subject of many future developments to fully determine the extent to which mixed films can improve surface characteristics. Co-polymerization is expected to help facilitate integration of inorganic systems with host bodies in the form of compatible coatings for implants, bio-active surfaces and materials which supporting the facile integration between two dissimilar systems. This type of synthesis may also facilitate the direct formation of simple peptide sequences on a surface, which addresses issues in both synthesis and attachment of various peptide chemistries to a substrate in a one step process. The co-polymerization synthesis method could be further adapted to other material combinations to create tailored biofunctional films for various interface applications, especially since the chemistries of the original monomers remain largely intact.

Future experiments with these material systems should focus on further characterization of the cross-linking and internal structure of films by techniques such as X-ray and neutron reflectivity. An in-depth understanding of the structure of the film would allow better control in the design and fabrication process. Additional compositional studies by NMR, especially in the case of co-polymerized films, would help to more accurately determine the nature of the co-polymerization and determine if truly random mixing occurs and to what degree.

Further testing of plasma polymerized amino acids and peptides can be done to evaluate cell adhesion and growth. These surfaces can be fabricated through two different approaches. The first is a direct sublimation deposition of a pre-fabricated peptide sequence used as the monomer. Assuming the monomers are stable under heating and easily vaporizable, they are expected to plasma polymerize as well, as has been observed in several initial trials. The second method involves the simultaneous deposition of three or four different amino acid, allowing them to mix and form a "plasma peptide" on their own as they are deposited. This is advantageous since peptide sequences that may be difficult or expensive to synthesize in large quantities, could be approximated on a surface through this method. Both routes offer plausible methods of surface modification and warrant further investigation. These types of films could potentially be applied to implant coatings, to enhance the facile integration into a host's body since the coatings can be easily applied to device surfaces for facile chemical modification in a one step process allowing for rapid modification.

Fabrication of a larger number of coated particles and free-standing structures must be demonstrated for plasma coated anisotropic particles to become a viable engineering manufacturing approach. The ability to rapidly modify many micron-sized particles with almost any chemistry in a single process is a significant manufacturing advantage. The process can be further streamlined by using sacrificial protecting layers, which are easier to work with. A material that is capable of being removed in a dry or single rinse state, such as one that easily breaks down under exposure to UV light or is water soluble might provide an alternate path to reduced post processing of these types of systems and become more environmentally friendly. Further studies are also needed to investigate more fully the potential of the free-standing half shells that are demonstrated

to ascertain their responsive nature, shape control ability and large scale manufacturing potential.

The use of PECVD in biological material and anisotropic coatings are emerging fields. There is tremendous potential for deposition of many different biological materials directly onto surfaces using a process free from any solution exposure and substrate adhesion difficulties. The challenges present in this type of study require interdisciplinary knowledge between materials science, bioengineering and plasma coatings to appropriately determine not only how to deposit unique materials, but how to guide the motivation behind which materials are of the most pressing importance to fully investigate. Further studies must be undertaken to fully characterize the structure of these films as well as in-depth studies investigating all amino acid and short peptide sequences. Detailed analysis of the nature of the bonding between multiple amino acids and the resulting peptide formation is also essential to understanding the limitations faced in future applications.

Complex ultrathin plasma polymer films represent an area of material science with an immense amount of potential growth, especially in biomedical, responsive photonic and functional surface applications. By depositing a wide range of highly functional, robust materials via PECVD on many different substrates, engineered ultrathin films can be designed to meet a wide range of future applications and challenges.

9.3 Dissemination of Results

9.3.1 Refereed publications directly related to this dissertation

1. **Anderson, K. D.**; Weber, R. B.; McConney, M. E.; Jiang, H.; Timothy, J. Bunning, Vladimir V. Tsukruk "Optically Enhanced Responsive Plasma Polymerized Ultrathin Films" *Polymer*, submitted.
2. **Anderson, K. D.**; Young, S. L.; Jiang, H; Jakubiak, R.; Bunning, T. J.; Naik, R. R.; Tsukruk, V. V. "Plasma Enhanced Co-Polymerization of Amino Acid and Synthetic Monomers" *Langmuir* **2012**, *28*, 1833-1845.
3. **Anderson, K. D.**; Marczewski, K.; Singamaneni, S.; Slocik, J. M.; Naik, R. R.; Bunning, T. J.; Tsukruk, V. V. "Plasma Amino Acid Coatings for a Conformal Growth of Titania Nanoparticles" *ACS Applied Materials and Interfaces* **2010**, 2, 2269-2281.
4. **Anderson, K. D.**; Luo, M.; Jakubiak, R.; Naik, R. R.; Bunning, T. J.; Tsukruk, V. V. "Robust Plasma Polymerized-Titania/Silica Janus Microparticles" *Chemistry of Materials* **2010**, 22, 3259-3264.
5. **Anderson, K. D.**; Slocik, J. M.; McConney, M. E.; Enlow, J. O.; Jakubiak, R.; Bunning, T. J.; Naik, R. R.; Tsukruk, V. V. "Facile Plasma Enhanced Deposition of Ultrathin Crosslinked Amino Acid Films for Conformal Biometallization" *Small* **2009**, 5, 741-749.

9.3.2 Publications from related studies

1. Kodyath, R.; Wang, J.; Combs, Z. A.; Chang, S.; Gupta, M. K.; **Anderson, K. D.**; Brown, R. J. C.; Tsukruk, V. V. "SERS Effects in Silver-decorated Cylindrical Nanopores" *Small* **2011**, *7*,3452-3457.
2. Lisunova, M. O.; Drachuk, I.; Shchepelina, O. A.; **Anderson, K. D.**; Tsukruk, V. V. "Direct Probing of Micromechanical Properties of Hydrogen-Bonded LbL Microcapsule Shells with different Chemical Compositions" *Langmuir* **2011**, *27*, 11157-11165.
3. Combs, Z. A.; Chang, S.; Clark, T.; Singamaneni, S.; **Anderson, K. D.**; Tsukruk, V. V. "Label-Free Raman Mapping of Surface Distribution of Protein A and IgG Biomolecules" *Langmuir* **2011**, *27*, 3198-3205.
4. McConney, M. E.; **Anderson, K. D.**; Brott, L. L.; Naik, R. R.; Tsukruk, V. V. "Bioinspired Material Approaches to Sensing" *Advanced Functional Materials* **2009**, 19, 2527-2544. *Feature Article.*

5. **Anderson, K. D.**; Lu, D. H.; McConney, M. E.; Han, T.; Reneker, D. H.; Tsukruk, V. V. "Hydrogel microstructures combined with electrospun fibers and photopatterning for shape and modulus control" *Polymer* **2008**, *49*, 5284-5293.
6. Peleshanko, S.; **Anderson, K. D.**; Goodman, M.; Determan, M. D.; Mallapragada, S. K.; Tsukruk, V. V. "Thermoresponsive Reversible Behavior of Multistimuli Pluronic®-Based Pentablock Copolymer at the Air-Water Interface" *Langmuir* **2007**, *23*, 25-30. *Invited paper*.
7. LeMieux, M. C.; Peleshanko, S.; **Anderson, K. D.**; Tsukruk, V. V. "Adaptive Nanomechanical Response of Stratified Polymer Brush Structures" *Langmuir* **2007**, *23*, 265-273.

9.3.3 Conference Presentations

1. **Anderson, K. D.**; Marczewski, K. M.; Slocik, J. M.; Jakubiak, R.; Naik, R. R.; Bunning, T. J.; Tsukruk, V. V. "Plasma-Enhanced Deposition of Ultrathin Crosslinked Amino Acid Films for Conformal Biomineralization" Poster Presentation, 3rd IC4N Conference Student Poster Competition, Crete, Greece. June 26-30, **2011**.
2. **Anderson, K. D.**; McConney, M. E.; Jakubiak, R.; Bunning, T. J.; Tsukruk, V. V. "Chemically-induced Responsive Thermal Volume Transformation with Ultrathin PECVD Polymers" Poster Presentation, Materials Research Society Spring 2011 Meeting, San Francisco, CA. April 25-29, **2011**.
3. **Anderson, K. D.**; Jakubiak, R.; Naik, R. R.; Bunning, T. J.; Tsukruk, V. V. "Robust Plasma Polymerized-Titania/Silica Janus Microparticles" Oral Presentation, Materials Research Society Spring 2011 Meeting, San Francisco, CA. April 25-29, **2011**.
4. **Anderson, K. D.**; Marczewski, K.; McConney, M. E.; Singamaneni, S.; Slocik, J. M.; Enlow, J. O.; Jakubiak, R.; Naik, R. R.; Bunning, T. J.; Tsukruk, V. V. "Plasma Polymerized Amino Acids for Surface Functionalization and Nanoparticle Reduction" Oral Presentation, Materials Research Society Spring 2011 Meeting, San Francisco, CA. April 25-29, **2011**.
5. **Anderson, K. D.**; Marczewski, K. B.; Singamaneni, S.; Slocik, J. M.; Jakubiak, R.; Naik, R. R.; Bunning, T. J.; Tsukruk, V. V. "Plasma Deposited Amino Acids for a Conformal Metallization of Photonic Polymeric Systems" Poster Presentation 2010 NanoTechnology for Defense Conference Atlanta, GA. May **2010**.

6. Jakubiak, R.; **Anderson, K. D.**; Slocik, J. M.; McConney, M. E.; Enlow, J. O.; Bunning, T. J.; Naik, R. R.; Tsukruk, V. V. “Plasma Polymerization for Bio-Assisted Fabrication of Nanostructures” Poster Presentation Spring 2010 MRS San Francisco, CA. April **2010**.
7. **Anderson, K. D.**; Slocik, J. M.; McConney, M. E.; Enlow, J. O.; Jakubiak, R.; Bunning, T. J.; Naik, R. R.; Tsukruk, V. V. “Plasma-Enhanced Deposition of Ultrathin Crosslinked Amino Acid Films for Conformal Biometallization” Poster Presentation Fall 2009 Materials Research Society, Boston, MA. December 1, **2009**.
8. **Anderson, K. D.**; McConney, M. E.; Slocik, J. M.; Enlow, J. O.; Jiang, H.; Bunning, T. J.; Naik, R. R.; Tsukruk, V. V. “Plasma Enhanced Deposition of Tyrosine Films for Biomineralization” Poster Presentation Air Force Research Laboratory/RX Biotech Review, Arlington VA. November 12-13, **2008**.

REFERENCES

[1] H. Jiang, W. E. Johnson, J. T. Grant, K. Eyink, E. M. Johnson, D. W. Tomlin, T. J. Bunning, *Chem. Mater.* **2003**, *15*, 340.

[2] W. E. Tenhaeff, L. D. McIntosh, K. K. Gleason, *Adv. Func. Mater.* **2010**, *20*, 1144.

[3] D. O. H. Teare, D. C. Barwick, W. C. E. Schofield, R. P. Garrod, A. Beeby, J. P. S. Badyal, *J. Phys. Chem. B* **2005**, *109*, 22407.

[4] H. Jiang, L. Hong, N. Venkatasubramanian, J. T. Grant, K. Eyink, K. Wiacek, S. Fries-Carr, J. Enlow, T. J. Bunning, *Thin Solid Films* **2007**, *515*, 3513.

[5] M. Yoshida, R. Langer, A. Lendlein, J. Lahann, *J. Macromol. Sci. C* **2006**, *46*, 347.

[6] S. Nejati, K. K. S. Lau, *Nano Lett.* **2011**, *11*, 419.

[7] M. E. Alf, A. Asatekin, M. C. Barr, S. H. Baxamusa, H. Chelawat, G. Ozaydin-Ince, C. D. Petruczok, R. Sreenivasan, W. E. Tenhaeff, N. J. Trujillo, S. Vaddiraju, J. Xu, K. K. Gleason, *Adv. Mater.* **2010** *22*, 1993.

[8] D. W. Hess, *J. Vac. Sci. Technol. A* **1984**, *2*, 244.

[9] G. Yang, X. Wang, Q. Xu, S. Wang, H. Tian, W. Zheng, *J. Solid State Chem.* **2009**, *182*, 966.

[10] Z. Chen, W. Ren, L. Gao, B. Liu, S. Pei, H.-M. Cheng, *Nat. Mater.* **2011**, *10*, 424

[11] P Xu, X. Ji, H. Yang, J. Qi, W. Zheng, V. Abetz, S. Jiang, J. Shen, *Mater. Chem. Phys.* **2010**, *119*, 249.

[12] R. Sreenivasan, K. K. Gleason, *Chem. Vapor Depos.* **2009**, *15*, 77.

[13] W. F. Gorham, *J. Polym. Sci, Part A: Polym. Chem.* **1966**, *4*, 3027.

[14] R. Förch, A. N. Chifen, A. Bousquet, H. L. Khor, M. Jungblut, L.-Q. Chu, Z. Zhang, I. Osey-Mensah, E.-K. Sinner, W. Knoll, *Chem. Vapor Depos.* **2007**, *13*, 280.

[15] H. D. Biederman, In *Plasma Polymer Films*; H. D. Biederman, Ed.; Imperial College Press: London, UK, **2004**.

[16] Y. Kang, J. J. Walish, T. Gorishnyy, E. L. Thomas, *Nat. Mater.* **2007**, *6*, 957.

[17] M. Kuzuya, A. Noguchi, H. Ito, S.-I. Kondo, N. Noda, *J. Polym. Sci. Pol. Chem.* **1991**, *29*, 1.

[18] D. W. Hess, *J. Vac. Sci. Technol. A* **1990**, *8*, 1677.

[19] W. E. Tenhaeff, K. K. Gleason, *Adv. Func. Mater.* **2008**, *18*, 979.

[20] J. Friedrich, G. Kühn, R. Mix, In *Plasma Processes and Polymers*; R. d'Agostino, P. Favia, C. Oehr, M. R. Wertheimer, Eds. Wiley-VCH Verlag GmbH & Co. KGaA: Weinheim, **2005**.

[21] S. G. Im, K. K. Gleason, *AICHE J.* **2011**, *57*, 276.

[22] K. K. S. Lau, Y. Mao, H. G. P. Lewis, S. K. Murthy, B. D. Olsen, L. S. Loo, K. K. Gleason, *Thin Solid Films* **2006**, *501*, 211.

[23] S. H. Baxamusa, K. K. Gleason, *Adv. Func. Mater.* **2009**, *19*, 3489.

[24] G. Ozaydin_Ince, K. K. Gleason, *Chem. Vap. Dep.* **2010**, *16*, 100.

[25] R. E. I. Shropp, *Thin Solid Films* **2009**, *517*, 3415.

[26] H. Yasuda, *Plasma Polymerization*, Academic Press, Inc. New York, **1985**.

[27] M. Karaman, S. E. Kooi, K. K. Gleason, *Chem. Mater.* **2008**, *20*, 2262.

[28] A. Choukourov, H. Biederman, D. Slavinska, L. Hanley, A. Grinevich, H. Boldyryeva, A. Mackova, *J. Phys. Chem. B* **2005**, *109*, 23086.

[29] S. Singamaneni, M. C. LeMieux, H. P. Lang, C. Gerber, Y. Lam, S. Zauscher, P. G. Datskos, N. V. Lavrik, H. Jiang, R. R. Naik, T. J. Bunning, V. V. Tsukruk, *Adv. Mater.* **2008**, *20*, 653.

[30] S. Bouaidat, C. Berendsen, P. Thomsen, S. Guldager Petersen, A. Wolff, J. Jonsmann, *Lab Chip* **2004**, *4*, 632

[31] J. M. Slocik, E. R. Beckel, H. Jiang, J. O. Enlow, J. S. Zabinski, T. J. Bunning, R. R. Naik, *Adv. Mater.* **2006**, *18*, 2095.

[32] H. E. Canavan, X. Cheng, D. J. Grahm, B. D. Ratner, D. G. Castner, *Langmuir* **2005**, *21*, 1949.

[33] S. Singamaneni, M. C. LeMieux, H. Jiang, T. J. Bunning, V. V. Tsukruk, *Chem. Mater.* **2007**, *19*, 129.

[34] S. Bouaidat, B. Winther-Jensen, S. Flygenring Christensen, J. Jonsmann, *Sensor. Actuat. A-Phys*. **2004**, *110*, 390.

[35] L. L. Atanasoska, J. C. Buchholz, G A. Somorjai, *Surf. Sci.* **1978**, *72*, 189.

[36] N. H. Lee, C. W. Frank, *Langmuir* **2003**, *19*, 1295.

[37] L. Adler-Abramovich, D. Aronov, P. Beker, M. Yevnin, S. Stempler, L. Buzhansky, G. Rosenman, E. Gazit, *Nat. Nanotechnol.* **2009**, *4*, 849.

[38] J. Shklovsky, P. Beker, N. Amdursky, E. Gazit, G. Rosenman, *Mater. Sci. Eng. B.* **2010**, *169*, 62.

[39] M. Reches, E. Gazit, *Nat. Nanotechnol.* **2006**, *1*, 195.

[40] P. A. Tamirisa, J. Koskinen, D. W. Hess, *Thin Solid Films* **2006**, *515*, 2618.

[41] P. A. Tamirisa, D. W. Hess, *Macromolecules* **2006**, 39, 7092.

[42] K. Chan, K. K. Gleason, *Langmuir* **2005**, *21*, 8930.

[43] G. P. López, B. D. Ratner, *J. Polym. Sci. Pol. Chem.* **1992**, *30*, 2415.

[44] K. D. Anderson, J. M. Slocik, M. E. McConney, J. O. Enlow, R. Jakubiak, T. J. Bunning, R. R. Naik, V. V. Tsukruk, *Small*, **2009**, *5*, 741.

[45] K. D. Anderson, K. Marczewski, S. Singamaneni, J. M. Slocik, R. R. Naik, T. J. Bunning, V. V. Tsukruk, *Appl. Mater. Inter.* **2010**, *2*, 2269.

[46] K. D. Anderson, M. Luo, R. Jakubiak, R. R. Naik, T. J. Bunning, V. V. Tsukruk, *Chem. Mater.* **2010**, *22*, 3259.

[47] H. U. Khan, M. E. Roberts, O. Johnson, R. Förch, W. Knoll, Z. Bao, *Adv. Mater.* **2010**, *22*, 4452.

[48] S. Singamaneni, M. E. McConney, V. V. Tsukruk, *Adv. Mater.* **2010**, *22*, 1263.

[49] Y. V. Pan, R. A. Wesley, R. Luginbuhl, D. D. Denton, B. D. Ratner, *Biomacromolecules* **2001**, *2*, 32.

[50] E. M. Johnson, S. J. Clarson, H. Jiang, W. Su, J. T. Grant, T. J. Bunning, *Polymer*, **2001**, *42*, 7215.

[51] M. C. LeMieux, M. E. McConney, Y.-H. Lin, S. Singamaneni, H. Jiang, T. J. Bunning, V. V. Tsukruk, *Nano Lett.* **2006**, *6*, 730.

[52] H. Biederman, D. Slavínská, *Surf. Coat. Tech.* **2000**, *125*, 371.

[53] J. Lahann, *Polym. Int.* **2006**, *55*, 1361.

[54] H.-Y. Chen, J. Lahann, *Langmuir* **2011**, *27*, 34.

[55] N. Mari-Buye, S. O'shaughnessy, C. Colominas, C. E. Semino, K. K. Gleason, S. Borros, *Adv. Func. Mater.* **2009**, *19*, 1276.

[56] H. Biederman, Y. Osada, *Plasma Polymerization Processes*, Elsevier, Amsterdam, **1992**.

[57] H. G. P. Lewis, D. J. Edell, K. K. Gleason, *Chem. Mater.* **2000**, *12*, 3488.

[58] M. Kuzuya, A. Noguchi, M. Ishikawa, A. Koide, K. Sawada, A. Ito, N. Noda, *J. Phys. Chem.* **1991**, *95*, 2398.

[59] M. Kuzuya, A. Noguchi, H. Ito, S.-I. Kondo, N. Noda, *J. Polym. Sci. A1* **1991**, *29*, 1

[60] D. Barton, R. D. Short, S. Fraser, J. W. Bradley, Chem. Commun. 2003, 348.

[61] P. N. Brookes, S. Fraser, R. D. Short, L. Hanley, E. Fuoco, A. Roberts, S. Hutton, *J. Electron Spectrosc.* **2001**, *21*, 281.

[62] D. B. Haddow, R. M. France, R. D. Short, J. W. Bradley, D. Barton, *Langmuir* **2000**, *15*, 5654.

[63] A. Michelmore, P. M. Bryant, D. A. Steele, K. Vasilev, J. W. Bradley, R. D. Short, *Langmuir* **2011**, *27*, 11943.

[64] D. Hegemann, M. M. Hossain, E. Körner, D. J. Balazas, *Plasma Process. Polym.* **2007**, *4*, 229.

[65] M. C. M. van de Sanden, *Plasma Process. Polym.* **2010**, *7*, 887.

[66] D. Hegemann, E. Körner, S. Guimond, *Plasma Process. Polym.* **2010**, *7*, 371.

[67] A. von Keudell, J. Benedikt, *Plasma Process. Polym.* **2010**, *7*, 376.

[68] D. Hegemann, E. Körner, K. Albrect, U. Schütz, S. Guimond, *Plasma Process. Polym.* **2010**, *7*, 889

[69] K. K. Gleason, *Plasma Process. Polym.* **2010**, *7*, 380.

[70] M. T. Seman, D. N. Richards, P. Rowlette, C. A. Wolden, *Chem. Vap. Dep.* **2008**, *14*, 296.

[71] S.-H. Cho, Z.-T. Park, J.-G. Kim, J.-H. Boo, *Surf. Coat. Tech.* **2003**, *174*, 1111.

[72] X. Cheng, H. E. Canavan, M. J. Stein, J. R. Hull, S. J. Kweskin, M. S. Wagner, G. A. Somorjai, D. G. Castner, B. D. Ratner, *Langmuir* **2005**, *21*, 7833.

[73] J. O. Enlow H. Jiang, J. T. Grant, K. Eyink, W. Su, T. J. Bunning, *Polymer* **2008**, *49*, 4042.

[74] C. A. Pfluger, R. L. Carrier, B. Sun, K. S. Ziemer, D. D. Burkey, *Macromol. Rapid Comm.* **2009**, *30*, 126.

[75] C. A. Pfluger, D. D. Burkey, L. Wang, B. Sun, K. S. Ziemer, R. L. Carrier, *Biomacromol.* **2010**, *11*, 1579.

[76] A. Choukourov, I. Gordeev, D. Arzhakov, A. Artemenko, A. Kylián, J. Kousal, O. Polonskyi, J. Pešička, D. Slavínská, H. Biederman, *Surf. Coat. Tech.* **2011**, *205*, 2830.

[77] J. Wiedemair, B. Balu, J.-S. Moon, D. W. Hess, B. Mizaikoff, C. Kranz, *Anal. Chem.* **2008**, *80*, 5260.

[78] G. T. Dobbs, B. Balu, C. Young, C. Kranz, D. W. Hess, B. Mizaikoff, *Anal. Chem.* **2007**, *79*, 9566.

[79] H. S. Jeon, J. Wyatt, D. Harper-Nixon, D. H. Weinkauf, *J. Polym. Sci. Pol. Phys.* **2004**, *42*, 2522.

[80] A. Nelson, B. W. Muir, J. Oldham, C. Fong, K. M .McLean, P. G. Hartley, S. K .Øiseth, M. James, *Langmuir* **2006**, *22*, 453.

[81] H. Kim, M. D. Foster, H. Jiang, S. Tullis, T. J. Bunning, C. F. Majkrzak, *Polymer* **2004**, *45*, 3175.

[82] H. S. Jeon, J. Wyatt, D. Harper-Nixon, D. H. Weinkauf, *J. Polym. Sci. Phys.* **2004**, *42*, 2522.

[83] A. Nelson, B. W. Muir, J. Oldham, C. Fong, K. M. McLean, P. G. Hartley, S. K. Øiseth, M. James, *Langmuir*, **2006**, *22*, 453.

[84] S. R. Peri, B. Habersberger, B. Akgun, H. Jiang, J. Enlow, T. J. Bunning, C. F. Majkrzak, M. D. Foster, *Polymer* **2010**, *51*, 4390.

[85] S. R. Peri, H. Kim, B. Akgun, J. Enlow, H. Jiang, T. J. Bunning, X. Li, M. D. Foster, *Polymer* **2010**, *51*, 3971.

[86] J. D. Whittle, R. D. Short, C. W. I. Douglas, J. Davies, Chem. Mater. 2000, *12*, 2664.

[87] X. Jiang, J. Bai, S. A. Gittens, H. Uludağ, Mat.-wiss. U. Werkstofftech. 2006, *37*, 462.

[88] I. Tokarev, S. Minko, *Soft Matter* **2009**, *5*, 511.

[89] C. Tarducci, W. C. E. Schofield, J. P. S. Badyal, *Chem. Mater.* **2002**, *14*, 2541.

[90] F. J. Aparicio, M. Holgado, A. Borras, I. Blaszczyk-Lezak, A. Griol, C. A. Barrios, R. Casquel, F. J. Sanza, H. Sohlström, M. Antelius, A. R. González-Elipe, A. Barranco, *Adv. Mater.* **2011**, *23*, 761.

[91] F. J. Aparicio, A. Borras, I. Blaszczyk-Lezak, P. Gröning, A. Álvarez-Herrero, M. Fernández-Rodríguez, A. R. González-Elipe, A. Barranco, *Plasma Process. Polym.* **2009**, *6*, 17.

[92] I. Blaszczyk-Lezak, F. J. Aparicio, A. Borrás, A. Barranco, A. Álvarez-Herrero, M. Fernández-Rodríguez, A. R. González-Elipe, *J. Phys. Chem. C* **2009**, *113*, 431.

[93] A. Barranco, P. Groening, *Langmuir* **2006**, *22*, 6719.

[94] Y. Xu, X. Zhu, Y. Dan, J. H. Moon, V. W. Chen, A. T. Johnson, J. W. Perry, S. Yang, S. *Chem. Mater*. **2008**, *20*, 1816.

[95] M. B. Dickerson, K. H. Sandhage, R. R. Naik, *Chem. Rev.* **2008**, *108*, 4935.

[96] S. Singamaneni, E. Kharlampieva, J.-H. Jang, M. E. McConney, H. Jiang, T. J. Bunning, E. L. Thomas, V. V. Tsukruk, *Adv. Mater*. **2010**, *22*, 1369.

[97] H. Jiang, K. O'Neill, J. T. Grant, S. Tullis, K. Eyink, W. E. Johnson, P. Fleitz, T. J. Bunning, *Chem. Mater.* **2004**, *16*, 1292.

[98] H. Jiang, K. Eyink, J. T. Grant, J. Enlow, S. Tullis, T. J. Bunning, *Chem. Vapor Depos.* **2008**, *14*, 286.

[99] G. Demirel, F. Buyukserin, *Langmuir* **2011**, *27*, 12533.

[100] S. P. Low, R. D. Short, D. A. Steele, *J. Adhes. Sci. Technol.* **2010**, *24*, 2215.

[101] P. Favia, M. Vulpio, R. Marino, R. d'Agostino, R. P. Mota, M. Catalano, Plasmas Polym. 2000, 5, 1

[102] L. M. Szott, M. J. Stein, B. D. Ratner, T. A. Horbett, *J. Biomed. Mater. Res.* **2011**, *96*, 150.

[103] C. Choi, D. Jung, D. W. Moon, T. G. Lee, *Surf. Interface Anal.* **2011**, *43*, 331.

[104] L. Tang, Y. Wu, R. B. Timmons, *J. Biomed. Res.* **1998**, *28*, 156.

[105] M. Malmsten, B. Lassen, K. Holmberg, V. Thomas, G. Quash, *J. Colloid Interf. Sci.* **1996**, *177*, 70.

[106] L. Detomaso, R. Gristina, G. S. Senesi, R. d'Agostino, P. Favia, *Biomaterials* **2005**, *26*, 3831.

[107] A. Harsch, J. Calderon, R. B. Timmons, G. W. Gross, *J. Neurosci. Methods* **2000**, *98*, 135.

[108] L. Addadi, S. Weiner, *Angew. Chem. Int. Ed. Engl.* **1992**, *31*, 153.

[109] L. Addadi, J. Moradian, E. Shay, N. G. Maroudas, S. Winer, *P. Natl. Acad. Sci. USA.* **1987**, *84*, 2732.

[110] E. Beniash, R. A. Metzler, R. S. K. Lam, P. U. P. A. Gilbert, *J. Struct. Biol.* **2009**, *166*, 133.

[111] S. Weiner, L. Addadi, *Annu. Rev. Mater. Res.* **2011**, *41*, 21.

[112] A. Dey, P. H. H. Bomans, F. A. Müller, J. Will, P. M. Frederik, G. de With, N. A. J. M. Sommerdijk, *Nat. Mater.* **2010**, *9*, 1010.

[113] K.-I. Sano, S. Yoshii, I. Yamashita, K. Shiba, *Nano Lett.* **2007**, *7*, 3201.

[114] E. Kharlampieva, J. M. Slocik, T. Tsukruk, R. R. Naik V. V. Tsukruk, *Chem. Mater.* **2008**, *20*, 5822.

[115] R. H. Jin, J. J. Yuan, *J. Mater. Chem.* **2005**, *15*, 4513.

[116] B. M. Rybak, K. N. Bergman, M. Ornatska, K. L. Genson, V. V. Tsukruk, *Langmuir,* **2006,** *22,* 1027.

[117] M. C. Daniel, D. Astruc, *Chem. Rev.* **2004**, *104*, 293.

[118] S. Si, T. K. Mandal, *Chem. Eur. J.* **2007**, *13*, 3160.

[119] E. Dujardin, C. I. Peet, G. Stubbs, J. N. Culver, S. Mann, *Nano Lett.* **2003**, *3*, 413.

[120] S. Mann, Biomineralization: Principles and Concepts in Bioinorganic Materials Chemistry, Oxford University Press. Oxford, **2001**.

[121] J. Xie, J. Y. Lee, D. I. C. Wang, *J. Phys. Chem. C* **2007**, *111*, 10226.

[122] R. Naik, S. J. Stringer, G. Agarwal, S. E. Jones, M. O. Stone, *Nat. Mater.* **2002,** *1*, 169.

[123] M. B. Dickerson, S. E. Jones, Y. Cai, G. Ahmad, R. R. Naik, N. Kröger, K. H. Sandhage, *Chem. Mater.* **2008**, *20*, 1578.

[124] J. M. Slocik, J. T. Moore, D. W. Wright, *Nano Lett.* **2002**, *2*, 169.

[125] M. N. Tahir, P. Théato, W. E. G. Müller, H. C. Schröder, A. Borejko, S. Faiß, A. Janshoff, J. Huth, W. Tremel, *Chem. Commun.* **2005**, 5533.

[126] S. H. Yang, K. Kang, I. S. Choi, *Chem. Asian. J.* **2008**, *3*, 2097.

[127] J. Wang, J. Xu, M. D. Goodman, Y. Chen, M. Cai, J. Shinar, Z. Lin, *J. Mater. Chem.* **2008**, *18*, 3270.

[128] N. Kröger, M. B. Dickerson, G. Ahmad, Y. Cai, M. S. Haluska, K. H. Sandhage, N. Poulsen, V. C. Sheppard, *Angew. Chem. Int. Ed.* **2006**, *45*, 7239.

[129] E. Kharlampieva, T. Tsukruk, J. M. Slocik, H. Ko, N. Poulsen, R. R. Naik, N. Kröger, V. V. Tsukruk, *Adv. Mater.* **2008,** *20,* 3274.

[130] S. Nejati, K. K. S. Lau, *Thin Solid Films* **2011**, *519*, 4551.

[131] K. J. Lee, J. Yoon, J. Lahann, *Curr. Opin. Colloid In.* **2011**, *16*, 195.

[132] J. Du, R. K. O'Reilly, *Chem. Soc. Rev.* **2011**, *40*, 2402.

[133] Tsukruk, V. V.; Bliznyuk, V. N. *Langmuir* **1998**, *14*, 446-455.

[134] M. E. McConney, S. Singamaneni, V. V. Tsukruk, *Polym. Rev.* **2010**, *50*, 235.

[135] V. V. Tsukruk, D. H. Reneker, *Polymer* **1995**, *36*, 1791.

[136] V. V. Tsukruk, *Rubber Chem. Technol.* **1997**, *70*, 430.

[137] *PeakForce QNM User Guide*, Bruker-Nano, **2010**

[138] M. D. Pashley, *Colloid. Surface* **1984**, *12*, 69.

[139] O. Piétrement, M. J. Troyon, *Colloid Interf. Sci.* **2000**, *226*, 166.

[140] New Characterization Techniques for Thin Polymer Films, Eds.: H. M. Tong, L. T. Nguyen, John Wiley & Sons: New York, United States, 1990.

[141] E. Kharlampieva, J. M. Slocik, S. Singamaneni, N. Poulsen, N. Kroger, R. R. Naik, V. V. Tsukruk, *Adv. Func. Mater.* **2009**, *19*, 2303.

[142] J. M. Slocik, R. R Naik, *Adv. Mater.* **2006,** *18*, 1988.

[143] J. M. Slocik, R. R Naik, M. O. Stone, D. W. Wright, *J. Mater. Chem.* **2005**, *15*, 749.

[144] N. Loges, G. Karlheinz, L. Nasdala, W. Tremel, *Langmuir* **2006**, *22*, 3073.

[145] A. L. Boskey, *Connect. Tissue Res.* **2003**, *44*, 5.

[146] H. P. Jennissen, M. Laub, *Material. Wiss. Werkst.* **2007**, *38*, 1035.

[147] Y. Jiang, D. Yang, L. Zhang, L. Li, Q. Sun, Y. Zhang , J. Li, Z. Jiang, *Dalton Trans.* **2008**, 4165.

[148] H. H. Klump, K. Koch, C. T. Lin, *S. Afr. J. Sci.* **2006**, *102*, 264.

[149] T. Ueno, N. Yokoi, S. Abe, Y. Watanabe, *J. Inorg. Biochem.* **2007**, *101*, 1667.

[150] T. Prozorov, S. K. Mallapragada, B. Narasimhan, L. Wang, P. Palo M. Nilsen-Hamilton, T. J. Williams, D. A. Bazylinski, R. Prozorov, P. C. Canfield, *Adv. Funct. Mater*. **2007**, *17*, 951.

[151] S. Areva, T. Peltola, E. Säilynoja, K. Laajalehto, M. Lindén, J. B. Rosenholm, *Chem. Mater.* **2002**, *14*, 1614.

[152] J. Ekeroth, A. Borgh, P. Konradsson, B. J. Liedberg, *J. Colloid Interf. Sci.* **2002**, *254*, 322.

[153] X. Mo, M. P. Krebs, S. M. Yu, *Small* **2006**, *4*, 526.

[154] G. Hodes, *Adv. Mater.* **2007**, *19*, 639.

[155] J. M. Slocik, M. O. Stone, R. R. Naik, *Small* **2005**, *11*, 1048.

[156] H. Lee, S. M. Dellatore, W. M. Miller, P. B. Messersmith, *Science* **2007**, *318*, 426.

[157] N. Wangoo, K. K. Bhasi, S. K. Mehta, C. R. Suri, *J. Colloid Interf. Sci.* **2008**, *323*, 247.

[158] K. Ariga, J. P. Hill, M. V. Lee, A. Vinu, R. Charvet, S. Acharya, *Sci. Technol. Adv. Mat.* **2008**, *9*, 014109.

[159] V. V. Tsukruk, *Prog. Polym. Sci.* **1997**, *22*, 247.

[160] G. Decher, *Science* **1997**, *277*, 1232.

[161] C. Jiang, V.V. Tsukruk, *Adv. Mater.* **2006**, *18*, 829.

[162] *Multilayer Thin Films: Sequential Assembly of Nanocomposite Materials* Eds.: G. Decher, J.-M. Lehn, J. Schlenoff, John Wiley & Sons: Weinheim, Germany, **2003**.

[163] F. Hua, Y. Lvov, T. Cui, *Thin Solid Films* **2004**, *449*, 222.

[164] D. Lee, M. F. Rubner, R. E. Cohen, *Nano Lett.* **2006**, *6*, 2305.

[165] T. Fukuoka, Y. Tachibana, H. Tonami, H. Uyama, S. Kobayashi, *Biomacromolecules* **2002**, *3*, 768.

[166] E. Katchalski, M. J. Sela, *J. Am. Chem. Soc.* **1953**, *75*, 5284.

[167] M. Seyama, Y. Iwasaki, S. Ogawa, I. Sugimoto, A. Tate, O. Niwa, *Anal. Chem.* **2005**, *77*, 4228.

[168] D. Klee, Z. Ademovic, A. Bosserhoff, H. Hoecker, G. Maziolid, H.-J. Erli, *Biomaterials* **2003**, *24*, 3663.

[169] S. Tone, T. Masawaki, T. Hamada, *J. Membrane Sci.* **1995**, *103*, 57.

[170] B. M. Wickson, J. L. Brash, *Colloid. Surface.* **1999**, *156*, 201.

[171] S. Kurosawa, E. Tawar-Kondo, N, Minoura, N. Kamo, *Sensor. Actuat. B-Chem.* **1997**, *43*, 175.

[172] S. Tone, T. Masawaki, K. Eguchi, *J. Membrane Sci.* **1996**, *118*, 31.

[173] S. J. Oldenberg, S. L. Westcott, R. D. Averitt, N. J. Halas, *J. Chem. Phys.* **1999**, *111*, 4729.

[174] J. Cho, F. Caruso, *Chem. Mater.* **2005**, *17*, 4547.

[175] P. Haaland, J. Targove, *Appl. Phys. Lett.* **1992**, *61*, 34.

[176] H.-H. Yu, J. W. Hutchinson, *Thin Solid Films* **2003**, *423*, 54.

[177] Y. Eom, L. Boogh, V. Michaud, P. Sunderland, J.-A. Månson, *Polym. Eng. Sci.* **2000**, *40*, 1281.

[178] T. Williams, M. W. Hayes, *Nature* **1966**, *209*, 769.

[179] Y. Zubavichus, A. Shaporenko, M. Grunze, M. Zharnikov, *J. Phys. Chem. B* **2007**, *111*, 9803.

[180] S. Kurosawa, N. Kamo, D. Matsui, Y. Kobatake, *Anal. Chem.* **1990**, *62*, 353.

[181] J. A. Theil, J. G. Brace, R. W. Knoll, *J. Vac. Sci. Technol. A* **1994**, *12*, 1365.

[182] J. D. S. Newman, G. J. Blanchard, *J. Nanopart. Res.* **2007**, *9*, 861.

[183] K.-K. Chia, R. E. Cohen, M. F. Rubner, *Chem. Mater.* **2008**, *20*, 6756.

[184] M. A. Hernandez-Perez, C. Garapon, C. Champeaux, J. C. Orlianges, *J. Phys: Conf. Ser.* **2007**, *59*, 724.

[185] L. I. Grace, R. Cohen, T. M. Dunn, D. M. Lubman, M. S. de Vries, *J. Mol. Spectrosc.* **2002**, *215*, 204.

[186] P. Crews, J. Rodríguez, M. Jaspars, *Organic Structure Analysis*, Oxford University Press, New York, **1998**.

[187] E. Pretsch, P. Bühlmann, C. Affolter, *Structure Determination of Organic Compounds*, Springer, Berlin, **2000**.

[188] C. Jeffryes, T. Gutu, J. Jiao, G. L. Rorrer, *J. Mater. Res.* **2008**, *23*, 3255.

[189] J. T. Koberstein, *J. Polymer Science, B-Polymer Physics* **2004**, *42*, 2942.

[190] J. A. Crowe, J. C. Genzer, *J. Am. Chem. Soc.* **2005**, *127,* 17610.

[191] P. M. Mendes, *Chem. Soc. Rev.***2008**, *37*, 2512.

[192] W. Senaratne, L. Andruzzi, C. K. Ober, *Biomacromolecules* **2005**, *6,* 2427.

[193] I. Tokarev, I. Tokareva, S. Minko, *Adv Mater.* **2008**, *20*, 2730.

[194] M. W. Urban, *Polym Rev.* **2006**, *46*, 329.

[195] D. V. Andreeva, D. Fix, H. Mohwald, D. G Shchukin, *Adv. Materials,* **2008**, *20,* 2789.

[196] T. P. Russell, *Science* **2002**, *297*, 964.

[197] V. V. Tsukruk, *Adv. Mater.* **2001**, *13,* 95.

[198] S. Singamaneni, M. E. McConney, M. C. LeMieux, H. Jiang, J. O. Enlow, T. J. Bunning, R. R. Naik, V. V. Tsukruk, *Adv. Mater.* **2007**, *19*, 4248.

[199] D. Julthongpiput, Y.-H. Lin, J. Teng, E. R. Zubarev, V. V. Tsukruk, *J. Am. Chem. Soc.* **2003**, *125*, 15912.

[200] A. Horváth, A. Beck, A. Sárkány, G. Stefler, Z. Varga, O. Geszti, L. Tóth, L. Guczi, *J. Phys. Chem. B* **2006**, *110*, 15417.

[201] M. F. Bertino, B. Smarsly, A. Stocco, A. Stark, *Adv. Func. Mater.* **2009**, *19*, 1235.

[202] M. C. Stuart, W. Huck, J. Genzer, M. Müller, C. Ober, M. Stamm, G. Sukhorukov, I. Szleifer, V. V. Tsukruk, M. Urban, F. Winnik, S. Zauscher, I. Luzinov, S. Minko, *Nat. Mater.* **2010,** *9,* 101.

[203] I. Luzinov, S. Minko, V. V. Tsukruk, *Soft Matter*, **2008,** *4,* 714.

[204] I. Luzinov, S. Minko, V. V. Tsukruk, *Prog. Polym. Sci.* **2004**, *29,* 635.

[205] R.-H. Jin, J.-J. Yuan, *Adv. Mater.* **2009**, *21*, 3750.

[206] M. T. Klem, M. Young, T. Douglas, *J. Mater. Chem.* **2008**, *18*, 3821.

[207] V. Kozlovskaya, E. Kharlampieva, S. Chang, R. Muhlbauer, V. V. Tsukruk, *Chem. Mater.* **2009**, *21*, 2158.

[208] V. Kozlovskaya, E. Kharlampieva, B. P. Khanal, P. Manna, E. R. Zubarev, V. V. Tsukruk, *Chem. Mater.* **2008**, *20*, 7474.

[209] O. Durupthy, J. Bill, F. Aldinger, *Cryst. Growth Des.* **2007**, *7*, 2696.

[210] Y. Zhao, W. Pérez-Segarra, Q. Shi, A. Wei, *J. Am. Chem. Soc.* **2005**, *127*, 7328.

[211] F. Dubois, B. Mahler, B. Dubertret, E. Doris, C. Mioskowski, *J. Am. Chem Soc.* **2007**, *129*, 482.

[212] J.-J. Yuan, R.-H. Jin, *Langmuir* **2010**, *26*, 4212.

[213] L. D. Bonifacio, B. V. Lotsch, D. P. Puzzo, F. Scotognella, G. A. Ozin, *Adv. Mater.* **2009**, *21*, 1641.

[214] D. P. Puzzo, L. D. Bonifacio, J. Oreopoulos, C. M. Yip, I. Manners, G. A. Ozin, *J. Mater. Chem.* **2009**, *19*, 3500.

[215] N. Hidalgo, M. E. Calvo, H. Míguez, *Small*, **2009**, *5*, 2309.

[216] J. S. King, E. Graugnard, O. M. Roche, D. N. Sharp, J. Scrimgeour, R. G. Denning, A. J. Turberfield, C. J. Summers, *Adv. Mater.* **2006**, *18*, 1561.

[217] J. H. Moon, S. Yang, W. T. Dong, J. W. Perry, A. Adibi, S. M. Yang, *Opt. Express* **2006**, *14*, 6297.

[218] L. Martinu, D. Poitras, *J. Vac. Sci. Technol. A* **2000**, *18*, 2619.

[219] M. Maldovan, E. L. Thomas, Periodic Materials and Interference Lithography: For Photonics, Phononics and Mechanics, Wiley-VCH, **2008**.

[220] C. K. Ullal, M. Maldovan, E. L. Thomas, G. Chen, Y.-J. Han, S. Yang, *Appl. Phys. Lett.* **2004**, *84*, 5434.

[221] J. H. Moon, J. Ford, S. Yang, *Polym. Adv. Tech.* **2006**, *17*, 83.

[222] T. Choi, J.-H. Jang, C. K. Ullal, M. C. Lemieux, V. V. Tsukruk, E. L. Thomas, *Adv. Funct. Mater.* **2006,** *16*, 1324.

[223] J.-H. Jang, C. K. Ullal, M. Maldovan, T. Gorishnyy, S. Kooi, C. Y. Koh, E. L. Thomas, *Adv. Func. Mater.* **2007**, *17*, 3027.

[224] T. Dammak, N. Fourati, Y. Abid, H. Boughzala, A. Mlayah, C. Minot, *Spectrochim. Acta A.* **2007**, *66*, 1097.

[225] J. Madhavan, S. Aruna, A. Anuradha, D. Premanand, I. V. Potheher, K. Thamizharasan, P. Sagayaraj, *Opt. Mater.* **2007**, *29*, 1211.

[226] M. Wolpert, P. Hellwig, *Spectrochim. Acta A* **2006**, *64*, 987.

[227] J. Madhavan, S. Aruna, P. C. Thomas, M. Vimalan, S. A. Rajasekar, P. Sagayaraj, *Cryst. Res. Technol.* **2007**, *42*, 59.

[228] S. J. La'verne, S. Srivastave, S. Srivastave, S. Srivastave, V. D. Gupta, *J. Polym. Sci. Pol. Phys.* **2010**, *48*, 128.

[229] H. G. Tompkins, E. A. Irene *Handbook of Ellipsometry* Springer Science & Business: New York, NY, **2005**.

[230] P. J. Roussel, J. Vanhellemont, H. E. Maes, *Thin Solid Films* **1993**, *234*, 423.

[231] B. Krajewska, W. Zaborska, *J. Mol. Catal. B-Enzym.* **1999**, *6*, 75.

[232] M. Sun, J. Chen, X. H. Liu, Y. F. Zhao, *J. Mol. Struc-Theochem* **2004**, *668*, 47.

[233] H. Jensen, A. Soloviev, Z. Li, R. G. Søgaard, *Appl. Surf. Sci.* **2005**, *246*, 239.

[234] C .M. Greenlief, J. M. White, C. S. Ko, R. J Gorte, *J. Phys. Chem.* **1985**, *89*, 5025.

[235] L. Jing, X. Sun, W. Cai, Z. Xu, Y. Du, H. Fu, *J. Phys. Chem. Solids* **2003**, *64*, 615.

[236] M .M. Rahman, K. M. Krishna, T. Soga, T. Jimbo, M. Umeno, *J. Phys. Chem. Solids* **1999**, *60*, 201.

[237] M. Ocana, J. V. Garcia-Ramos, C. J. Serna, *J. Am. Ceram. Soc.* **1992**, *75*, 2010.

[238] T. D. Robert, L. D. Laude, V. M. Geskin, R. Lazzaroni, R. Gouttebaron, *Thin Solid Films* **2003**, *440*, 268.

[239] S. N. Kasarova, N. G. Sultanova, C. D. Ivanov, I. D. Nikolov, *Opt. Mater.* **2007**, *29*, 1481.

[240] N. Sbai, J. Perrière, B. Gallas, E. Millon, W. Seiler, M. C. Bernard, *J. Appl. Phys.* **2009**, *104*, 033529.

[241] N. .B. Abaffy, P. Evans, G. Triani, D. McCulloch, *Proc. SPIE* **2008**, *7041*, 704109.

[242] A. Bendavid, P. J. Martin, E. W. Preston, *Thin Solid Films* **2008**, *517*, 494.

[243] H.-Q. Jiang, Q. Wei, Q.-X. Cao, X. Yao, *Ceram. Int.* **2008**, *34*, 1039.

[244] J. Aarik, A. Aidla, H. Mändar, T. Uustare, M. Schuisky, A. J. Hårsta, *Cryst. Growth* **2002**, *242*, 189.

[245] A. Kasikov, J. Aarik, H. Mändar, M. Moppel, M. Pärs, T. Uustare, *J. Phys. D Appl. Phys.* **2006**, *39*, 54.

[246] J. Aarik, A. Aidla, A.-A. Kiisler, T. Uustare, V. Sammelselg, *Thin Solid Films* **1997**, *305*, 270.

[247] S. Singamaneni, S. Chang, J.-H. Jang, W. Davis, E. L. Thomas, V. V. Tsukruk, *Phys. Chem. Chem. Phys.* **2008**, *10*, 4093.

[248] S. Singamaneni, K. Bertoldi, S. Chang, J. H. Jang, E. L. Thomas, M. Boyce, V. V. Tsukruk, *Adv. Func. Mater.* **2009**, *19*, 1426.

[249] S. Singamaneni, K. Bertoldi, S. Chang, J. H. Jang, E. L. Thomas, M. Boyce, V. V. Tsukruk, *ACS. Appl. Mater. Interfaces* **2009**, *1*, 42.

[250] O. Wichterle, D. Lim, *Nature* **1960**, *165*, 117.

[251] R. Jeyanthi, K. P. Rao, *Biomaterials* **1990**, *11*, 238.

[252] R. K. Bose, K. K. S. Lau, *Biomacromolecules* **2010**, *11*, 2116.

[253] C. P Quinn, C. P. Pathak, A. Heller, J. A. Hubbell, *Biomaterials* **1995**, *16*, 389.

[254] D. Wang, C. G. Williams, F. Yang, J. H. Elisseeff, *Adv. Func. Mater.* **2004**, *14*, 1152.

[255] H. Jiang, J. T. Grant, K. Eyink, S. Tullis, J. Enlow, T. J. Bunning, *Polymer*, **2005**, *46*, 8178.

[256] A. Borras, J. Cotrino, A. R. González-Elipe, *J. Electrochem. Soc.* **2007**, *154*, 152.

[257] R. Alvarez, P. Romero-Gomez, J. Gil-Rostra, J. Cotrino, F. Yubero, A. Palmero, A. R. González-Elipe, *J. Appl. Phys.* **2010**, *108*, 064316.

[258] K.-H Ahn, Y.-B. Park, D.-W. Park, *Surf. Coat. Tech.* **2003**, *171*, 198.

[259] H. Jiang, J. T. Grant, J. Enlow, W. Su, T. J. Bunning, *J. Mater. Chem.* **2009**, *19*, 2234.

[260] V. R. Rai, S. Agarwal, *J. Phys. Chem. C* **2009**, *113*, 12962.

[261] K. Sweers, K. van der Werf, M. Bennink, V. Subramaniam, *Nanoscale Res. Lett.* **2011**, *6*, 270.

[262] C. P. Fictorie, J. F. Evans, W. L. Gladfelter, *J. Vac. Sci. Technol. A* **1994**, *12*, 1108.

[263] R. L. Spear, R. Tamayev, K. R. Fath, I. A. Banerjee, *Colloid. Surface. B* **2007**, *60*, 158.

[264] V. V. Tsukruk, I. Luzinov, D. Julthongpiput, *Langmuir* **1999**, *15*, 3029.

[265] I Luzinov, D. Julthongpiput, A. Liebmann-Vinson, T. Cregger, M. D. Foster, V. V. Tsukruk, *Langmuir* **2000**, *16*, 504.

[266] J. T. Grant, H. Jiang, S. Tullis, W. E. Johnson, K. Eyink, P. Fleitz, T. J. Bunning, *Vacuum* **2005**, *80*, 12.

[267] P .G. De Gennes, *Rev.* Mod*. Phys.* **1992**, *64*, 645.

[268] A. Perro, S. Reculusa, S. Ravaine, E. Bourgeat-Lami, E. Duguet, *J. Mater. Chem.* **2005**, *15*, 3745.

[269] R. Chatterjee, S. K. Mitra, S. Bhattacharjee, *Langmuir* **2011**, *27*, 8787.

[270] T. Ondarcuhu, P. Fabre, E. Rafael, M. Veyssie, *J. Phys.-Paris* **1990**, *51*, 1527.

[271] C. De Michele, S. Gabrielli, P. Tartaglia, F. Sciortino, *J. Phys. Chem. B* **2006**, *110*, 8064.

[272] L. Hong, S. Jiang, S. Granick, S. *Langmuir* **2006**, *22*, 9495.

[273] N. Glaser, D. J. Adams, A. Böker, G. Krausch, *Langmuir* **2006**, *22*, 5227.

[274] S. Jiang, M. J. Schultz, Q. Chen, J. S. Moore, S. Granick, *Langmuir* **2008**, *24*, 10073.

[275] S. Berger, A. Synytska, L. Ionov, K. J. Eichhorn, M. Stamm, *Macromolecules* **2008**, *41*, 9669.

[276] R. Erhardt, A. Böker, H. Zettl, H. Kaya, W. Pyckhout-Hintzen, G. Krausch, V. Abetz, A. H. E. Müller, *Macromolecules* **2001**, *34*, 1069.

[277] S. Jiang, S. Granick, *Langmuir* **2008**, *24*, 2438.

[278] Z. Li, D. Lee, M. F. Rubner, R. E. Cohen, *Macromolecules* **2005**, *38*, 7876.

[279] A. Perro, F. Meunier, V. Schmitt, S. Ravaine, *Colloid. Surface. A.* **2009**, *332*, 57.

[280] X. Y. Ling, I. Y. Phang, C. Acikgoz, M. D. Yilmaz, M. A. Hempenius, G. J. Vancso, J. Huskens, *Angew. Chem. Int. Edit.* **2009**, *48*, 7677.

[281] O. Cayre, V. N. Paunov, O. D. Velev, *J. Mater. Chem.* **2003**, *13*, 2445.

[282] T. Nisisako, T. Torii, T. Takahashi, Y. Takizawa, *Adv. Mater.* **2006**, *18*, 1152.

[283] S. Pradhan, L.-P. Xu, S. Chen, *Adv. Func. Mater.* **2007**, *17*, 2385.

[284] A. G. Vanakaras, *Langmuir* **2006**, *22*, 88.

[285] L. Nie, S. Liu, W. Shen, D. Chen, M. Jiang, *Angew. Chem. Int. Ed.* **2007**, *46*, 6321.

[286] L. Hong, A. Cacciuto, E. Luijten, S. Granick, *Nano. Lett.* **2006**, *6*, 2510.

[287] A. Walther, X. Andre, M. Drechsler, V. Abetz, A. H. E. Müller, *J. Am. Chem. Soc.* **2007**, *129*, 6187.

[288] K. Roh, D. C. Martin, J. Lahann, *Nat. Mater.* **2005**, *4*, 759.

[289] M. Fialkowski, A. Bitner, B. A. Grzybowski, *Nat. Mater.* **2005**, *4*, 93.

[290] G. Zhang, D. Wang, H. Möhwald, *Angew. Chem.* **2005**, *44*, 7767.

[291] L. Hong, A. Cacciuto, E. Luijten, S. Granick, *Langmuir* **2008**, *24*, 621.

[292] R. K. Shah, J. W. Kim, D. A. Weitz, *Adv. Mater.* **2009**, *21*, 1949.

[293] A. Walther, A. H. E. Müller, *Soft Matter* **2008**, *4*, 663.

[294] S. Jiang, S. Granick, *J. Chem. Phys.* **2007**, *127*, 161102.

[295] K. H. Roh, M. Yoshida, J. Lahann, *Mat.-wiss. u. Werkstofftech.* **2007**, *38*, 1008.

[296] M. Yoshida, K. H. Roh, J. Lahann, *Biomaterials* **2007**, *28*, 2446.

[297] C. J. Behrend, J. N. Anker, B. H. McNaughton, M. Brasuel, M. A. Philbert, R. Kopelman, *J. Phys. Chem. B*, **2004**, *108*, 10408.

[298] Y. K. Takahara, S. Ikeda, S. Ishino, K. Tachi, K. Ikeue, T. Sakata, T. Hasegawa, H. Mori, M. Matsumura, B. J. Ohtani, *J. Am. Chem. Soc.* **2005**, *127*, 6271.

[299] B. P. Binks, P. D. I. Fletcher, *Langmuir* **2001**, *17*, 4708.

[300] H. Wang, N. J. Halas, *Nano Lett.* **2006**, *6*, 2945.

[301] A. Walther, M. Hoffmann, A. H. E. Müller, *Angew. Chem. Int. Ed.* **2008**, *47*, 711.

[302] S. G. Jang, D. G. Choi, C. J. Heo, S. Y. Lee, S. M. Yang, *Adv. Mater.* **2008**, *20*, 4862.

[303] J.-Q. Cui, I. Kretzschmar, *Langmuir* **2006**, *22*, 8281.

[304] M. D. McConnell, M. J. Kraeutler, S. Yang, R. J. Composto, *Nano Lett.* **2010**, *10*, 603.

[305] R. M. Erb, N. J. Jenness, R. L. Clark, B. B. Yellen, *Adv. Mater.* **2009**, *21*, 4825.

[306] S. Limb, K. K. S. Lau, D. J. Edell, E. F. Gleason, K. K. Gleason, K. K. *Plasmas Polym.* **1999**, *4*, 21.

[307] K. S. Schanze, A. H. Shellton, *Langmuir* **2009**, *25*, 13698.

[308] Y. Ma, W. F. Dong, M. A. Hempenius, H. Mohwald, G. J. Vancso, *Nat. Mater.* **2006**, *5*, 724.

[309] J. H. He, Y.-H. Lin, M. E. McConney, V. V. Tsukruk, Z. L. Wang, G. Bao, *J. Appl. Phys.,* **2007,** *102,* 084303.

[310] R. Sato-Berrú, R. Redón, A. Vázquez-Olmos, J. M. Saniger, *J. Raman Spectrosc.* **2009**, *40*, 376.

[311] T. J. White, N. V. Tabiryan, S. V. Serak, U. A. Hrozhyk, V. P. Tondiglia, H. Koerner, R. A. Vaia, T. J. Bunning, *Soft Matter* **2008**, *4*, 1796.

[312] S. Schmidt, H. Motschman, T. Hellweg, R. von Klitzing, *Polymer*, **2008**, *49*, 749.

[313] S. Peleshanko, K. D. Anderson, M. Goodman, M. D. Determan, S. K. Mallapragada, V. V. Tsukruk, *Langmuir* **2007**, *23*, 25.

[314] W. Xu, X. Yin, G. He, J. Zhao, H. Wang, *Soft Matter* **2012**, *8*, 3105.

[315] D. Matsukuma, K. Yamamoto, T. Aoyagi, *Langmuir* **2006**, *22*, 5911.

[316] E. Bucio, G. Burillo, E. Adem, X. Coqueret, *Macromol. Mater. Eng.* **2005**, *290*, 745.

[317] M. E. Alf, T. A. Hatton, K. K. Gleason, *Thin Solid Films* **2011**, *519*, 4412.

[318] M. E. Alf, P. D. Godfrin, T. A. Hatton, K. K. Gleason, *Macromol. Rapid Commun.* **2010**, *31*, 2166.

[319] M. C. LeMieux, S. Peleshanko, K. D. Anderson, V. V. Tsukruk, *Langmuir* **2007**, *23*, 265.

[320] M. Delcea, S. Schmidt, R. Palankar, P. A. L. Fernandes, A. Fery, H. Möhwald, A. G. Skirtach, *Small* **2010**, *6*, 2858.

[321] Y. M. Lee, J. K. Shim, *Polymer*, **1997**, *38*, 1227.

[322] M. E. Alf, T. A. Hatton, K. K. Gleason, *Polymer* **2011**, *52*, 4429.

[323] H. Tu, C. E. Heitzman, P. V. Braun, *Langmuir* **2004**, *20*, 8313.

[324] H. Jiang, J. T. Grant, S. Tullis, K. Eyink, P. Fleitz, T. J. Bunning, *Polymer*, **2004**, *45*, 8475.

[325] K. D. Anderson, S. L. Young, H. Jiang, R. Jakubiak, T. J. Bunning, R. R. Naik, V. V. Tsukruk, *Langmuir* **2012**, 28, 1833.

[326] A. Niskanen, K. Arstila, M. Leskelä, M. Ritala, *Chem. Vap. Deposition* **2007**, *13*, 152.

VITA

Kyle Anderson was born in Omaha, Nebraska on April 17th, 1984. He grew up in the Des Moines Metro Area in central Iowa attending West Des Moines Valley High School and participating in many youth organizations including the Boy Scouts of America where he earned the rank of Eagle Scout. He the continued his education at Iowa State University in the Department of Materials Science and Engineering earning a bachelor's degree in materials engineering in 2007 with specializations in polymeric and electronic materials. During his time at ISU, he worked as an undergraduate research assistant in Prof. Tsukruk's laboratory and Argonne National Laboratory. He was also actively involved as a tutor for chemistry and physics. Kyle began his graduate work at the Georgia Institute of Technology in 2007 and had the opportunities to travel to Wright-Patterson Air Force Base and the University of Bayreuth in Germany to conduct research. In his time away from the lab, Kyle enjoys a range of outdoor activities including long distance running, hiking, biking, climbing and reading about personal finance. He will begin his career at The Dow Chemical Company near Houston, TX upon graduation.